UNIVERSITY OF LEEDS

Engineering Functional Partial Joint Replacements: A Soft Solution To A Hard Problem

Robert Joseph Elkington

Submitted in accordance with the requirements for the degree of PhD Mechanical Engineering

The University of Leeds

Faculty of EPS, School Of Mechanical Engineering

February 2025

Intellectual Property and Publication Statement

The candidate confirms that the work submitted is his own, except where work which has formed part of jointly-authored publications has been included. The contribution of the candidate and the other authors to this work has been explicitly indicated below. The candidate confirms that appropriate credit has been given within the thesis where reference has been made to the work of others.

Publications in the Journal Of The Mechanical Behavior Of Biomedical Materials, Tribology International, and Langmuir are Open Access and do not infringe on the rights of the journal. In papers listed below the primary author (Robert Joseph Elkington) conducted all experimental studies, data evaluation and publication preparation. All other authors contributed to funding acquisition, conceptualisation and proofing of articles prior to publication.

1. Highly lubricious SPMK-g-PEEK implant surfaces to facilitate rehydration of articular cartilage. Elkington RJ, Hall RM, Beadling AR, Pandit H, Bryant MG. *Journal Of The Mechanical Behavior Of Biomedical Materials* (Nov 2023)

2. Engineering tribological rehydration of cartilage interfaces: Assessment of potential polyelectrolyte mechanisms. Elkington RJ, Hall RM, Beadling AR, Pandit H, Bryant MG. *Tribology International* (May 2024)

3. Brushing up on cartilage lubrication: Polyelectrolyte-enhanced tribological rehydration. Elkington RJ, Hall RM, Beadling AR, Pandit H, Bryant MG. (May 2024) *Langmuir*

4. Performance Parity In Cartilage Repair: SPMK-g-PEEK Versus Cartilage-Cartilage Interfaces. Elkington RJ, Pryce G, Keeling D, Hall RM, Beadling AR, Pandit H, Bryant

MG. [Submitted to the *Journal Of The Mechanical Behavior Of Biomedical Materials*]

Acknowledgments

There once was a stoic graduate of engineering, busy every day in their research lab. One day, the stoic graduate's experiment failed. "Oh no," lamented the labmates, "What terrible luck, this will surely delay you." "We'll see," pronounced the stoic graduate.

The next week, having appraised the hardware, the stoic graduate yielded useful data. "You are so lucky! Finally, data! Surely you can begin your paper now?" "We'll see," asserted the stoic graduate.

The following week, after a granular analysis of the data, the stoic's hypothesis appeared flawed. "How unlucky!" sighed the labmates. "Frustrating to have lost so much time to unavailing results." "We'll see," maintained the stoic graduate.

The next week, exciting, novel, and unanticipated behaviours emerged from the data. "How lucky!" exclaimed the labmates. "You surely can derive three papers from follow-up experiments!" "We'll see," avowed the stoic graduate.

And so on, and so forth, the stoic graduate continued for four years, eventually completing their PhD thesis.

While reflecting on the broader philosophies learned through the pursuit of a PhD, this narrative certainly does not set out to imply pessimism from my peers. The most significant lesson learned is that science requires an approach of tenacity, rationality, and equanimity. None of which would not have been possible without the people who have supported me through this journey. So, let the credits roll:

First and foremost, to my lab mates: thank you for providing an endless supply of motivation and mirth — Philipp, Sam, Naveen, Manoj, Beril, Pedro, Thawhid, Greg P, Greg dB, Josh, Edona, Faizal, Raihan, Ryan A, Ryan C, Yasmin, Dave, Mike J, Oliver, Issy, and Charlotte-

Beth. You have all reminded me a day without laughter is a day wasted.

To my family — Sarah, Andy, Andrew, Nicholas, Peter, Chris, and Annie — your unwavering support has been the foundation of all my academic adventures.

To my friends, who have kept life fun along the way — too many to name, but you know who you are — thanks for being the perfect escape from the grind. A smorgasbord of hikers, climbers, and hedonists (Joe).

And, of course, my academic mentors, who have guided me with patience and wisdom: Rob, for making Leeds feel like home from day one; Hemant, for taking me knee deep into orthopaedic surgery; Richard, for teaching me the nuanced interpersonal skills required to succeed in academia; and MVP Mike who has been an assiduous, sympathetic and pragmatic mentor throughout — couldn't have done this without your support and friendship!

Abstract

Arthritis often leads to joint replacement, where metal and plastic or ceramic components are used to restore function. While effective, these replacements can fail over time, leading to complex and unpredictable revision surgeries. In many cases, arthritis affects only one side of the joint, making partial joint replacement (hemiarthroplasty or focal cartilage repair) a less invasive alternative. However, replacing soft cartilage with hard metallic surfaces in current hemiarthroplasty devices often results in poor outcomes, as the stiff implants reduce contact area and increase stress on the remaining cartilage, potentially causing further degeneration.

This thesis explores the use of polyelectrolyte functionalised biomaterials as cartilage interfacing surfaces, focusing on SPMK-g-PEEK — a biomimetic interface composed of 3-sulfopropyl methacrylate potassium salt (SPMK) tethered to a polyetheretherketone (PEEK) substrate, inspired by the natural biopolyelectrolytes in synovial fluid. SPMK-g-PEEK surfaces form a highly hydrated, compliant layer ($\sim$5 μm thick) due to their dense coverage of hydrophilic sulphonic acid groups, which supports aqueous boundary lubrication and promotes cartilage interstitial fluid recovery.

Under aqueous conditions, SPMK-g-PEEK exhibits ultra-low friction coefficients ($\mu < 0.02$), consistent across physiologically relevant speeds (0.1 – 200 mm/s) and contact pressures (0.25 –2 MPa), mimicking the tribological properties of natural cartilage. Additionally, these surfaces facilitate a novel mechanism of polyelectrolyte-enhanced tribological rehydration (PETR), promoting cartilage interstitial fluid recovery even in static contact areas. This mechanism supports continuous lubrication and contrasts with conventional theories that attribute cartilage rehydration to hydrodynamic fluid entrainment facilitated by convergent cartilage contact geometries. PETR is attributed to the combined effects of fluid confinement within the contact gap and the enhanced elastohydrodynamic behaviour of surface tethered polyelectrolytes.

This work not only enhances the understanding of cartilage tribology but also offers a promising strategy for developing joint replacement materials that more effectively replicate the natural function of cartilage. The implications extend to advancing the design of next-generation implants for focal cartilage repair, offering new potential for improved patient outcomes in orthopaedic applications.

Nomenclature

Abbreviations

μEHL Micro elastohydrodynamic lubrication

AFM Atomic Force Microscopy

CoCrMo Cobalt-Chrome-Molybdenum

CoF Coefficient of Friction

cSCA Convergent Stationary Contact Area

EDX Energy Dispersive Spectroscopy

FTIR Fourier Transform Infrared Spectroscopy

IFP Interstitial Fluid Pressurisation

MCA Migrating Contact Area

MPC 2-(Methacryloyloxy)ethyl 2-(trimethylammonio)ethyl phosphate

PB Polymer Brush

PB-EHL Polymer brush enhanced elastohydrodynamic lubrication

PBS Phosphate Buffered Saline

PEEK Polyether-ether-ketone

PETR Polyelectrolyte Enhanced Tribological Rehydration

SCA Stationary Contact Area

SEM Scanning Electron Microscopy

SPMK 3-Sulfopropyl methacrylate potassium salt

SPMK-g-PEEK SPMK-grafted-PEEK

THR Total Hip Replacement

TJR Total Joint Replacement

TKR Total Knee Replacement

WCA Water Contact Angle

Engineering Variables & Units

μ or μ_{eff} (Effective) Coefficent of Friction (CoF) (-)

μ_{eq} Equilibrium CoF, $F' = 0$, zero IFP condition (-)

μ_F Final CoF (-)

μ_S Startup CoF (-)

τ Time constant (s)

ε Strain (%)

ε_{eq} Equilibrium Strain, $F' = 0$, zero IFP condition (%)

ε_F Final Strain (%)

ε_r Strain Recovery (%)

F' Fluid Load Fraction (-)

h Cartilage height (μm)

h_0 Swollen cartilage height (μm)

R_a Arithmetic Roughness (nm or μm)

t Time (s)

F_X Tangential force (N)

F_Z Normal force (N)

Contents

List of Figures

List of Tables

Chapter 1

Literature Review

> "Cartilages...are spread on some parts of them [bones], such as the joints, to make them smooth...serving as a grease for the joints...Nature has...covered each member of the joint with cartilage and then poured over a greasy, glutinous fluid, providing every joint an easy movement and protection against wear."
>
> — Galen, *On the Usefulness of Various Parts of the Body, AD 175 [1]*

1.1 Introduction

The earliest documented observation of cartilage dates back to Aristotle in the fourth century BC, who described it as *pliable flesh* covering the articulating bones. The epigraph above details the next significant advancement; the first recorded description of the lubricating attributes of cartilage, made by the Greek physician Galen in AD 175. He observed the *smooth* nature of cartilage tissue and the presence of a *greasy, glutinous fluid* that facilitates lubrication, *easy movement and protection against wear* within synovial joints [1, 2]. Comprehensive anatomical studies of articular cartilage did not commence until the early 19th century. These investigations revealed the avascular and hierarchically organised structure of collagen within cartilage tissue [2]. This foundational knowledge paved the way for the 20th century's in-depth exploration of biphasic cartilage biomechanics [3] and the roles of hydrophilic biopolyelectrolytes, which are present on cartilage surfaces and free in the synovial fluid, in providing aqueous

boundary lubrication [4, 5]. The poroelastic mechanics of cartilage, which provide mechanisms of hydration lubrication, fluid load support, and fluid recovery, are now recognised as crucial to the functionality and longevity of articular cartilage in synovial joints [6, 7].

The 19th century also marked the first orthopaedic osteotomy procedure to correct hip arthritis being pioneered by naval surgeon John Rhea Barton. Following this, a variety of implant materials were explored including, plastic, pig bladders, metals and ivory [8]. But it took until the 1950's, and Sir John Charnely, to introduce the first reliable low friction metal-on-metal hip replacement implant system and consistent manufacturing along with surgical methods for up to a 70% survival rate after 30 years [9]. Now the global orthopaedic implant industry is valued at over $60 Billion (c. 2022) [10] and sustains the development of advanced surgical techniques and metallic, ceramic, and polymeric materials offering optimised tribological interfaces to provide long lasting joint replacements. Currently, patients receiving total hip or knee replacements generally have a 90% likelihood of implant functionality after 15 years [11].

Alarmingly, the demographic needing surgical joint interventions is both increasing and skewing younger [12]. As younger patients undergo these procedures, the frequency of complex and costly revision surgeries is expected to rise significantly, reflecting an increased overall demand for such interventions [13]. One strategy to mitigate this trend is the early use of less invasive joint repairs, such as focal repair of articular cartilage lesions, to delay the need for total joint replacement, thereby extending the time before more invasive procedures become necessary. However, the hard metallic or ceramic biomaterials commonly used in for articulating against cartilage are limited in their ability to support the low friction environment. This limitation arises from their high modulus, which focuses the contact area and disrupts biphasic cartilage fluid load support [14, 15]. Additionally, their non-porous and non-hydrated nature diminishes effective aqueous and biphasic lubrication of cartilage [16, 17]. While tissue-engineered solutions hold promise for cartilage restoration, they are currently hindered by restrictive clinical indications and prolonged healing periods, which limit their clinical adoption [18].

In order to bridge the gap between the limitations of hard biomaterials and clinical challenges of tissue engineered solutions, a class of engineered materials is required that are optimised for supporting the physiological aqueous friction and biphasic fluid load support of interfacing cartilage. Hydrogels, due to their high water content and biphasic network structure, have been shown to provide aqueous lubrication and high fluid support, effectively mimicking the

biomechanical properties of cartilage [19, 20, 21]. However, due to the high water content of hydrogels, the clinical translation is impeded by implant integration into surrounding tissue [22]. Implant surfaces functionalised with hydrophilic polyelectrolytes, reminiscent of native biopolyelectrolytes on the superficial cartilage surface, onto implantable biomaterials have been utilised clinically which afford the benefits of aqueous lubricious interfaces. Polyethylene doped with hyaluronic acid (BioPoly, USA) [23] have been employed for cartilage resurfacing, and polyethylene grafted with hydrophilic polymer brushes (Aquala, Koycera Medical, Japan) [24] have been employed to reduce wear in total hip replacements.

This thesis endeavours to further contribute to the research corpus of bioinspired surface grafted polyelectrolyte interfaces. Reflecting on Galen's initial observations of Nature's synovial lubricating mechanisms, it seeks to explore the use of surface grafted polyelectrolytes specifically against articular cartilage interfaces, elucidating a soft solution to the hard problem of biomimetic partial joint repair. This approach necessitates a thorough analysis of synovial function, current orthopaedic trends, and the fundamental tribology that underpins cartilage operation. It culminates in exploring the promising biotribology of *polymer brush* interfaces, valued for their lubricious and biomimetic properties.

1.2 Synovial Joint Overview

1.2.1 Anatomy of Synovial Joints

The human body contains three types of joints when classified by their binding tissues: fibrous joints such as sutures which are formed of dense regular collagen fibres; cartilaginous joints such as intervertebral discs which are joined entirely by cartilage; and the most mobile, synovial joints which are separated by a synovial cavity but bound by surrounding connective tissue [25]. Different types of synovial joints, such as the knee, shoulder, and hip joints, provide 1 to 3 degrees of freedom (i.e. flexion/extension, abduction/adduction, and internal/external rotation). Figure 1.1 shows the hyaline (smooth) articular cartilage covered bone surfaces which are lubricated by synovial fluid contained within the synovial membrane. Joint stability is provided by a fibrous articular capsule and surrounding accessory ligaments[25].

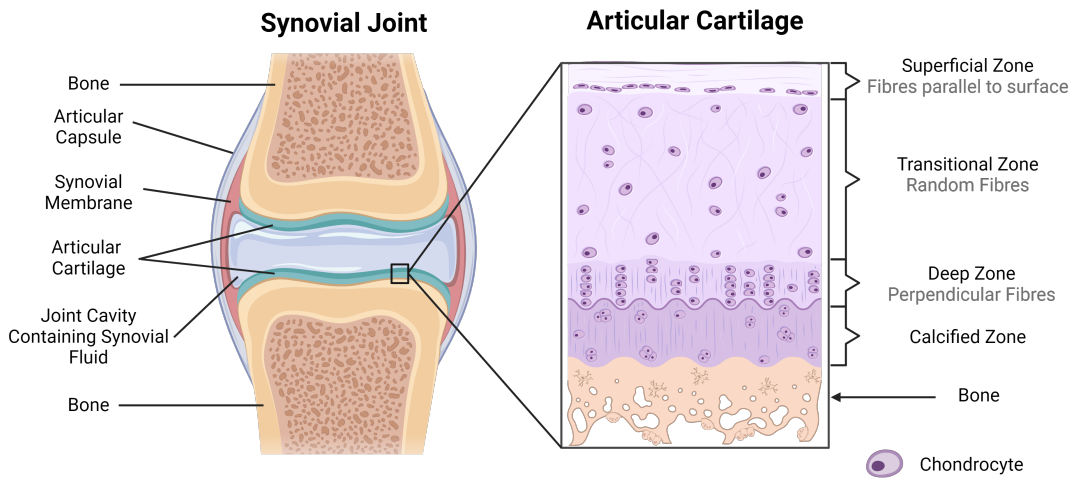

Figure 1.1: Illustration of a synovial joint and structure of articular cartilage.

In healthy synovial joints the articular bone surfaces are covered with a 2 - 4 mm thick viscoelastic porous articular cartilage layer. The physiological purpose of cartilage is to provide a low friction articulating interface and to transfer loads from the bone across the joint. Contrary to popular belief, it is not primarily a shock absorbing tissue, but it is deformable to distribute joint loads, reduce contact stresses, and dissipate impact energy through activities of daily living [26, 27]. By wet weight, cartilage is $\approx$ 70 - 80% water, $\approx$ 20% fibrous matrix proteins (mainly type-II collagen and proteoglycans) and $\approx$ 2 - 5% chondrocytes, the highly specialised and only cell-type which maintain the cartilaginous matrix constituents [28, 29]. The behaviour of chondrocytes (i.e. matrix synthesis and degradation) is determined by presence of cytokines within the synovial capsule and mechanotransduction [28, 30]. Cartilage is devoid of a vascular structure and has limited capacity for healing. The preservation of the cartilage relies on protecting the structure, maintaining hydration of the matrix, and lubricating efficacy of synovial fluid in mitigating surface damage [27].

Figure 1.1 shows the structure of the articular cartilage collagenous matrix divided into 3 distinct regions. The superficial zone is in contact with the opposing cartilage surface and synovial fluid which protects the rest of the cartilage structure from the compressive, shear, and tensile forces generated during joint articulation. This region is approximately 8 - 10% of the cartilage structure and is populated by flattened chondrocytes and tangential collagen to provide the tensile strength for this protection. The cartilage surface is relatively rough with an arithmetic roughness (R_a) measured between 1 - 3 μm [31, 32, 33]. The wide variation in results

is attributable both to the roughness measurement technique used and drying of the cartilage as it is investigated *ex vivo* [34, 31]. The surface of the superficial zone is a delicate acellular region of thin collagen fibrils covered with a highly hydrated $\sim$ 1 - 4 μm thick macromolecular complex composed of adsorbed synovial fluid constituents to provide boundary lubrication [35, 36]. The chemistry and composition of the superficial macromolecular complex is discussed in greater detail in Section 1.3.3. The transitional zone is functionally the bridge between the superficial and radial zones to resist compressive forces. The deep zone provides the most resistance to compressive forces, it contains the lowest concentration of water and is populated by thick collagen fibrils [27].

Water is the main component of cartilage, with the highest content in the superficial zone ($\approx$ 80%) and the lowest in the deep zone ($\approx$ 65%) [29]. This water can be either bound (hydration water) or unbound [28]. Hydrophilic macromolecular species are pervasive throughout the cartilage structure to maintain hydration (bound water). These include aggrecan and hyaluronic acid (HA) which together form larger hydrophilic bottle-brush HA-aggrecan complexes (Figure 1.3) [29, 28, 37, 38]. Within the deeper zones these enhance compressive resistance, whereas in the superficial zone contribute to boundary lubrication of cartilage which is discussed in greater detail in Section 1.3.3 [27, 38]. Water within cartilage is instrumental to preserving its health, flow of interstitial water due to pressure gradients across the tissue supplies nutrients to the chondrocytes and matrix, and interstitial fluid pressure carries the bulk of the joint load to shield the matrix from overloading [39, 40, 37].

Healthy synovial fluid is a clear or pale yellow viscous liquid. It has a neutral pH (7.4 $\pm$ 0.4), provides joint lubrication, load attenuation, cytoprotection and acts as a transport medium. Only a small fluid volume occupies each joint, typically less than 10 mL is in large joints like the knee[41, 42, 25]. Synovial fluid is a transudate of blood plasma, consisting of approximately 94 - 95% water, 0.7 - 0.8% inorganic salts, and 2.5% proteins (mainly albumin and γ-globulin) [43], along with specialised lubricating species produced by type-B synoviocytes. These include phospholipds, HA, and lubricin (proteoglycan-4, possessing a mucin-like structure, Figure 1.3), all of which possess hydrophilic characteristics and are postulated to contribute to the adsorbed macromolecular complex on cartilage to support lubrication [28, 29, 44]. Table 1.1 shows the concentrations of the main synovial fluid constituents for samples aspirated from healthy human knee joints [45, 44].

Constituent	Median Concentration (Q1 - Q3)
Total protein (mg/mL)	37.9 (31.0 - 51.0)
Albumin (mg/mL)	29.1 (19.1 - 37.2)
Lubricin (mg/mL)	0.364 (0.305 - 0.405)
Hyaluronic acid (mg/mL)	2.0 (0.8 - 3.4)
Phospholipids (mg/mL)	0.312 (0.125 - 0.513)
Viscosity (mPa/s)	7.3 (3.6 - 60.7)

Table 1.1: Median values (first quartile - third quartile) of synovial fluid constituents for healthy human knees (n = 26) [45], with the exception of Lubricin (n = 24) [44].

This section introduces the structural and biochemical characteristics of articular cartilage, alluding to the importance of fluid flow and macromolecular hydration of cartilage for biomechanical function. Section 1.3 will discuss the tribological context of these properties focusing on interstitial fluid pressurisation (Section 1.3.4) and the mechanism of the superficial macromolecular complex on boundary lubrication (Section 1.3.3). These factors are essential for the lifetime function of cartilage, and their deterioration can both contribute to or indicate joint disease [40, 44].

1.2.2 Joint Disease And Osteoarthritis

Osteoarthritis (OA) is the most prevalent form of joint arthritis and cause of disability in the UK. It is estimated up to 8.5 million people in the UK suffer with joint pain attributable to osteoarthritis. Symptoms vary person to person, early symptoms include low-level pain and stiffness but overtime the condition may become chronic leading to debilitating joint pain and loss of mobility. The total cost to the UK economy is estimated to be up to 1% of the GDP due to sick leave, treatment, and community and social service costs [46].

Many factors contribute to the initiation and progression of OA; their individual contribution can vary widely and include obesity, trauma or ligament damage, genetic predisposition or age-related degradation of synovial fluid constituents [47, 48]. Early in the OA process, the balance between the synthesis and degradation of the cartilage matrix components is disrupted. Articular cartilage degradation is driven by the disruption of chondrocyte function and inflammatory mediators leading which promote inflammation and stimulate the production of catabolic enzymes that degrade the collagen structure [40]. As cartilage degrades, leading to localised cartilage fibrillation and joint space narrowing, pain can result in altered joint mechanics which can further stress the cartilage and the underlying bone, compounding further cartilage erosion

exacerbated by increasing shear stresses and friction [49, 50]. Whilst localised cartilage defects can improve or stabilise over time, defects tend to progress in patients with symptomatic OA as avascular articular cartilage has limited capacity to fully heal [51, 52, 53]. Full thickness cartilage defects and joint space narrowing are a reliable and independent indication for progression to future total joint affection [54]. The ability to slow OA progression depends upon many intrinsic (location, size, shape of the defect, nature of repair etc.) and extrinsic (ligament damage, load, further trauma, vascular insults, altered mechanics etc.) factors. Consequently, repair of the affected cartilage area can slow down or stop the progression of OA [55, 48].

Around 50% of over 65's have some X-ray evidence of cartilage damage or joint space narrowing relating to arthritis [46] and up to 63% of patients undergoing knee arthroscopy have evidence of articular cartilage lesions [56]. A range of lifestyle, pharmacological and non-pharmacological treatments are effective for the management of arthritis, however in late stage OA and chronic cases surgical intervention is required. During the early stages of symptomatic OA, non surgical interventions such as viscosuplementation of hyaluronic acid or non-steroidal anti inflammatory drugs can be recommended. Whilst these treatments offer effective short term pain management, there is no evidence that these are chondroprotective nor slow the progression of OA [57, 58]. Alternatively, local restorative techniques for articular cartilage repair include subchondral drilling and microfractures to stimulate production of fibrocartilaginous repair tissue and osteochondral autografts. Though, these both require long healing periods, limited long term performance, and are not considered a silver bullet for the therapeutic challenges of symptomatic articular cartilage disease [59]. Depending on the severity and location(s) of cartilage lesions, partial or full joint replacements are the most common surgical intervention [60, 61].

1.2.3 Joint Arthroplasty

Total joint arthroplasty (TJA), replacement of both damaged joint surfaces with prosthetic components, is the most common intervention for late stage symptomatic joint disease to alleviate pain and restore joint function. The most common procedures are total knee arthroplasty (TKA) and total hip arthroplasty (THA), which involve the substitution of the knee and hip joint surfaces, respectively, with metallic, ceramic or polymeric materials. Historically, joint replacement success has been limited to larger joints, with the most common joint arthroplasty surgeries being the hip followed by knee, shoulder, ankle, shoulder, and elbow [62]. However, ongoing research is currently active in addressing the challenges of replacement of small joints

like fingers or toes and more complex joints such as the temporomandibular joint [63].

Despite the success in mobility restoration and pain reduction, these techniques have limitations, including wear of the prosthetic materials, risk of infection, and the eventual need for revision surgeries, especially in younger and more active patients [64]. TJA utilises hard biomaterials such as cobalt-chromium-molybdenum (CoCr), ultra-high molecular weight polyethylene (UHMWPE), and ceramics like alumina [65]. These materials are used in various contact pair configurations, including CoCr-on-CoCr, UHMWPE-on-CoCr, and alumina-on-alumina [66]. However, use of CoCr can lead to deleterious material wear-corrosion processes resulting in the release of cytotoxic metallic ions [67]. Furthermore, release of polyethylene or CoCr wear debris lead to osteolysis and aseptic loosening of the implant [68]. Use of ceramics implant surfaces can drastically reduce materials wear and associated aseptic loosening, but in cases of failure (due to abnormal loading or material defects) is catastrophic producing sharp fragmented debris which severely damage surrounding tissues [69]. Notwithstanding these materials limitations, TJA requires the removal of substantial native bone and cartilage, posing significant challenges for subsequent revision surgeries in terms of operative planning, surgical success, functional outcomes, and implant longevity [70].

Development of minimally invasive joint arthroplasty is ongoing, motivated by shortened rehabilitation times and preservation of remaining healthy articular surfaces [71]. For example, unicompartmental (partial) knee replacements (UKA) are gaining popularity because they involve replacing only the damaged compartment of the knee rather than the entire joint. However, since UKA often employs the same biomaterials mentioned earlier, they remain susceptible to similar failure modes [72]. Additionally, UKA has higher revision rates compared to total knee arthroplasty (TKA) [72, 73].

1.2.4 Rise of Joint Replacement Surgery

In 2019 over 240,000 full, partial, and revision joint replacement surgeries were performed in the UK [62]. Worldwide, these rates continue to trend upwards, for example from 2007 and 2017 overall hip replacement surgeries have increased by 30% and knee replacement by 40% [74]. This is primarily due to the rising rates of arthritis and requirements for joint repair interventions in younger patients [75, 76]. By 2030 it is projected that 52% of primary total hip replacements and 55% of total knee replacements will be implanted in patients younger than

65, with the highest increase in patients aged 45 - 55 [12].

Population studies following patients over 70 who have received TJA of the hip or knee reveal that the lifetime risk of premature failure and subsequent revision surgery is below 5%, with 10 and 20 year implant survival rates above 95% and 85% respectively [13]. However, the risk of lifetime implant failure, necessitating costly and complex revision surgeries, is significantly higher in younger patients. Depending on the patient's sex and implant type, the lifetime revision risk for those younger than 60 varies between 15% and 35%, with the median time to revision being 4.4 years [13]. Another cohort study tracking patients under 55 following THR found a 63% 10-year revision survival rate [77]. Similarly, the 12-year survival rate for patients under 60 undergoing TKR is approximately 82%. Furthermore, when considering revision and patient pain as endpoints, the survival rate decreases to 59% [78]. The incidence of total joint replacements in younger patients is increasing, and the existing precedence of total or partial joint arthroplasty often result in poor function and high revision rates, contributing to a growing population burdened with high care costs and disability [79].

1.2.5 Cartilage Resurfacing

Resurfacing of the affected cartilage area can provide immediate pain relief and functional improvement, whilst also attenuating the progression of osteoarthritis. Both engineered biomaterials and tissue engineering approaches have been explored, offering minimally invasive solutions which retain healthy tissue and can be implanted to match the geometry of the defect [80, 81]. These solutions offer earlier interventions for osteoarthritis and can delay the need for TJA and mitigate the risk of subsequent revision surgeries in younger patients [82, 81].

Hemiarthroplasty, a technique for replacing only one entire joint surface, is suitable for patients with healthy cartilage on the opposing surface, typically within hip and shoulder joints [83, 84]. It offers benefits such as improved joint stability, reduced risk of wear debris-related aseptic loosening, shorter operating times, and a more 'natural' intervention that many patients prefer [85, 86]. Hemiarthroplasty employ metallic or ceramic biomaterials, which are notably stiffer than the native compliant articular cartilage [87]. Furthermore, the geometry of most joints is non-axisymmetric but most engineered implants are axisymmetric potentially leading to further deviation from the natural contact mechanics [88]. Leading to cartilage erosion of the mating surface with incidences as high as 40 - 60% [89, 90] and high articular cartilage wear rates of 0.34

± 0.35 mm/year of cartilage [91]. The use of stiff materials in hemiarthroplasty alters natural joint mechanics, reducing the contact area by up to 40% increasing peak stresses by 500% [14, 15]. Due to these limitations, hemiarthroplasty is predominantly performed on elderly patients with reduced mobility where the risks of a longer surgery and excessive bleeding are significant [86, 92]. For patients with appropriate clinical indications, femoral head hemiarthroplasty has a 5-year revision rate of approximately 2.3–2.8% [83], while shoulder hemiarthroplasty shows a notably higher 5-year revision rate of around 10% [84].

Focal resurfacing systems made of CoCr such as the HemiCAP (Arthrosurface, USA) or Episealer (Episurf Medical, Sweden) are suitable for the repair of localised full thickness cartilage lesions [81]. Short term patient outcomes after two years are promising, with a 2.5% failure rate after 2 years [93] and improved patient outcomes compared to cartilage transplantation or microfracture [94]. However, revision rates increase overtime [95], showing signs of osteoarthritis progression and degenerative changes after 5 years [96, 97] and a concerning 23% re-operation rate with conversion to total arthroplasty after 7 years [82]. Failure is attributed to erosion of the opposing cartilage surface and subsequent progression of joint disease, ultimately due to high contact pressures against articular cartilage which compromises fluid-pressure dependent load support [98, 99, 100, 101]. Furthermore, concerns around tribocorrosion of CoCr surfaces and Co and Cr ion interactions with mating cartilage surfaces have been raised, contributing to the current EUs narrative around limiting the use of Co and Cr containing implants [102, 103].

Self-lubricating biosynthetic materials, such as Biopoly (BioPoly LLC, USA), designed to mimic articular cartilage surfaces, have been recently developed. Biopoly is made from ultra-high molecular weight polyethylene doped with hyaluronic acid on the surface. It demonstrates lower friction coefficients compared to CoCr [23] and leads to improved patient outcomes when compared to microfracture at 2-5 years [104, 105]. However, there is currently no information on the long-term efficacy of BioPoly. Evidence suggests higher revision rates compared to HemiCAP, indicating susceptibility to similar failure modes [106].

1.2.6 Future of Articular Cartilage Repair

Ultimately, the gold standard for treating cartilage lesions is the regeneration of healthy articular cartilage through tissue engineering approaches. Autologous chondrocyte implantation, involving the use of scaffolds or cell-seeded scaffolds, has been explored extensively by researchers,

with only a few approaches advancing to human clinical trials [107, 108]. This remains a significant clinical challenge, primarily limited to younger patient cohorts below 30-35 years of age [107]. The treatment is often associated with long healing times (over nine months [109]) and inconsistent patient outcomes, largely due to inadequate integration, cell leakage, and failure to replicate the mechanical properties of natural cartilage [107, 108, 110].

There is an urgent need for alternative material solutions optimised to interface directly with cartilage and serve as suitable implants for focal joint resurfacing [92]. These materials aim to maximise tissue preservation and delay the necessity for total joint replacement, especially in younger patients. By providing a long-lasting focal cartilage repair device that supports the function of opposing cartilage, these materials can reduce the risk of erosion and slow the progression of osteoarthritis. The ideal material should exhibit reduced stiffness to match that of cartilage [87, 21], providing a biomimetic analogue of cartilage as the orthopaedic implant surface. The design of such materials must be informed by the mechanical and tribological properties of cartilage, leading to a bioinspired solution that effectively restores joint function.

1.3 A Tribological Perspective Of Cartilage Biomechanics

1.3.1 Articular Cartilage Friction

Synovial joints must withstand high contact stresses throughout a lifespan exceeding 80 years. *In vivo* pressure-sensing instrumented prostheses [111, 112], *ex vivo* loading studies [113, 114, 115], and mathematical modelling [116, 117] have measured spatially averaged synovial joint pressures ranging from 0.1 to 5 MPa, with peak stresses reaching up to 18 MPa [111, 5] under static (standing) and dynamic (gait) conditions. For healthy function, the mechanical integrity of the articular cartilage tissue must be protected by effective friction dissipation. Conversely, abnormally high friction strongly correlates with the pathogenesis of degenerative joint disease such as osteoarthritis [118, 5].

The Coefficient of Friction (CoF, μ) is the ratio of the tangential force F_X resisting the motion of two surfaces in contact to the normal applied force F_Z, described by Equation 1.1.

$$\mu = \frac{F_X}{F_Z} \tag{1.1}$$

The first human synovial joint pendulum experiments, conducted in 1936 by Jones on the interphalangeal joint of an amputated finger, demonstrated the CoF to be as low as 0.02 [119]. Subsequent measurements for entire synovial joint systems have have reported values ranging from 0.001 - 0.03 [120, 121, 122, 123]. However, friction measurements of *in vivo* joints are inherently challenging due to additional energy dissipation from the distortion of ligaments and connective tissues, as well as the difficulty in maintaining unperturbed contact geometry [5, 124]. Sliding of small osteochondral explants on flat synthetic countersurfaces (e.g. glass) allows for the direct CoF measurement and a detailed study of cartilage tribological mechanisms. Various *in vitro* approaches have been used to study boundary and mixed fluid film lubrication regimes of cartilage, generally corroborating the low steady-state CoF range of 0.003 to 0.02 [124, 5]. However, it should be noted that benchtop cartilage experiments are complex and dependant on their specified configuration, which will be discussed in detail in subsequent sections.

1.3.2 Cartilage Lubrication Models

The history of understanding cartilage lubrication in synovial joints has evolved significantly since the early 20th century, revealing a complex and multi-modal mechanism influenced by the biphasic nature of cartilage, boundary lubricants, loading conditions, and joint health [125, 126, 127]. Since the 1930's many competing theories have been proposed and superseded one another as experiments and understanding became more sophisticated.

Early theories, inspired by traditional engineering bearings, proposed hydrodynamic lubrication as the principal mechanism. In the 1930s, MacConail suggested that the unique geometry of synovial joints creates a convergent wedge, facilitating fluid film lubrication [128]. Supporting this, logarithmic decay of motion in synovial joint pendulum tests appeared consistent with fluid film lubrication rather than boundary lubrication which would be expected to give a linear decay [119]. Dowson later proposed an elastohydrodynamic solution for synovial lubrication [129]. However, subsequent findings challenged these theories as the calculated film thicknesses for hydrodynamic and elastohydrodynamic theories, $\sim 0.1\ \mu m$ and 1 - 4 μm respectively, were much thinner than the roughness of cartilage (1 - 5 μm), leading to doubts about the viability of fluid film theories alone [126].

By the mid-20th century, increasingly sophisticated approaches began to emerge to elucidate cartilage lubrication. McCutchen proposed a weeping lubrication theory in the 1960s, which

highlighted the role of biphasic cartilage properties; under load, cartilage would exude fluid, acting like a self-pressurised hydrostatic bearing while also supporting boundary lubrication [130, 131]. Weeping lubrication offered a substantive explanation for why synovial joint friction is independent of speed and time-sensitive to loading without discounting the role of boundary lubrication, which in the 1970's was supported by the isolation of lubricin and its role in providing a structured hydrated boundary lubrication layer [4, 132]. This led to the concept that a hydrated squeeze film is maintained between loaded cartilage surfaces by specific constituents of the synovial fluid and tissues, suggesting a mechanism of ultra-filtration where fluid flows down the pressure gradient into cartilage leaving behind a hydrated gel-like film to provide boundary lubrication [133, 134, 5].

Subsequent theories expanded on these ideas, including boosted [135], biphasic [136], and interstitial [39, 137] lubrication. Although variations exist among these theories, there is a consensus that interstitial fluid pressure bears the majority of the load, leaving only a minimal portion to be supported by the solid matrix [138, 139, 140]. Consequently, the frictional forces transmitted through the solid phase are reduced, resulting in lower shear forces. The remaining normal force occurring at between solid contact of opposing cartilage surfaces are then dissipated by the gel-like macromolecular constituents of the boundary lubricating layer [5, 28, 141]. Experimental evidence supports mixed or boundary lubrication regimes, such that synovial joint friction is measured independent of speeds [142] (boundary lubrication) or decreasing with velocity [143] (mixed lubrication) [28, 144]. Direct observations of *in vivo* and cadaveric demonstrate the pressure distribution in hip contact areas is highly nonuniform [111, 145], strongly suggesting that high pressure regions are in boundary contact (as the fluid between them is squeezed out to adjacent lower pressure regions) [5]. Therefore explicating the mechanisms of boundary lubrication must take into account the lubrication dynamics of the surface macromolecular constituents.

Figure 1.2 shows a schematic of the multiscale tribology of articular cartilage. The synovial joint is composed of a conformal contact area of self-mated poroviscoelastic articular cartilage, with the loaded cartilage area migrating over the synovial surface during gait and movement. The majority of the joint loading is supported through interstitial fluid pressurisation, resulting in a high fluid load fraction. Consonantly, during loading interstitial fluid exude from the porous cartilage modulates fluid pressurisation and facilitates biphasic lubrication. At the

microscale, on the surface of the articular cartilage there is an approximately 1 - 4 μm thick gel-like superficial macromolecular complex of hyaluronic acid, phospholipids, HA-aggrecan, free aggrecan, and lubricin which provides boundary lubrication to dissipate friction in areas of interfacing cartilage contact [146, 147, 28].

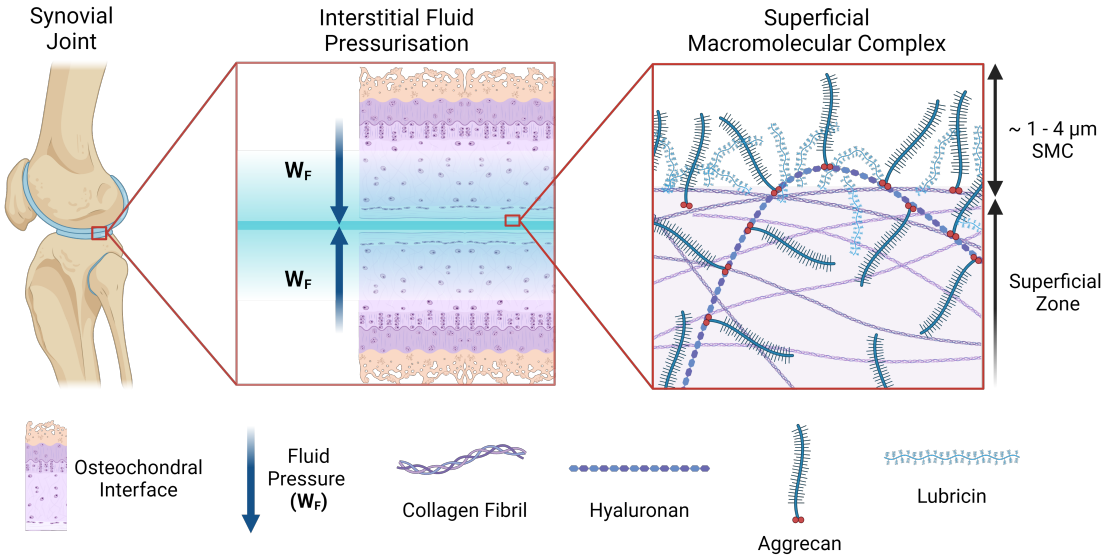

Figure 1.2: Schematic showing the multiscale tribological function of cartilage. **Synovial Joint:** covered with approximately 2 - 4 mm of articular cartilage [148]. **Interstitial Fluid Pressurisation:** upwards of 90% of an articular joint's load is borne over interstitial fluid pressure [139, 149]. **Superficial Macromolecular Complex:** $\sim$ 1 - 4 μm thick gel-like complex of free aggrecan, HA-aggrecan, and lubricin on the superficial osteochondral surface [28, 150, 151].

Understanding the lubrication mechanics of cartilage requires delineation of two key aspects. At the macroscale level, Section 1.3.4 examines the mechanics of contact area migration and the interplay between cartilage rehydration and dehydration, which collectively regulate interstitial fluid pressurisation (IFP) [149]. At the microscale level, Section 1.3.3 discusses the biotribology of the superficial macromolecular complex which provides boundary lubrication [28, 147, 152].

1.3.3 Boundary Lubrication of Synovial Joints

The surface of articular cartilage is coated with a lubricious gel-like acellular non-collagenous superficial macromolecular complex [153, 152, 154]. Measurements using atomic force microscopy (AFM) and scanning electron microscopy (SEM) reveal a thickness of between $\sim$ 1 - 4 μm [35, 155, 153, 156, 152] and AFM force-indentation demonstrate a low moduli of 9 $\pm$ 2 kPa [157]. This superficial layer is highly hydrated, primarily composed of synovial macromolecular

constituents (Section 1.2.1); hyaluronic acid (HA), a linear polysaccharide; the proteoglycan aggrecan; the glycoprotein lubricin; as well as phosopholipds [5, 152]. Each of these constituents possess hydrophilic domains and are implicated in facilitating the aqueous boundary lubrication of articular surfaces [28, 5, 151, 147].

Figure 1.3 shows a schematic of lubricin, aggrecan, and HA-aggrecan complexes. Lubricin is composed of a core protein with positively charged end domains, denoted as N-terminus and C-terminus domains (ND & CD) which associate with the negatively charged cartilage matrix [28, 158]. The central mucin-like domain is heavily glycosylated, populated with approximately 180 O-linked oligosaccharides attached to the protein backbone, resulting in a bottle brush structure with a molecular weight of $\sim$ 250 kDa ($\sim$ 250 kg/mol) [159, 158, 28]. The central oligosaccharides are negatively charged, due to the high concentration of hydroxyl groups ($-OH$), which form hydration shells in physiological conditions [28]. SEM measurements have shown lubricin is approximately $\sim$ 200 $\pm$ 50 nm free length with a width of $<$ 5 nm [158, 28]. Aggrecan is composed of a core protein with end globular domains (G1 - G3) and a link protein (LP) and covalently attached glycosaminoglycan chains resulting in a molecular weight of 2 - 4 MDa [29]. The large central mucin-like domain contains approximately 20 - 50 keratan sulphate chains ($\sim$ 6 - 8 kDa) with an extended length of 10 - 20 nm, and approximately 100 chondroitin sulphate chains ($\sim$ 10 - 30 kDa) with an extended length of 20 - 60 nm [29]. These side chains are composed of sulfonic acid (SO_3^-) and carboxylic acid (COO^-) groups which provide a high density of negative charges to form hydration shells [28, 5, 29]. Resulting in a highly hydrated bottle brush structure in physiological conditions, measuring a diameter of approximately 80 - 100 nm and $\sim$ 400 nm length as measured by AFM of species in mature human cartilage [160, 29]. Up to 100 aggrecan can non-covalently attach at one end via its link-protein (LP) to HA, forming large HA-aggrecan supramolecular bottle-brush structures with a high molecular weight of 50 - 200 MDa [29, 161, 162]. Resulting a large complexes with a free length of a few microns, and a similar aspect ratio to aggrecan, with a $\sim$ 1 μm width as measured by AFM and SEM [29, 161, 163]. However these complexes can differ, the length of the HA backbone can vary from 0.1 - 4 μm [164], and HA has also been shown to associate with phospholipids (composed of a hydrophilic polar head and hydrophobic apolar fatty acid tail) [5, 165, 166].

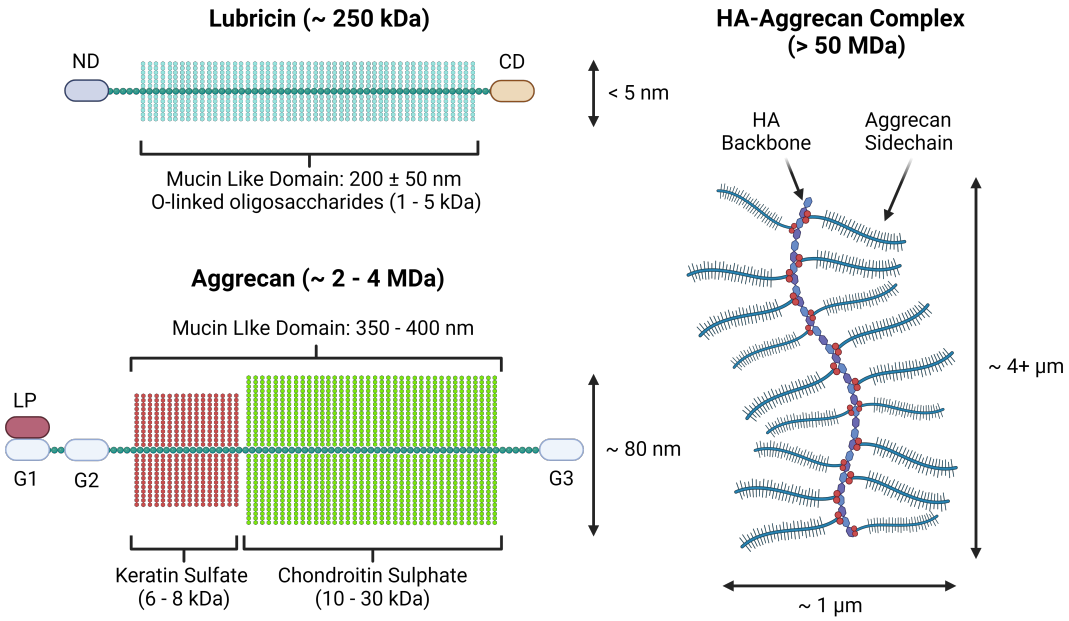

Figure 1.3: Schematic of lubricating glycoproteins, Lubricin and Aggrecan, along with HA-Aggrecan supramolecular complex highlighting the bottle brush-like structure and large mucin-like hydrated domains.

Experiments to determine the true macromolecular conformation of an *in vivo* cartilage surface are extremely difficult; mainly due to degradation of excised cartilage, disturbances to the surface during analysis, and difficulty in reproducing and maintaining *in vivo* synovial surface conditions *in vitro*. Biochemical analysis of fresh cartilage surfaces identify sulphated glycosaminoglycan ($\sim$ 61 μg/cm^2) consistent with keratan and chondroitin sulphate found on aggrecan, and phospholipids ($\sim$ 51 μg/cm^2, predominantly phosphatidylcholine) [152, 167]. Lubricin (often referred to as superficial zone protein) has also been identified adsorbed on the surface of articular cartilage within the superficial macromolecular complex [168, 147]. This is consistent with observations that the amorphous surface complex extends from the superficial zone, rather than wholly physisorbed [152, 153]. The result of the combined adsorption of lubricin in synovial fluid and aggrecan, HA, and HA-aggrecan produced by chrondrocytes in the cartilage superficial zone [147, 141]. The schematic shown in Figure 1.2, reflects the brush-like phase of the superficial macromolecular complex originally proposed by Jacob Klein [147, 5, 169]. Attributing the interactions between synovial constituents to provide a self assembling gel-like macromolecular complex with lubrication attributed to the hydration sheaths bound to the hydrophilic domains of the constituent biopolyelectrolytes [170, 5, 171]. However the specific conformation of the complex has not been directly demonstrated, this model is

based on reductive analysis of synovial constituents, though the 'brush-like' structure affording hydration lubrication and deformation without failure is widely accepted [166, 29, 172].

Several groups have measured the boundary lubrication properties of the different synovial constituents attached to model nanoscale surfaces in aqueous conditions, summarised in Table 1.2. Highlighting the synergistic efficacy between constituents under physiological pressures (0.5 - 10 MPa), notably showing the high CoF of HA alone (μ = 0.2 - 0.5 [173, 174]) compared to Aggrecan + HA (μ = 0.02 - 0.03 [173]) or phospholipids (phosphorycholine) + HA (μ = 0.001 [175]). This reflects observations detailed in more extensive review articles [5, 28], highlighting that synovial boundary lubrication is not attributable to any single constituent, rather synergy between them. Macroscale cartilage tribological studies primarily focus on the viscous fluid-film lubrication properties of synovial fluid [126], rather than superficial macromolecular complex species, but do generally demonstrate synovial fluid yields CoF approximately half that of aqueous solutions (i.e. water, PBS, ringers solution) [176, 149, 177]. However, tribological studies of SCA cartilage pins interfaced with cartilage plates [152] or glass [178] demonstrate removal of the superficial macromolecular complex does not significantly alter CoF. As during loaded-sliding (10 mm linear reciprocating, 4 mm/s, $\sim$ 0.4 MPa contact pressure, in ringers solution), the superficial macromolecular complex is shown to regenerate evidenced by presence of phospholipids and sulphated glycosaminoglycans exude from the cartilage following testing [152, 141]. Whilst there is uncertainty of the specific conformation of the synovial supramolecular complex, low CoF under physiological loads are achieved through an emergent mechanism of *hydration lubrication* facilitated by the highly hydrophilic constituents [28, 170, 5].

Table 1.2: Measured CoF for different synovial boundary lubricants in aqueous conditions on model surfaces. SFB = Surface Force Balance. SFA = Surface Force Apparatus.

Boundary Layer	Substrate	CoF (μ)	Load (MPa)	Speed (μm/s)	Apparatus	Ref
HA	Mica	0.2 - 0.5	0.5	0.3 - 3	SFB	[173, 174]
Aggrecan + HA	Mica	0.02 - 0.03	1	0.3	SFB	[173]
Lubricin	Mica	0.03 - 0.4	0.6	1	SFA	[179]
Lubricin + HA	Mica	0.09 - 0.4	up to 4	1 - 100	SFA	[180]
Phosphorylcholine	Mica	0.001	up to 18	0.5	SFB	[181]
Phosphorycholine + HA	Mica	0.001	up to 10	0.1 - 1.5	SFB	[175]

1.3.3.1 Hydration Lubrication

Hydration lubrication occurs where hydration shells surrounding charges act as a highly effective lubricating boundary layer. Water has a large electric dipole (approximately 1.85 D (Debye))

due to its bent asymmetric structure and electrically polarised H-O bonds, termed a *polar* molecule due to the net dipole [182]. Therefore, in the vicinity of an ion, water will form a tenaciously attached hydration shell as shown in Figure 1.4. The shells are extremely resistant to dehydration and thus are able to withstand high pressures due to the large energy that would be required to break apart the shells. For example in the case of an Na^+ ion the dehydration energy is 80 ± 20 kJ/mol [170, 5, 183].

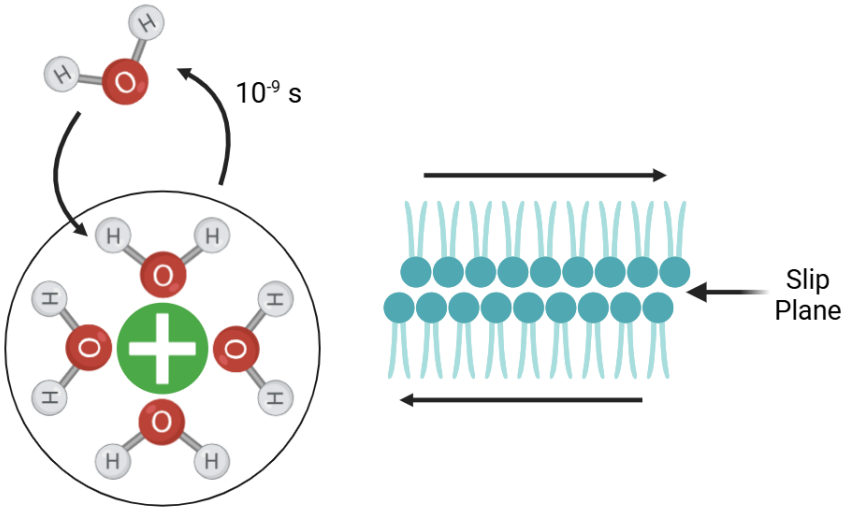

Figure 1.4: Left: Hydrated shell exchanging water molecule. Right: ultra-low friction slip plane between two hydrated layers of cohesive phospholipid heads.

Overlapping hydration shells of nearby charges will lead to short range steric hydration repulsion, which between two hydrated surfaces would prevent adhesive van der Waals contact [170, 184]. Each individual water molecule in the shell is able to rapidly exchange positions with the surrounding bulk water or with water in adjacent hydration shells. The exchange rate can be on the order of 10^{-9} s^{-1} for an alkali metal (i.e. Na^+ ion) to 10^{-4} s^{-1} for a Cr^{3+} ion [170, 183]. In a tribological contact the rapid relaxation dynamics mean providing the shear rate ($\dot{\gamma}$) is below the exchange rate ($\dot{\gamma} > \omega_{exchange}$) hydration shells will behave fluidly under shear to dissipate friction [170]. Experiments isolating hydration lubrication phenomena using a surface force balance (SFB) reveal CoF of ≤ 0.002 at pressures up to 3 MPa with hydration shells estimated to support loads of up to 1 GPa (for Na^+ ions) [183, 184, 170]. The hydrated slip plane between headgroups of one class of phospholipid, comprising of a negative PO_4^- next to a positive $N^+(CH_3)_3$ (Figure 1.4), provide extremely low CoF ($\sim 2 \times 10^{-5}$) up to pressures of 12 MPa [185, 5].

Hydration lubrication provides resistance to normal forces to keep surfaces separated and a

fluid like response to shear, culminating to a highly lubricious and robust frictional dissipation synovial boundary lubrication layer [5]. Wear of opposing surfaces is inevitable, however the synovial macromoleular complex constitutes of molecular species pervasive in the synovial environment and the molecular interactions are physical rather than chemical (i.e. due to charge–charge, charge–dipole, or van der Waals forces) hence regeneration of the boundary film can be near spontaneous [5, 147].

1.3.4 Interstitial Fluid Pressurisation

Ateshian's Interstitial Fluid Pressurisation (IFP) theory currently stands as the predominant model for understanding cartilage biphasic lubrication [149, 137]. It elucidates the time-dependent inverse relationship between friction and interstitial pressure, as substantiated by both experimental [186, 187] and theoretical [137] evidence. IFP theory described by Equation 1.2, $\mu_{\text{eff}}(t)$ is the observed time-dependent coefficient of friction (CoF). $W(t)$ is the applied load, and $W^P(t)$ is the portion of this load supported by interstitial pressure. φ represents the fraction of direct solid-to-solid contact area, μ_{eq} is the CoF at equilibrium, achieved when the fluid pressure is effectively zero. Typically equilibrium CoF (μ_{eq}) are reported in the region of 0.2 - 0.3 for saline, and approximately half that in synovial fluid [149, 186, 177, 188, 176]. Due to the relatively small solid-to-solid contact area ($< 2\%$ [137]), Equation 1.2 is also often simplified into $\mu_{eff}(t) = (1-F')\mu_{eq})$ where F' denotes the aggregate fluid load support fraction ($F' \approx W^P(t)/W(t)$) [149].

$$\mu_{eff}(t) = \left[1 - (1-\varphi)\frac{W^P(t)}{W(t)}\right]\mu_{eq} \equiv (1-F')\mu_{eq} \tag{1.2}$$

IFP theory is underpinned by the poroviscoelastic mechanics of cartilage which is described by biphasic theory, for which the reader is referred to Van Mow [189] for a complete analytical description. Later, computational models have developed biphasic poroviscoelastic non-linear descriptions implemented for advanced articular cartilage full knee joint finite element models [190]. In summary, during sustained periods of loading as the cartilage undergoes deformation, interstitial fluid is exude and subsequently pressurisation subsides. Figure 1.5a shows cartilage displacement during confined compression until an equilibrium state is reached [191]. Concurrently, this results in diminishing fluid load support (F'), shown in Figure 1.5b, as fluid pressurisation subsides and load is transferred to the solid matrix [191, 138]. Meaning that

IFP theory (Eq. 1.2) relies on a loading-sliding state of low cartilage strain in order to sustain cartilage hydration [187, 137]. A corollary of this is IFP theory can also be derived in terms of strain ($\varepsilon(t)$), Equation 1.3, where ε_{eq} corresponds to the equilibrium cartilage compressive strain (zero fluid pressure condition) [187, 149].

$$\mu_{eff}(t) = \mu_{eq}(1 - F') = \mu_{eq}\frac{\varepsilon(t)}{\varepsilon_{eq}} \tag{1.3}$$

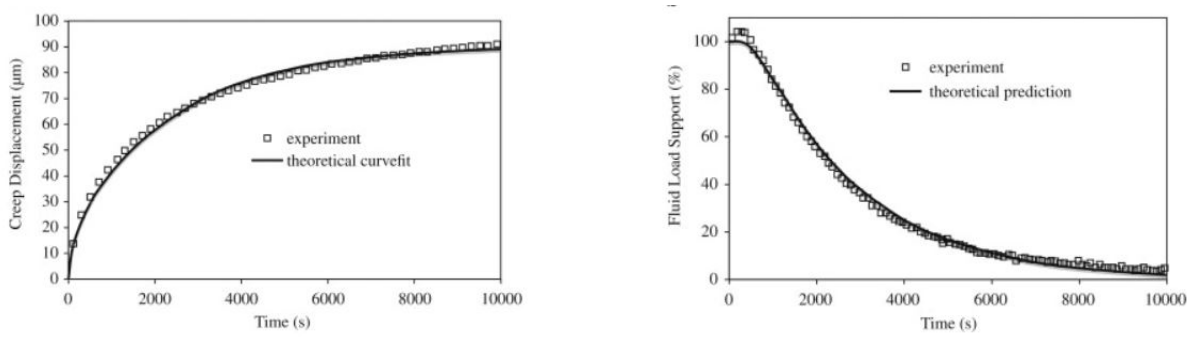

(a) (b)

Figure 1.5: Bovine cartilage confined creep compression (no sliding) response. 1.5a Experimental temporal creep deformation fitted to biphasic theory. 1.5b Ratio of interstitial fluid pressure to applied stress (F') fitted to biphasic theory. Reproduced from [191] under CC-BY-NC-ND.

In vivo studies of tibiofemoral cartilage have measured strain (ϵ) across a range of activities including; gait ($\epsilon \sim 7$ - 23 %)[192]; 10 minutes after jogging ($\epsilon \sim 4$ %)[193]; and knee bending ($\epsilon \sim 3$ - 8 %)[194]. Whereas, periods of sustained loading such as sitting or standing will inevitably lead to substantial fluid exudation, with periods of sustained loading (i.e. inactivity such as sitting or standing) shown to lead to cartilage strains up to 50% [195]. Cartilage has been shown to recover interstitial fluid due to free swelling driven by the viscoelastic recovery of cartilage when unloaded in a supine position [193] and also during physical activity between intermittent periodic loading as the cartilage contact area migrates [196, 197]. Low strain observed during activity, demonstrates native mechanism of interstitial fluid recovery (rehydration) during activity to compete with loading induced exudation. Without rehydration, loss of interstitial fluid pressurisation would overload the collagen extracellular matrix leading to high CoF and wear [3, 5] which is detrimental to cartilage health [198]. Furthermore, interstitial fluid transport is required to maintain cell viability [199], provide solute transport and metabolic waste removal [200, 201].

1.3.4.1 Free Swelling Rehydration

During transient loading articular cartilage can recover interstitial fluid through osmotic swelling, free swelling when unloaded, or through slower passive swelling in areas of nominal unloading [186, 202]. Figure 1.6 shows two sliding contact configurations which examine cartilage CoF and IFP theory using excised bovine cartilage by Caligaris [186]. A stationary contact area (SCA) configuration consists of constantly loaded flat cartilage plug (4 mm diameter) sliding against a glass plate. This is analogous to unconfined compression, as there is limited capacity for the constantly loaded cartilage area to recover interstitial fluid [149]. The migrating contact area (MCA) consists of a glass lens (18 mm radius) sliding against a bovine condyle, allowing cartilage to rehydrate through free swelling during unloaded intervals [186]. Both sliding experiments were conducted under submerged conditions in saline for 3600 s, with identical sliding parameters (6.3 N load, ± 10 mm displacement, 1 mm/s velocity). The recorded CoF μ_{eff} are summarised in Table 1.3. For the SCA configuration, μ_{eff} increases monotonically up to $\mu_{eff} = 0.214$ which corresponds to the maximal μ_{eq} CoF corresponding to a total loss of fluid pressurisation [186, 139, 149]. Conversely for the MCA configuration, μ_{eff} decreases slightly from startup to a sustain low CoF of $\mu_{eff} = 0.024$. Throughout sliding the unloaded areas of cartilage can recuperate hydration through free swelling, sustaining minimal compressive strain with the fluid load fraction (F') supporting up to 90% of the applied load [186, 149].

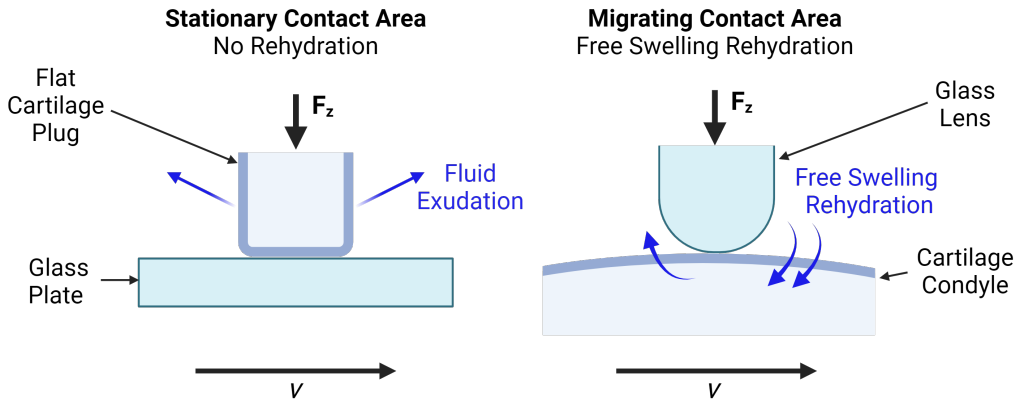

Figure 1.6: Schematic of a static cartilage contact area (SCA) configuration, analogous to unconfined compression, and migrating contact area (MCA) configuration.

μ_{eff}	Initial (t = 0 s)	Steady State
SCA: Cartilage Plug - Glass Plate	0.034 ± 0.005	0.214 ± 0.039
MCA: Glass Lens - Cartilage Condlye	0.014 ± 0.005	0.024 ± 0.010

Table 1.3: Measured CoF (μ_{eff}) of SCA and MCA cartilage contact configurations under the same testing conditions (saline lubricant, 6.3 N load ($\sim$ 0.3 MPa), 1 mm/s velocity, ± 10 mm reciprocating sliding distance, duration = 3600 s). Data from [186].

Finite element analysis studies corroborate that free swelling alone can maintain interstitial fluid [203, 204, 205], however there is no theoretical analysis for the passive swelling hypothesis of joint rehydration and maintenance of low strains during activity [206]. There are established theoretical concerns with the feasibility of this hypothesis. Primarily rehydration must compensate for substantial fluid pressures on the order of 1 - 5 MPa contact stresses [207], whereas passive rehydration is governed by lower osmotic pressures which are limited to 1 - 10% of the competing exudation stress [206]. Furthermore, given the relative amount of time any region spends in contact versus free swelling, it is unlikely that osmotic inflow could balance exudation [206, 199].

1.3.4.2 Tribological Rehydration

Moore and Burris introduced a second mechanism of cartilage interstitial fluid recovery called tribological rehydration, employing a novel convergent stationary contact area (cSCA) configuration. [206, 208]. This setup, depicted in Figure 1.7a, utilises a constantly loaded convex cartilage plug with a larger diameter ($\geq$ 18 mm) differentiating it from a SCA by creating a curved wedge entrainment zone [206]. The convergent inlet zone provides a region of hydrodynamic pressurisation which at speeds greater than 30 mm/s surpasses the interstitial fluid pressure of cartilage, facilitating fluid recovery and lower strain and CoF [206, 208, 7]. At high speeds of 60 mm/s under constant loading ($\sim$ 0.25 MPa), the cSCA configuration could sustain physiological CoF of $\mu_{eff} \sim 0.02$ and lower overall cartilage compression of $\sim$ 60 μm compared to an SCA control ($\mu_{eff} \sim 0.27$, compression $\sim$ 160 μm) [206]. As this is a hydrodynamic process the magnitude of tribological rehydration scales with speed, at 60 mm/s cartilage samples were able to maintain $\sim$ 90% fluid load support (F') [206, 208]. Compared to passive swelling, the cSCA configuration has demonstrated that cartilage rehydration can occur up to seven times faster [202]. Sliding induced tribological rehydration is capable of recovering cartilage strain following a period of compressive strain. Figure 1.7b depicts SCA and cSCA cartilage

following a period of compressive strain (ε_C), upon the onset of sliding the SCA strain continues to increase ($\varepsilon_{SCA} \rightarrow \varepsilon_{eq}$), conversely for the cSCA strain reduces ($\varepsilon_{cSCA} < \varepsilon_C$) indicating rehydration [209, 210, 211, 212].

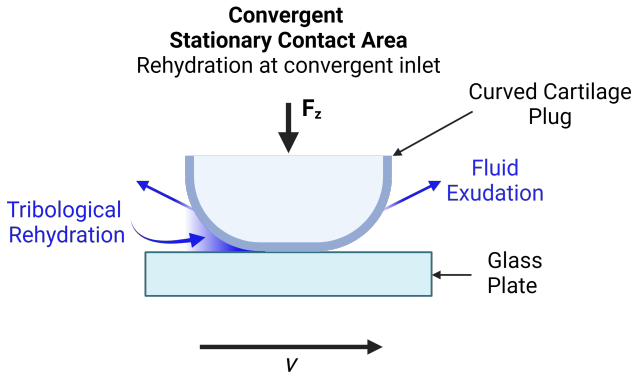

(a)

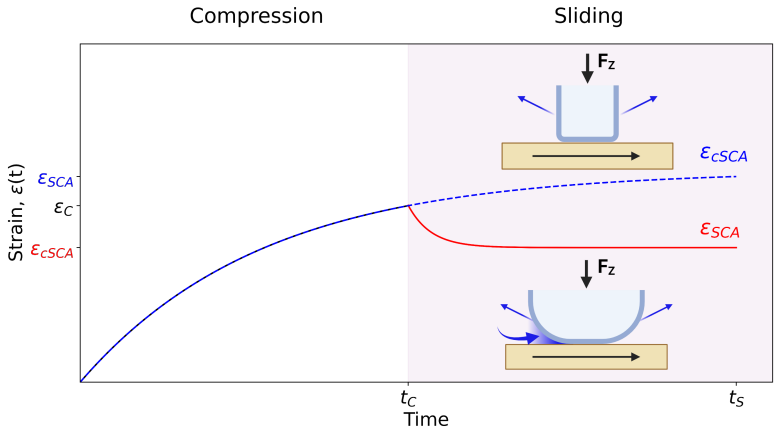

(b)

Figure 1.7: 1.7a. Schematic of a convergent stationary contact area (cSCA) cartilage plug sliding against a glass plate, showing the convergent inlet region of hydrodynamic pressurisation to facilitate tribological rehydration [140]. 1.7b. Illustrative strain profile for a cSCA and SCA cartilage explants undergoing a period of compression-strain (ε_C), followed by sliding-under-compression against a hard impermeable substrate. Upon sliding, the cSCA cartilage explant recovers strain ($\varepsilon(t = t_S) = \varepsilon_{cSCA} < \varepsilon_C$) through tribological rehydration, facilitated by hydrodynamic fluid pressurisation at the convergent wedge leading edge. In contrast, the SCA cartilage explant is analogous to unconfined compression, with no capacity for rehydration, and strain increases throughout sliding ($\varepsilon(t = t_S) = \varepsilon_{SCA} \rightarrow \varepsilon_{eq}$) diminishing interstitial fluid pressurisation. Blue arrows indicate interstitial fluid flow. [211, 212].

For cSCA contacts at the end of sliding (t_S), the overall strain recovery ($\varepsilon_r = \varepsilon_C$ - ε_{cSCA}) quantifies interstitial rehydration. Following compression (30 minutes, $\sim$ 0.25 MPa), upon the onset of sliding (30 minutes, $\sim$ 0.25 MPa, 80 mm/s) cSCA exhibit a high startup CoF ($\mu(t = t_C)$) of $\sim$ 0.11. Table 1.4 shows following sliding of cSCA cartilage in PBS the reduced

strain recovery and lower final CoF ($\varepsilon_r \sim 6\%$, $\mu_{eff} = 0.024$) comply with IFP theory (Eq. 1.3). Whereas, cSCA cartilage sliding synovial fluid exhibit greater reduction ($\varepsilon_r \sim 9\%$, $\mu_{eff} = 0.004$), highlighting the enhanced lubricity and fluid pressurisation of viscous synovial fluid facilitating greater fluid recovery [211, 199]. However, this study does not directly address if the synovial fluid macromolecular constituents enhance fluid confinement in the contact gap, or if rehydration is solely attributable to increased fluid-film viscosity and subsequent boosted pressurisation.

Table 1.4: Comparison of final CoF (μ_{eff} (t = t_S)) and recovered strain following compression (30 minutes) and sliding (30 minutes) of cSCA cartilage, under constant loading ($\sim$ 0.25 MPa) and sliding speeds of 80 mm/s [211].

Lubricant	μ_{eff} (t = t_S)	Recovered Strain (ε_r)
PBS	0.020	$\sim$ 6 %
Synovial Fluid	0.004	$\sim$ 9 %

Tribological rehydration does provide a mechanistic explanation consistent with low strains observed during activity for conformal joints and recovery of cartilage strain following inactivity [206, 199]. From a health perspective, effective tribological rehydration has been demonstrated to mitigate chrondrocyte death in benchtop sliding experiments [199] and facilitate solute transport within cartilage [213, 201]. However, tribological testing so far has only demonstrated low strain recovery ($\varepsilon_r \sim 6$ - 9%) compared to strain recovery required following high strain periods of inactivity ($\varepsilon \sim 50\%$). Secondly, tribological rehydration requires high speeds above 30 mm/s, whereas synovial joints operate across a velocity range of 0 - 100 mm/s [199] which are slower depending on activity or those with reduced mobility.

1.3.4.3 Fluid Flow In The Cartilage Contact Gap

Experimental observations of competitive tribological rehydration to counteract compressive exudation are only demonstrated for cartilage against impermeable counterfaces (i.e. glass) with the underpinning assumption that fluid reuptake occurs due to hydrodynamic pressurisation of entrained fluid films [206, 202]. Computational biphasic modelling of cSCA tribological rehydration demonstrate that hydrodynamic pressurisation, and subsequently fluid pressure induced flow into the porous cartilage, peaks at the contact inlet and propagates a rehydration front across the contact area. Specifically within the contact area, the micro-scale roughness of cartilage provides localised percolation interfacial gaps for rehydration [7].

For matched cartilage, there are two paths of fluid flow in the cartilage gap, one is lateral outflow across the perimeter of the contact gap (fluid loss) and the other is fluid exchange with the interfacing cartilage (counter-surface fluid recovery) [214]. Computational models suggest that pressurised synovial fluid confinement between the micro-roughness of cartilage can contribute to fluid exchange (recovery) between interfacing cartilage surfaces [214, 215, 216]. However these inconsistently account for the hydrated macromolecular interlayer present on the cartilage surface. Viscous synovial fluid does suggest enhanced fluid pressurisation both experimentally [177, 211] and in modelling approaches [215, 217]. Whereas potential surface bound fluid-pressure dynamics of synovial macromolecular species are overlooked, with their presence generally assumed to reduce cartilage permeability and restrict fluid flow [215, 172, 215]. This is a subtle contradiction to address, to the authors knowledge no experimental studies of matched cartilage interfaces directly characterise fluid flow within the contact gap, instead they focus on MCA rehydration (Sec. 1.3.4.1).

The presence of the macromolecular complex on the articular surface are expected to attenuate permeability and enhance interstitial fluid pressurisation [187, 172, 215]. Though, this hypothesis has not been tested directly. Tribological studies have demonstrated equilibrium CoF of cartilage sliding in synovial fluid is around half that of saline [188, 186, 177, 149] and enhanced strain recovery (Tab. 1.4) [211, 199]. Indicating that native synovial macromolecular constituents can enhance both boundary lubrication and interstitial fluid pressurisation [187]. Computational models of attenuated cartilage permeability in the presence of the macromolecular surface complex indicate up to 26× increased fluid support compared to a model with no surface complex [172]. The role of the superficial macromolecular complex can feasibly contribute to explaining low *in vivo* cartilage strains in tandem with osmotic swelling and tribological rehydration, however their specific role on modulating interstitial fluid load support should be studied directly.

1.3.5 Tribological Studies Of Biomaterials Interfaced With Cartilage

Tribometer studies of continuous sliding of small diameter cartilage plugs (SCA) against hard CoCr or polymer counterfaces demonstrate CoF of 0.2 - 0.4 after 60 minutes of sliding [16, 218, 219, 17, 124] with CoF increasing up to as high as 0.7 after 500 minutes sliding [218]. Optical and histological analyses of cartilage following such studies reveal significant deleterious cartilage damage, including delamination and fibrillation [17, 16]. Contrary to this, pendu-

lum friction simulator studies of stainless steel or CoCr surfaces against articulating cartilage condyles sustain CoF between 0.04 - 0.1, and generally support the use of hard biomaterials in hemiarthroplasty [121, 220, 221]. Such experiments are closer representation of native conformal joint mechanics of cartilage in synovial joints, and hence allow for cartilage contract migration and convergent hydrodynamic wedge mechanics necessary for cartilage rehydration [140, 186]. Tribometer studies of CoCr biomaterials interfaced with cartilage demonstrate that these materials do not support aqueous boundary lubrication of cartilage. Furthermore, continuous sliding in a static contact configuration is sensitive to the compression-induced loss of cartilage interstitial fluid pressurisation [186, 206], failing to mimic the modes of cartilage rehydration necessary to sustain low CoF representative of physiological joints (Sec. 1.3.4).

For the assessment of candidate biomaterials proposed to support aqueous boundary lubrication and biphasic interstitial load support, the assessment of CoF as a sole performance indicator can be tenuous. Section 1.3.4 describes that a high degree of cartilage interstitial fluid pressurisation must be maintained to sustain low friction and the mechano-biological function of cartilage [149, 201]. However tribometer studies exploring the use of hydrogels or polymer brush (see Sec. 1.4 for a further discussion) interfaces as biomimetic cartilage materials often only consider CoF against either hard counterfaces (e.g. glass) [222, 223, 224, 225, 19, 226, 227] or cartilage [228, 229, 219, 230]. In particular, cartilage sliding against polymer brush functionalised interfaces demonstrate sustained low CoF of 0.02 - 0.05 which indicate effective replication of aqueous boundary lubrication [228, 230]. However, these methods do not directly assess the materials' capacity to regulate the recovery of cartilage interstitial fluid. Instead, they often infer sustained IFP hydration by observing the maintenance of physiological CoF levels, relying on the understanding of the biphasic properties of these materials [226, 227]. Therefore, early stage tribometer studies of promising cartilage mimetic biomaterials would be enhanced through simultaneous measurement of cartilage CoF alongside strain to measure temporal interstitial fluid modulation, akin to Figure 1.7b.

1.4 Surface Grafted Polyelectrolytes

1.4.1 Polyelectrolyte Biomimicry

Synthetic polyelectrolytes have attracted significant attention because they mimic the biopolyelectrolyte constituents native to synovial fluid (Fig. 1.3), which provide aqueous boundary

lubrication in synovial joints [28, 151]. Macromolecular systems of surface grafted polyelectrolytes, *polymer brushes*, have been extensively investigated for their biomimetic properties, where the presence of hydrophilic groups provide hydration lubrication [165, 28, 231]. Leading to the exploration of microgels with tethered bottle-brush polymers for synthetic synovial fluid [232, 233] and grafted to orthopaedic biomaterials to facilitate low friction hydration lubrication [28, 234, 151].

Enumerate grafted polyelectrolyte compositions have been explored by various research groups, in a wide array of nano-to-macroscale contact configurations, which are summarised in extensive literature reviews [28, 235, 236, 151]. Notably, MPC (2-(methacryloyloxy)ethyl phosphorylcholine) polymer brushes, with highly hydrophilic zwitterionic phosphorylcholine functional groups, have attracted significant attention to mimic synovial aqueous boundary lubrication [237, 238, 28, 239, 234]. Table 1.5 summarises two surface force experiments of end grafted MPC (linear brush, Fig. 1.8) [237] and MPC grafted to a methyl-methacrylate backbone, end tethered in a looped configuration reminiscent of lubricin or aggrecan (bottle brush) [238]. Sliding under physiological pressures (2 - 20 MPa), both matched polymer brush configurations sustain low CoF consistent with native synovial biopolyelectrolytes (Tab. 1.2), attributed to effective hydration lubrication [28, 237, 238, 240]. Furthermore, this demonstrates the polyelectrolyte character (i.e. bottle-brush versus linear-brush) itself is not necessarily essential for low friction boundary lubrication, but rather the essential characteristic is sufficient hydration for aqueous lubrication and swelling to prevent contact between opposing surfaces [165, 28, 240].

Table 1.5: Surface force experiments of MPC (2-(methacryloyloxy)ethyl phosphorylcholine) grafted to mica substrates in a linear-brush and bottle-brush configuration, sliding in aqueous conditions (water) under physiological pressures [237, 238].

MPC Conformation	Height (nm)	CoF (μ)	Load (MPa)	Speed (μm/s)	Apparatus	Ref
Linear-Brush	~ 40	$10^{-5} - 10^{-3}$	7.5 - 20	0.3	SFB	[237]
Bottle-Brush	~ 200	$10^{-3} - 10^{-1}$	2	0.1 - 20	SFA	[238]

This section will focus specifically on surface grafted linear polyelectrolytes, introducing their conformation (Section 1.4.2), propensity for aqueous lubrication (Section 1.4.3) and finally their orthopaedic applications with a focus on MPC (Section 1.4.4). Aiming to highlight the potential for synthetic polyelectrolytes to significantly enhance the performance and longevity of orthopaedic implants by mimicking the natural boundary lubrication mechanisms of cartilage.

1.4.2 Linear Polymer Brush Interfaces

1.4.2.1 Polymer Conformation

Surfaces functionalised with polymer brushes are achieved through chemically grafting polymeric molecules at one end to a planar substrate (a 2D type). The conformation, and subsequently layer thickness, are controlled by the grafting density (ρ_g) of the polymer. In a good solvent a high grafting density (where the distance is small between grafting sites) steric repulsion will cause chain stretching to yield a brush-like conformation with the polymer standing normal to the substrate giving a thick film. Lower graft densities will give other, flatter conformations termed mushroom or semi-stretched structures as shown in Figure 1.8 [236, 241].

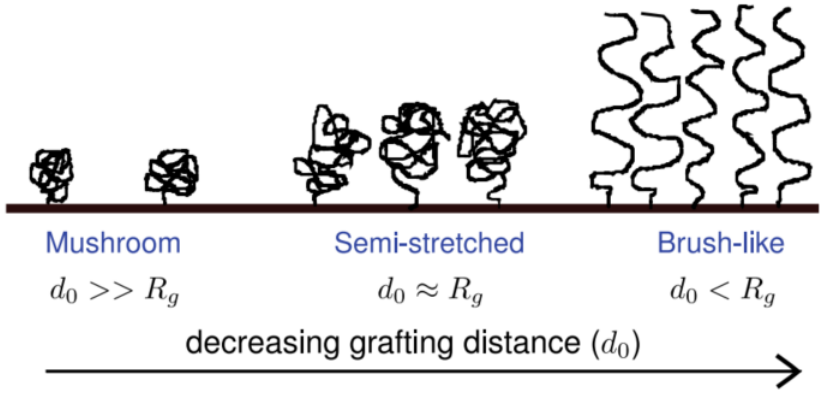

Figure 1.8: Surface grafted polymer conformations as a function of graft density. Adapted from [241]

The conformation is determined by the distance d_0 between polymer graft sites and the radius of gyration R_g of the polymer chain in the bulk solution. When $d_0 >> R_g$ a mushroom conformation occurs, $d_0 \approx R_g$ a semi-stretched conformation is realised, and when $d_0 < R_g$ the polymer chains stretch to a brush like conformation. The critical grafting density for brush-like conformation (ρ_g*) can be approximated to $\rho_g* \sim d_0^{-2} < R_g^{-2}$. An increase in brush layer thickness and graft density corresponds to lower CoF as the PB layer rigidity and amount of bound solvent is increased [241, 242]. Notably, polymer brushes are increasingly being employed to reduce friction in water-lubricated systems, achieving levels approaching those observed in natural systems like synovial joints [242].

1.4.2.2 Polymer Brush Grafting

There are two main approaches to polymer surface grafting; *grafting to* where polymers are adsorbed directly to the substrate (e.g. dipping and crosslinking); and *grafting from* approaches of surface initiated polymerisation where monomers are polymerised from an initiator [151]. *Grafting to* density is limited due to the requirement for polymers to diffuse through already attached polymers to reach the reactive graft sites at the surface, yielding thinner films. Hence *grafting from* is the preferred and most practical method for synthesising high density polymer brush conformations. This can be achieved through atom transfer radical polymerisation (ATRP), reversible addition-fragmentation chain-transfer polymerisation, or photoiniferter mediated polymerisation for accurate control of ρ_g and therefore film thickness, structure, and functional properties [151, 243, 236].

It is also possible to directly graft polymer brushes directly to polyether-ether-ketone (PEEK) [244] and polyethylene variants (e.g. UHMWPE, HXLPE) [245], both of which are biocompatible polymer's routinely used in medical devices [246], using a single step grafting to UV photopolymerisation method. PEEK polymer is comprised of an aromatic backbone molecular chain with ketone and ether functional groups. The presence of a benzophenone unit (an aryl ketone) in the molecular structure, which when irradiated by UV undergoes a pincolization reaction to form a semi-benzopinocal radical (ketyl radical) which act as photoinitatiors, can be exploited for self initiated grafting for direct polymerisation of functional monomers onto the PEEK surface without using a photoinitiator [247, 244, 248]. The surface grafted polymer conformation on PEEK is commensurate with UV exposure time, because the polymer density and molecular weight is increased by successive radical generation through UV initiation of the benzophenone groups [249, 248].

1.4.3 Aqueous Lubrication Of Polymer Brushes

Both hydrophilic neutral (polar) polymers and those containing ionisiable groups (polyelectrolytes) can be exploited for aqueous lubrication [151]. Neutral polymer brushes consist of polar monomers and interact with water through hydrogen bonding [236]. Polyelectrolytes are comparatively much more robust and lubricious than neutral polymers. Stronger ion-dipole interactions between charged groups and water yield a tenacious hydration shell and compression resistance is improved due to generation of osmotic pressures borne through dissociation of

ionic groups in water [236, 250]. Repulsion between ionic groups sustains brush conformation under high contact pressures (> 100 MPa) and resist dehydration, providing a highly hydrated boundary lubricating interface preventing contact with the substrate [251, 252, 165, 28]. Furthermore, water confined within the polymer brush can support a high fluid load fraction and shield the polymer chains from mechanical damage, mitigating wear [253].

Hydrophilic polymer brush friction dissipation pathways are multiscale. At the nanoscale, polymer brush interfaces facilitate effective hydration lubrication, with energy dissipated during shear of sub-nanometer hydration shells (Sec. 1.3.3.1 and discussion of MPC surface force experiments in Sec. 1.4.1) [236, 183]. Whereas, macroscale low friction performance of polymer brushes is largely attributed to the high entropic forces sustaining the brush conformation to separate sliding surfaces while maintaining a fluid (low shear strength, low hydrodynamic drag) film between them [254, 255, 256]. Matched polymer brush surfaces (PB vs. PB) have been the subject of notably more nanoscale and macroscale studies than polymer brushes versus unfunctionalised interfaces (e.g. PB vs. Glass) [165, 236]. For the matched case (PB vs. PB) excluded volume effects of the polymer brush interface entropically resist interpenetration, exhibiting very low adhesion and sustaining a fluid-like interface [236, 151]. Asymmetric systems (e.g. PB vs. Glass) can still sustain comparatively low CoF providing the polymer brush remains between the surfaces (i.e. no wear or collapse) to sustain a fluid-like interface [165, 257]. Effective asymmetric polymer brush lubrication necessitates high grafting densities and hydrophilicity to maintain a robust, hydrated boundary layer capable of sustaining surface separation under high load conditions [258].

Table 1.6: Hydrophilic polymer brushes grafted to Si wafers (∼ 50 nm PB dry thickness) slid against an unfunctionalised glass ball (PB vs. Glass) and a polymer brush functionalised glass ball (PB vs. PB) at 1.5 mm/s with a contact pressure of 140 MPa. (DHMA: 2,3-dehydroxypropyl methacrylate, MTAC: 2-(methacryloyloxy)ethyltrimethylammonium chloride, SPMK: 3-sulfopropyl methacrylate potassium salt, MPC: 2-methacryloyloxyethyl phosphorylcholine) Data from [259, 260].

Monomer	Functional group	Graft Density (ρ_g) (nm^{-2})	Surface free energy (γ_{SL}) (mJ/m^2)	Static WCA	CoF (μ) PB vs. Glass	CoF (μ) PB vs. PB
DHMA	hydroxy (neutral)	0.36	48.1	60°	0.19	0.15
MTAC	ammonium (cationic)	0.20	72.3	12°	0.12	0.08
SPMK	sulfonic acid (anionic)	>0.1	72.9	7°	0.04	0.03
MPC	phosphorylcholine (zwitterionic)	0.23	73.6	3°	0.07	0.04

Table 1.6 compares the characteristics of neutral and ionic polymer brushes grafted (ATRP)

to Si wafers. Notably, the polyelectrolyte functionalised surfaces (MTAC, SPMK, MPC) have surface energies in the region of 72 - 74 mJ/m^2, similar to that of water (72.8 mJ/m^2), exhibiting high hydrophilicity and correspondingly low water contact angles (WCA) [260, 259]. Sliding against a glass probe at a speed of 1.5 mm/s and high contact pressure of 140 MPa in aqueous conditions, demonstrates the enhanced lubricity of polyelectrolyte grafted surfaces (μ(neutral) $> \mu$(polyelectrolyte)). The low CoF was achieved by polyelectrolytes is attributed to the strong electrostatic repulsion between the ionic groups and tenaciously bound hydration shells resisting dehydration [259, 261].

At speeds greater than 1.5 mm/s, CoF generally decreases, with speed ranges between 10 - 100 mm/s sustaining coefficients of friction in the range of 0.01 - 0.04 for MTAC, SPMK and MPC [259, 260]. At low speeds, CoF is typically higher due to the concentration of PB's increasing effective viscosity and resisting shear flow [236]. At increasing sliding speeds, extended polymer chains continue to influence the interfacial viscosity which has a net smoothing effect to damp frictional transitions between boundary and fluid film lubrication (an elastoviscous regime) [262, 236]. Fluid film interferometry studies reveal a *polymer brush-enhanced elastohydrodynamic regime* (PB-EHL), where polyelectrolytes behave as viscosity modifiers to significantly enhance fluid film formation at speeds as low as 0.1 mm/s [263, 264]. For an MTAC-grafted-glass disc sliding against a glass probe under a pressure of approximately 140 MPa, the fluid film thickness increased from approximately 30 nm to 130 nm at speeds ranging from 10 to 1000 mm/s, while the CoF remained consistently low ($\mu \sim 0.02$) [264]. In contrast in the absence of MTAC, water alone cannot sustain a fluid film due to its low viscosity exhibiting an immeasurably thin lubricating layer resulting in high CoF ($\mu \sim 0.2$) [264]. Owing to surface separation and low speed PB-EHL, aqueous lubrication by polymer brushes generally demonstrate a weaker dependence on sliding speed compared to Stribeck analysis of conventional lubricated engineering interfaces [254, 264, 265, 151, 236].

The nanoscale testing (Tab. 1.5) demonstrate PB's capability to support hydration lubrication, and the macroscale tribometer studies (Tab. 1.6) indicate effective aqueous lubrication at pressures an order of magnitude above typical physiological levels. However, the experiments detailed in Table 1.6 were relatively short-term, consisting of 450 cycles and a total sliding distance of 18 meters. Under the high pressure of 140 MPa, evidence of PB wear was observed at the end of testing [259]. The development and validation of polyelectrolyte interfaces for

orthopaedic applications necessitate the optimisation of PB grafted thickness and significantly longer physiologically relevant testing periods. Section 1.4.4 will discuss in greater detail the progress with MPC and SPMK polyelectrolytes in extended testing and medical applications.

1.4.4 Orthopaedic Applications Of Polymer Brushes

The proposed biomimetic attributes of polymer brushes, particularly their low CoF under physiological pressures and speeds, have driven their translation into orthopaedic medical devices. A notable example is the development and clinical implementation of MPC functionalised hip implant surfaces, *Aquala* (Kyocera Medical, Japan) [239, 234]. This provides a comprehensive case study of the research rationale and workflow for polyelectrolyte functionalised orthopaedic interfaces. Following this, development of SPMK functionalised devices will be briefly discussed, due to the functional similarities with MPC in terms of biocompatibility and potential biomedical applications [266].

1.4.4.1 2-methacryloyloxyethyl phosphorylcholine (MPC)

2-methacryloyloxyethyl phosphorylcholine (MPC) is a biocompatible methacrylate containing neutrally charged highly hydrophilic phosphorylcholine groups. The phosphorylcholine group is zwitterionic containing a negative PO_4^- and a positive $N^+(CH_3)_3$ group [184]. Surface grafted MPC polymer brushes have attracted significant attention as biomimetic surfaces. Primarily due to the similarity of the phosphorylcholine groups to the phospholipids and biopolyelectrolytes native to synovial fluid and the articular surface adsorbed supramolecular complex facilitating hydration lubrication [267, 184, 268, 237]. The zwitterionic groups are highly hydrated, with up to 15 water molecules in the primary hydration shell [184], supporting hydration lubrication (Tab. 1.5) [237]. Furthermore, MPC is biocompatible [269] and its high water content facilitates the easy detachment of proteins, providing effective antibiofouling properties [270]. MPC-grafted polyethylene has been shown to reduce bacterial adhesion by a factor of 100 compared to unfunctionalised polyethylene [271]. Alongside orthopaedic applications, MPC functionalised surfaces have been explored for use on medical devices such as intravascular stents, catheters, soft contact lenses, and artificial heart and lung valves [269, 272].

Bioinspired THR designs composed of MPC grafted to polyethylene acetabular components have been demonstrated to drastically reduce wear and friction against CoCr femoral components [234, 184, 273, 274, 275, 239]. They have also been explored as potential surface

coatings for hemiarthroplasty [228, 267, 230], which is discussed later in Section 1.4.5. Surface functionalisation of MPC is *grafted from* cross linked polyethylene (MPC-CLPE) through UV photopolymerisation ($\lambda = 350 \pm 50$ nm, 5 mW/cm^2 intensity, using a benzophenone photoinitiator) by immersing the CLPE substrate in a 0.5 mol/L MPC monomer aqueous solution at 60 °C [234, 273, 274, 275]. Table 1.7 shows that for a range of UV irradiation times (0 - 180 minutes) the grafted thickness of the MPC can be controlled [234]. WCA and ball-on-plate tribometer testing of MPC-CLPE (CoCr ball, 31 MPa pressure, 25 mm reciprocating distance, 50 mm/s speed) demonstrates grafting times of above 45 minutes yields surfaces indicative of a polymer brush conformation (WCA $< 17°$, $\mu < 0.04$).

Hip simulator testing (ISO Standard 14242-3, against a 26 mm CoCr femoral head) of MPC-CLPE acetabular components for 5×10^6 cycles show greatly reduced wear compared (gravimetric wear < 0 mg) to the unfunctionalised CLPE control (gravimetric wear ~ 26 mg) [234]. The negative gravimetric wear is attributed to trapping of excess water in the MPC coating upon removal. This is consistent with MPC-CLPE hip simulator studies showing reduction of up to 80% frictional torque [276], and longer studies of 2 $\times10^7$ cycles in which the number and volume of wear particles is decreased by by 68.7% and 98.2% respectively compared to unfunctionalised CLPE liners [239]. MPC-PEEK acetabular components have been explored in the same experimental setup, displaying similar efficacy in reducing friction and wear [248].

Grafting Time (minutes)	WCA (deg)	Dry Thickness (nm)	CoF (μ)	Gravimetric Wear (mg)
0 (untreated CLPE)	90	0	0.08	25
11	77	0	0.07	-
23	53	30	0.07	11
45	17	95	0.04	-2
90	15	105	0.01	-5
180	15	110	0.03	-5

Table 1.7: Static water contact angle (WCA), grafted layer thickness, tribometer CoF, and gravimetric wear follow 5×10^6 (ISO Standard 14242-3, against a 26 mm CoCr femoral head) of MPC grafted to cross linked polyethylene (MPC-CLPE). Data from [234].

The affinity for MPC surface coatings to reduce wear is attributed to effective aqueous lubrication and repulsion of proteins preventing adhesive interaction with the adsorbed proteins on the CoCr countersurface [277, 228, 237]. This provided a promising solution to reducing incidence of periprosthetic osteolysis and subsequent aseptic loosening attributed to high friction and

wear of polyethylene implant components [239]. Leading to the development of MPC grafted highly cross linked polyethylene (HXLPE) acetabular liners manufactured by Kyocera Medical (Japan) marketed under the name *Aquala* as 'next generation hip joint capsules to prevent aseptic loosening' for the Japanese market since 2011 [278]. Between November 2011 and January 2019 more than 52,000 MPC-HXLPE *Aquala* artificial hip joint devices have been implanted in patients [24]. Follow up examinations of the clinical and radiographic outcomes after three (N = 80) and five (N = 68) years for Aquala acetabular components articulating against a 26 - 28 mm CoCr femoral component were promising [279, 280]. The initial post-operative wear during the first year was measured at a mean of 0.22 mm, aligning with the performance of other HXLPE liners. Mean steady state wear across both studies was measured to be 0.002 mm/year, a substantial improvement compared to the measured steady state wear for ungrafted HXLPE liners of 0.02 - 0.05 mm/ year. Radiograph analysis showed no signs of periprosthetic osteolysis, self reported pain scores were low, resultant joint mobility was on par with other established THR surgeries, and self reported health surveys showed a marked improvement in health related quality of life [279, 280].

However, studies analysing retrieved Aquala acetabular liners (retrieved due to death or other comorbidities, rather than implant failing) report vastly reduced and inconsistent concentrations of MPC polymer remaining on the bearing surfaces. Across two retrieval studies taking place 3 - 36 months after implantation, each liner underwent X-ray Photoelectron Spectroscopy (XPS) and Fourier-Transformed Infrared Spectroscopy (FTIR) analysis which showed no traces of MPC polymer remaining on the bearing surfaces in the loaded areas [281, 278]. The absence of MPC indicates a chain scission failure mode rather than gradual depolymerisation, evident after as little as three months [281]. This degradation could be attributed to hydrolysis of the ester bond in the methacrylate group [266, 282, 283, 284]. Chain scission due to oxidative covalent bond cleavage of MPC has also been observed in the presence of hydrogen peroxide (H_2O_2) [285, 286], which can be produced by the inflammatory response following orthopaedic surgery [287, 288].

1.4.4.2 3-sulfopropyl methacrylate potassium salt (SPMK)

3-sulfopropyl methacrylate potassium salt (SPMK) is a biocompatible methacrylate containing a potassium sulfonate group ($-SO_3^-K^+$) [266, 265]. These groups are ionisable, enabling them to dissociate in aqueous environments leaving hydrophilic sulfonate ions (SO_3^-) tethered to the

polymer backbone [265], capable of holding up to 12 water molecules in the first hydration shell [289]. Reminiscent of the bioinspired philosophy of MPC brush grafted surfaces, sulfonate ions are also one of the same functional groups present on aggrecan (Fig. 1.3) within the superficial macromolecular complex [28].

SPMK polymer brush grafted surfaces elicit similar aqueous lubrication to MPC (Tab. 1.6) [259, 260]. With another study demonstrating that SPMK grafted PEEK (SPMK-g-PEEK) can sustain low CoF ($\mu < 0.01$) against CoCr under contact pressure of $\sim$ 40 MPa , following a long UV photopolymerisation time of 90 minutes ($\lambda = 350 \pm 50$ nm) [290]. However, this study does not measure the grafted thickness. SPMK-g-PEEK has also demonstrated biocompatibility and long-term antibiofouling properties, effectively inhibiting the formation and attachment of cellular and protein biofilms [266].

Building on the case study of MPC development for orthopaedic surfaces in Section 1.4.4.1, SPMK surfaces exhibit comparable and consistent tribological and functional properties to MPC. However, compared to MPC, there has been limited progress in exploiting SPMK for medical biomaterials. SPMK polymer brush grafted surfaces have been positioned as infection resistant coatings for orthopaedic materials [266, 291, 292], lubricious coatings for catheters [265], and also microgel coatings for artificial synovial fluid [232]. However despite their potential as an enabling technology, these applications are still in the very early stages of research, primarily serving as the basis for literature context and early-stage studies. There are currently no indications of further development or translation towards preclinical validation.

1.4.5 Polymer Brushes For Cartilage Resurfacing

There are a limited number of studies that have investigated the interaction between polymer brush surfaces and cartilage. One group reports that MPC grafted to CoCr surfaces, when slid against bovine SCA cartilage, sustained low CoF of $\sim$ 0.02 after $5{\times}10^3$ reciprocating sliding cycles (1 Hz, 25 mm reciprocating distance), with little load dependency across a range of 1 - 10 N ($\sim$ 15 - 150 kPa) [228, 267]. Another study reports that for polyurethane coated with an MPC copolymer brush sliding against convex bovine cartilage plugs, over a total sliding distance of 60 meters across an increasing speed range of 0 to 100 mm/s, and under an estimated contact pressure of 0.55 - 2 MPa, the CoF remained stable between 0.05 and 0.07 [230]. Both groups conducted subsequent histological analyses of the cartilage counterfaces, revealing no

evidence of cartilage damage, which they attributed to the efficacy of aqueous polyelectrolyte lubrication in maintaining physiological CoF levels and preventing cartilage degradation [228, 267, 230]. However, as discussed in Section 1.3.5, these studies do not analyse cartilage strain and subsequently IFP effects.

The role of biopolyelectrolytes has been broached as a mechanism which can support cartilage IFP (Sec. 1.3.4.3) [187, 172]. Whilst this has not been tested directly, matched cartilage surfaces treated with interpenetrating polymer networks (IPN) - a subtly different system from polymer brushes, where two or more polymer networks are physically entangled but not covalently bonded - containing MPC in torsional disc-on-disc SCA cartilage experiments (0.8 MPa, 22 mm/s rotational velocity, 3 hours) demonstrated a lower steady-state CoF of 0.03 compared to untreated samples (CoF $\sim$ 0.06). Notably, these experiments showed a significant reduction in temporal strain for IPN-treated samples, with the resultant strain (ε) $\sim$ 22% lower. This reduction is attributed to the IPNs' ability to decrease hydraulic permeability and the hydrophilic groups of MPC holding free water, enriching the hydration of cartilage [293]. Surfaces functionalised with polyelectrolytes clearly demonstrate the benefits of enhanced aqueous lubrication of cartilage. Furthermore, recent studies have demonstrated that polymer brush terminated hydrogels can enhance rehydration through a sliding-induced hydrodynamic effect, counteracting fluid exudation and preserving lubrication under load [294, 295]. This mechanism closely parallels the natural tribological rehydration observed in cartilage, where a hydrodynamic wedge effect at the contact interface facilitates fluid inflow and bound hydrophilic polyelectrolytes maintain hydration at the interface [294]. Given that polymer brush modified surfaces have already shown efficacy in reducing cartilage strain and promoting sustained lubrication, the potential role of surface bound polyelectrolytes in supporting IFP due to decreased hydraulic permeability or supporting tribological rehydration of cartilage remains unexplored and warrants further investigation.

1.5 Conclusion

This comprehensive literature review has elucidated several critical insights into the biomechanical and tribological challenges of cartilage resurfacing and the promising role of polyelectrolyte interfaces in addressing these challenges. Traditional hard biomaterials, such as cobalt-chromium-molybdenum (CoCr) alloys, for cartilage resurfacing are only effective for short-term

clinical intervention and often only indicated for elderly patients [86, 92]. Inevitably, these materials lead to high friction, increased wear, and ultimately erosion of the opposing cartilage surfaces [89, 90, 91, 101, 100]. The use of hard biomaterials in cartilage resurfacing are insufficient to replicate the natural biomechanics of the cartilage, substantially reducing the contact area and increasing contact pressures [14, 15], which compromise low friction aqueous boundary lubrication and interstitial fluid load support which underpin native articular cartilage function.

Polyelectrolyte interfaces, especially those mimicking the biopolyelectrolyte constituents within the synovial environment, have emerged as promising candidates for bioinspired total joint replacement surfaces [234]. These interfaces exhibit significant potential for hydration lubrication, a critical aspect of aqueous boundary lubrication. The ability of polyelectrolyte interfaces to form highly hydrated boundary layers offers a biomimetic solution that closely replicates the hydrated macromolecular complex on articular cartilage surfaces [28, 170, 151]. However there is a paucity of research exploring polyelectrolyte functionalised surfaces for cartilage resurfacing. Given the structural and functional congruence between polyelectrolytes and the synovial macromolecular complex, it is plausible to anticipate effective integration of these materials at the cartilage interface, limited studies have already highlighted the advantageous low friction properties of MPC functionalised surfaces interfaced with cartilage [228, 267, 230].

The development of cartilage mimicking biomaterials should not only focus on providing effective boundary lubrication but also on supporting interstitial fluid pressurisation, a critical factor for sustaining cartilage health (i.e. low strain, solute transport, and mechano-biological function) [201, 206]. Hence both aqueous boundary lubrication and interstitial fluid maintenance should considered interdependently. Thus, evaluating the strain of interfacing cartilage in conjunction with friction measurements is crucial to ensure these materials truly replicate the natural function of cartilage. This thesis highlights that polyelectrolyte brush interfaces could feasibly influence cartilage interstitial fluid pressurisation. These interfaces may achieve this either by reducing hydraulic permeability [172, 293] or otherwise through supporting interstitial fluid recovery (i.e. rehydration) [211].

This study will focus on elucidating the tribological mechanisms, specifically aqueous lubrication and interstitial fluid pressurisation, between engineered polyelectrolytes and articular cartilage. By closely mimicking the natural synovial environment, bioinspired polyelectrolyte interfaces offer a promising avenue for improving the outcomes of cartilage resurfacing. This advancement

could enable earlier joint repair interventions for younger patients who would otherwise be candidates for total joint replacement, a procedure with limited longevity.

References

[1] Margaret Tallmadge May et al. *Galen on the usefulness of the parts of the body: peri chreias moriōn [romanized form] de usu partium*, volume 1. Cornell University Press, 1968.

[2] TG Benedek. A history of the understanding of cartilage. *Osteoarthritis and cartilage*, 14(3):203–209, 2006.

[3] Van C Mow and Rik Huiskes. *Basic orthopaedic biomechanics & mechano-biology*. Lippincott Williams & Wilkins, 2005.

[4] WH Davis Jr, SL Lee, and L Sokoloff. A proposed model of boundary lubrication by synovial fluid: structuring of boundary water. 1979.

[5] Sabrina Jahn, Jasmine Seror, and Jacob Klein. Lubrication of articular cartilage. *Annual review of biomedical engineering*, 18(1):235–258, 2016.

[6] GN De Boer, N Raske, S Soltanahmadi, D Dowson, MG Bryant, and RW Hewson. A porohyperelastic lubrication model for articular cartilage in the natural synovial joint. *Tribology International*, 149:105760, 2020.

[7] Carmine Putignano, David Burris, Axel Moore, and Daniele Dini. Cartilage rehydration: The sliding-induced hydrodynamic triggering mechanism. *Acta Biomaterialia*, 125:90–99, 2021.

[8] Edward T Habermann. Total joint replacement: an overview. In *Seminars in roentgenology*, volume 21, pages 7–19. Elsevier, 1986.

[9] John J Callaghan, Peter Bracha, Steve S Liu, Somyot Piyaworakhun, Devon D Goetz, and Richard C Johnston. Survivorship of a charnley total hip arthroplasty: a concise follow-up, at a minimum of thirty-five years, of previous reports. *JBJS*, 91(11):2617–2621, 2009.

[10] Straits Research. Orthopedic device market report, 2024. Accessed on 20 April 2024.

[11] Justin S Chang and Fares S Haddad. Long-term survivorship of hip and knee arthroplasty. *The bone & joint journal*, 102(4):401–402, 2020.

[12] Steven M. Kurtz, Edmund Lau, Kevin Ong, Ke Zhao, Michael Kelly, and Kevin J. Bozic. Future young patient demand for primary and revision joint replacement: National projec-

tions from 2010 to 2030. *Clinical Orthopaedics and Related Research*, 467(10):2606–2612, 2009.

[13] Lee E Bayliss, David Culliford, A Paul Monk, Sion Glyn-Jones, Daniel Prieto-Alhambra, Andrew Judge, Cyrus Cooper, Andrew J Carr, Nigel K Arden, David J Beard, et al. The effect of patient age at intervention on risk of implant revision after total replacement of the hip or knee: a population-based cohort study. *The Lancet*, 389(10077):1424–1430, 2017.

[14] Ryan Willing, Graham J.W. King, and James A. Johnson. Contact mechanics of reverse engineered distal humeral hemiarthroplasty implants. *Journal of Biomechanics*, 48(15):4037–4042, 2015.

[15] Ryan Willing, Michael Lapner, Graham J.W. King, and James A. Johnson. In vitro assessment of the contact mechanics of reverse-engineered distal humeral hemiarthroplasty prostheses. *Clinical Biomechanics*, 29(9):990–996, 2014.

[16] SMT Chan, CP Neu, K Komvopoulos, AH Reddi, and PE Di Cesare. Friction and wear of hemiarthroplasty biomaterials in reciprocating sliding contact with articular cartilage. *Journal of Tribology*, 110(4), 2011.

[17] Sevan R Oungoulian, Krista M Durney, Brian K Jones, Christopher S Ahmad, Clark T Hung, and Gerard A Ateshian. Wear and damage of articular cartilage with friction against orthopedic implant materials. *Journal of biomechanics*, 48(10):1957–1964, 2015.

[18] Lijie Zhang, Jerry Hu, and Kyriacos A Athanasiou. The role of tissue engineering in articular cartilage repair and regeneration. *Critical Reviews™ in Biomedical Engineering*, 37(1-2), 2009.

[19] Kai Chen, Xuehui Yang, Dekun Zhang, Linmin Xu, Xin Zhang, and Qingliang Wang. Biotribology behavior and fluid load support of pva/ha composite hydrogel as artificial cartilage. *Wear*, 376:329–336, 2017.

[20] Axel C Moore, Matthew G Hennessy, Liebert Parreiras Nogueira, Susan J Franks, Matteo Taffetani, Hyejeong Seong, Yoo K Kang, Wei Shen Tan, Gregor Miklosic, R El Laham, et al. Fiber reinforced hydrated networks recapitulate the poroelastic mechanics of articular cartilage. *Acta Biomaterialia*, 167:69–82, 2023.

[21] Wei S Tan, Axel C Moore, and Molly M Stevens. Minimum design requirements for a poroelastic mimic of articular cartilage. *Journal of the mechanical behavior of biomedical materials*, 137:105528, 2023.

[22] Kara L Spiller, Suzanne A Maher, and Anthony M Lowman. Hydrogels for the repair of articular cartilage defects. *Tissue engineering part B: reviews*, 17(4):281–299, 2011.

[23] James Cruickshank and Jon Smith. Next-generation cartilage repair and the prearthroplasty patient prearthroplasty artificial implants part a: Biopoly. *Operative Techniques in Sports Medicine*, 30(4):150964, 2022.

[24] Kazuhiko Ishihara. Revolutionary advances in 2-methacryloyloxyethyl phosphorylcholine polymers as biomaterials. *Journal of Biomedical Materials Research - Part A*, 107(5):933–943, 2019.

[25] Susan Standring, Harold Ellis, J Healy, D Johnson, A Williams, P Collins, and C Wigley. Gray's anatomy: the anatomical basis of clinical practice. *American journal of neuroradiology*, 26(10):2703, 2005.

[26] T. D. Stewart. Tribology of artificial joints. *Orthopaedics and Trauma*, 24(6):435–440, 2010.

[27] Alice J. Sophia Fox, Asheesh Bedi, and Scott A. Rodeo. The basic science of articular cartilage: Structure, composition, and function. *Sports Health*, 1(6):461–468, 2009.

[28] Weifeng Lin and Jacob Klein. Recent progress in cartilage lubrication. *Advanced Materials*, 33(18):2005513, 2021.

[29] Anna A Cederlund and Richard M Aspden. Walking on water: revisiting the role of water in articular cartilage biomechanics in relation to tissue engineering and regenerative medicine. *Journal of the Royal Society Interface*, 19(193):20220364, 2022.

[30] Moonsoo Jin, Eliot H Frank, Thomas M Quinn, Ernst B Hunziker, and Alan J Grodzinsky. Tissue shear deformation stimulates proteoglycan and protein biosynthesis in bovine cartilage explants. *Archives of biochemistry and biophysics*, 395(1):41–48, 2001.

[31] P. A. Smyth, R. Rifkin, R. L. Jackson, and R. R. Hanson. The average roughness and fractal dimension of articular cartilage during drying. *Scanning*, 36(3):368–375, 2014.

[32] R S Sayles, T R S Thomias, J Anderson, I Haslock, and A Unsworth. Measurement of the surface microgeometry of articular cartilage. pages 257–267, 1979.

[33] H. Forster and J. Fisher. The influence of continuous sliding and subsequent surface wear on the friction of articular cartilage. *Proceedings of the Institution of Mechanical Engineers, Part H: Journal of Engineering in Medicine*, 213(4):329–345, 1999.

[34] Siddharth Ghosh, James Bowen, Kyle Jiang, Daniel M. Espino, and Duncan E.T. Shepherd. Investigation of techniques for the measurement of articular cartilage surface roughness. *Micron*, 44(1):179–184, 2013.

[35] Joe T Rexwinkle, Heather K Hunt, and Ferris M Pfeiffer. Characterization of the surface and interfacial properties of the lamina splendens. *Frontiers of Mechanical Engineering*, 12:234–252, 2017.

[36] Yoshinori Sawae, Teruo Murakami, Kenji Matsumoto, and Masayuki Horimoto. Study on morphology and lubrication of articular cartilage surface with atomic force microscopy. *Toraibarojisuto/Journal of Japanese Society of Tribologists*, 45(2):150–157, 2000.

[37] Van C Mow and W Michael Lai. Recent developments in synovial joint biomechanics. *Siam Review*, 22(3):275–317, 1980.

[38] Jasmine Seror, Yulia Merkher, Nir Kampf, Lisa Collinson, Anthony J Day, Alice Maroudas, and Jacob Klein. Articular cartilage proteoglycans as boundary lubricants: structure and frictional interaction of surface-attached hyaluronan and hyaluronan–aggrecan complexes. *Biomacromolecules*, 12(10):3432–3443, 2011.

[39] C. G. Armstrong, W. M. Lai, and V. C. Mow. An analysis of the unconfined compression of articular cartilage. *Journal of Biomechanical Engineering*, 106(2):165–173, 1984.

[40] Manoj Rajankunte Mahadeshwara, Maisoon Al-Jawad, Richard M Hall, Hemant Pandit, Reem El-Gendy, and Michael Bryant. How do cartilage lubrication mechanisms fail in osteoarthritis? a comprehensive review. *Bioengineering*, 11(6):541, 2024.

[41] Mihai Roman, Sorin Fleaca, Adrian Boicean, Dan Bratu, Victoria Birlutiu, Luca Rus, Cristian Tantar, and Sebastian Mitariu. Assesment of synovial fluid ph in osteoarthritis of the hip and knee. *Revista de Chimie -Bucharest- Original Edition-*, 68:1340–1342, 06 2017.

[42] Stuart Metcalfe and Ian Reilly. Common Foot and Ankle Conditions. *Foot and Ankle Injection Techniques*, pages 153–167, 2010.

[43] Sergey Ermakov, Alexandr Beletskii, Oleg Eismont, and Vladimir Nikolaev. *Liquid crystals in biotribology: Synovial joint treatment*. Springer, 2015.

[44] Marta Krystyna Kosinska, Taryn E Ludwig, Gerhard Liebisch, Ruiyan Zhang, Hans-Christian Siebert, Jochen Wilhelm, Ulrich Kaesser, Reinhard B Dettmeyer, Heiko Klein, Bernd Ishaque, et al. Articular joint lubricants during osteoarthritis and rheumatoid arthritis display altered levels and molecular species. *PloS one*, 10(5):e0125192, 2015.

[45] Adéla Galandáková, Jitka Ulrichová, Kateřina Langová, Adéla Hanáková, Martin Vrbka, Martin Hartl, and Jiri Gallo. Characteristics of synovial fluid required for optimization of lubrication fluid for biotribological experiments. *Journal of Biomedical Materials Research - Part B Applied Biomaterials*, 105(6):1422–1431, 2017.

[46] National Institute For Health And Clinical Excellence. Osteoarthritis: the care and management of osteoarthritis. https://www.nice.org.uk/guidance/cg177/documents/osteoarthritis-update-final-scope2, 2014.

[47] Michele M. Temple-Wong, Shuwen Ren, Phu Quach, Bradley C. Hansen, Albert C. Chen, Akihiko Hasegawa, Darryl D. D'Lima, Jim Koziol, Koichi Masuda, Martin K. Lotz, and Robert L. Sah. Hyaluronan concentration and size distribution in human knee synovial fluid: Variations with age and cartilage degeneration. *Arthritis Research and Therapy*, 18(1):1–8, 2016.

[48] David Murray, Christopher Dodd, John Goodfellow, and John OConnor. *Unicompartmental Arthroplasty with the Oxford Knee (2nd Edition)*. Goodfellow Publishers Limited, 2011.

[49] Timothy M Griffin and Farshid Guilak. The role of mechanical loading in the onset and progression of osteoarthritis. *Exercise and sport sciences reviews*, 33(4):195–200, 2005.

[50] Farshid Guilak. Biomechanical factors in osteoarthritis. *Best practice & research Clinical rheumatology*, 25(6):815–823, 2011.

[51] ML Davies-Tuck, Anita E Wluka, Y Wang, AJ Teichtahl, Graeme Jones, Changhai Ding,

and Flavia Maria Cicuttini. The natural history of cartilage defects in people with knee osteoarthritis. *Osteoarthritis and Cartilage*, 16(3):337–342, 2008.

[52] Darby A Houck, Matthew J Kraeutler, John W Belk, Rachel M Frank, Eric C McCarty, and Jonathan T Bravman. Do focal chondral defects of the knee increase the risk for progression to osteoarthritis? a review of the literature. *Orthopaedic journal of sports medicine*, 6(10):2325967118801931, 2018.

[53] Y Wang, Changhai Ding, Anita E Wluka, S Davis, Peter Robert Ebeling, Graeme Jones, and Flavia Maria Cicuttini. Factors affecting progression of knee cartilage defects in normal subjects over 2 years. *Rheumatology*, 45(1):79–84, 2006.

[54] Joshua S Everhart, Moneer M Abouljoud, J Caid Kirven, and David C Flanigan. Full-thickness cartilage defects are important independent predictive factors for progression to total knee arthroplasty in older adults with minimal to moderate osteoarthritis: data from the osteoarthritis initiative. *JBJS*, 101(1):56–63, 2019.

[55] Tom Minas, Andreas H. Gomoll, Shahram Solhpour, Ralf Rosenberger, Christian Probst, and Tim Bryant. Autologous chondrocyte implantation for joint preservation in patients with early osteoarthritis. *Clinical Orthopaedics and Related Research*, 468(1):147–157, 2010.

[56] Walton W Curl, Jonathan Krome, E Stanley Gordon, Julia Rushing, Beth Paterson Smith, and Gary G Poehling. Cartilage injuries: a review of 31,516 knee arthroscopies. *Arthroscopy: The Journal of Arthroscopic & Related Surgery*, 13(4):456–460, 1997.

[57] Michael Benke and Benjamin Shaffer. Viscosupplementation treatment of arthritis pain. *Current pain and headache reports*, 13:440–446, 2009.

[58] Leslie J Crofford. Use of nsaids in treating patients with arthritis. *Arthritis research & therapy*, 15:1–10, 2013.

[59] F. V. Sciarretta. 5 to 8 years follow-up of knee chondral defects treated by PVA-H hydrogel implants. *European Review for Medical and Pharmacological Sciences*, 17(22):3031–3038, 2013.

[60] E. B. Hunziker. Articular cartilage repair: Basic science and clinical progress. A review of the current status and prospects. *Osteoarthritis and Cartilage*, 10(6):432–463, 2002.

[61] S N Redman, S F Oldfield, and C W Archer. Current Strategies For Articular Cartilage Repair. 44(0), 2005.

[62] National Joint Registry. NJR 17th Annual Report 2020. https://reports.njrcentre.org.uk/Portals/0/PDFdownloads/NJR%2017th%20Annual%20Report%202020.pdf, 2020.

[63] L Guarda-Nardini, D Manfredini, and G Ferronato. Temporomandibular joint total replacement prosthesis: current knowledge and considerations for the future. *International journal of oral and maxillofacial surgery*, 37(2):103–110, 2008.

[64] Kevin L Ong, Edmund Lau, Jeremy Suggs, Steven M Kurtz, and Michael T Manley. Risk of subsequent revision after primary and revision total joint arthroplasty. *Clinical Orthopaedics and Related Research®*, 468:3070–3076, 2010.

[65] Kalpana S Katti. Biomaterials in total joint replacement. *Colloids and surfaces B: Biointerfaces*, 39(3):133–142, 2004.

[66] J Pajarinen, T-H Lin, T Sato, Z Yao, and SB Goodman. Interaction of materials and biology in total joint replacement–successes, challenges and future directions. *Journal of materials chemistry B*, 2(41):7094–7108, 2014.

[67] Emmanuel Gibon, Derek F Amanatullah, Florence Loi, Jukka Pajarinen, Akira Nabeshima, Zhenyu Yao, Moussa Hamadouche, and Stuart B Goodman. The biological response to orthopaedic implants for joint replacement: Part i: Metals. *Journal of Biomedical Materials Research Part B: Applied Biomaterials*, 105(7):2162–2173, 2017.

[68] Nicholas A Hodges, Eric M Sussman, and Jan P Stegemann. Aseptic and septic prosthetic joint loosening: Impact of biomaterial wear on immune cell function, inflammation, and infection. *Biomaterials*, 278:121127, 2021.

[69] B Sonny Bal, Jonathan Garino, Michael Ries, and Mohamed N Rahaman. Ceramic materials in total joint arthroplasty. In *Seminars in Arthroplasty*, volume 17, pages 94–101. Elsevier, 2006.

[70] Neil P Sheth, Marcelo Batista Bonadio, and Marco Kawamura Demange. Bone loss in revision total knee arthroplasty: evaluation and management. *JAAOS-Journal of the American Academy of Orthopaedic Surgeons*, 25(5):348–357, 2017.

[71] William J Hozack, Martin Krismer, Michael Nogler, Peter M Bonutti, Franz Rachbauer, Jonathan L Schaffer, and William J Donnelly. *Minimally invasive total joint arthroplasty*. Springer Science & Business Media, 2012.

[72] J-A Epinette, B Brunschweiler, P Mertl, D Mole, A Cazenave, The French Society for the Hip, et al. Unicompartmental knee arthroplasty modes of failure: wear is not the main reason for failure: a multicentre study of 418 failed knees. *Orthopaedics & Traumatology: Surgery & Research*, 98(6):S124–S130, 2012.

[73] Hannah A Wilson, Rob Middleton, Simon GF Abram, Stephanie Smith, Abtin Alvand, William F Jackson, Nicholas Bottomley, Sally Hopewell, and Andrew J Price. Patient relevant outcomes of unicompartmental versus total knee replacement: systematic review and meta-analysis. *bmj*, 364, 2019.

[74] OECD. Health at a Glance 2019. https://www.oecd-ilibrary.org/content/publication/4dd50c09-en, 2019.

[75] Elena Losina, Thomas S Thornhill, Benjamin N Rome, John Wright, and Jeffrey N Katz. The dramatic increase in total knee replacement utilization rates in the united states cannot be fully explained by growth in population size and the obesity epidemic. *The Journal of Bone and Joint Surgery. American volume.*, 94(3):201, 2012.

[76] Ian J Wallace, Steven Worthington, David T Felson, Robert D Jurmain, Kimberly T Wren, Heli Maijanen, Robert J Woods, and Daniel E Lieberman. Knee osteoarthritis has doubled in prevalence since the mid-20th century. *Proceedings of the National Academy of Sciences*, 114(35):9332–9336, 2017.

[77] PTH Lee, DL Lakstein, B Lozano, O Safir, J Backstein, and AE Gross. Mid-to long-term results of revision total hip replacement in patients aged 50 years or younger. *The bone & joint journal*, 96(8):1047–1051, 2014.

[78] A. J. Price, D. Longino, J. Rees, R. Rout, H. Pandit, K. Javaid, N. Arden, C. Cooper, A. J. Carr, C. A.F. Dodd, D. W. Murray, and D. J. Beard. Are pain and function better measures of outcome than revision rates after TKR in the younger patient? *Knee*, 17(3):196–199, 2010.

[79] B Willem Schreurs and Gerjon Hannink. Total joint arthroplasty in younger patients: heading for trouble? *The lancet*, 389(10077):1374–1375, 2017.

[80] Cecilia Pascual-Garrido, Erika Daley, Nikhil N Verma, and Brian J Cole. A comparison of the outcomes for cartilage defects of the knee treated with biologic resurfacing versus focal metallic implants. *Arthroscopy: The Journal of Arthroscopic & Related Surgery*, 33(2):364–373, 2017.

[81] Gerben M van Buul, Jaroslaw Stanclik, Johan van Der Stok, Joseph M Queally, and Turlough O'Donnell. Focal articular surface replacement of knee lesions after failed cartilage repair using focal metallic implants: a series of 132 cases with 4-year follow-up. *The Knee*, 29:134–141, 2021.

[82] Jens Ole Laursen and Martin Lind. Treatment of full-thickness femoral cartilage lesions using condyle resurfacing prosthesis. *Knee Surgery, Sports Traumatology, Arthroscopy*, 25:746–751, 2017.

[83] Sophie Moerman, Nina MC Mathijssen, Wim E Tuinebreijer, Anne JH Vochteloo, and Rob GHH Nelissen. Hemiarthroplasty and total hip arthroplasty in 30,830 patients with hip fractures: data from the dutch arthroplasty register on revision and risk factors for revision. *Acta orthopaedica*, 89(5):509–514, 2018.

[84] JV Rasmussen, A Polk, AK Sorensen, Bo Sanderhoff Olsen, and S Brorson. Outcome, revision rate and indication for revision following resurfacing hemiarthroplasty for osteoarthritis of the shoulder: 837 operations reported to the danish shoulder arthroplasty registry. *The bone & joint journal*, 96(4):519–525, 2014.

[85] Yiqiong Zhao, Dong Fu, Kai Chen, Guodong Li, Zhengdong Cai, Yan Shi, and Xiaobing Yin. Outcome of hemiarthroplasty and total hip replacement for active elderly patients with displaced femoral neck fractures: A meta-analysis of 8 randomized clinical trials. *PLoS ONE*, 9(5):1–7, 2014.

[86] M. P.J. Van Den Bekerom, E. F. Hilverdink, I. N. Sierevelt, E. M.B.P. Reuling, J. M. Schnater, H. Bonke, J. C. Goslings, C. N. Van Dijk, and E. L.F.B. Raaymakers. A comparison of hemiarthroplasty with total hip replacement for displaced intracapsular fracture of the femoral neck: A randomised controlled multicentre trial in patients aged 70 years and over. *Journal of Bone and Joint Surgery - Series B*, 92(10):1422–1428, 2010.

[87] Carolyn Berkmortel, G Daniel G Langohr, Graham King, and James Johnson. Hemiarthroplasty implants should have very low stiffness to optimize cartilage contact stress. *Journal of Orthopaedic Research®*, 38(8):1719–1726, 2020.

[88] G. Daniel G. Langohr, Ryan Willing, John B. Medley, Graham J.W. King, and James A. Johnson. Contact analysis of the native radiocapitellar joint compared with axisymmetric and nonaxisymmetric radial head hemiarthroplasty. *Journal of Shoulder and Elbow Surgery*, 24(5):787–795, 2015.

[89] B Y Michael H Huo and Nathan F Gilbert. Total Hip Arthroplasty and Hemiarthroplasty in mobile, independant patients with a displaced intracapsular fracture of the femoral neck. *Journal of Bone and Joint Surgery - Series B*, pages 2133–2147, 2005.

[90] Abidemi Adenikinju, James D. Slover, and Kenneth A. Egol. Rapid Acetabular Chondrolysis following Hemiarthroplasty of the Hip: A Poor Prognostic Sign. *Case Reports in Orthopedics*, 2019:1–8, 2019.

[91] Yee Suk Kim, Young Ho Kim, Kyu Tae Hwang, and Il Yong Choi. The cartilage degeneration and joint motion of bipolar hemiarthroplasty. *International Orthopaedics*, 36(10):2015–2020, 2012.

[92] Nicholas A Kenney and Kevin W Farmer. Minimally invasive versus conventional joint arthroplasty. *PM&R*, 4(5):S134–S140, 2012.

[93] Johannes Holz, Tim Spalding, Tarek Boutefnouchet, Pieter Emans, Karl Eriksson, Mats Brittberg, Lars Konradsen, Clemens Kösters, Peter Verdonk, Magnus Högström, et al. Patient-specific metal implants for focal chondral and osteochondral lesions in the knee; excellent clinical results at 2 years. *Knee Surgery, Sports Traumatology, Arthroscopy*, 29:2899–2910, 2021.

[94] Paul Jermin, Jill Mulrain, and Nikhil Sharma. The benefits of focal resurfacing implants over articular cartilage grafting in the knee. *Orthopaedics and Trauma*, 2023.

[95] Hany Elbardesy, Matthew Nagle, Lydia Simmons, and James Harty. The partial femoral condyle focal resurfacing (hemicap-unicap) for treatment of full-thickness cartilage defects, systematic review and meta-analysis. *Acta Orthop Belg*, 87(1):93–102, 2021.

[96] GM van Buul, E Thompson, R Lutchumun, G O'Toole, and T O'Donnell. Partial articular

resurfacing secondary to pediatric hip chondroblastoma curettage with a 5-yearfollow-up: A case report. *JBJS Case Connector*, 11(1):e20, 2021.

[97] Panayiotis D Megaloikonomos, Christoph Becher, Johan Van der Stok, and Turlough O'Donnell. Femoral condyle resurfacing using an inlay metal implant: low revision rate of 266 patients in a 5–10 years follow-up. *Archives of Orthopaedic and Trauma Surgery*, pages 1–9, 2023.

[98] Yaghoub Dabiri and LePing Li. Focal cartilage defect compromises fluid-pressure dependent load support in the knee joint. *International journal for numerical methods in biomedical engineering*, 31(6):e02713, 2015.

[99] Frank Vizesi. The creation and repair of osteochondral defects and the effect on the opposing surfaces. 2008.

[100] Leif Ryd, Katarina Flodström, and Michael T Manley. Patient-specific implants for focal cartilage lesions in the knee: implant survivorship analysis up to seven years post-implantation. *Surg Technol Int*, 38:379–386, 2020.

[101] Carl A Kirker-head, David C Van Sickle, Steve W Ek, and John C Mccool. Safety of , and Biological and Functional Response to , a Novel Metallic Implant for the Management of Focal Full-Thickness Cartilage Defects : Preliminary Assessment in an Animal Model Out to 1 Year. (May):1095–1108, 2006.

[102] B Stojanović, C Bauer, C Stotter, T Klestil, S Nehrer, F Franek, and M Rodríguez Ripoll. Tribocorrosion of a cocrmo alloy sliding against articular cartilage and the impact of metal ion release on chondrocytes. *Acta biomaterialia*, 94:597–609, 2019.

[103] Gary Eichenbaum, Jared T Wilsey, Gion Fessel, Qing-Qing Qiu, Laura Perkins, Philippe Hasgall, Andrew Monnot, Sharlee L More, Natalie Egnot, Jorge Sague, et al. An integrated benefit-risk assessment of cobalt-containing alloys used in medical devices: Implications for regulatory requirements in the european union. *Regulatory Toxicology and Pharmacology*, 125:105004, 2021.

[104] Dinesh Nathwani, Michael McNicholas, Alister Hart, Jonathan Miles, and Vladimir Bobic. Partial resurfacing of the knee with the biopoly implant: interim report at 2 years. *JBJS Open Access*, 2(2):e0011, 2017.

[105] Dinesh Nathwani, Michael McNicholas, Alister Hart, Jonathan Miles, and Vladimir Bobić. The biopoly partial resurfacing knee implant provides beneficial clinical outcomes: a concise follow-up, at 5 years, of a previous report. *JBJS Open Access*, 8(4):e23, 2023.

[106] Şahin Çepni, Enejd Veizi, Mesut Tahta, Enes Uluyardımcı, Mohammed JT Abughalwa, and Çetin Işık. Focal metallic inlay resurfacing prosthesis in articular cartilage defects: short-term results of 118 patients and 2 different implants. *Archives of Orthopaedic and Trauma Surgery*, 140:209–218, 2020.

[107] J Holz, A Ilg, R Kaiser, and S Schneider. Mini-review on mini-metal implants for focal cartilage lesions. *Clin Surg. 2021; 6*, 3056.

[108] Vikrant Rai, Matthew F Dilisio, Nicholas E Dietz, and Devendra K Agrawal. Recent strategies in cartilage repair: a systemic review of the scaffold development and tissue engineering. *Journal of biomedical materials research Part A*, 105(8):2343–2354, 2017.

[109] Shane J Nho, Michael J Pensak, Daniel A Seigerman, and Brian J Cole. Rehabilitation after autologous chondrocyte implantation in athletes. *Clinics in sports medicine*, 29(2):267–282, 2010.

[110] Eleftherios A Makris, Andreas H Gomoll, Konstantinos N Malizos, Jerry C Hu, and Kyriacos A Athanasiou. Repair and tissue engineering techniques for articular cartilage. *Nature Reviews Rheumatology*, 11(1):21–34, 2015.

[111] WA Hodge, RS Fijan, KL Carlson, RG Burgess, WH Harris, and RW3458248 Mann. Contact pressures in the human hip joint measured in vivo. *Proceedings of the National Academy of Sciences*, 83(9):2879–2883, 1986.

[112] Kjirste C Morrell, W Andrew Hodge, David E Krebs, and Robert W Mann. Corroboration of in vivo cartilage pressures with implications for synovial joint tribology and osteoarthritis causation. *Proceedings of the National Academy of Sciences*, 102(41):14819–14824, 2005.

[113] D Adams and SA Swanson. Direct measurement of local pressures in the cadaveric human hip joint during simulated level walking. *Annals of the rheumatic diseases*, 44(10):658–666, 1985.

[114] AM Ahmed and DL Burke. In-vitro of measurement of static pressure distribution in synovial joints—part i: Tibial surface of the knee. 1983.

[115] Abdul M Ahmed. In-vitro measurement of static contact pressure distribution in synovial joints. In *Mechanics Computing in 1990's and Beyond*, pages 579–583. ASCE.

[116] Paul Brinckmann, Wolfgang Frobin, and E Hierholzer. Stress on the articular surface of the hip joint in healthy adults and persons with idiopathic osteoarthrosis of the hip joint. *Journal of Biomechanics*, 14(3):149–156, 1981.

[117] M Ipavec, RA Brand, DR Pedersen, B Mavčič, V Kralj-Iglič, and A Iglič. Mathematical modelling of stress in the hip during gait. *Journal of Biomechanics*, 32(11):1229–1235, 1999.

[118] CP Neu, AH Reddi, K Komvopoulos, TM Schmid, and PE Di Cesare. Increased friction coefficient and superficial zone protein expression in patients with advanced osteoarthritis. *Arthritis & Rheumatism*, 62(9):2680–2687, 2010.

[119] Eric S. Jones. Joint lubrication. *The Lancet*, page 1043, 1936.

[120] IC Clarke, R Contini, and RM Kenedi. Friction and wear studies of articular cartilage: a scanning electron microscope study. 1975.

[121] L McCann, I Udofia, S Graindorge, E Ingham, Z Jin, and J Fisher. Tribological testing of articular cartilage of the medial compartment of the knee using a friction simulator. *Tribology International*, 41(11):1126–1133, 2008.

[122] LP Müller, J Degreif, L Rudig, D Mehler, H Hely, and PM Rommens. Friction of ceramic and metal hip hemi-endoprostheses against cadaveric acetabula. *Archives of orthopaedic and trauma surgery*, 124:681–687, 2004.

[123] Brian K Jones, Krista M Durney, Clark T Hung, and Gerard A Ateshian. The friction coefficient of shoulder joints remains remarkably low over 24 h of loading. *Journal of biomechanics*, 48(14):3945–3949, 2015.

[124] H Forster and J Fisher. The influence of loading time and lubricant on the friction of articular cartilage. *Proceedings of the Institution of Mechanical Engineers, Part H: Journal of Engineering in Medicine*, 210(2):109–119, 1996.

[125] Zhongmin JIN, Sophie WILLIAMS, Joanne TIPPER, Eileen INGHAM, and John FISHER. Tribology of Hip Joints from Natural Hip Joints, Cartilage Substitution, Artificial Replacements to Cartilage Tissue Engineering. *Journal of Biomechanical Science and Engineering*, 1(1):69–81, 2006.

[126] Duncan Dowson. Bio-tribology. *Faraday Discussions*, 156:9–30, 2012.

[127] Alessandro Ruggiero. Milestones in Natural Lubrication of Synovial Joints. *Frontiers in Mechanical Engineering*, 6(July):1–6, 2020.

[128] M A Macconaill. The Function of Intra-Articular Fibrocartilages, with Special Reference to the Knee and Inferior Radio-Ulnar Joints. *Journal of anatomy*, 66(Pt 2):210–27, 1932.

[129] D. Dowson. Modes of lubrication in human hip joints. *Proc Instn Mech Engrs*, 181(37):45 – 53, 1967.

[130] C. W. McCutchen. The frictional properties of animal joints. *Wear*, 5(1):1–17, 1962.

[131] McCutchen. Mechanism of animal joints: Sponge-hydrostatic and Weeping Bearings. 184, 1959.

[132] David A Swann, STUART Sotman, MARVIN DixoN, and CAROLYN Brooks. The isolation and partial characterization of the major glycoprotein (lgp-i) from the articular lubricating fraction from bovine synovial fluid. *Biochemical Journal*, 161(3):473–485, 1977.

[133] W Michael Lai and Van C Mow. Ultrafiltration of synovial fluid by cartilage. *Journal of the Engineering Mechanics Division*, 104(1):79–96, 1978.

[134] GR Higginson and T Unsworth. The lubrication of natural joints, 1981.

[135] D. Dowson, A. Unsworth, and V. Wright. Analysis of 'Boosted Lubrication' in Human Joints. *Journal of Mechanical Engineering Science*, 12(5):364–369, 1970.

[136] Van C. Mow and W. Michael Lai. Recent Developments in Synovial Joint Biomechanics. *SIAM Review*, 22(3):275–317, 1980.

[137] Gerard A. Ateshian. The role of interstitial fluid pressurization in articular cartilage lubrication. *Journal of Biomechanics*, 42(9):1163–1176, 2009.

[138] GA Ateshian, Huiqun Wang, and WM Lai. The role of interstitial fluid pressurization and surface porosities on the boundary friction of articular cartilage. 1998.

[139] Gerard A Ateshian. The role of interstitial fluid pressurization in articular cartilage lubrication. *Journal of biomechanics*, 42(9):1163–1176, 2009.

[140] Axel C Moore. *Independent and competing roles of fluid exudation and rehydration in cartilage mechanics and tribology*. University of Delaware, 2017.

[141] Teruo Murakami, Yoshinori Sawae, and Maki Ihara. Protective mechanism of articular cartilage to severe loading: roles of lubricants, cartilage surface layer, extracellular matrix and chondrocyte. *JSME International Journal Series C Mechanical Systems, Machine Elements and Manufacturing*, 46(2):594–603, 2003.

[142] CW McCutchen. Lubrication of and by articular cartilage. In *Cartilage*, pages 87–107. Elsevier, 1983.

[143] ZM Jin and D Dowson. Elastohydrodynamic lubrication in biological systems. *Proceedings of the Institution of Mechanical Engineers, Part J: Journal of Engineering Tribology*, 219(5):367–380, 2005.

[144] J O'kelly, A Unsworth, D Dowson, DA Hall, and V Wright. A study of the role of synovial fluid and its constituents in the friction and lubrication of human hip joints. *Engineering in Medicine*, 7(2):73–83, 1978.

[145] NY Afoke, PD Byers, and WCrt Hutton. Contact pressures in the human hip joint. *The Journal of Bone & Joint Surgery British Volume*, 69(4):536–541, 1987.

[146] JinJing Liao, David W Smith, Saeed Miramini, Bruce S Gardiner, and Lihai Zhang. Investigation of role of cartilage surface polymer brush border in lubrication of biological joints. *Friction*, pages 1–18, 2021.

[147] Jacob Klein. Molecular mechanisms of synovial joint lubrication. *Proceedings of the Institution of Mechanical Engineers, Part J: Journal of Engineering Tribology*, 220(8):691–710, 2006.

[148] Alice J Sophia Fox, Asheesh Bedi, and Scott A Rodeo. The basic science of articular cartilage: structure, composition, and function. *Sports health*, 1(6):461–468, 2009.

[149] Axel C Moore, Jordyn Lee Schrader, Jaclyn J Ulvila, and David L Burris. A review of methods to study hydration effects on cartilage friction. *Tribology-Materials, Surfaces & Interfaces*, 11(4):202–214, 2017.

[150] Matej Daniel. Boundary cartilage lubrication: Review of current concepts. *WMW*, 164(5-6):88–94, 2014.

[151] Nicholas D Spencer. *Aqueous lubrication: natural and biomimetic approaches*, volume 3. World Scientific, 2014.

[152] S Graindorge, W Ferrandez, E Ingham, Z Jin, P Twigg, and J Fisher. The role of the surface amorphous layer of articular cartilage in joint lubrication. *Proceedings of the Institution of Mechanical Engineers, Part H: Journal of Engineering in Medicine*, 220(5):597–607, 2006.

[153] JS Jurvelin, DJ Müller, M Wong, D Studer, A Engel, and EB Hunziker. Surface and subsurface morphology of bovine humeral articular cartilage as assessed by atomic force and transmission electron microscopy. *Journal of structural biology*, 117(1):45–54, 1996.

[154] T Murakami, Y Sawae, M Horimoto, and M Noda. Role of surface layers of natural and artificial cartilage in thin film lubrication. In *Tribology Series*, volume 36, pages 737–747. Elsevier, 1999.

[155] R Fujioka, T Aoyama, and T Takakuwa. The layered structure of the articular surface. *Osteoarthritis and Cartilage*, 21(8):1092–1098, 2013.

[156] P Kumar, M Oka, J Toguchida, M Kobayashi, E Uchida, T Nakamura, and K Tanaka. Role of uppermost superficial surface layer of articular cartilage in the lubrication mechanism of joints. *The Journal of Anatomy*, 199(3):241–250, 2001.

[157] R Crockett, S Roos, P Rossbach, C Dora, W Born, and H Troxler. Imaging of the surface of human and bovine articular cartilage with esem and afm. *Tribology letters*, 19:311–317, 2005.

[158] David A Swann, Henry S Slayter, and Fred H Silver. The molecular structure of lubricating glycoprotein-i, the boundary lubricant for articular cartilage. *Journal of biological chemistry*, 256(11):5921–5925, 1981.

[159] Liaqat Ali, Sarah A Flowers, Chunsheng Jin, Eric Paul Bennet, Anna-Karin H Ekwall,

and Niclas G Karlsson. The o-glycomap of lubricin, a novel mucin responsible for joint lubrication, identified by site-specific glycopeptide analysis. *Molecular & Cellular Proteomics*, 13(12):3396–3409, 2014.

[160] Laurel Ng, Alan J Grodzinsky, Parth Patwari, John Sandy, Anna Plaas, and Christine Ortiz. Individual cartilage aggrecan macromolecules and their constituent glycosaminoglycans visualized via atomic force microscopy. *Journal of structural biology*, 143(3):242–257, 2003.

[161] LAWRENCE Rosenberg, WILHELMINE Hellmann, and AK Kleinschmidt. Electron microscopic studies of proteoglycan aggregates from bovine articular cartilage. *Journal of Biological Chemistry*, 250(5):1877–1883, 1975.

[162] Timothy E Hardingham and Amanda J Fosang. Proteoglycans: many forms and many functions. *The FASEB journal*, 6(3):861–870, 1992.

[163] Timothy E Hardingham. Cartilage; aggrecan-link protein-hyaluronan aggregates. *Glycoforum*, 2:A5, 1998.

[164] JA Buckwalter and LC Rosenberg. Electron microscopic studies of cartilage proteoglycans. direct evidence for the variable length of the chondroitin sulfate-rich region of proteoglycan subunit core protein. *The Journal of biological chemistry*, 257(16):9830–9839, 1982.

[165] Andra Dedinaite. Biomimetic lubrication. *Soft Matter*, 2012.

[166] Weifeng Lin, Zhang Liu, Nir Kampf, and Jacob Klein. The role of hyaluronic acid in cartilage boundary lubrication. *Cells*, 9(7):1606, 2020.

[167] AV Sarma, GL Powell, and M LaBerge. Phospholipid composition of articular cartilage boundary lubricant. *Journal of orthopaedic research*, 19(4):671–676, 2001.

[168] Carl R Flannery, Clare E Hughes, Barbara L Schumacher, Debbie Tudor, Margaret B Aydelotte, Klaus E Kuettner, and Bruce Caterson. Articular cartilage superficial zone protein (szp) is homologous to megakaryocyte stimulating factor precursor and is a multifunctional proteoglycan with potential growth-promoting, cytoprotective, and lubricating properties in cartilage metabolism. *Biochemical and biophysical research communications*, 254(3):535–541, 1999.

[169] Jacob Klein. Repair or replacement–a joint perspective. *Science*, 323(5910):47–48, 2009.

[170] Sabrina Jahn and Jacob Klein. Hydration lubrication: the macromolecular domain. *Macromolecules*, 48(15):5059–5075, 2015.

[171] Teruo Murakami, Seido Yarimitsu, Nobuo Sakai, Kazuhiro Nakashima, Tetsuo Yamaguchi, and Yoshinori Sawae. Importance of adaptive multimode lubrication mechanism in natural synovial joints. *Tribology International*, 113(November 2016):306–315, 2017.

[172] JinJing Liao, David W Smith, Saeed Miramini, Bruce S Gardiner, and Lihai Zhang. Investigation of role of cartilage surface polymer brush border in lubrication of biological joints. *Friction*, pages 1–18, 2022.

[173] Jasmine Seror, Yulia Merkher, Nir Kampf, Lisa Collinson, Anthony J Day, Alice Maroudas, and Jacob Klein. Normal and shear interactions between hyaluronan–aggrecan complexes mimicking possible boundary lubricants in articular cartilage in synovial joints. *Biomacromolecules*, 13(11):3823–3832, 2012.

[174] Marcel Benz, Nianhuan Chen, and Jacob Israelachvili. Lubrication and wear properties of grafted polyelectrolytes, hyaluronan and hylan, measured in the surface forces apparatus. *Journal of Biomedical Materials Research Part A: An Official Journal of The Society for Biomaterials, The Japanese Society for Biomaterials, and The Australian Society for Biomaterials and the Korean Society for Biomaterials*, 71(1):6–15, 2004.

[175] Jasmine Seror, Linyi Zhu, Ronit Goldberg, Anthony J Day, and Jacob Klein. Supramolecular synergy in the boundary lubrication of synovial joints. *Nature communications*, 6(1):6497, 2015.

[176] TA Schmidt and RL Sah. Effect of synovial fluid on boundary lubrication of articular cartilage. *OsteoArthritis and cartilage*, 15(1):35–47, 2007.

[177] H Forster and J Fisher. The influence of continuous sliding and subsequent surface wear on the friction of articular cartilage. *Proceedings of the Institution of Mechanical Engineers, Part H: Journal of Engineering in Medicine*, 213(4):329–345, 1999.

[178] R Krishnan, M Caligaris, Robert L Mauck, Clark T Hung, KD Costa, and Gerard A Ateshian. Removal of the superficial zone of bovine articular cartilage does not increase its frictional coefficient. *Osteoarthritis and cartilage*, 12(12):947–955, 2004.

[179] Bruno Zappone, Marina Ruths, George W Greene, Gregory D Jay, and Jacob N Is-

raelachvili. Adsorption, lubrication, and wear of lubricin on model surfaces: polymer brush-like behavior of a glycoprotein. *Biophysical journal*, 92(5):1693–1708, 2007.

[180] Saurabh Das, Xavier Banquy, Bruno Zappone, George W Greene, Gregory D Jay, and Jacob N Israelachvili. Synergistic interactions between grafted hyaluronic acid and lubricin provide enhanced wear protection and lubrication. *Biomacromolecules*, 14(5):1669–1677, 2013.

[181] Raya Sorkin, Nir Kampf, Linyi Zhu, and Jacob Klein. Hydration lubrication and shear-induced self-healing of lipid bilayer boundary lubricants in phosphatidylcholine dispersions. *Soft Matter*, 12(10):2773–2784, 2016.

[182] JC Del Valle, C Aragó, MI Marqués, and JA Gonzalo. Paraelectric response of water in the range 0–100 c. *Ferroelectrics*, 466(1):166–180, 2014.

[183] Liran Ma, Anastasia Gaisinskaya-kipnis, Nir Kampf, and Jacob Klein. Origins of hydration lubrication. *Nature Communications*, pages 8–13, 2015.

[184] Jacob Klein. Hydration lubrication. *Friction*, 1(1):1–23, 2013.

[185] Ronit Goldberg, Avi Schroeder, Gilad Silbert, Keren Turjeman, Yechezkel Barenholz, and Jacob Klein. Boundary Lubricants with Exceptionally Low Friction Coeffi cients Based on 2D Close-Packed Phosphatidylcholine Liposomes. pages 3517–3521, 2011.

[186] Matteo Caligaris and Gerard A Ateshian. Effects of sustained interstitial fluid pressurization under migrating contact area, and boundary lubrication by synovial fluid, on cartilage friction. *Osteoarthritis and Cartilage*, 16(10):1220–1227, 2008.

[187] Ramaswamy Krishnan, Monika Kopacz, and Gerard A Ateshian. Experimental verification of the role of interstitial fluid pressurization in cartilage lubrication. 22:565–570, 2004.

[188] Charles W McCutchen. The frictional properties of animal joints. *Wear*, 5(1):1–17, 1962.

[189] Van C Mow, SC Kuei, W Michael Lai, and Cecil G Armstrong. Biphasic creep and stress relaxation of articular cartilage in compression: theory and experiments. 1980.

[190] Lorenza Mattei, Eleonora Campioni, Mario Alberto Accardi, and Daniele Dini. Finite element analysis of the meniscectomised tibio-femoral joint: implementation of advanced

articular cartilage models. *Computer methods in biomechanics and biomedical engineering*, 17(14):1553–1571, 2014.

[191] Michael A Soltz and Gerard A Ateshian. Experimental verification and theoretical prediction of cartilage interstitial fluid pressurization at an impermeable contact interface in confined compression. *J. Biomech.*, 31(10):927–934, 1998.

[192] Fang Liu, Michal Kozanek, Ali Hosseini, Samuel K Van de Velde, Thomas J Gill, Harry E Rubash, and Guoan Li. In vivo tibiofemoral cartilage deformation during the stance phase of gait. *J. Biomech.*, 43(4):658–665, 2010.

[193] Hattie C Cutcliffe, Keithara M Davis, Charles E Spritzer, and Louis DeFrate. The characteristic recovery time as a novel, noninvasive metric for assessing in vivo cartilage mechanical function. *Ann. Biomed. Eng.*, 48:2901–2910, 2020.

[194] Felix Eckstein, Marcus Tieschky, Sonja Faber, Karl-Hans Englmeier, and Maximilian Reiser. Functional analysis of articular cartilage deformation, recovery, and fluid flow following dynamic exercise in vivo. *J. Anat. Embryol.*, 200:419–424, 1999.

[195] C Herberhold, S Faber, T Stammberger, M Steinlechner, R Putz, KH Englmeier, M Reiser, and F Eckstein. In situ measurement of articular cartilage deformation in intact femoropatellar joints under static loading. *Journal of biomechanics*, 32(12):1287–1295, 1999.

[196] BE Ingelmark and RAGNAR Ekholm. A study on variations in the thickness of articular cartilage in association with rest and periodical load; an experimental investigation on rabbits. *Upsala lakareforenings forhandlingar*, 53(1-2):61–74, 1948.

[197] Jamie M Benson. *Clarifying cartilage mechanics during contact, separation, and migration (PhD Thesis)*. Univ. Delaware, 2023.

[198] Dennis R Carter, Gary S Beaupré, Marcy Wong, R Lane Smith, Tom P Andriacchi, and David J Schurman. The mechanobiology of articular cartilage development and degeneration. *Clinical Orthopaedics and Related Research®*, 427:S69–S77, 2004.

[199] Margot S Farnham, Kyla F Ortved, David L Burris, and Christopher Price. Articular cartilage friction, strain, and viability under physiological to pathological benchtop sliding conditions. *CMBE*, 14(4):349–363, 2021.

[200] Alan J Grodzinsky, Marc E Levenston, Moonsoo Jin, and Eliot H Frank. Cartilage tissue remodeling in response to mechanical forces. *Annu. Rev. Biomed. Eng.*, 2(1):691–713, 2000.

[201] Brian T Graham, Axel C Moore, David L Burris, and Christopher Price. Sliding enhances fluid and solute transport into buried articular cartilage contacts. *Osteoarthritis and cartilage*, 25(12):2100–2107, 2017.

[202] Steven Voinier, AC Moore, Jamie M Benson, C Price, and David Lawrence Burris. The modes and competing rates of cartilage fluid loss and recovery. *Acta Biomaterialia*, 138:390–397, 2022.

[203] Gerard A Ateshian and Huiqun Wang. A theoretical solution for the frictionless rolling contact of cylindrical biphasic articular cartilage layers. *Journal of biomechanics*, 28(11):1341–1355, 1995.

[204] SS Pawaskar, ZM Jin, and J Fisher. Modelling of fluid support inside articular cartilage during sliding. *Proceedings of the Institution of Mechanical Engineers, Part J: Journal of Engineering Tribology*, 221(3):165–174, 2007.

[205] Mario Alberto Accardi, Daniele Dini, and Philippa M Cann. Experimental and numerical investigation of the behaviour of articular cartilage under shear loading—interstitial fluid pressurisation and lubrication mechanisms. *Tribology International*, 44(5):565–578, 2011.

[206] Axel C Moore and David L Burris. Tribological rehydration of cartilage and its potential role in preserving joint health. *Osteoarthritis and cartilage*, 25(1):99–107, 2017.

[207] Richard A Brand. Joint contact stress: a reasonable surrogate for biological processes? *The Iowa orthopaedic journal*, 25:82, 2005.

[208] David L Burris and Axel C Moore. Cartilage and joint lubrication: new insights into the role of hydrodynamics. *Biotribology*, 12:8–14, 2017.

[209] Margot S Farnham, Riley E Larson, David L Burris, and Christopher Price. Effects of mechanical injury on the tribological rehydration and lubrication of articular cartilage. *Journal of the mechanical behavior of biomedical materials*, 101:103422, 2020.

[210] Meghan E Kupratis, Ahmed E Gure, Kyla F Ortved, David L Burris, and Christopher

Price. Comparative tribology: articulation-induced rehydration of cartilage across species. *Biotribology*, 25:100159, 2021.

[211] Margot S Farnham, Kyla F Ortved, Jeffrey S Horner, Norman J Wagner, David L Burris, and Christopher Price. Lubricant effects on articular cartilage sliding biomechanics under physiological fluid load support. *Tribology Letters*, 69:1–14, 2021.

[212] Robert J Elkington, Richard M Hall, Andrew R Beadling, Hemant Pandit, and Michael G Bryant. Engineering tribological rehydration of cartilage interfaces: Assessment of potential polyelectrolyte mechanisms. *Tribology International*, page 109822, 2024.

[213] Brian T Graham, Axel C Moore, David L Burris, and Christopher Price. Mapping the spatiotemporal evolution of solute transport in articular cartilage explants reveals how cartilage recovers fluid within the contact area during sliding. *Journal of Biomechanics*, 71:271–276, 2018.

[214] JinJing Liao, David W Smith, Saeed Miramini, Namal Thibbotuwawa, Bruce S Gardiner, and Lihai Zhang. The investigation of fluid flow in cartilage contact gap. *Journal of the Mechanical Behavior of Biomedical Materials*, 95:153–164, 2019.

[215] JinJing Liao, David W Smith, Saeed Miramini, Bruce S Gardiner, and Lihai Zhang. A coupled contact model of cartilage lubrication in the mixed-mode regime under static compression. *Tribology International*, 145:106185, 2020.

[216] Yabin Wu and Stephen J Ferguson. The influence of cartilage surface topography on fluid flow in the intra-articular gap. *Computer methods in biomechanics and biomedical engineering*, 20(3):250–259, 2017.

[217] Mo Sadique, Sapna Ratan Shah, Sunil Kumar Sharma, and Sardar MN Islam. Effect of significant parameters on squeeze film characteristics in pathological synovial joints. *Mathematics*, 11(6):1468, 2023.

[218] Ewen Northwood and John Fisher. A multi-directional in vitro investigation into friction, damage and wear of innovative chondroplasty materials against articular cartilage. *Clinical Biomechanics*, 22(7):834–842, 2007.

[219] Feng Li, Yonglin Su, Jianping Wang, Gang Wu, and Chengtao Wang. Influence of dynamic load on friction behavior of human articular cartilage, stainless steel and polyvinyl alcohol

hydrogel as artificial cartilage. *Journal of Materials Science: Materials in Medicine*, 21:147–154, 2010.

[220] L McCann, E Ingham, Z Jin, and J Fisher. An investigation of the effect of conformity of knee hemiarthroplasty designs on contact stress, friction and degeneration of articular cartilage: a tribological study. *Journal of biomechanics*, 42(9):1326–1331, 2009.

[221] D Groves, J Fisher, and S Williams. In-vitro simulation of natural hip and hip hemiarthroplasty joints. In *Orthopaedic Proceedings*, volume 99, pages 148–148. Bone & Joint, 2017.

[222] Piers E Milner, Maria Parkes, Jennifer L Puetzer, Robert Chapman, Molly M Stevens, Philippa Cann, and Jonathan RT Jeffers. A low friction, biphasic and boundary lubricating hydrogel for cartilage replacement. *Acta biomaterialia*, 65:102–111, 2018.

[223] Yu-Song Pan, Dang-Sheng Xiong, and Ru-Yin Ma. A study on the friction properties of poly (vinyl alcohol) hydrogel as articular cartilage against titanium alloy. *Wear*, 262(7-8):1021–1025, 2007.

[224] Mark E Freeman, Michael J Furey, Brian J Love, and Jeanne M Hampton. Friction, wear, and lubrication of hydrogels as synthetic articular cartilage. *Wear*, 241(2):129–135, 2000.

[225] Michelle M Blum and Timothy C Ovaert. Low friction hydrogel for articular cartilage repair: evaluation of mechanical and tribological properties in comparison with natural cartilage tissue. *Materials Science and Engineering: C*, 33(7):4377–4383, 2013.

[226] D Baykal, RJ Underwood, K Mansmann, M Marcolongo, and SM Kurtz. Evaluation of friction properties of hydrogels based on a biphasic cartilage model. *Journal of the mechanical behavior of biomedical materials*, 28:263–273, 2013.

[227] Teruo Murakami, Seido Yarimitsu, Kazuhiro Nakashima, Nobuo Sakai, Tetsuo Yamaguchi, Yoshinori Sawae, and Atsushi Suzuki. Biphasic and boundary lubrication mechanisms in artificial hydrogel cartilage: A review. *Proceedings of the Institution of Mechanical Engineers, Part H: Journal of Engineering in Medicine*, 229(12):864–878, 2015.

[228] Masayuki Kyomoto, Toru Moro, Ken-ichi Saiga, Fumiaki Miyaji, Hiroshi Kawaguchi, Yoshio Takatori, Kozo Nakamura, and Kazuhiko Ishihara. Lubricity and stability of poly (2-methacryloyloxyethyl phosphorylcholine) polymer layer on co–cr–mo surface for hemi-

arthroplasty to prevent degeneration of articular cartilage. *Biomaterials*, 31(4):658–668, 2010.

[229] Feng Li, Anmin Wang, and Chengtao Wang. Analysis of friction between articular cartilage and polyvinyl alcohol hydrogel artificial cartilage. *Journal of Materials Science: Materials in Medicine*, 27:1–8, 2016.

[230] J. Rogers Foy, P. F. Williams, G. L. Powell, K. Ishihara, N. Nakabayashi, and M. Laberge. Effect of phospholipidic boundary lubrication in rigid and compliant hemiarthroplasty models. *Proceedings of the Institution of Mechanical Engineers, Part H: Journal of Engineering in Medicine*, 213(1):5–18, 1999.

[231] Motoyasu Kobayashi, Masami Terada, and Atsushi Takahara. Polyelectrolyte brushes: a novel stable lubrication system in aqueous conditions. *Faraday discussions*, 156(1):403–412, 2012.

[232] Guoqiang Liu, Zhilu Liu, Na Li, Xiaolong Wang, Feng Zhou, and Weimin Liu. Hairy polyelectrolyte brushes-grafted thermosensitive microgels as artificial synovial fluid for simultaneous biomimetic lubrication and arthritis treatment. *ACS applied materials & interfaces*, 6(22):20452–20463, 2014.

[233] Guoqiang Liu, Yang Feng, Xiaohua Gao, Zhuo Chen, Nan Zhao, Feng Zhou, and Weimin Liu. Synovial fluid-inspired biomimetic lubricating microspheres: Zwitterionic polyelectrolyte brushes-grafted microgels. *Friction*, 11(6):938–948, 2023.

[234] Masayuki Kyomoto, Toru Moro, Yoshio Takatori, Hiroshi Kawaguchi, and Kazuhiko Ishihara. Cartilage-mimicking, high-density brush structure improves wear resistance of crosslinked polyethylene: a pilot study. *Clinical Orthopaedics and Related Research®*, 469:2327–2336, 2011.

[235] Suzanne Giasson and Nicholas D Spencer. Aqueous lubrication with polymer brushes. *Aqueous Lubrication*, pages 183–218, 2014.

[236] Piotr Mocny and Harm Anton Klok. Tribology of surface-grafted polymer brushes. *Molecular Systems Design and Engineering*, 1(2):141–154, 2016.

[237] Meng Chen, Wuge H Briscoe, Steven P Armes, and Jacob Klein. Lubrication at physiological pressures by polyzwitterionic brushes. *science*, 323(5922):1698–1701, 2009.

[238] Xavier Banquy, Joanna Burdynska, Dong Woog Lee, Krzysztof Matyjaszewski, and Jacob Israelachvili. Bioinspired bottle-brush polymer exhibits low friction and amontons-like behavior. *Journal of the American Chemical Society*, 136(17):6199–6202, 2014.

[239] Toru Moro, Yoshio Takatori, Masayuki Kyomoto, Kazuhiko Ishihara, Masami Hashimoto, Hideya Ito, Takeyuki Tanaka, Hirofumi Oshima, Shigeyuki Tanaka, and Hiroshi Kawaguchi. Long-term hip simulator testing of the artificial hip joint bearing surface grafted with biocompatible phospholipid polymer. *Journal of Orthopaedic Research*, 32(3):369–376, 2014.

[240] Weifeng Lin and Jacob Klein. Hydration lubrication in biomedical applications: From cartilage to hydrogels. *Accounts of materials research*, 3(2):213–223, 2022.

[241] Jitendra Kumar Katiyar, P Ramkumar, TVVLN Rao, and J Paulo Davim. Tribology in materials and applications, 2020.

[242] Mohamed A Abdelbar, James P Ewen, Daniele Dini, and Stefano Angioletti-Uberti. Polymer brushes for friction control: Contributions of molecular simulations. *Biointerphases*, 18(1), 2023.

[243] Neil Ayres. Polymer brushes: Applications in biomaterials and nanotechnology. *Polymer Chemistry*, 1(6):769–777, 2010.

[244] Hiroki Nakano, Yuri Noguchi, Sachiro Kakinoki, Mai Yamakawa, Issey Osaka, and Yasuhiko Iwasaki. Highly Durable Lubricity of Photo-Cross-Linked Zwitterionic Polymer Brushes Supported by Poly(ether ether ketone) Substrate. 2020.

[245] Dangsheng Xiong, Yaling Deng, Nan Wang, and Yuanyuan Yang. Influence of surface pmpc brushes on tribological and biocompatibility properties of uhmwpe. *Applied surface science*, 298:56–61, 2014.

[246] Jeffrey M Toth. Biocompatibility of peek polymers. In *PEEK biomaterials handbook*, pages 107–119. Elsevier, 2019.

[247] Jianping Deng, Lifu Wang, Lianying Liu, and Wantai Yang. Developments and new applications of uv-induced surface graft polymerizations. *Progress in polymer science*, 34(2):156–193, 2009.

[248] Masayuki Kyomoto, Toru Moro, Shihori Yamane, Masami Hashimoto, Yoshio Takatori,

and Kazuhiko Ishihara. Poly (ether-ether-ketone) orthopedic bearing surface modified by self-initiated surface grafting of poly (2-methacryloyloxyethyl phosphorylcholine). *Biomaterials*, 34(32):7829–7839, 2013.

[249] Ahmed Yousaf, Aleeza Farrukh, Zehra Oluz, Eylül Tuncel, Hatice Duran, Sema Yiyit Doğan, Turgay Tekinay, Habib Ur Rehman, and Basit Yameen. UV-light assisted single step route to functional PEEK surfaces. *Reactive and Functional Polymers*, 83:70–75, 2014.

[250] Siddhartha Das, Meneka Banik, Guang Chen, Shayandev Sinha, and Rabibrata Mukherjee. Polyelectrolyte brushes: theory, modelling, synthesis and applications. *Soft Matter*, 11(44):8550–8583, 2015.

[251] RM Pashley. Hydration forces between mica surfaces in aqueous electrolyte solutions. *Journal of colloid and interface science*, 80(1):153–162, 1981.

[252] J Matthew D Lane, Michael Chandross, Mark J Stevens, and Gary S Grest. Water in nanoconfinement between hydrophilic self-assembled monolayers. *Langmuir*, 24(10):5209–5212, 2008.

[253] Rosa M Espinosa-Marzal, Robert M Bielecki, and Nicholas D Spencer. Understanding the role of viscous solvent confinement in the tribological behavior of polymer brushes: A bioinspired approach. *Soft Matter*, 9(44):10572–10585, 2013.

[254] Nicholas D Spencer. Aqueous lubrication with poly (ethylene glycol) brushes. *Tribology Online*, 9(4):143–153, 2014.

[255] Jacob Klein, Eugenia Kumacheva, Diana Mahalu, Dvora Perahia, and Lewis J Fetters. Reduction of frictional forces between solid surfaces bearing polymer brushes. *Nature*, 370(6491):634–636, 1994.

[256] Seunghwan Lee and Nicholas D Spencer. Achieving ultralow friction by aqueous, brush-assisted lubrication. In *Superlubricity*, pages 365–396. Elsevier, 2007.

[257] Nir Kampf, Jean-François Gohy, Robert Jérôme, and Jacob Klein. Normal and shear forces between a polyelectrolyte brush and a solid surface. *Journal of Polymer Science Part B: Polymer Physics*, 43(2):193–204, 2005.

[258] Masayuki Kyomoto, Toru Moro, Fumiaki Miyaji, Masami Hashimoto, Hiroshi

Kawaguchi, Yoshio Takatori, Kozo Nakamura, and Kazuhiko Ishihara. Effect of 2-methacryloyloxyethyl phosphorylcholine concentration on photo-induced graft polymerization of polyethylene in reducing the wear of orthopaedic bearing surface. *Journal of Biomedical Materials Research Part A: An Official Journal of The Society for Biomaterials, The Japanese Society for Biomaterials, and The Australian Society for Biomaterials and the Korean Society for Biomaterials*, 86(2):439–447, 2008.

[259] Motoyasu Kobayashi and Atsushi Takahara. Tribological properties of hydrophilic polymer brushes under wet conditions. *Chemical Record*, 10(4):208–216, 2010.

[260] Moyotasu Kobayashi, Yuki Terayama, Tatsuya Ishikawa, Masami Terada, Hiroe Soejima, Daiki Murakami, and Atsushi Takahara. Applications of surface initiated atrp to the preparation of polyelectrolyte brushes for antifouling, adhesion control, friction control. In *Progress in Controlled Radical Polymerization: Materials and Applications*, pages 183–195. ACS Publications, 2012.

[261] Girma Biresaw. *Surfactants in Tribology, Volume 3*. CRC Press, 2013.

[262] Alison C Dunn, W Gregory Sawyer, and Thomas E Angelini. Gemini interfaces in aqueous lubrication with hydrogels. *Tribology Letters*, 54:59–66, 2014.

[263] LI Jinpeng, YANG Shuyan, WU Yang, LI Xinming, GUO Feng, and ZHOU Feng. Correlation between water film thickness and tribological behavior of polymer brush in aqueous lubrication. *Tribology*, 41(6):858–869, 2021.

[264] Motoyasu Kobayashi, Hiroyoshi Tanaka, Myo Minn, Joichi Sugimura, and Atsushi Takahara. Interferometry study of aqueous lubrication on the surface of polyelectrolyte brush. *ACS Applied Materials & Interfaces*, 6(22):20365–20371, 2014.

[265] JL Lanigan, S Fatima, TV Charpentier, A Neville, D Dowson, and M Bryant. Lubricious ionic polymer brush functionalised silicone elastomer surfaces. *Biotribology*, 16:1–9, 2018.

[266] Yunlong Yu, Marco Cirelli, Pengfei Li, Zhichao Ding, Yue Yin, Yucheng Yuan, Sissi De Beer, G Julius Vancso, and Shiyong Zhang. Enhanced stability of poly (3-sulfopropyl methacrylate potassium) brushes coated on artificial implants in combatting bacterial infections. *Industrial & Engineering Chemistry Research*, 58(47):21459–21465, 2019.

[267] Masayuki Kyomoto, Toru Moro, Yasuhiko Iwasaki, Fumiaki Miyaji, Hiroshi Kawaguchi,

Yoshio Takatori, Kozo Nakamura, and Kazuhiko Ishihara. Superlubricious surface mimicking articular cartilage by grafting poly (2-methacryloyloxyethyl phosphorylcholine) on orthopaedic metal bearings. *Journal of Biomedical Materials Research Part A: An Official Journal of The Society for Biomaterials, The Japanese Society for Biomaterials, and The Australian Society for Biomaterials and the Korean Society for Biomaterials*, 91(3):730–741, 2009.

[268] Kazuhiko Ishihara. Highly lubricated polymer interfaces for advanced artificial hip joints through biomimetic design. (March):1–13, 2015.

[269] Kazuhiko Ishihara. Revolutionary advances in 2-methacryloyloxyethyl phosphorylcholine polymers as biomaterials. *Journal of Biomedical Materials Research Part A*, 107(5):933–943, 2019.

[270] Tatsuro Goda, Tomohiro Konno, Madoka Takai, and Kazuhiko Ishihara. Photoinduced phospholipid polymer grafting on parylene film: Advanced lubrication and antibiofouling properties. *Colloids and Surfaces B: Biointerfaces*, 54(1):67–73, 2007.

[271] Masayuki Kyomoto, Takeo Shobuike, Toru Moro, Shihori Yamane, Yoshio Takatori, Sakae Tanaka, Hiroshi Miyamoto, and Kazuhiko Ishihara. Prevention of bacterial adhesion and biofilm formation on a vitamin e-blended, cross-linked polyethylene surface with a poly (2-methacryloyloxyethyl phosphorylcholine) layer. *Acta Biomaterialia*, 24:24–34, 2015.

[272] Yasuhiko Iwasaki and Kazuhiko Ishihara. Cell membrane-inspired phospholipid polymers for developing medical devices with excellent biointerfaces. *Science and Technology of Advanced Materials*, 13(6), 2012.

[273] Toru Moro, Hiroshi Kawaguchi, Kazuhiko Ishihara, Masayuki Kyomoto, Tatsuro Karita, Hideya Ito, Kozo Nakamura, and Yoshio Takatori. Wear resistance of artificial hip joints with poly (2-methacryloyloxyethyl phosphorylcholine) grafted polyethylene: comparisons with the effect of polyethylene cross-linking and ceramic femoral heads. *Biomaterials*, 30(16):2995–3001, 2009.

[274] Masayuki Kyomoto, Toru Moro, Tomohiro Konno, Hiroaki Takadama, Noboru Yamawaki, Hiroshi Kawaguchi, Yoshio Takatori, Kozo Nakamura, and Kazuhiko Ishihara. Enhanced wear resistance of modified cross-linked polyethylene by grafting with poly (2-

methacryloyloxyethyl phosphorylcholine). *Journal of Biomedical Materials Research Part A*, 82(1):10–17, 2007.

[275] Masayuki Kyomoto, Toru Moro, Fumiaki Miyaji, Masami Hashimoto, Hiroshi Kawaguchi, Yoshio Takatori, Kozo Nakamura, and Kazuhiko Ishihara. Effects of mobility/immobility of surface modification by 2-methacryloyloxyethyl phosphorylcholine polymer on the durability of polyethylene for artificial joints. *Journal of Biomedical Materials Research Part A: An Official Journal of The Society for Biomaterials, The Japanese Society for Biomaterials, and The Australian Society for Biomaterials and the Korean Society for Biomaterials*, 90(2):362–371, 2009.

[276] Toru Moro, Yoshio Takatori, Kazuhiko Ishihara, Tomohiro Konno, Yorinobu Takigawa, Tomiharu Matsushita, Ung I.L. Chung, Kozo Nakamura, and Hiroshi Kawaguchi. Surface grafting of artificial joints with a biocompatible polymer for preventing periprosthetic osteolysis. *Nature Materials*, 3(11):829–836, 2004.

[277] Masayuki Kyomoto, Toru Moro, Kenichi Saiga, Masami Hashimoto, Hideya Ito, Hiroshi Kawaguchi, Yoshio Takatori, and Kazuhiko Ishihara. Biomimetic hydration lubrication with various polyelectrolyte layers on cross-linked polyethylene orthopedic bearing materials. *Biomaterials*, 33(18):4451–4459, 2012.

[278] Shine Tone, Masahiro Hasegawa, Leonardo Puppulin, Giuseppe Pezzotti, and Akihiro Sudo. Surface modifications and oxidative degradation in MPC-grafted highly cross-linked polyethylene liners retrieved from short-term total hip arthroplasty. *Acta Biomaterialia*, 66:157–165, 2018.

[279] Toru Moro, Yoshio Takatori, Sakae Tanaka, Kazuhiko Ishihara, Hiromi Oda, Yoon Taek Kim, Takashige Umeyama, Eisei Fukatani, Hideya Ito, Masayuki Kyomoto, Hirofumi Oshima, Takeyuki Tanaka, Hiroshi Kawaguchi, and Kozo Nakamura. Clinical safety and wear resistance of the phospholipid polymer-grafted highly cross-linked polyethylene liner. *Journal of Orthopaedic Research*, 35(9):2007–2016, 2017.

[280] Yoshio Takatori, Toru Moro, Kazuhiko Ishihara, Morihide Kamogawa, Hiromi Oda, Takashige Umeyama, Yoon Taek Kim, Hideya Ito, Masayuki Kyomoto, Takeyuki Tanaka, Hiroshi Kawaguchi, and Sakae Tanaka. Clinical and radiographic outcomes of total hip replacement with poly(2-methacryloyloxyethyl phosphorylcholine)-grafted highly cross-

linked polyethylene liners: Three-year results of a prospective consecutive series. *Modern Rheumatology*, 25(2):286–291, 2015.

[281] Takashi Hosoi, Masahiro Hasegawa, Elia Marin, Narifumi Kishida, Akihiro Sudo, Wenliang Zhu, and Giuseppe Pezzotti. MPC-grafted highly cross-linked polyethylene liners retrieved from short-term total hip arthroplasty : Further evidences for the unsuitability of the MPC method. (February):1–11, 2020.

[282] Kathryn A Melzak, Kai Yu, Deng Bo, Jayachandran N Kizhakkedathu, and José L Toca-Herrera. Chain length and grafting density dependent enhancement in the hydrolysis of ester-linked polymer brushes. *Langmuir*, 31(23):6463–6470, 2015.

[283] Nariye Cavusoglu Ataman and Harm-Anton Klok. Degrafting of poly (poly (ethylene glycol) methacrylate) brushes from planar and spherical silicon substrates. *Macromolecules*, 49(23):9035–9047, 2016.

[284] Yunlong Yu, G Julius Vancso, and Sissi de Beer. Substantially enhanced stability against degrafting of zwitterionic pmpc brushes by utilizing pgma-linked initiators. *European polymer journal*, 89:221–229, 2017.

[285] Tomoaki Uchiyama, Yoshihiro Kiritoshi, Junji Watanabe, and Kazuhiko Ishihara. Degradation of phospholipid polymer hydrogel by hydrogen peroxide aiming at insulin release device. *Biomaterials*, 24(28):5183–5190, 2003.

[286] Yong Du, Jingyao Gao, Tingting Chen, Chao Zhang, Jian Ji, and Zhi-Kang Xu. Understanding the oxidative stability of antifouling polymer brushes. *Langmuir*, 33(29):7298–7304, 2017.

[287] Emanuela Galliera, Luca Massaccesi, Giuseppe Banfi, Elena De Vecchi, Vincenza Ragone, and Massimiliano M Corsi Romanelli. Effect of oxidative stress on bone remodeling in periprosthetic osteolysis. *Clinical Reviews in Bone and Mineral Metabolism*, 19(1):14–23, 2021.

[288] Albert van der Vliet and Yvonne MW Janssen-Heininger. Hydrogen peroxide as a damage signal in tissue injury and inflammation: murderer, mediator, or messenger? *Journal of cellular biochemistry*, 115(3):427–435, 2014.

[289] Dietmar Paschek and Ralf Ludwig. Specific ion effects on water structure and dynamics beyond the first hydration shell. *Angew. Chem., Int. Ed*, 50(2):352–353, 2011.

[290] Patcharida Chouwatat, Tomoyasu Hirai, Keiko Higaki, Yuji Higaki, Hung-Jue Sue, and Atsushi Takahara. Aqueous lubrication of poly (etheretherketone) via surface-initiated polymerization of electrolyte monomers. *Polymer*, 116:549–555, 2017.

[291] Narges Hadjesfandiari, Kai Yu, Yan Mei, and Jayachandran N Kizhakkedathu. Polymer brush-based approaches for the development of infection-resistant surfaces. *Journal of Materials Chemistry B*, 2(31):4968–4978, 2014.

[292] Shaifali Dhingra, Shivangi Sharma, and Sampa Saha. Infection resistant surface coatings by polymer brushes: strategies to construct and applications. *ACS Applied Bio Materials*, 5(4):1364–1390, 2022.

[293] Benjamin G Cooper, TB Lawson, Brian D Snyder, and Mark W Grinstaff. Reinforcement of articular cartilage with a tissue-interpenetrating polymer network reduces friction and modulates interstitial fluid load support. *Osteoarthritis and cartilage*, 25(7):1143–1149, 2017.

[294] Yunlei Zhang, Carmine Putignano, Changmin Qi, Weiyi Zhao, Bo Yu, Shuanhong Ma, Daniele Dini, and Feng Zhou. Sliding-induced rehydration in hydrogels for restoring lubrication and anticreeping capability. *The Journal of Physical Chemistry Letters*, 15(45):11328–11334, 2024.

[295] Mingming Rong, Hui Liu, Michele Scaraggi, Yanyan Bai, Luyao Bao, Shuanhong Ma, Zhengfeng Ma, Meirong Cai, Daniele Dini, and Feng Zhou. High lubricity meets load capacity: cartilage mimicking bilayer structure by brushing up stiff hydrogels from sub-surface. *Advanced Functional Materials*, 30(39):2004062, 2020.

Chapter 2

Objectives and Structure

2.1 Objectives

A biocompatible polyelectrolyte functionalised implant surface will be developed and assessed for its ability to provide biomimetic lubrication. This involves achieving low physiological friction levels and the capacity to modulate interstitial fluid pressurisation of articular cartilage to mitigate progression of joint disease of interfacing tissue. Ultimately, the goal is to ascertain whether a biomimetic polyelectrolyte approach can yield effective tribological performance akin to healthy, biologically matched cartilage-cartilage contacts. Furthermore, by developing mechanistic insights into the biotribology of polyelectrolyte-cartilage interfaces, this research aims to deepen the understanding of the sparsely postulated role of native biopolyelectrolytes in supporting cartilage interstitial fluid recovery and pressurisation.

The following objectives have been established to assess the success of this project:

2.1.1 Objective 1. Development and Validation of Biocompatible Polyelectrolyte Functionalised Biomaterial

This objective focuses on creating a hydrophilic and compliant polyelectrolyte-functionalised biomaterial. The aim is to demonstrate that this surface significantly reduces friction compared to unfunctionalised materials. By employing benchtop tribometer studies which measure both strain and friction, the study seeks to establish that polyelectrolyte surfaces can sustain cartilage interstitial fluid pressurisation, elucidating their superiority over current hard biomaterials. This will involve comprehensive surface analysis for repeatable surface synthesis and friction testing

under representative physiological conditions.

2.1.2 Objective 2. Characterisation of Rehydration Capability

This objective aims to assess the ability of the developed polyelectrolyte-functionalised material to rehydrate interfacing articular cartilage. Emphasis will be placed on demonstrating a novel mode of cartilage rehydration, distinct from traditional mechanisms (tribological rehydration or free swelling). This will involve detailed experimental investigations to measure the extent of rehydration by directly assessing cartilage strain recovery, providing insights into the material's effectiveness in maintaining cartilage function.

2.1.3 Objective 3. Empirical Development Of A Mechanistic Tribological Framework For Polyelectrolyte - Cartilage Interfaces

The goal of this objective is to develop a comprehensive tribological framework for understanding the interactions between polyelectrolyte surfaces and cartilage. This will include a deep mechanistic analysis of the material's tribological properties and the underlying principles of polyelectrolyte-enhanced lubrication and rehydration. By elucidating the fundamental mechanisms at play, this research will contribute to the broader field of cartilage biotribology and support the development of advanced biomaterials.

2.1.4 Objective 4. Comparative Analysis of Biomimetic Capabilities

This objective involves contrasting the performance of polyelectrolyte-functionalised materials with known mechanisms of cartilage rehydration and lubrication observed in native cartilage-cartilage interfaces. The aim is to demonstrate the potential of these materials for biomimetic cartilage resurfacing, emphasizing their ability to replicate the natural friction and rehydration characteristics of healthy cartilage. This comparative analysis will highlight the advantages of polyelectrolyte surfaces in restoring joint function and mitigating disease progression.

2.2 Thesis Outline

This thesis is composed of the following four journal papers which constitute the main body of this thesis and broadly correspond to each research objective. To present this work cohesively, the chapter manuscripts have been edited to minimise repeated information, primarily by con-

densing the introductions and cross-referencing common methods sections. These are presented in chronological order to be read as an omnibus of the work conducted:

Objective 1 - Chapter 3: Highly lubricious SPMK-g-PEEK implant surfaces to facilitate rehydration of articular cartilage. Elkington RJ, Hall RM, Beadling AR, Pandit H, Bryant MG. *Journal Of The Mechanical Behavior Of Biomedical Materials* (Nov 2023)

Objective 2 - Chapter 4: Engineering tribological rehydration of cartilage interfaces: Assessment of potential polyelectrolyte mechanisms. Elkington RJ, Hall RM, Beadling AR, Pandit H, Bryant MG. *Tribology International* (May 2024)

Objective 3 - Chapter 5: Brushing up on cartilage lubrication: Polyelectrolyte-enhanced tribological rehydration. Elkington RJ, Hall RM, Beadling AR, Pandit H, Bryant MG. (May 2024) *Langmuir*

Objective 4 - Chapter 6: Performance Parity In Cartilage Repair: SPMK-g-PEEK Versus Cartilage-Cartilage Interfaces. Elkington RJ, Pryce G, Keeling D, Hall RM, Beadling AR, Pandit H, Bryant MG. [Submitted to the *Journal Of The Mechanical Behavior Of Biomedical Materials*]

Finally, **Chapter 7** delineates the key research findings of each manuscript, contextualises the clinical and mechanistic implications of the study, discusses the limitations beyond those described in each manuscript, and outlines future work to advance this research.

2.3 Priori: Materials Choice Of SPMK-g-PEEK

The aim of this project is to develop mechanistic understanding of polyelectrolyte functionalised implant materials. MPC has gained attention as a biomimetic polyelectrolyte (Section 1.4.4.1) as it contains a zwitterionic phosphorycholine group which mimics the phosphatidylcholine group native to the phospholipds within the superficial macromolecular complex on cartilage [1, 2]. Similarly, SPMK contains an anionic sulfonic acid group, which dissociate into sulfonate ions, which have also been identified on proteoglycans within the superficial macromolecular complex [3, 4]. Both SPMK and MPC can be used to produce biomimetic end tethered hydrophilic polyelectrolytes with a high density of bound hydration shells for aqueous lubrication [5]. This work focuses exclusively on 3-sulfopropyl methacrylate potassium salt (SPMK) end-grafted onto a PEEK substrate (SPMK-g-PEEK). The choice of materials was straightforwardly motivated

by cost considerations, with SPMK priced at £161 per 100 grams, significantly more affordable than MPC at £15,100 per 100 grams (prices from Sigma-Aldrich, July 2024). Furthermore, both SPMK and PEEK have been demonstrated to be biocompatible materials [6, 7], and hence could be considered a viable orthopaedic bearing surfaces.

This body of work remains focused on the functional and material characteristics of polyelectrolytes interfaced with cartilage, utilising SPMK-g-PEEK as a paradigmatic case study, no further consideration is given to optimising the chemical species employed nor developing exploitable intellectual property for clinical translation. As discussed in Section 1.2, the limitations of current orthopaedic materials highlight the need for improved cartilage repair interfaces. However, the development of specific exploitable materials should be undertaken by specialised institutions. The reader is directed to the recent Beauhurst and Royal Academy of Engineering *Spotlight on Spinouts Report: UK Academic Spinout Trends (April 2024)* to learn more about the abominably high equity stakes imposed by the University of Leeds relative to other UK academic institutions [8]. High equity stakes which demotivate researchers to pursue technology translation, financially impede venture capital investment and subsequently hinder scaling to market readiness or acquisition [9, 10].

References

[1] AV Sarma, GL Powell, and M LaBerge. Phospholipid composition of articular cartilage boundary lubricant. *Journal of orthopaedic research*, 19(4):671–676, 2001.

[2] Anna A Cederlund and Richard M Aspden. Walking on water: revisiting the role of water in articular cartilage biomechanics in relation to tissue engineering and regenerative medicine. *Journal of the Royal Society Interface*, 19(193):20220364, 2022.

[3] Weifeng Lin and Jacob Klein. Recent progress in cartilage lubrication. *Advanced Materials*, 33(18):2005513, 2021.

[4] Van C Mow and W Michael Lai. Recent developments in synovial joint biomechanics. *Siam Review*, 22(3):275–317, 1980.

[5] Motoyasu Kobayashi and Atsushi Takahara. Tribological properties of hydrophilic polymer brushes under wet conditions. *Chemical Record*, 10(4):208–216, 2010.

[6] Yunlong Yu, Marco Cirelli, Pengfei Li, Zhichao Ding, Yue Yin, Yucheng Yuan, Sissi De Beer, G Julius Vancso, and Shiyong Zhang. Enhanced stability of poly (3-sulfopropyl methacrylate potassium) brushes coated on artificial implants in combatting bacterial infections. *Industrial & Engineering Chemistry Research*, 58(47):21459–21465, 2019.

[7] Jeffrey M Toth. Biocompatibility of peek polymers. In *PEEK biomaterials handbook*, pages 107–119. Elsevier, 2019.

[8] Beauhurst and Royal Academy of Engineering. Spotlight on spinouts 2024, April 2024. Accessed: July 12, 2024.

[9] Weiwei Liu, Zhile Yang, and Kexin Bi. Forecasting the acquisition of university spin-outs: An rbf neural network approach. *Complexity*, 2017(1):6920904, 2017.

[10] Tim Minshall, Bill Wicksteed, Céline Druilhe, Andrea Kells, Michael Lynskey, and Jelena Širaliova. The role of spin-outs within university research commercialisation activities: Case studies from 10 uk universities. In *New Technology-Based Firms in the New Millennium*, volume 6, pages 185–201. Emerald Group Publishing Limited, 2008.

Chapter 3

Highly lubricious SPMK-g-PEEK implant surfaces to facilitate rehydration of articular cartilage

3.1 Abstract

To enable long lasting osteochondral defect repairs which preserve the native function of synovial joint counter-face, it is essential to develop surfaces which are optimised to support healthy cartilage function by providing a hydrated, low friction and compliant sliding interface. PEEK surfaces were modified using a biocompatible 3-sulfopropyl methacrylate potassium salt (SPMK) through UV photo-polymerisation, resulting in a ∼350 nm thick hydrophilic coating rich in hydrophilic anionic sulfonic acid groups. Characterisation was done through Fourier Transformed Infrared Spectroscopy, Focused Ion Beam Scanning Electron Microscopy, and Water Contact Angle measurements.

Using a Bruker UMT TriboLab, bovine cartilage sliding tests were conducted with real-time strain and shear force measurements, comparing untreated PEEK, SPMK functionalised PEEK (SPMK-g-PEEK), and Cobalt Chrome Molybdenum alloy (CoCr). Tribological tests over 2.5 hours at physiological loads (0.75 MPa) revealed that SPMK-g-PEEK maintains low friction ($\mu < 0.024$) and minimises strain, significantly reducing shear forces on the cartilage interface and promoting interstitial fluid pressurisation. Post-test analysis showed no notable damage to the

cartilage interfacing against the SPMK functionalised surfaces.

The application of a constitutive biphasic cartilage model to the experimental strain data reveals that SPMK surfaces increase the interfacial permeability of cartilage in sliding, facilitating fluid and strain recovery. Unlike previous demonstrations of sliding-induced tribological rehydration requiring specific hydrodynamic conditions, the SPMK-g-PEEK introduces a novel mode of tribological rehydration operating at low speeds and in a stationary contact area. SPMK-g-PEEK surfaces provide an enhanced cartilage counter-surface, which provides a highly hydrated and lubricious boundary layer along with supporting biphasic lubrication.

Soft polymer surface functionalisation of orthopaedic implant surfaces are a promising approach for minimally invasive synovial joint repair with an enhanced bioinspired polyelectrolyte interface for sliding against cartilage. These hydrophilic surface coatings offer an enabling technology for the next generation of focal cartilage repair and hemiarthroplasty implant surfaces.

3.2 Introduction

Polyelectrolyte functionalised surfaces offer a biomimetic surface treatment that replicates the large hydrophilic domained biomolecules found on the superficial macromolecular complex of cartilage with industrial scalability [1, 2]. Research into polyelectrolyte functionalised surfaces against cartilage remains limited, with Ishihara demonstrating MPC coated CoCr sliding against cartilage sustains low friction coefficients of < 0.01 and does not noticeably damage cartilage surfaces [3]. However, the majority of work in this area focuses on applications in the THR acetabulum interface, and principally elucidates the favourable lubrication properties of polyelectrolyte surfaces as enabled by the zwitterionic functional groups which provide a highly hydrated sliding interface [4, 5]. Further mechanistic insight into how polyelectrolyte surface treatments can support native cartilage function is required. SPMK-g-PEEK surfaces were been prepared via UV initiated polymerisation [6, 7] and their biotribological performance is characterised against cartilage.

This research hypothesises that hydrated SPMK-g-PEEK surfaces will enable surfaces capable of sustaining and promoting effective hydration lubrication at cartilage interfaces. By promoting hydration and dissipating friction, cartilage trauma can be mitigated by supporting the natural modes of lubrication and interstitial fluid load support. This study will investigate

the tribological performance of a SPMK polyelectrolyte functionalised PEEK (SPMK-g-PEEK) surface will be investigated, comparing it to unfunctionalised PEEK and CoCr surfaces, when interacting with articular cartilage under physiological loads. Coefficient of friction (CoF) and real time strain measurement will be used to analyse the cartilage response sliding against SPMK-g-PEEK. Low CoF will demonstrate effective aqueous lubrication, whilst a reduced cartilage strain compared to an unfunctionalised PEEK control will evidence enhanced fluid load support. Following testing, cartilage samples will be examined to quantify wear along with evidence of cartilage fibrillation or damage to the collagen matrix, indicating a breakdown in fluid load support. Ultimately, this study aims to evaluate the performance of SPMK-g-PEEK and its suitability for supporting physiological synovial tribology, specifically aimed at sustained lubricity and improved fluid load support in cartilage.

3.3 Materials and Methodology

3.3.1 Materials

Victrex PEEK 450G was purchased from RS Components (UK) as a flat 5 mm thick sheet and cut into square samples of 25 × 25 mm. Surgical implant grade cobalt chrome alloy bar conforming to ASTM F1537-20 was purchased from Oracle Special Metals Ltd (Berkshire, UK). All PEEK and CoCr samples underwent a sequential polishing regimen to achieve a target surface roughness (R_a) of 100 nm. The protocol entailed progressive grinding with abrasive papers of P240, P400, P800, and P1200 grits, followed by napless polishing using diamond and silica oxide suspensions with particle sizes ranging from 3 to 0.04 μm. Following polishing, surface topography was validated using a Talysurf PGI NOVUS profilometer.

The monomer 3-sulfopropyl methacrylate potassium salt (SPMK, CAS No. 31098-21-2) in powder form, with a purity of greater than 98%, and phosphate buffered saline tablets (Product No. 524650) were purchased from Sigma Aldrich (UK) and used as received.

3.3.2 Cartilage Plugs

Cartilage plugs, each ⌀7.2 mm in diameter, were extracted from the patellofemoral grooves of bovine stifle joints acquired from John Penny & Sons, Leeds, UK. The selected specimens originated from bovines that were sacrificed for a food distribution service, consequently it is not possible to record a precise age and hence had an age range associated with 1 - 2 years old.

Cartilage plug extraction was performed using an 8 mm trephine bur (with an internal 7.2 mm diameter) in a high speed 30,000 rpm rotary tool. During drilling a steady stream of phosphate buffered saline was used to ensure cartilage plugs were not damaged due to frictional heating. Following extraction, each cartilage plug underwent a thorough inspection for visible defects and geometric inconsistencies. To ensure uniformity in the subsequent analyses, plugs displaying greater than 0.2 mm planar height difference across the cartilage surface were systematically excluded to maintain consistency in sample geometry across the study. The samples were cryopreserved (−18°C) in PBS and thawed for at least 12 hours prior to testing in a refrigerated environment, followed by acclimatisation to room temperature for an additional 2 hours immediately before testing. Single cycles of freezing and thawing have demonstrated no difference in tribological properties compared to fresh articular cartilage samples [8]. The osmolarity and ion concentrations of PBS emulates the isotonic body fluid environment which provides a suitable storage and immersion fluid for cartilage to prevent cartilage swelling, deformation, and maintain tissue hydration, it is routinely used during *in vitro* cartilage tribological testing [9, 10]

3.3.3 Hydrophilic functionalisation of PEEK

SPMK functionalised PEEK samples were prepared with reference to the method developed by Kobayashi for MPC [6, 7]. Polished PEEK samples were washed in acetone for 30 minutes in an ultrasonic bath, washed with isopropanol, and then dried in a stream of air. SPMK aqueous solution was prepared at a 1 mol/L concentration and purged with nitrogen for 2 hours to remove oxygen. In a glove box flooded with nitrogen cleaned PEEK substrates were immersed in the SPMK solution and exposed to 5 mW/cm^2 ultraviolet (UV) light at a 365 nm wavelength (Analytik Jena UVP Crosslinker CL-3000L) for 90 minutes for a total UV exposure of 27 J/cm^2. Following photopolymerisation, functionalised PEEK samples were washed with isopropanol and deionised water to remove excess unreacted monomer.

Hydrophilic surfaces can be prepared through surface initiated polymerisation using a grafting-from approach of polymerising SPMK monomer onto PEEK substrates. PEEK comprises of an aromatic backbone molecular chain with ketone and ether functional groups. The presence of a benzophenone unit (an aryl ketone) in the molecular structure, which when irradiated by UV undergoes a pinacolization reaction to form a semi-benzopinocal radical (i.e. ketyl radicals) which act as a photoinitiator as shown in Figure 3.1(a). This can be exploited for self initiated surface graft polymerisation enabling direct grafting of functional SPMK polymers onto the

PEEK surface without using a photoinitiator [11]. Anionic sulfonic acid groups (Figure 3.1(b)) in the SPMK structure have a high affinity for water and in aqueous conditions provide a highly hydrated lubricious soft interface [7].

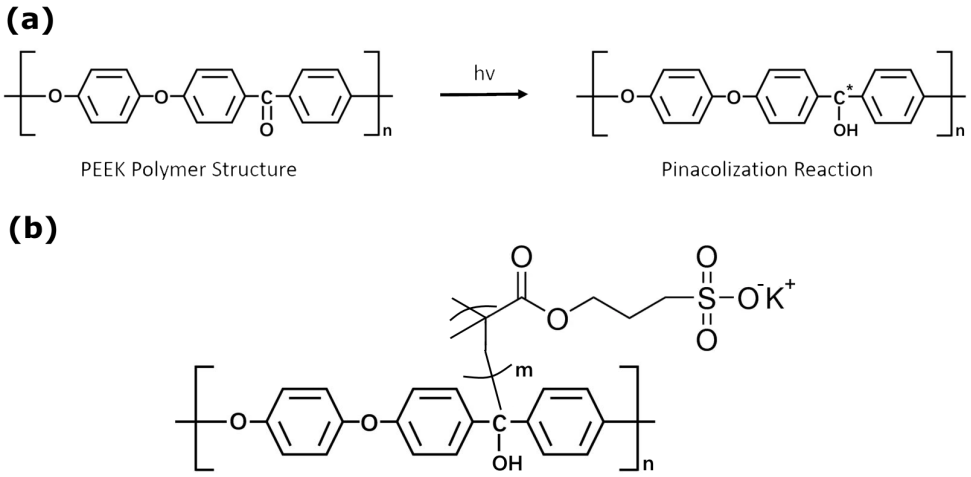

Figure 3.1: (a) A benzophenone unit exposed to ultraviolet irradiation a pinacolization reaction is induced, forming a semi-benzopinocal (ketyl) radical that acts as a photoinitiator. (b) SPMK-grafted-PEEK achieved through grafting-to of the SPMK monomer showing the anionic sulfonic functional group.

3.3.4 FTIR

Fourier Transformed Infrared Spectroscopy with an attenuated total reflection module (FTIR-ATR) was performed using a Spotlight 400 (Perkin Elmer, Massachusetts USA) to confirm the presence of grafted polymer following UV initiated photopolymerisation.

IR spectra were obtained from 16 scans with four repeats at four different locations on each grafted PEEK surface between 650 - 4000 cm^{-1} at a resolution of 4 cm^{-1}. Transmittance profiles were then compared to SpectraBase FTIR-ATR database to confirm the presence of SPMK on the PEEK surface.

3.3.5 Wettability

Water contact angle (WCA) measurements were performed by dropping 10 μL of purified Milli-Q water from a fixed height of 40 mm onto the sample surface all in ambient temperatures (298 K). After allowing the water droplet to wet the surface and become static for 30 s, the droplet is illuminated using an Attension Theta Tensiometer (Nanoscale Instruments, Phoenix, USA) producing a high contrast image of the droplet imaged with a CMOS camera. Attension Theta

software was used to determine the water contact angle in air. Each measurement was repeated 5 times to calculate an average WCA measurement.

3.3.6 Focused Ion Beam - Scanning Electron Microscopy

A Helios G4 CX Dual Beam (FEI, USA) Scanning Electron Microscope with a precise Focussed Ion Beam (FIB-SEM) was used to measure the dry film thickness of the SPMK grafted PEEK surfaces. Prior to analysis, samples were dehydrated in a vacuum and coated with a 20 nm of iridium. Samples were then placed in the FIB-SEM microscope and a layer of platinum was deposited on the surface via an electron and ion beam. Both of these processes were necessary to ensure the SPMK surface would be preserved throughout the gallium ion beam FIB cross sectioning. A $3 \times 10 \times 10$ μm section was milled to expose a cross section of the SPMK-g-PEEK interface which was then imaged under SEM to observe the dry film thickness. Two cross sections were taken on separate SPMK-g-PEEK samples to enable a representative calculation of dry SPMK film thickness, four measurements of SPMK thickness were taken in each milled cross section to calculate an overall average thickness.

3.3.7 Mechanical Testing

A Bruker UMT Tribolab fitted with a reciprocating linear drive and custom built lubricant bath was used to perform cartilage-pin on CoCr, PEEK, and SPMK-g-PEEK plates. Plate samples were fixed in the bath and cartilage pins were fixed to a rigid load and displacement transducer. During testing samples were fully submerged in PBS as an isotonic test fluid to simulate a physiological environment and subsequently mitigate cartilage swelling and maintain a hydrated equilibrium representative of an *in vivo* environment. A schematic of the experimental setup is shown in Figure 3.2a.

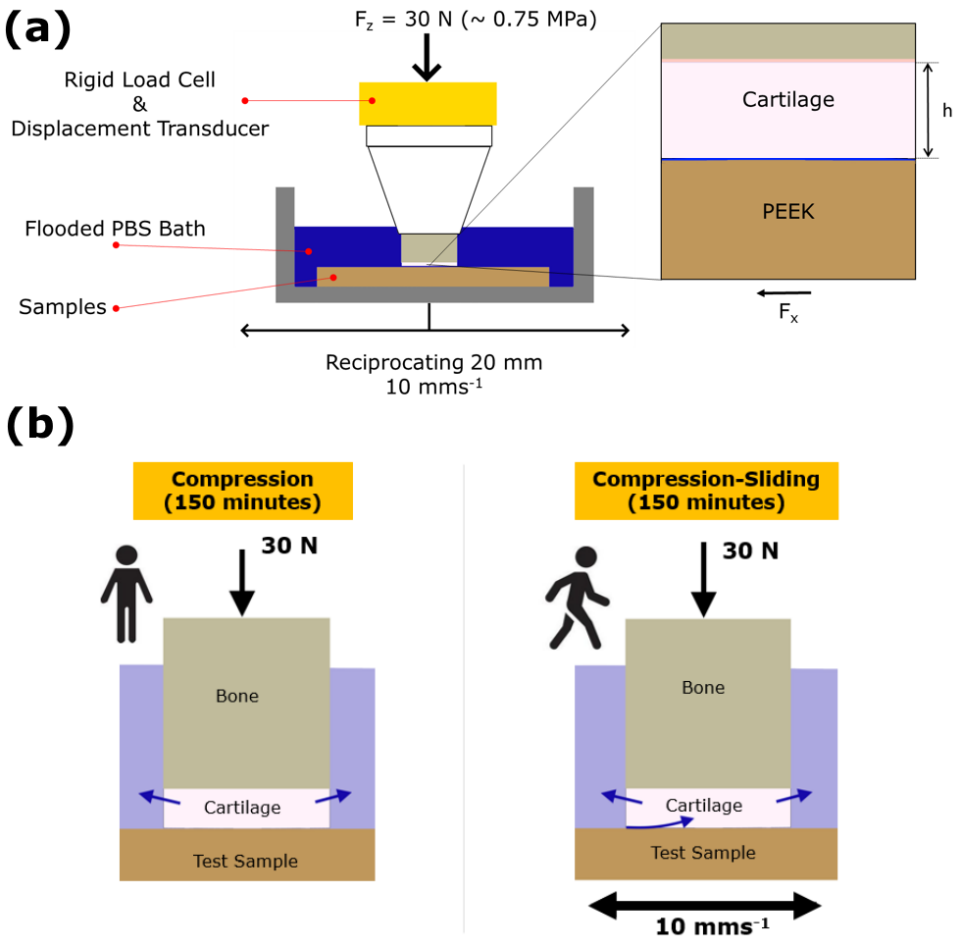

Figure 3.2: (a) Schematic of cartilage pin on plate testing on the Bruker UMT (b) the testing regimes employed in the study: compression where a 30 N load is applied and held for 150 minutes and compression-sliding where a 30 N load is applied with a reciprocating sliding speed of 10 mm/s.

Throughout testing closed loop control enabled simultaneous measurement of the Coefficient of Friction (μ) and cartilage compressive strain (ε):

$$\mu = \frac{F_x}{F_z} \tag{3.1}$$

$$\varepsilon = \frac{\Delta h}{h_0} \times (100\%) \tag{3.2}$$

where F_X and F_Z are the measured forces in the tangential ($\mathbf{x}$) and normal ($\mathbf{z}$) directions respectively, h_0 is the swollen full thickness of the cartilage, and Δh is the compressed cartilage height.

Throughout testing a constant normal load (F_Z) of 30 ± 3 N is applied and maintained with PID control. This corresponds to a physiologically representative spatially averaged contact pressure of approximately 0.75 MPa for human hip and tibiofemoral joints [12, 13]. Figure 3.2(b) show the two 150 minute testing regimes employed. Unconfined compression of a constant applied 30 N load for 150 minutes and the time dependent strain response of cartilage is recorded against PEEK, SPMK-g-PEEK, and CoCr (each N = 3).

Table 3.1 summarises the compression-sliding routines which applied a constant load of 30 N throughout a 9000 s test of cartilage pin-on-plate reciprocating sliding. SPMK-g-PEEK (N = 4) and PEEK (N = 4) plates were slid against cartilage pins with a 20 mm stroke length for 2250 cycles. The smaller 25 mm diameter CoCr plates (N = 3) underwent sliding with a 10 mm stroke length for 4500 cycles. The sliding stage underwent a sawtooth displacement profile, as such the velocity profile consisted of alternating periods of constant positive and negative velocities at a speed of 10 mm/s. For each sample test this equates to a total sliding distance of 90 m.

	SPMK-g-PEEK	**PEEK**	**CoCr**
Load	30 N	30 N	30 N
Speed	10 mm/s	10 mm/s	10 mm/s
Reciprocating Distance	20 mm	20 mm	10 mm
Test Length	9000 s	9000 s	9000 s
Total Sliding Distance	90 m	90 m	90 m

Table 3.1: Compression-Sliding test parameters for SPMK-g-PEEK, PEEK, and CoCr tests. All tests lasted 9000 s with a constant applied load of 30 N, constant speed of 10 mm/s and total sliding distance of 90 m.

The unconfined compression tests serve as a baseline measurement of cartilage strain without any sliding induced rehydration. The compression-sliding data can then be directly compared to the strain responses of the pin-on-plate sliding tests using the same contact geometry to quantify sliding induced cartilage rehydration. Coefficient of Friction (CoF), μ, and strain, ε, are reported as a single average value for each reciprocating cycle. Both values are calculated from the mid 50% of the reciprocating cycle, with the value from each cycle calculated from the mean of the forward and backward stroke, in order to calculate CoF during steady state sliding. The strain response of cartilage throughout mechanical testing was fitted using a custom script written in Python 3.7 to understand the viscoelastic time dependent creep by fitting to the biphasic theory equation [14]. All mathematical code was written using scripts enabled by

pandas, NumPy along with curve fitting using SciPy non-linear least squares fit algorithm [15].

3.3.8 Cartilage Surface Analysis

Following testing cartilage pins were stored in 10% neutral buffered formalin using CellPath CellStor Pre-filled Specimen Containers at room temperature. Prior to analysis cartilage samples were washed and soaked thoroughly in phosphate buffered saline. Measurement of the cartilage height was performed on a Keyence VHX-7000 with a 20× magnification calibrated with a reference scale accurate to ± 0.1 μm, enabling accurate pixel measurements to be taken on sample images. Four images were taken of each cartilage plug of the transverse plane, with the cartilage plug rotated about its long axis of symmetry by 90° between each image. This generated a set of four images which show the full 360° of the cartilage swollen height. Using Keyence measurement software the line of best fit was plotted along the tidemark (calcified cartilage-bone interface) along with the top surface of the cartilage, the average cartilage height between the fitted lines is then calculated. Full thickness cartilage height (h_0) is calculated from the average of the four images taken per sample. An annotated image demonstrating the measurement procedure is shown in Figure 3.3.

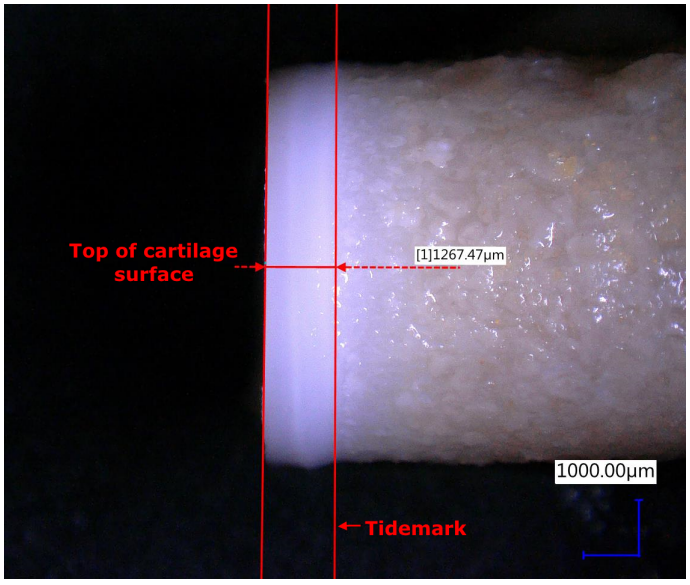

Figure 3.3: Measurement of cartilage layer height using images taken on a Keyence VHX-7000 analysed using the supplied Keyence measurement suite.

Accutrans (a casting silicone used for taking transfer moulds) replicas of the cartilage plug surface were analysed using an Infinite Focus Optical 3D Measurement Microscope (Alicona, USA). Macroscopic images were taken over the entire surface of the plug to identify significant

wear artefacts and fibrillation. Additionally, microscale measurements over an area of 0.5 mm width across the centre of the cartilage plugs determine the roughness of the cartilage indicating surface degradation.

Roughness measurements were taken on the cartilage sample after undergoing sliding against PEEK, SPMK-g-PEEK and CoCr, along with unused fresh cartilage plugs as a control. Roughness profiles were taken over the central 4 mm of each cartilage plug, a cut off filter with a wavelength of 250 μm was used to remove profile features caused by bubbles in the the silicone moulds or the uneven geometry of natural cartilage. For each of the sliding counter-face materials, an average value of the cartilage roughness following sliding was calculated.

3.4 Results

3.4.1 FTIR-ATR

Figure 3.4 shows the FTIR-ATR spectra of unfunctionalised PEEK and SPMK-g-PEEK samples. CoCr is not included as it did not include any notable IR absorption peaks. IR absorption peaks for the ester carbonyl group C=O (1721 cm^{-1}) and sulfonate group S=O (1045 cm^{-1}) are clearly observed, indicating successful UV initiated polymer grafting of SPMK to the PEEK substrate [16]. A broad adsorption peak around 3400 cm^{-1} also indicates water bound at the hydrophilic sulfonic acid groups of the SPMK [17].

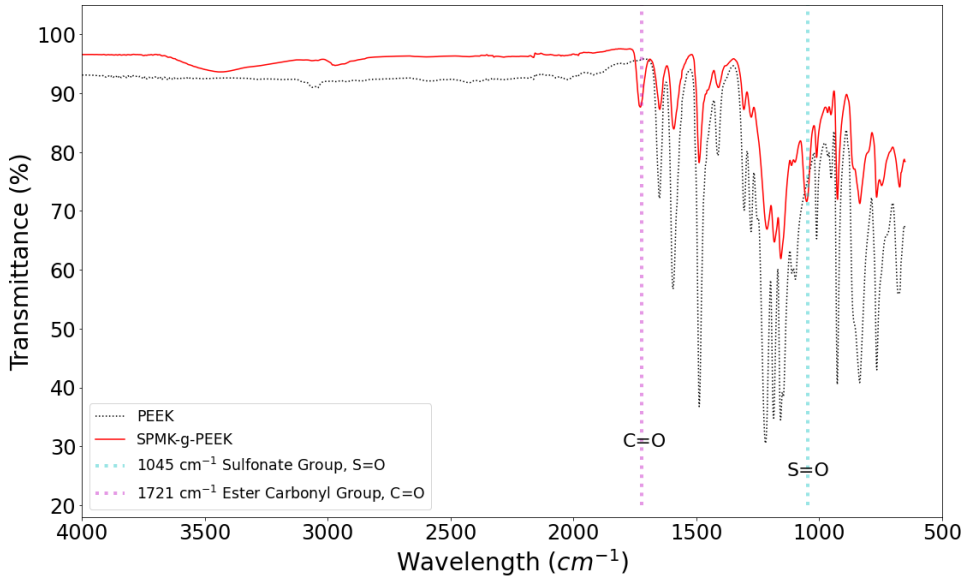

Figure 3.4: FTIR-ATR Spectra of unfunctionalised PEEK and SPMK-g-PEEK with IR absorption peaks for ester carbonyl and sulfonate groups shown.

3.4.2 Water Contact Angle

Static water contact angle (WCA) measurements shown in Figure 3.5 demonstrate that SPMK functionalisation is able to modify the surface wettability of a hydrophobic PEEK substrate, substantially enhancing the hydrophilic properties. PEEK and CoCr yielded higher WCA of 82.7° ± 2.2° and 76.7° ± 6.2° respectively corresponding to a hydrophobic surface eliciting a low surface energy. SPMK-g-PEEK had a static WCA of 33.5° ± 3.1° demonstrating a high surface energy and affinity for water, providing an interface optimised for retaining a fluid film in an aqueous environments [18, 6, 7]. A decrease of 49.2° of WCA was observed between PEEK versus SPMK-g-SPMK.

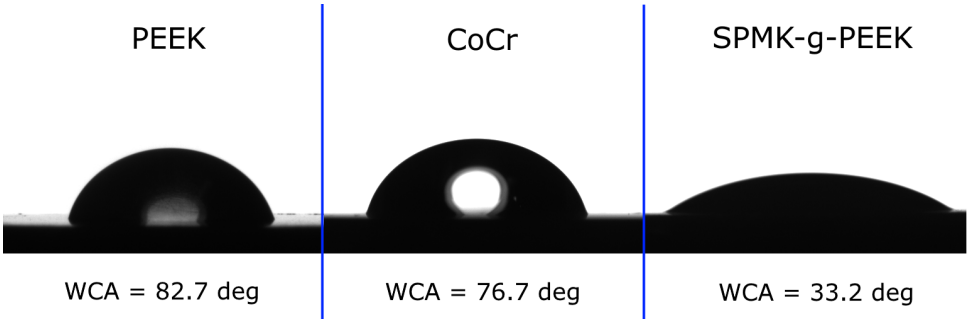

Figure 3.5: Static water contact angle (WCA) images and measurements for unfunctionalised PEEK 82.7° ± 2.2° (N = 5), CoCr 6.7° ± 6.2° (N = 5), and SPMK-g-PEEK 33.5° ± 3.1° (N = 5).

3.4.3 FIB-SEM Dry Film Thickness

Figure 3.6 show the FIB-SEM cross section and dry layer thickness of SPMK-g-PEEK surfaces. An average dry film thickness of 397 ± 47 nm (N = 8) was observed on SPMK-g-PEEK samples. FIB-SEM also indicated a layer of uniform thickness and distribution across the surfaces within the area analysed. The 'crackled' surface appearance is attributed to dehydration (under ultra high vacuum) and application of the protective Platinum layer.

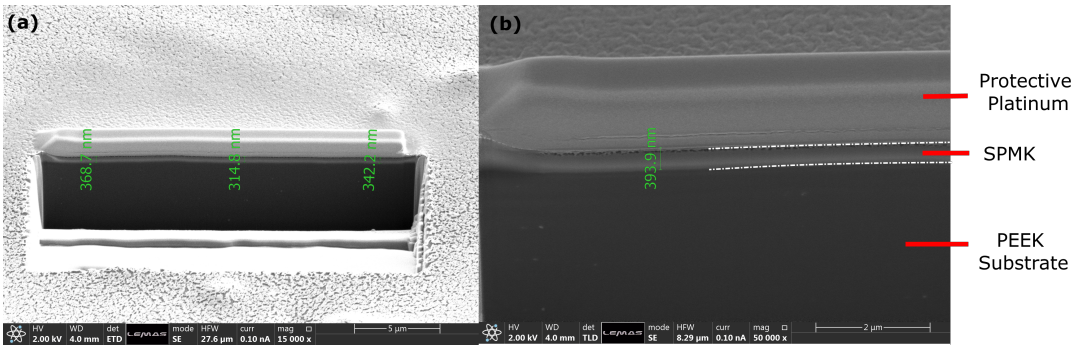

Figure 3.6: FIB-SEM cross section images of SPMK-g-PEEK showing (a) milled section for analysis which enabled measurement of the dry SPMK layer height using SEM at 15,000× and (b) 50,000× magnification with annotation on material conformation of analysed surface. Green markings demonstrate measurement of local SPMK layer thickness on the PEEK substrate.

3.4.4 Continuous pin-on-plate sliding

The evolution of CoF during sliding is shown in Figure 3.7(a). PEEK and CoCr surfaces slid against a static cartilage pin exhibited an increasing CoF up to a high final CoF (μ_F) of 0.45 ± 0.04 and 0.35 ± 0.04 respectively at the end of the test. In contrast, SPMK-g-PEEK maintained a low CoF throughout the test duration increasing monotonically to μ_F of 0.024 ± 0.01. The startup CoF μ_S (t = 1 s) and final CoF μ_F (t = 9000 s) are summarised in table 3.2.

Figure 3.7(b) show the cartilage strain evolution for the Compression and Compression-Sliding experiments. This was characterised by an initial rapid increase in strain where interstitial fluid is rapidly exude from the cartilage (t < 3600 s), followed by a steadier creep towards strain equilibrium.

For the Compression tests no sliding induced rehydration of the cartilage plug is possible, and benchmarks the maximum expected fluid exudation and final cartilage strain response after 9000 s of loading. For unconfined compression a typical biphasic creep response was observed with average values for PEEK ε_F of 49.7 ± 7.8%, SPMK-g-PEEK ε_F of 55.0 ± 5.4% and CoCr ε_F of 59.6 ± 12%. Each value is summarised in Table 3.2. When considering the uncertainty in each dataset it can be concluded that the strain response for cartilage with no sliding reduce rehydration broadly yields an final strain of $\varepsilon_F \sim$ 45% - 65%.

In-situ cartilage strain measurement during the Compression-Sliding tests presented a similar monotonic relationship. The final strain ε_F for PEEK and CoCr was 52.5 ± 7.5% and 39.8 ± 5.0% respectively. SPMK-g-PEEK yielded the lowest ε_F of 26.3 ± 7.6%, demonstrating functionalisation of PEEK surfaces with SPMK is able to effectively halve the final strain when

sliding against cartilage.

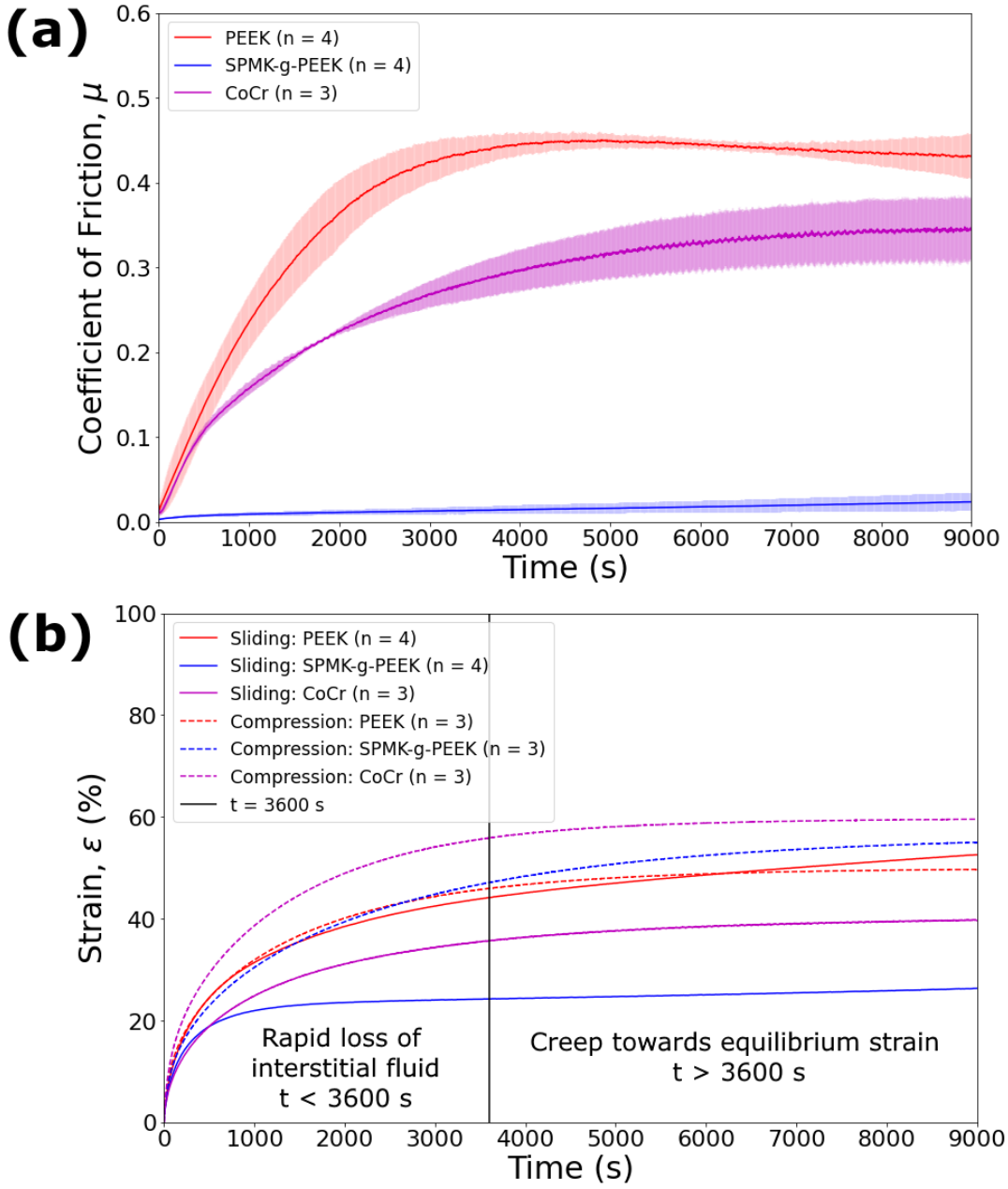

Figure 3.7: (a) Dynamic friction per reciprocating sliding cycle for a cartilage pin sliding against PEEK, SPMK-g-PEEK, and CoCr under a constant 30 N load, 20 mm reciprocating distance at a speed of 10 mm/s. Error bars show one standard deviation in each reciprocating cycle for each material data set. (b) Compression and Compression-Sliding (mean strain per reciprocating sliding cycle) for cartilage against PEEK, SPMK-g-PEEK and CoCr surfaces. Error bars are omitted for figure clarity, see Table 3.2.

Sample	Compression	Compression-Sliding		
	Final Strain ε_F (%)	Startup CoF μ_S (t = 1 s)	Final CoF μ_F (t = 9000 s)	Final Strain ε_F (%)
PEEK	49.7 ± 7.8 (N = 3)	0.020 ± 0.007	0.451 ± 0.040	52.5 ± 7.5 (N = 4)
SPMK-g-PEEK	55.0 ± 5.4 (N = 3)	0.003 ± 0.001	0.0242 ± 0.011	26.3 ± 7.6 (N = 4)
CoCr	59.6 ± 12 (N = 3)	0.016 ± 0.005	0.353 ± 0.041	39.8 ± 5.0 (N = 3)

Table 3.2: Average startup CoF (μ_S), final CoF (μ_F) and final strain (ε_F) after 9000 s of compression or sliding against cartilage for the PEEK, CoCr, and SPMK-g-PEEK. The error values correspond to one standard deviation of each average value.

3.4.5 Cartilage Surface Analysis

Figures 3.8 show Accutrans moulds taken of cartilage pin surfaces for sliding against (a) PEEK (b) SPMK-g-PEEK and (c) CoCr surfaces respectively. Analysis of cartilage pins sliding against PEEK show deep scratches and fibrillation in the surface, tearing of the cartilage surface is due to high shear forces at the interface during testing. No notable scratches or fibrillation were observed on the cartilage surface interfacing with SPMK-g-PEEK or CoCr samples.

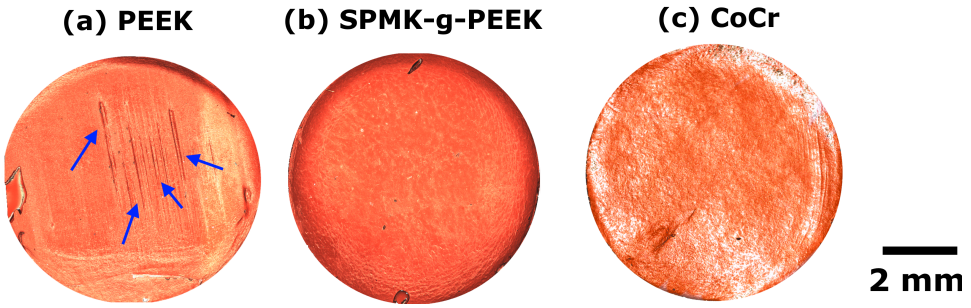

Figure 3.8: Images of Accutrans moulds of cartilage pins following 9000 s sliding against (a) PEEK showing localised fissuring and fibrillation of cartilage surface marked with blue arrows and (b) SPMK-g-PEEK exhibiting no notable deleterious wear to cartilage surface and (c) CoCr showing evidence of surface fibrillation. For each sample, it should be noted that the appearance of blister like defects at the sample edges are air bubble artefacts during the Accutrans moulding process.

For each test the mean average arithmetic roughness (R_a) and maximum valley height (R_z) are calculated to quantify cartilage surface fibrillation (roughness, R_a) and any localised tearing (R_z), summarised in Table 3.3. The largest features (maximum peak/valley height) were observed on the PEEK (Figure 3.8(a)) samples corresponding to tearing in the cartilage surface. Broad peaks and valleys with large feature heights of 14.19 ± 8.15 μm indicate significant damage to the cartilage, compared to an unused cartilage control with feature heights of 5.33 ± 0.54 μm. Similarly cartilage sliding against PEEK exhibits a increase in roughness with R_a values

of 2.49 ± 0.52 μm compared to the cartilage control with an R_a of 1.04 ± 0.09 μm. Cartilage sliding on CoCr exhibited maximum feature heights of 3.18 ± 1.01 μm and roughness values of 0.64 ± 0.20 μm. Cartilage sliding on SPMK-g-PEEK samples yielded maximum feature heights and average roughness in the ranges of 2.70 ± 0.77 μm and 0.69 ± 0.16 μm respectively. Compared to the cartilage control, sliding against CoCr and SPMK-g-PEEK reduced the cartilage roughness, effectively flattening the rough profile of natural cartilage.

Name	R_z / μm	R_a / μm
PEEK (N = 4)	14.19 ± 8.20	2.49 ± 0.52
SPMK-g-PEEK (N = 4)	2.70 ± 0.77	0.69 ± 0.16
CoCr (N = 2)	3.18 ± 1.01	0.64 ± 0.20
Fresh Cartilage (N = 3)	5.33 ± 0.54	1.04 ± 0.09

Table 3.3: Mean maximum valley height (R_z) and arithmetic roughness (R_a) measured for cartilage samples following sliding against PEEK, SPMK-g-PEEK, and CoCr, along with unused (fresh) cartilage control samples. Due to improper storage after testing, one CoCr interfacing cartilage plug was rendered unsuitable for post-testing surface analysis and roughness measurement.

3.5 Discussion

Focal metallic cartilage resurfacing is an emerging clinical procedure that offers a solution between the biologic repair and total joint arthroplasty for active patients with early stage osteoarthritis and full-thickness cartilage defects. The advantages of this technique include local management of the defect retaining healthy tissues, maintaining joint stability with surfaces contoured to be congruent with the natural joint. However, osteoarthritis progression, persisting pain along with cartilage erosion and the subsequent high revision rate is common in the medium to long term. Strategies to reduce erosion and promote adjacent cartilage tissue health may enable better outcomes at the medium-long term.

3.5.1 Surface and tribological properties of SPMK-g-PEEK

PEEK substrates were successfully grafted with end tethered SPMK polyelectrolytes via surface initiated photopolymerisation induced by the benzophenone groups in PEEK. Following surface modification, FTIR-ATR confirmed successful grafting of SPMK-g-PEEK confirming the presence of anionic sulfonate functional groups. These functional groups play a crucial role in maintaining the polymer brush structure under high loads through electrostatic repulsive in-

teractions and high affinity for water promote a highly hydrated interface in aqueous conditions [7, 17]. Water contact angle measurements demonstrate SPMK surface functionalisation reduces the PEEK WCA of 82.7° ± 2.2° to a highly wettable WCA of 33.5° ± 3.1° for SPMK-g-PEEK, essential for highly lubricious performance in aqeuous environments.

The nanoscale layer thickness of the dry SPMK of 397 ± 47 nm determined by FIB-SEM measurements is approximately four times thicker than comparable applications of polyelectrolyte polymer brush functionalised surfaces developed by Ishihara. [4]. Measurements of dry surface coatings of MPC on polyethylene are reported to be in the region of 80 - 100 using transmission electron microscopy on functionalised surface cross sections. MPC functionalised surfaces exhibit high lubricity in aqueous environments and have been incorporated into polyethylene acetabular cups in total hip replacement [19, 20]. The significantly thicker dry film coating compared to those in the aforementioned studies raises questions about the exact polymer conformation at the surface and will be subject to further investigation.

Throughout sliding tests against cartilage, SPMK-g-PEEK sustained a low CoF ranging between 0.003 - 0.024 which are comparable to the CoF measured for healthy cartilage-cartilage interfaces. Cadaveric hip pendulum experiments designed to emulate gait have measured cartilage-cartilage contacts having a CoF in the range of 0.01 - 0.04 [21, 22, 23]. Similarly, benchtop cartilage pin-on-plate tribometer tests at loads in the range of 0.2 - 0.4 MPa have demonstrated cartilage steady state CoF in the range of 0.05 - 0.07 [24, 25]. Anionic polyelectrolyte surfaces are able to facilitate hydration lubrication, whereby tenaciously bound water molecules at the functional groups maintain a highly hydrated sliding interface [2, 26]. Through surface force balance observations based on synthetic end tethered polyelectrolytes, a lubrication mechanism enabled through hydration lubrication proposed by Klein hypothesises that boundary synovial lubrication can be attributed to hydration lubrication enabled by the hydrophilic macromolecule complexes (hyaluronic acid, aggrecan, and phospholipids) at the superficial cartilage interface which maintain a fluid like lubrication layer and dissipate friction via exchange of water ions between hydration shells [27, 28, 2].

In comparison, untreated PEEK ($\mu_F = 0.45$) and CoCr ($\mu_F = 0.35$) surfaces do not exhibit sustained hydration-enabled lubrication, resulting in rapid increases in CoF beyond levels observed in healthy cartilage-cartilage contacts. The lack of sustained lubrication in these materials can be attributed to their lower affinity for surface water as demonstrated by high water contact

angles, especially in the case of PEEK, which exhibits the lowest surface energy. The improved wettability of CoCr compared to PEEK provides a slightly improved hydrophilic interface that can partially support lubrication at the interface [29]. This allows for some degree of biphasic lubrication, which will maintain the hydration state of the interfacing cartilage. While the direct relationship between water contact angle and friction is not linear and remains a research gap, these factors collectively contribute to reducing the coefficient of friction at the cartilage - CoCr interface.

The interstitial fluid and pressure loss in cartilage under an applied load is closely linked to the changes in CoF. When the cartilage is initially loaded, the interstitial fluid pressure (IFP) plays a crucial role in supporting most of the applied load. However, as the load persists, the interstitial fluid is gradually exude out of the cartilage, leading to a transfer of load to the solid collagen matrix. This transition causes an increase in the CoF as both a higher load is transferred to the solid interface and weeping lubrication become diminished. After a sustained period of loading (i.e. $t > 3600$ s) almost all of the interstitial fluid is forced out of the cartilage, an equilibrium state of strain and CoF is reached where the load is primarily supported by the solid collagen matrix [30, 31].

The study design, which involved using 7.2 mm diameter flat cartilage plugs, facilitated a static contact area and arrested tribological rehydration attributable to hydrodynamic wedge effects, enabling a more controlled analysis [30, 32, 10]. Use of a stationary contact area enabled a direct comparison of sliding-compression tests to unconfined compression data, which benchmarks the time-dependent cartilage strain response.

Following 9000 s of unconfined compression against PEEK, a final strain of $\varepsilon_F = 49.7 \pm 7.8\%$ was observed, representing a state of maximal loss of IFP under a load of 30 N. In comparison, the final strain during sliding against PEEK was measured at $\varepsilon_F = 52.5 \pm 7.5\%$, which, considering the strain error, indicates a comparable state of IFP loss. Cartilage sliding against CoCr demonstrated some extent of IFP was retained, with an $\varepsilon_F = 39.8 \pm 5.0\%$, approximately 20% lower than the total strain observed in the unconfined compression control. The wettability of CoCr provides a slightly improved hydrophilic interface to support lubrication. This also supports the hydration state of the interfacing cartilage, enabling some biphasic lubrication. While the direct link between WCA and friction is not linear, these factors together play a vital role in reducing the coefficient of friction on the CoCr surface.

One of the key findings of this study is the notable reduction in the final strain observed with SPMK-g-PEEK, with ε_F measured at 26.3 ± 7.6%. This represents a significant decrease of approximately 47% in the expected IFP loss compared to the unconfined compression control (ε_F = 55.0 ± 5.4%). These findings provide compelling evidence that SPMK polyelectrolyte functionalised surfaces are able to support sliding induced rehydration and modulate interstitial fluid flow, through a novel mechanism independent of hydrodynamic fluid inflow. The most likely explanation is the interplay of hydration lubrication and sustained biphasic fluid load support. The highly hydrophilic nature of the SPMK-g-PEEK surfaces provides a boundary lubricating layer, maintaining a low CoF at the interface. Additionally, the tenaciously bound hydrated species provide a hydrated region which, during sliding, facilitates the influx of fluid into the contact interface and its absorption into the cartilage surface.

Deleterious cartilage fibrillation was only observed in cartilage samples sliding against unfunctionalised PEEK and CoCr (Fig. 3.8) while no notable damage was found in pins sliding against SPMK-g-PEEK. Similarly, cartilage sliding against PEEK showed increased roughness (R_a) and valley height (R_z) compared to the fresh cartilage control and samples sliding against SPMK and CoCr (Table 3.3). The high CoF and strain behaviour during PEEK sliding demonstrates a total loss of IFP, leading to a situation where the majority of load in the contact is borne on the solid collagen phase leading to high shear forces and failure in the collagen fibre matrix.

3.5.2 Biphasic Theory Analysis

In the context of the presented minimised strain behaviour for SPMK-g-PEEK (Figure 3.9), the application of biphasic theory analysis has been employed to elucidate and provide an explanation for the encouraging observations related to coefficient of friction (CoF), strain, and the mitigated cartilage damage achieved with SPMK-g-PEEK surfaces compared to unfunctionalised biomaterial surfaces. The fluid flow-dependent viscoelastic behaviour of cartilage is commonly described using biphasic theory [14]. This model for cartilage creep behaviour is shown in Eq. 3.3 which for a time constant τ the asymptotic creep towards strain equilibrium ($\varepsilon(t)$) can be described. The characteristic time constant τ_c quantifies the time to reaching compressive creep equilibrium [33, 34].

$$\varepsilon(t) = -\frac{\sigma}{H_A}\left[1 - 2\sum_{n=0}^{\infty}\frac{1}{M}e^{-(\frac{M}{\tau})t}\right] \tag{3.3}$$

and

$$M = \pi^2 \left(n + \frac{1}{2} \right)^2 \tag{3.4}$$

$$\tau = \frac{h^2}{H_A k} \tag{3.5}$$

where ε = strain, t = time, τ = time constant, τ_c = characteristic time constant, h = cartilage thickness, σ = applied stress, H_a = aggregate modulus, and k = permeability.

For quantitative temporal analysis of the time-dependent cartilage strain behaviour during the initial hour of biphasic creep (t $<$ 3600 s, see Fig. 3.7(b)) a 5th order approximation (0 $\leq$ n $<$ 5) of Eq. 3.3 is fitted to the strain data using a nonlinear least squares fit algorithm to calculate characteristic time constants (τ_c). A 5th order approximation was deemed suitable for fitting since $log(t_{max}/t_{min}) = log(9000/0.1) = 5.0$. This approximation was chosen because it sufficiently represents variations in the data without overcomplicating the model, as evidenced by the logarithmic ratio of the time data, which equals 5.0.

The quality of the curve fit is assessed through calculating the coefficient of determination, R-squared (R^2) using Eq. 3.6.

$$R^2 = 1 - \frac{\sum_t \left(\varepsilon_t - \varepsilon(t) \right)^2}{\sum_t \left(\varepsilon_t - \bar{\varepsilon} \right)^2} \tag{3.6}$$

Figure 3.9 shows the fitting of the biphasic strain equation (Eq. 3.3) to the strain response of cartilage samples during unconfined compression (no sliding) and sliding against PEEK, SPMK-g-PEEK and CoCr surfaces during the initial 3600 s of testing. Table 3.4 summarises the parameters calculated by fitting the biphasic strain equation of the characteristic time constant τ_c, the quality of the biphasic fit R^2, and the final strain after the 3600 s period of analysis $\varepsilon(t = 3600s)$.

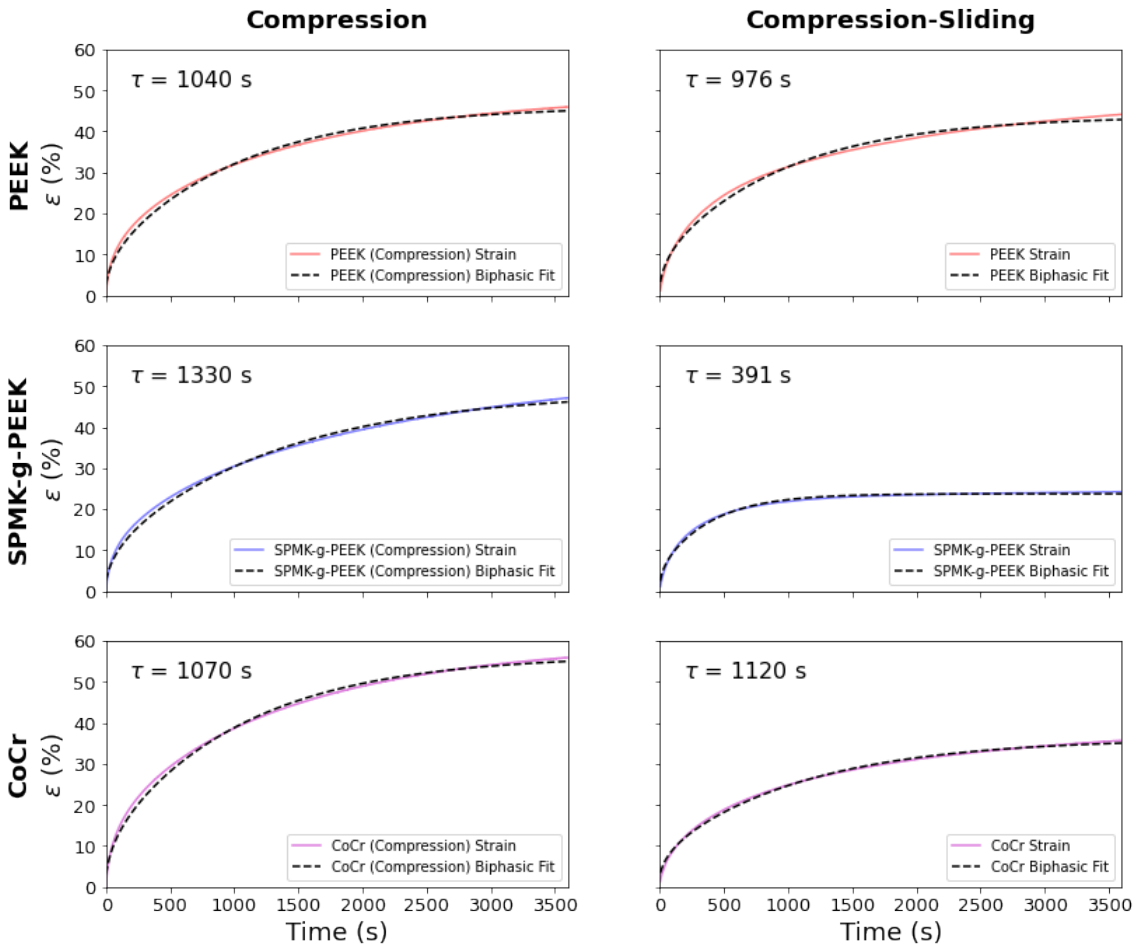

Figure 3.9: Fitting of the biphasic theory model (Eq. 3.3) to the first hour (t < 3600 s) of the cartilage during the Compression and Compression Sliding experiments for PEEK, SPMK-g-PEEK and CoCr. The biphasic time constant (τ) is annotated for each experiment

Cartilage sliding against PEEK and CoCr surfaces yielded τ_c of 976 s and 1120 s respectively, which are both within 10% of the corresponding compression control experiments (τ_c = 1040 s and 1070 s respectively), and hence indicate little evidence of altered interstitial fluid exudation during sliding. Early experiments designed to probe the viscoelastic properties of cartilage in compression consistently demonstrate the time to reaching equilibrium strain to be in excess of 1000 s and align with the CoCr and PEEK data presented in Table 3.4 [35, 14].

SPMK-g-PEEK surfaces reached the lowest final strain in a significantly shorter time with τ_c = 391 s, demonstrating that the effective permeability of the interfacing cartilage increases (Eq. 3.5). Interestingly, the corresponding compression control for SPMK-g-PEEK yields an increased time constant of τ_c = 1330 s compared to the unfunctionalised PEEK control, implying a reduced interfacial permeability. Finite Element Analysis modelling of polyelectrolytes on the superficial cartilage surface predict that permeability is reduced by the presence of a polymer

brush border [36]. This contradiction demonstrates firstly that cartilage rehydration is triggered by sliding, and secondly the most likely explanation for the reduced final strain and short time constant during sliding is due to a competitive exudation-rehydration fluid flow.

Sample	**Compression**			**Compression-Sliding**		
	τ_c	R^2	$\varepsilon(t = 3600s)$	τ_c	R^2	$\varepsilon(t = 3600s)$
PEEK	1040	0.994	45.9 (92% ε_F)	976	0.992	44.1 (84% ε_F)
SPMK-g-PEEK	1330	0.995	47.1 (86% ε_F)	391	0.992	24.2 (92% ε_F)
CoCr	1070	0.996	55.9 (94% ε_F)	1120	0.997	35.7 (90% ε_F)

Table 3.4: Time constant τ_c are calculated by fitting the biphasic theory model (Eq. 3.3) to the first 60 minutes (t < 3600 s) of strain data in Fig 3.9. R^2 scores the quality of fit using Eq. 3.6. Strain at t = 3600 s is also given along with the ratio against final strain after 9000 s of Compression / Compression-Sliding (ε_F).

In order to analyse the steadier approaching equilibrium strain, a linear regression (Eq. 3.7) is fitted to the strain response in the final 90 minutes of the test (3600 s $\leq t \leq$ 9000 s). In this final time period cartilage will be approaching the maximum final strain ($\varepsilon(t >$ 3600 s) $\xrightarrow{\text{linear}}$ ε_F), such that the gradient of the linear regression (β, Eq. 3.8) will express the rate of change of strain and subsequently the sample propensity to maintain a stable strain equilibrium.

$$\varepsilon(t) = \varepsilon(t = 3600s) + \beta t \qquad \text{for} \qquad t \geq 3600\ s \tag{3.7}$$

$$\beta = \frac{\sum_{i=3600}^{9000} (t_i - \bar{t})\,(\varepsilon_i - \bar{\varepsilon})}{\sum_{i=3600}^{9000} (t_i - \bar{t})^2} \tag{3.8}$$

Figure 3.10 shows the long term creep behaviour and subsequent cartilage equilibrium strain rate by fitting a linear regression (Eq. 3.8) to the strain response in the final 90 minutes ($3600s \leq t \leq 9000s$) of testing. Table 3.5 summarises the slope of the linear regression (β) expressed as increase in strain per minute and the coefficient of determination R^2 quality of linear regression fit.

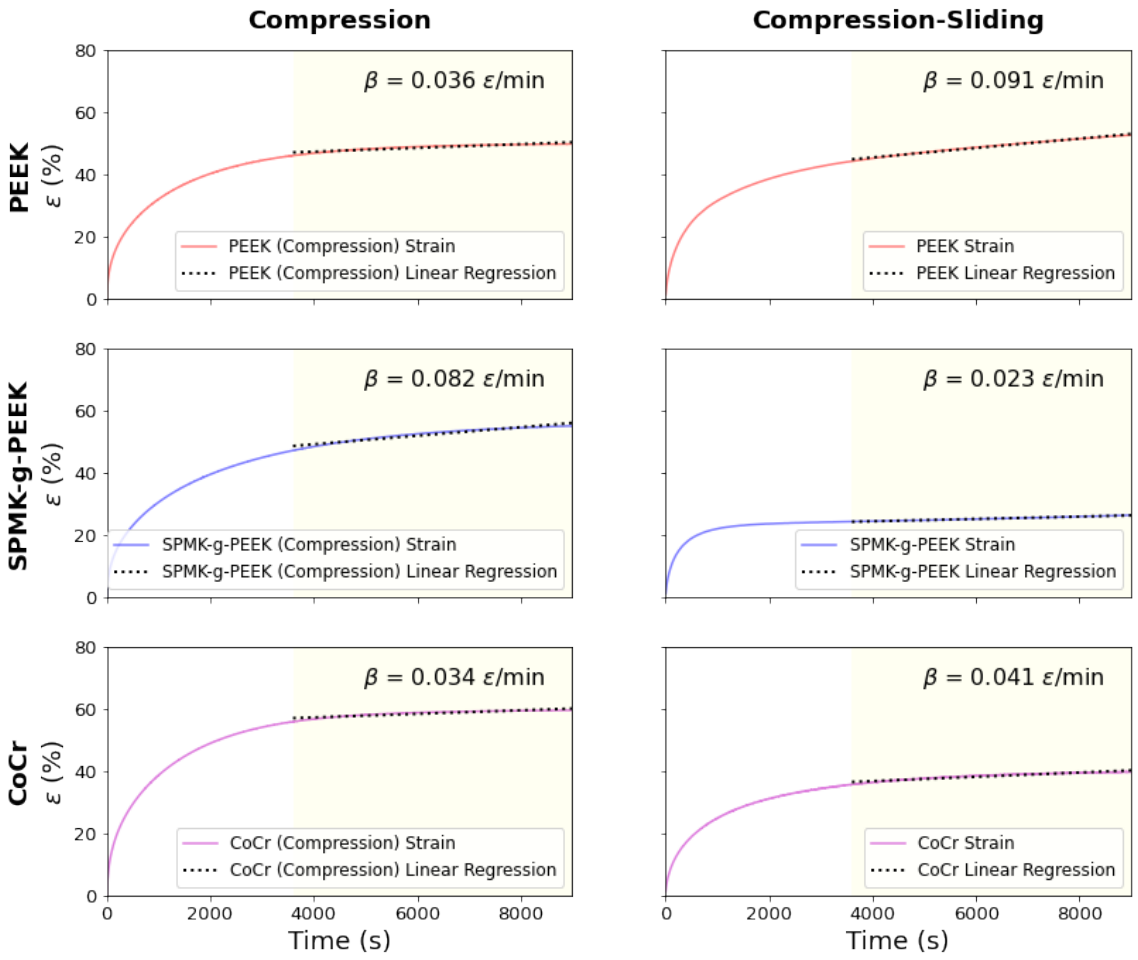

Figure 3.10: Linear regression (Eq. 3.8) fitted to the final 90 minutes ($3600s \leq t \leq 9000s$) of Compression and Compression-Sliding tests against PEEK, SPMK-g-PEEK and CoCr. he strain rate for this period β is annotated in terms of ϵ (%) / minute.

Sample	**Compression**		**Compression-Sliding**	
	β, Strain (%) / minute	R^2	β, Strain (%) / minute	R^2
PEEK (N = 4)	3.6 $\times 10^{-2}$	0.941	9.1 $\times 10^{-2}$	0.996
SPMK-g-PEEK (N = 4)	8.2 $\times 10^{-2}$	0.971	2.3 $\times 10^{-2}$	0.997
CoCr (N = 3)	3.4 $\times 10^{-2}$	0.926	4.1 $\times 10^{-2}$	0.941

Table 3.5: Slope of the linear regression (β, Eq. 3.8) given as increase in Strain (%) / minute, and R^2 quality of fit score.

The equilibrium cartilage strain creep behaviour for each test can be directly compared through the approximated linear strain rate (β) during the final phase of each test ($3600s \leq t \leq 9000s$). Sliding cartilage against SPMK-g-PEEK demonstrated the most favourable behaviour, with the lowest strain rate of 0.023 ε/minute, indicating the most stable progression towards final strain. Throughout compression-sliding tests the physics of fluid exudation of cartilage remain

unchanged, thus the reduced creep indicates a competitive rehydration mechanism facilitated by the SPMK interface.

Cartilage sliding against PEEK yielded the highest strain rate of 0.091 ε/minute, indicating the greatest depletion of interstitial fluid and failure to approach a steady final equilibrium. This could be attributed to the ongoing breakdown of the collagen matrix due to high shear forces, as evidenced by observed surface damage and fibrillation (Fig. 3.8). Ultimately, such degradation would lead to reduced mechanical strength and reduced water retention capacity of cartilage.

Sliding strain rates for CoCr and the unconfined compression control exhibited comparable rates of 0.034 and 0.041 ε/minute respectively. These rates align the performance of CoCr closer to a balanced state, falling between the extremes of the SPMK-g-PEEK and PEEK. While SPMK-g-PEEK demonstrated a favourable progression towards the final strain state, and PEEK showed a tendency towards fluid depletion and collagen breakdown, CoCr's behavior represents a moderate response that neither excels in rehydration nor fails in maintaining interstitial fluid as observed by the overall reduced strain. The strain rates for CoCr provides further insight into its tribological efficacy as a biomaterial for use in articulation against cartilage, and subsequent affinity to maintain fluid load support and improved lubricity compared to PEEK.

SPMK-g-PEEK samples exhibited a substantially reduced biphasic time constant during sliding (τ_c = 391 s, over a 60% reduction compared to the unconfined compression control) and the minimal long term strain rate (β = 0.023 ε/minute). Cartilage rehydration is onset by sliding, akin to *tribological rehydration* elucidated by Burris and Moore [37, 32, 38, 39]. Nonetheless, unlike previous investigations illustrating tribological rehydration that necessitates velocities surpassing 30 mm/s and a convergent wedge configuration to generate adequate hydrodynamic pressures for cartilage rehydration, this study introduces a distinct mechanism of polyelectrolyte enhanced tribological rehydration that is independent of conventional hydrodynamic tribological rehydration [37]. This is achieved through the use of a compliant wetting surface, the hydrophilic and hydrated nature of the SPMK layer provides a means to deliver water and replenish water at the cartilage interface, promoting and maintaining hydration.

It is hypothesised that during compression, polymer brushes may generate a high fluid pressure caused by the intensified excluded volume between polymer chains. This increased excluded volume leads to an augmented osmotic pressure within the brush interface, resulting in elevated fluid pressure [40]. Hence, it is conjectured that if the osmotic pressure within the polymer

brush is greater than the interstitial fluid pressure of cartilage, this could drive the flow of fluid back into the cartilage, thereby maintaining a greater proportion of fluid load support during sliding and reduced overall strain.

3.5.3 Limitations and Future Work

3.5.3.1 Validity of biphasic model

Fitting the biphasic model (Eq. 3.3) to the total strain response for each sample (Fig 3.7) over the full 9000 s tests was unsuitable for PEEK and SPMK where the long term creep did not strictly follow an exponential decay with a single time constant. Hence the biphasic model was only fit to the first 3600 s of sliding tests where the contact strain is dominated by the time dependent biphasic fluid flow out of cartilage. A linear fit (Eq. 3.8) was then used to model to the long term creep. Both of these metrics then enabled direct comparison of time dependent strain during sliding tests to the expected behaviour of cartilage in unconfined compression.

During the creep towards final strain phase ($t > 3600$ s) PEEK exhibited the greatest creep rate and final strain which reflects the fibrillation observed on the cartilage surface analysis following testing. During sliding tearing of the cartilage surface will both affect the real contact area and alter the aggregate modulus of the cartilage, which are assumed to be constant when modelling biphasic theory.

The biphasic model utilised in this study, initially introduced by Van Mow [14] and later expanded upon by Armstrong [41], offers a one dimensional solution that describes the temporal creep response of cartilage under confined and unconfined compression. However, this model does not consider material deformations resulting from shear forces at the interface during sliding. In the context of this study, the biphasic model is employed to examine the characteristic time constant associated with cartilage creep equilibrium, as has been done in previous research involving the assessment of in vivo cartilage mechanical function using MRI data [33].

To further elucidate the temporal behaviour of interstitial fluid pressure in cartilage during sliding and investigate the impact of polymer brush interfaces, future studies should employ constitutive models that incorporate cartilage poroelastic lubrication mechanisms. These advanced models will provide a more comprehensive understanding of how the pressure of the cartilage interstitial fluid is influenced by polymer brush interfaces over time [42].

3.5.3.2 Further insight into polyelectrolyte interactions

The contact dynamics between two polyelectrolyte surfaces have previously demonstrated that steric repulsion between opposing brushy interfaces entropically favours a liquid interface to regulate polyelectrolyte interpenetration between opposing surfaces [43, 44]. In the experiments presented within this study, a polyelectrolyte functionalised surface could be expected to favourably interact with the macromolecules on the cartilage plug samples, however following harvesting all samples were washed with PBS which has been shown to disrupt and potentially remove the natural boundary lubricating layer [43]. Further investigations into the interactions between synthesised polyelectrolyte surfaces (SPMK-g-PEEK) and synovial surfaces will provide additional insights into the beneficial interactions of SPMK functionalised biomaterials for their application in focal cartilage defect repair.

While this study provides valuable insights into the tribological properties of SPMK-g-PEEK and the supported cartilage fluid load bearing capacity, it has certain limitations that merit further investigation to fully elucidate fluid rehydration mechanisms at play. One limitation is the lack of direct measurements of cartilage interstitial fluid pressure during sliding. Future work should explore experimental setups to monitor interstitial fluid pressure in real-time, providing a more comprehensive understanding of the fluid load bearing capacity of the interfaces. Additionally, the long-term durability of SPMK-g-PEEK surfaces under physiologically representative conditions warrants investigation to assess their potential clinical applications.

3.6 Conclusions

This study demonstrates that surfaces functionalised with SPMK-g-PEEK exhibit tribological characteristics associated with effective hydration lubrication (evidenced by high wettability and the lowest coefficient of friction) and favourable modulation of interstitial fluid pressure (indicated by the lowest final strain (ε_F), strain rate (β), and characteristic time constant (τ_c)). These findings align with the two main mechanisms that contribute to the high lubricity and longevity of healthy cartilage in synovial joints; hydration lubrication and sustained biphasic fluid load support [25, 28].

The following four key conclusions demonstrate the efficacy of SPMK-g-PEEK:

1. Hydrophilic Surface Coating: The one-step grafting procedure successfully creates a highly

hydrophilic SPMK-g-PEEK surface, enabling effective hydration lubrication. This coating demonstrates the ability to sustain a low coefficient of friction (μ) during startup and steady-state sliding against cartilage, with μ maintained below 0.024.

2. Minimised Cartilage Final Strain: SPMK-g-PEEK surfaces exhibit the ability to significantly reduce cartilage strain during sliding. Facilitating the retention of a higher proportion of interstitial fluid and enhanced fluid load support compared to untreated biomaterials.

3. Effective Fluid Load Support: The improved fluid load support is attributed to the reduced effective cartilage permeability and the subsequent rehydration of cartilage initiated by sliding against SPMK-g-PEEK.

4. Novel Tribological Rehydration: Unlike previous models, which require specific conditions for hydrodynamic pressure-induced rehydration, SPMK-g-PEEK introduces a new mode of polyelectrolyte enabled tribological rehydration. This polymer brush enabled mechanism operates independently of hydrodynamics, underscoring the capability of the surface to facilitate fluid delivery to the cartilage interface.

In conclusion, SPMK-g-PEEK surfaces emerge as a promising candidate for the next generation of osteochondral defect repairs, aiming to promote functional and healthy cartilage. The combination of hydration lubrication and sustained biphasic fluid load support allows these surfaces to mitigate damage, alleviate excessive loading on the collagen matrix, and support cartilage biphasic viability. Created through a one-step grafting process, this highly hydrophilic and sterile surface coating offers benefits that include enhanced lubrication, maintained hydration, and prevention of cartilage damage. Future research should hone in on the long-term durability of SPMK-g-PEEK under physiologically representative conditions, the exploration of innovative focal repair device concepts, and the development of improved patient treatment pathways, thereby unlocking its full potential in supporting the health of interfacing cartilage.

References

[1] Kazuhiko Ishihara. Biomimetic materials based on zwitterionic polymers toward human-friendly medical devices. *Science and Technology of Advanced Materials*, 23(1):498–524, 2022.

[2] Meng Chen, Wuge H Briscoe, Steve P Armes, Hagai Cohen, and Jacob Klein. Robust, biomimetic polymer brush layers grown directly from a planar mica surface. *ChemPhysChem*, 8(9):1303–1306, 2007.

[3] Masayuki Kyomoto, Toru Moro, Ken-ichi Saiga, Fumiaki Miyaji, and Hiroshi Kawaguchi. Lubricity and stability of poly (2-methacryloyloxyethyl phosphorylcholine) polymer layer on Co – Cr – Mo surface for hemi-arthroplasty to prevent degeneration of articular cartilage. *Biomaterials*, 31(4):658–668, 2010.

[4] Masayuki Kyomoto, Toru Moro, Yoshio Takatori, Hiroshi Kawaguchi, Kozo Nakamura, and Kazuhiko Ishihara. Self-initiated surface grafting with poly(2-methacryloyloxyethyl phosphorylcholine) on poly(ether-ether-ketone). *Biomaterials*, 31(6):1017–1024, 2010.

[5] Kazuhiko Ishihara. Highly lubricated polymer interfaces for advanced artificial hip joints through biomimetic design. (March):1–13, 2015.

[6] Motoyasu Kobayashi and Atsushi Takahara. Tribological properties of hydrophilic polymer brushes under wet conditions. *Chemical Record*, 10(4):208–216, 2010.

[7] Motoyasu Kobayashi and Atsushi Takahara. Polyelectrolyte brushes : a novel stable lubrication system in aqueous conditions. pages 403–412, 2012.

[8] H. Forster and J. Fisher. The influence of continuous sliding and subsequent surface wear on the friction of articular cartilage. *Proceedings of the Institution of Mechanical Engineers, Part H: Journal of Engineering in Medicine*, 213(4):329–345, 1999.

[9] S. M.T. Chan, C. P. Neu, K. Komvopoulos, A. H. Reddi, and P. E. Di Cesare. Friction and wear of hemiarthroplasty biomaterials in reciprocating sliding contact with articular cartilage. *Journal of Tribology*, 133(4):1–7, 2011.

[10] DL Burris, L Ramsey, BT Graham, C Price, and AC Moore. How sliding and hydrodynamics contribute to articular cartilage fluid and lubrication recovery. *Tribology Letters*, 67:1–10, 2019.

[11] Hiroki Nakano, Yuri Noguchi, Sachiro Kakinoki, Mai Yamakawa, Issey Osaka, and Yasuhiko Iwasaki. Highly Durable Lubricity of Photo-Cross-Linked Zwitterionic Polymer Brushes Supported by Poly(ether ether ketone) Substrate. 2020.

[12] W A Hodge and W H Harris. Contact pressures in the human hip joint measured in vivo. 83(May):2879–2883, 1986.

[13] Richard A Brand. Joint contact stress: a reasonable surrogate for biological processes? *The Iowa orthopaedic journal*, 25:82, 2005.

[14] Van C Mow, SC Kuei, W Michael Lai, and Cecil G Armstrong. Biphasic creep and stress relaxation of articular cartilage in compression: theory and experiments. *Journal of biomechanical engineering*, 102(1):73–84, 1980.

[15] Pauli Virtanen, Ralf Gommers, Travis E Oliphant, Matt Haberland, Tyler Reddy, David Cournapeau, Evgeni Burovski, Pearu Peterson, Warren Weckesser, Jonathan Bright, et al. Scipy 1.0: fundamental algorithms for scientific computing in python. *Nature methods*, 17(3):261–272, 2020.

[16] Patcharida Chouwatat, Tomoyasu Hirai, Keiko Higaki, Yuji Higaki, Hung Jue Sue, and Atsushi Takahara. Aqueous lubrication of poly(etheretherketone) via surface-initiated polymerization of electrolyte monomers. *Polymer*, 116:549–555, 2017.

[17] J. L. Lanigan, S. Fatima, T. V. Charpentier, A. Neville, D. Dowson, and M. Bryant. Lubricious ionic polymer brush functionalised silicone elastomer surfaces. *Biotribology*, 16(March):1–9, 2018.

[18] Kock-Yee Law. Definitions for hydrophilicity, hydrophobicity, and superhydrophobicity: getting the basics right, 2014.

[19] Kazuhiko Ishihara. Highly lubricated polymer interfaces for advanced artificial hip joints through biomimetic design. *Polymer Journal*, 47(9):585–597, 2015.

[20] Tatsuro Goda, Tomohiro Konno, Madoka Takai, Toru Moro, and Kazuhiko Ishihara. Biomimetic phosphorylcholine polymer grafting from polydimethylsiloxane surface using photo-induced polymerization. *Biomaterials*, 27(30):5151–5160, 2006.

[21] I. C. Clarke, R. Contini, and R. M. Kenedi. Friction and Wear Studies of Articular Carti-

lage: a Scanning Electron Microscopic Study. *American Society of Mechanical Engineers (Paper)*, (74 -Lub-37):358–366, 1974.

[22] A Unsworth, D Dowson, and V Wright. Some new evidence on human joint lubrication. *Annals of the rheumatic diseases*, 34:277–285, 1975.

[23] Wright V Dowson D, Unsworth A. The Finctional Behavior of Human Synovial Joints-Part I: Natural Joints. (July):369–376, 1975.

[24] Ewen Northwood and John Fisher. A multi-directional in vitro investigation into friction, damage and wear of innovative chondroplasty materials against articular cartilage. *Clinical Biomechanics*, 22(7):834–842, 2007.

[25] J Katta, SS Pawaskar, ZM Jin, E Ingham, and J Fisher. Effect of load variation on the friction properties of articular cartilage. *Proceedings of the Institution of Mechanical Engineers, Part J: Journal of Engineering Tribology*, 221(3):175–181, 2007.

[26] Weifeng Lin and Jacob Klein. Control of surface forces through hydrated boundary layers. *Current Opinion in Colloid & Interface Science*, 44:94–106, 2019.

[27] Sabrina Jahn and Jacob Klein. Hydration Lubrication: The Macromolecular Domain. *Macromolecules*, 48(15):5059–5075, 2015.

[28] Sabrina Jahn, Jasmine Seror, and Jacob Klein. Lubrication of articular cartilage. *Annual review of biomedical engineering*, 18:235–258, 2016.

[29] Zenon Pawlak, Wieslaw Urbaniak, and Adekunle Oloyede. The relationship between friction and wettability in aqueous environment. *Wear*, 271(9-10):1745–1749, 2011.

[30] Axel C Moore, Jordyn Lee Schrader, Jaclyn J Ulvila, and David L Burris. A review of methods to study hydration effects on cartilage friction. *Tribology-Materials, Surfaces & Interfaces*, 11(4):202–214, 2017.

[31] Ramaswamy Krishnan, Monika Kopacz, and Gerard A. Ateshian. Experimental verification of the role of interstitial fluid pressurization in cartilage lubrication. *Journal of Orthopaedic Research*, 22(3):565–570, 2004.

[32] David L. Burris and Axel C. Moore. Cartilage and Joint Lubrication: New Insights Into the Role of Hydrodynamics. *Biotribology*, 12(September):8–14, 2017.

[33] Hattie C Cutcliffe, Keithara M Davis, Charles E Spritzer, and Louis DeFrate. The characteristic recovery time as a novel, noninvasive metric for assessing in vivo cartilage mechanical function. *Annals of biomedical engineering*, 48(12):2901–2910, 2020.

[34] CG Armstrong and Van C Mow. Variations in the intrinsic mechanical properties of human articular cartilage with age, degeneration, and water content. *The Journal of bone and joint surgery. American volume*, 64(1):88–94, 1982.

[35] JOHN M COLETTI JR, WAYNE H AKESON, and SAVIO LY WOO. A comparison of the physical behavior of normal articular cartilage and the arthroplasty surface. *Journal of Bone and Joint Surgery*, 54(1):147–160, 1972.

[36] JinJing Liao, David W Smith, Saeed Miramini, Bruce S Gardiner, and Lihai Zhang. Investigation of role of cartilage surface polymer brush border in lubrication of biological joints. *Friction*, 10(1):110–127, 2022.

[37] Steven Voinier, AC Moore, Jamie M Benson, C Price, and David Lawrence Burris. The modes and competing rates of cartilage fluid loss and recovery. *Acta Biomaterialia*, 138:390–397, 2022.

[38] A. C. Moore and D. L. Burris. Tribological rehydration of cartilage and its potential role in preserving joint health. *Osteoarthritis and Cartilage*, 25(1):99–107, 2017.

[39] Meghan E Kupratis, Ahmed E Gure, Kyla F Ortved, David L Burris, and Christopher Price. Comparative tribology: articulation-induced rehydration of cartilage across species. *Biotribology*, 25:100159, 2021.

[40] Cangyi Chen, Ping Tang, Feng Qiu, and An-Chang Shi. Excluded volume effects in compressed polymer brushes: A density functional theory. *The Journal of Chemical Physics*, 142(12):124904, 2015.

[41] C. G. Armstrong, W. M. Lai, and V. C. Mow. An analysis of the unconfined compression of articular cartilage. *Journal of Biomechanical Engineering*, 106(2):165–173, 1984.

[42] GN De Boer, N Raske, S Soltanahmadi, MG Bryant, and RW Hewson. Compliant-poroelastic lubrication in cartilage-on-cartilage line contacts. *Tribology-Materials, Surfaces & Interfaces*, 14(3):151–165, 2020.

[43] Bruno Zappone, Marina Ruths, George W. Greene, Gregory D. Jay, and Jacob N. Is-

raelachvili. Adsorption, lubrication, and wear of lubricin on model surfaces: Polymer brush-like behavior of a glycoprotein. *Biophysical Journal*, 92(5):1693–1708, 2007.

[44] Noa Iuster, Odeya Tairy, Michael J. Driver, Steven P. Armes, and Jacob Klein. Cross-Linking Highly Lubricious Phosphocholinated Polymer Brushes: Effect on Surface Interactions and Frictional Behavior. *Macromolecules*, 50(18):7361–7371, 2017.

Chapter 4

Engineering tribological rehydration of cartilage interfaces: assessment of potential polyelectrolyte mechanisms

4.1 Abstract

Articular cartilage, primarily composed of water and collagen, is vital for synovial joint function. Traditional hard biomaterials like ceramic or CoCr used in hemiarthroplasty often result in abnormal contact pressures and premature implant failure. This study investigates the tribological properties of polyelectrolyte functionalised PEEK (SPMK-g-PEEK) in contact with cartilage, proposing a solution to these issues by augmenting interstitial fluid recovery and effective aqueous lubrication.

This study demonstrates a new mode of polyelectrolyte-enhanced tribological rehydration where SPMK-g-PEEK achieves low friction and promotes interstitial fluid recovery during sliding, independent of traditional hydrodynamic theories. This results in a rapid stabilisation of the coefficient of friction (CoF) to levels comparable to natural cartilage (CoF $\sim$ 0.01) and aids in approximately 8% cartilage strain recovery, indicating effective tribological rehydration even under cartilage degradation or altered osmotic conditions.

Furthermore, it is demonstrated that lubrication and rehydration against an SPMK-g-PEEK interface depend minimally on biphasic lubrication but significantly on the hydrophilic sulfonic

acid groups of SPMK, which act as a fluid reservoir. Our findings suggest SPMK-g-PEEK as a promising biomaterial for cartilage interfacing implants that offer low friction and modulate cartilage interstitial fluid pressure. This study enhances our understanding of biotribological interactions and contributes to the development of joint replacement materials that support the natural function of cartilage.

4.2 Introduction

Chapter 3 introduces modified PEEK surfaces functionalised with SPMK (SPMK-g-PEEK) as a 350 nm thick hydrophilic coating rich in anionic sulfonic acid groups [1]. SPMK is a biocompatible surface treatment [2], which when used as an orthopaedic implant coating for articulating against cartilage can actively support tissue hydration [3]. Tribological testing against SCA bovine cartilage demonstrates that SPMK-g-PEEK maintains low friction, minimises cartilage strain, and reduces stress at the cartilage interface. Notably, SPMK-g-PEEK was found to support a greater interstitial fluid equilibrium, exhibited as a reduced cartilage strain [1, 4]. SPMK-g-PEEK sliding against cartilage provides fluid recovery through polyelectrolyte-enhanced tribological rehydration.

This study aims to elucidate the underlying mechanisms governing cartilage rehydration mediated by SPMK-g-PEEK and explore different tribological and adverse physiological conditions to examine the suitability of polyelectrolyte modified implant surfaces for synovial joint repair. By employing a flat SCA cartilage area (Fig. 1.7), no converging entrainment zone is present at the cartilage interface, meaning any cartilage rehydration observed is independent of conventional hydrodynamic tribological rehydration facilitated by a convergent wedge geometry [5].

4.3 Materials and Methodology

4.3.1 Materials

SPMK monomer, PBS, and 5 mm thick PEEK (450G. Victrex, UK) sectioned into 25 × 25 mm square samples with a surface roughness (R_a) of approximately 100 nm are employed in this study, as detailed in Section 3.3.1.

4.3.2 Tissue samples

SCA cartilage plugs, each 7.2 mm in diameter, were extracted from the patellofemoral grooves of bovine stifle joints using the methodology described in Section 3.3.2.

4.3.3 UV Photopolymerisation

Figure 4.1 demonstrates the UV initiated atom transfer radical polymerisation (ATRP) workflow by which 3-Sulfopropyl methacrylate potassium salt (SPMK) was grafted onto the surface of polished PEEK samples to produce SPMK-g-PEEK [1, 6, 7]. The resulting SPMK-g-PEEK surfaces end tethered polyelectrolyte interface possess anionic sulfonic acid groups, providing a hydrophilic, lubricious interface developed for biotribological applications. Detailed methodologies and associated chemistry are described in a prior publication on SPMK-g-PEEK (Sec. 3.3.3) [1].

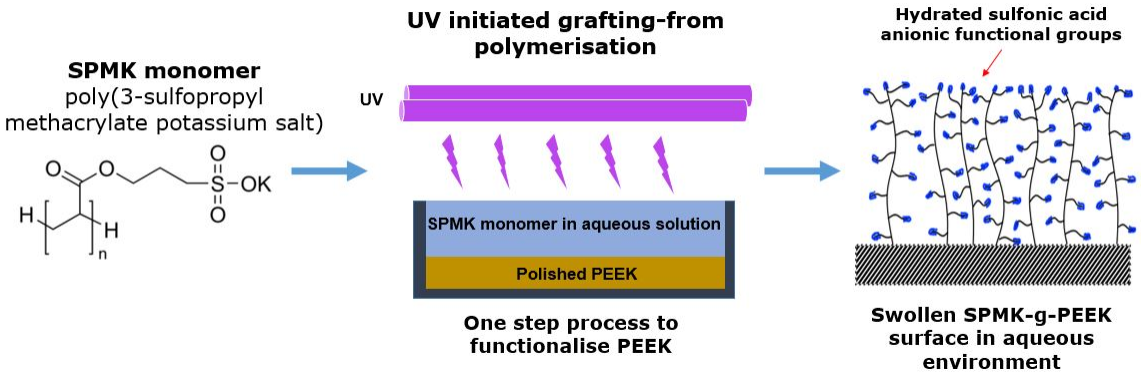

Figure 4.1: SPMK-g-PEEK workflow. SPMK monomer is dissolved at a 1 mol/L concentration in deionised water. The polished PEEK sample is then submerged in the aqueous SPMK solution and undergoes UV (365 nm) photopolymerisation for 90 minutes at an intensity of 5 mW/cm^2. Following grafting, the SPMK-g-PEEK sample is washed under a stream of deionised water to remove any unreacted monomer.

4.3.4 Mechanical Testing

A Bruker UMT Tribolab equipped with a reciprocating linear drive and a custom lubricant bath was employed for cartilage-pin tribological assessment against unfunctionalised PEEK and SPMK-g-PEEK plates. The testing apparatus fully submerged samples in phosphate-buffered saline (PBS) to simulate physiological osmotic conditions, thereby mitigating cartilage swelling and sustaining a hydrated equilibrium analogous to an *in vivo* environment. Closed-loop control concurrently measured the CoF (μ, Eq. 3.1) and the compressed cartilage height of cartilage (Δh) to calculate strain, ε (Eq. 3.2). This data collection protocol is the same as described

in Section 3.3.7, using a Keyence VHX-7000 microscope at 20× zoom to measure the swollen height (h_0) of cartilage to calculate strain (Sec. 3.3.8).

Throughout this study, only 7.2 mm diameter cartilage plugs were used, this was determined to be the largest cartilage plug that can be harvest from bovine condyles and still provide a SCA (Fig. 1.7) [1]. This is necessitated by the requirement to minimise any contribution of tribological rehydration borne through convergent wedge effects, in order to observe alternative mechanisms of tribological rehydration. Similarly during sliding tests a low speed of 10 mm/s was used to further minimise rehydration from previously described hydrodynamic effects.

Figure 4.2 shows the rehydration cycle testing protocol used to determine cartilage strain recovery after a period of interstitial fluid loss (also described in Fig. 1.7b). The protocol consists of an initial 30-minute compression phase, succeeded by a 30-minute compression-sliding phase at a linear reciprocating velocity of 10 mm/s over a sliding distance of 20 mm. Importantly, the cartilage remains under a constant normal load (F_Z) of 30 ± 3 N throughout the test, regulated via PID control. This load corresponds to a spatially averaged physiological contact pressure of approximately 0.75 MPa [8, 9].

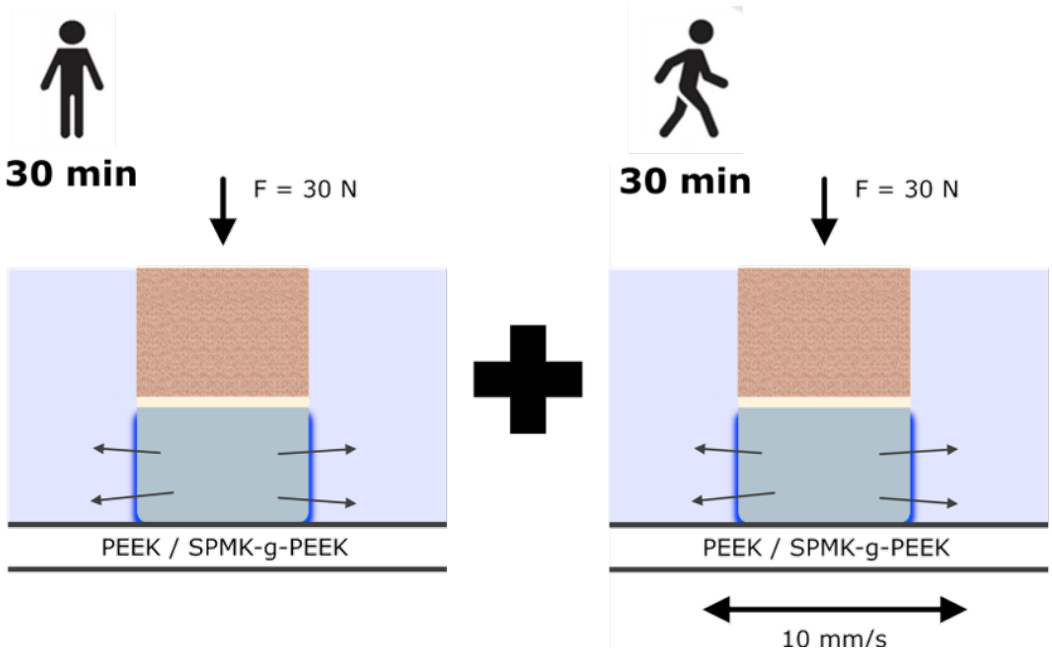

Figure 4.2: Schematic of the cartilage pin on plate UMT testing showing the physiological testing protocol of the compression (30 minute) and compression-sliding (30 minute) cycles.

For the evaluation of mechanical properties, Coefficient of Friction (CoF) and strain were averaged over the mid 50% of each reciprocating cycle to assess steady-state sliding conditions.

Strain response, characterised as viscoelastic time-dependent creep, was analysed through a custom Python 3.7 script based on a standard linear solid model.

4.3.5 Experimental Overview

To comprehensively understand the tribological behaviour of SCA cartilage against PEEK and SPMK-g-PEEK a systematic series of experiments were performed. The scope encompassed analysing the rehydration cycle (Fig. 4.2) for PEEK and SPMK-g-PEEK surfaces against freshly harvested and damaged cartilage samples, with inhibited rehydration, and for an overlapping 'unreplenished' contact zone. The methodologies adopted for each experimental condition, along with the underlying rationale, are discussed in the subsequent sections, and the specific experimental conditions are concisely summarised in Table 4.1. To ensure repeatability experiments were conducted triplicate (N = 3) for each test condition to ascertain average CoF and strain evolution during throughout the rehydration cycle.

Table 4.1: Summary of experimental conditions for the Rehydration Cycle, Abraded Cartilage, Inhibited Rehydration, and Overlapping SCA datasets. Every experiment underwent the rehydration cycle loading profile (Fig. 4.2b) and all experiments were conducted triplicate (N = 3) for each distinct set of conditions

Experiment	Interface	Cartilage	Lubricant	Stroke Length
Rehydration Cycle	- PEEK - SPMK-g-PEEK	Undamaged	PBS	20 mm
Abraded Cartilage	- PEEK - SPMK-g-PEEK	Abraded	PBS	20 mm
Diminished Rehydration	SPMK-g-PEEK	Undamaged	2M NaCl	20 mm
Overlapping SCA	SPMK-g-PEEK	Undamaged	PBS	1 mm 3.5 mm 7 mm

4.3.5.1 Rehydration Cycle

PEEK and SPMK-g-PEEK were tested against undamaged 7.2 mm SCA cartilage plugs undergoing the rehydration cycle defined in Fig. 4.2 in PBS lubricant. This experiment provides the preliminary assessment of the compression recovery and tribological performance between the unfunctionalised PEEK and SPMK modified surfaces.

4.3.5.2 Abraded Cartilage

SCA cartilage plugs were abraded using 250 µm grit paper, undergoing a 600 mm traversal while altering the orientation of the cartilage surface. This technique was employed to ensure the generation of a non-directional, uniformly damaged surface profile [10, 11]. Removal of the superficial zone is analogous to a situation of early cartilage degradation, and from a biomechanical perspective provides a more porous interface [10, 12]. Both PEEK and SPMK-g-PEEK surfaces underwent the rehydration cycle against damaged SCA cartilage to understand the fluid recovery mechanics of damaged tissue.

4.3.5.3 Diminished Rehydration

Rehydration cycles were performed in a 2 mol/L NaCl solution to impose a substantial osmotic gradient to inhibit rehydration and biphasic tribology of cartilage. This condition aims to isolate the contribution of hydration lubrication at the SPMK interface by inhibiting interstitial fluid recovery thus limiting the contribution of biphasic lubrication.

4.3.5.4 Overlapping SCA

Hydrogel and cartilage lubrication theories demonstrate that limiting hydration at the sliding interface through a short reciprocating overlapping stroke results in starvation of the contact area, consequently leading to elevated friction [13, 14]. Concentrating on a confined 'overlapping' regime, characterised by a stroke length shorter than the contact width, facilitates the investigation of the lubrication efficacy of SPMK-g-PEEK in an overlapped contact, analogous to the operational conditions of numerous physiological joints [14]. During overlap, the SPMK surface remains constantly constrained to prevent free swelling, thereby challenging the optimal hydration of the polyelectrolyte interface. Investigating different reciprocating lengths of 1, 3.5, and 7 mm enabled comparison of varying degrees of contact area overlap, in particular a non-replenished 'overlapping' regime where the stroke length is shorter than the contact width (1 mm and 3.5 mm sliding distances). For each test a peak velocity of 10 mm/s is maintained over the duration of the 1800 s sliding phase, hence for each test a total sliding distance of 18 m is achieved.

4.4 Results

Following unconfined compression and resultant interstitial fluid exudation from the cartilage, the initiation of sliding produced markedly low CoF of less than 0.01 when articulated against SPMK-g-PEEK samples. This was accompanied by notable interstitial fluid re-uptake and corresponding strain recovery. The summarised data for the Startup CoF (μ_S), Final CoF (μ_F), strain post-compression (ε_C), final strain post-sliding (ε_F), and recovered strain ($\varepsilon_r = \varepsilon_C - \varepsilon_F$) across rehydration cycles are presented in Table 4.2 highlighting the key experimental findings for tests defined in Table 4.1. The uncertainty values represent one standard deviation for CoF and strain at the start of sliding t = 1800 s (μ_S & ε_C respectively) and CoF and strain at the end of the sliding-rehydration phase at t = 3600 s (μ_F & ε_F respectively). The recovered strain (ε_r) is calculated as the mean strain recovery and standard deviation across each repeated rehydration cycle. The high standard deviation for strain values reflect the mechanical and poroviscoelastic variability of cartilage samples across unique bovine specimens and patellofemoral location of harvesting, these are consistent with previous studies of cartilage tribology with strain uncertainties of $> \pm 5\%$ [15, 16, 1].

Table 4.2: Consolidated data reflecting the Startup CoF (μ_S), Final CoF (μ_F), strain post-compression (ε_C), and post-sliding (ε_F), along with the recovered strain ($\varepsilon_r = \varepsilon_C - \varepsilon_F$) for the sliding (rehydration) phase, encompassing all experiments summarised in Table 4.1.

Test	μ_S (-)	μ_F (-)	ε_C (%)	ε_F (%)	ε_r (%)
Rehydration Cycles					
PEEK	0.234 ± 0.069	0.378 ± 0.021	40.72 ± 1.97	49.10 ± 3.05	-8.39 ± 1.24
SPMK-g-PEEK	0.010 ± 0.003	0.005 ± 0.001	41.02 ± 7.33	32.10 ± 5.90	8.05 ± 1.21
Abraded					
PEEK	0.188 ± 0.076	0.298 ± 0.073	34.34 ± 5.15	38.25 ± 3.53	-3.91 ± 1.76
SPMK-g-PEEK	0.014 ± 0.001	0.006 ± 0.001	35.89 ± 2.84	23.82 ± 4.84	12.06 ± 1.96
Diminished Rehydration					
NaCl - SPMK-g-PEEK	0.012 ± 0.002	0.005 ± 0.001	45.44 ± 4.94	43.83 ± 6.21	1.61 ± 1.72
Overlapping SCA					
1 mm	0.022 ± 0.015	0.004 ± 0.004	39.90 ± 2.79	33.88 ± 2.25	6.01 ± 0.58
3.5 mm	0.012 ± 0.002	0.009 ± 0.004	40.42 ± 5.31	32.16 ± 7.19	7.43 ± 1.71
7 mm	0.012 ± 0.007	0.008 ± 0.005	44.98 ± 9.82	36.41 ± 9.53	7.79 ± 0.68

4.4.1 Rehydration Cycles

As illustrated in Figure 4.3, the behaviour of SCA cartilage in contact with unfunctionalised PEEK (Fig 4.3a) and SPMK-g-PEEK (Fig 4.3b) during the rehydration cycles reveals distinct differences in compression recovery and tribological efficacy. At the onset of sliding cartilage SCA sliding against PEEK did not exhibit any compression recovery, rather exhibiting an additional $8.39 \pm 1.24\%$ further strain as interstitial fluid continued to be irreversibly efflux under load, yielding a final strain of $\varepsilon_F = 49.1 \pm 3.05\%$. Concurrently, the friction increases from an initial $\mu_S = 0.23 \pm 0.07$ up to $\mu_F = 0.38 \pm 0.02$ at the end of the test without reaching a steady equilibrium. The increasing strain and CoF during sliding indicates a continuing breakdown in biphasic lubrication, inhibiting hydration at the interface and loss of interstitial fluid pressurisation. Conversely, for SPMK-g-PEEK the cartilage strain recovered by $8.05 \pm 1.21\%$ during sliding, demonstrating re-uptake of interstitial fluid upon the onset of sliding for a final reduced strain of $\varepsilon_F = 32.1 \pm 5.9\%$. The hydrated interface facilitates a low startup $\mu_S = 0.01 \pm 0.003$ and marginally decreased to a stable CoF of $\mu_F = 0.005 \pm 0.001$ observed throughout the majority of the 30 minute sliding cycle.

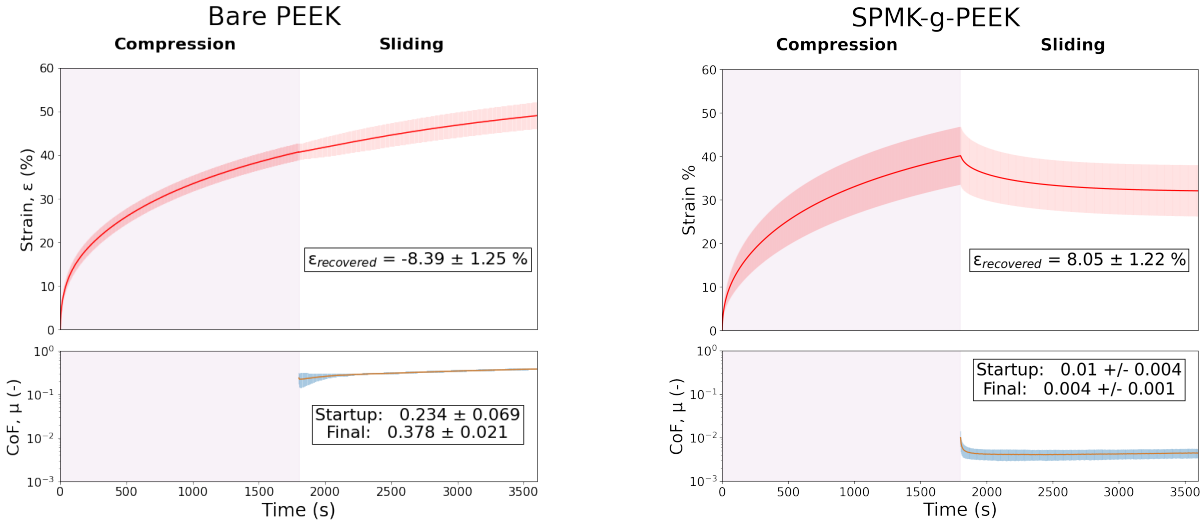

(a) PEEK (b) SPMK-g-PEEK

Figure 4.3: Compression and CoF data for the rehydration cycles of (a) unfunctionalised PEEK (N = 3) showing no evidence of rehydration upon the onset of sliding and (b) SPMK-g-PEEK (N = 3) showing strain recovery upon sliding.

4.4.2 Abraded Cartilage

Figure 4.4 shows the rehydration cycle for cartilage which has been abraded with sandpaper to simulate damaged cartilage, sliding against PEEK (Fig 4.4a) and SPMK-g-PEEK (Fig 4.4b).

In relation to the healthy cartilage benchmarks in Figure 4.3a, abraded cartilage sliding against PEEK exhibits reduced post compression strain of $\varepsilon_C = 34.3 \pm 5.2\%$ which upon the onset of sliding continues to increase at a reduced rate towards a final strain of $\varepsilon_F = 38.3 \pm 3.5\%$, culminating in a ε_r increase of $3.9 \pm 1.8\%$. The startup $\mu_S = 0.19 \pm 0.08$ is comparable to the undamaged cartilage case, and increases quickly towards a quasi-steady and final $\mu_F = 0.30 \pm 0.07$.

Abraded cartilage sliding against SPMK-g-PEEK recovers a greater fraction of cartilage strain ($\varepsilon_r = 12.1 \pm 2.0\%$) compared to the undamaged control in Fig 4.3b. The CoF trend matches the healthy cartilage benchmark, with a startup $\mu_S = 0.005 \pm 0.001$ quickly stabilising to a final equilibrium $\mu_F = 0.006 \pm 0.001$. Demonstrating that for a scenario where cartilage has been biomechanically diminished, SPMK-g-PEEK still provides an interface that can support the biphasic and hydrated boundary tribology of cartilage.

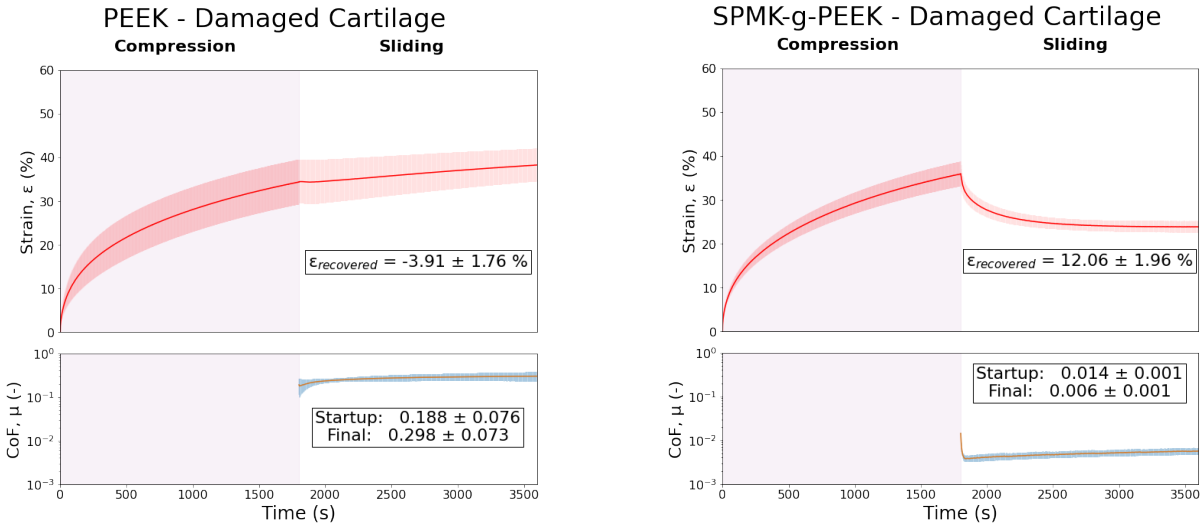

(a) PEEK (b) SPMK-g-PEEK

Figure 4.4: Compression and CoF data for the rehydration cycles of (a) unfunctionalised PEEK (b) SPMK-g-PEEK against cartilage samples that have been abraded with 250 μm grit sandpaper.

4.4.3 Diminished Rehydration

Figure 4.5 shows the average compression and friction data for the rehydration cycle of cartilage against SPMK-g-PEEK immersed in a 2mol/L NaCl solution to inhibit the rehydration of articular cartilage. The high osmotic gradient of the salt solution likely contributed to the high strain following the compression phase ($\varepsilon_C = 45.4 \pm 4.9\%$), and also minimal strain recovery during sliding where interstitial fluid recovery was inhibited, resulting in a recovery of only

$\varepsilon_r = 1.6 \pm 1.7\%$ but nonetheless during sliding the SPMK-g-PEEK did facilitate cartilage rehydration. The frictional characteristics are consistent with those observed for SPMK-g-PEEK in a phosphate-buffered saline (PBS) control environment (Fig 4.3b). Initial startup friction initiates at $\mu_S = 0.012 \pm 0.002$ and swiftly plateaus to a stable $\mu_F = 0.005 \pm 0.001$.

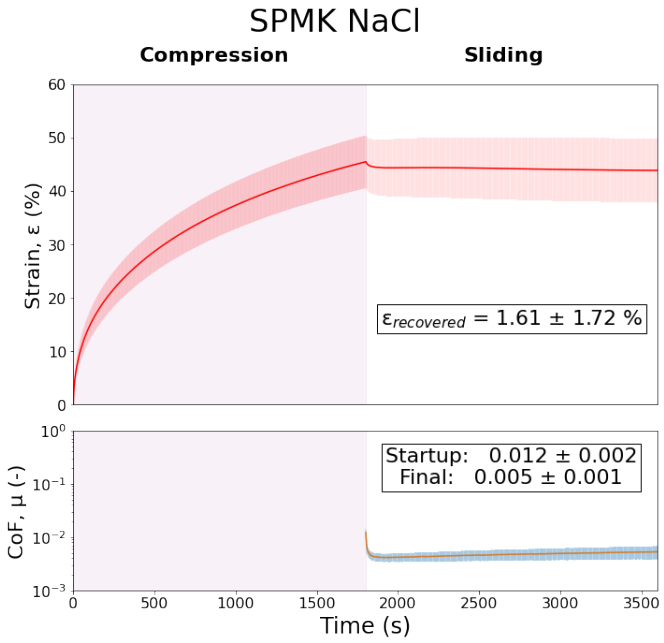

Figure 4.5: Compression and CoF data for the rehydration cycle of SPMK-g-PEEK samples submerged in 2mol/L NaCl water to inhibit fluid flow.

4.4.4 Overlapping Contact Area

Figure 4.6 displays the mean strain and frictional response for three distinct stroke lengths, 1 mm, 3.5 mm, and 7 mm, corresponding to the sliding phase of the rehydration cycle, as depicted in Figure 4.2. These profiles exemplify three unique contact configurations characterised by different degrees of overlap, enabling assessment of whether SPMK-g-PEEK can effectively promote cartilage rehydration and enhance lubrication whilst the SPMK polyelectrolyte interface is constrained from free-swelling between strokes.

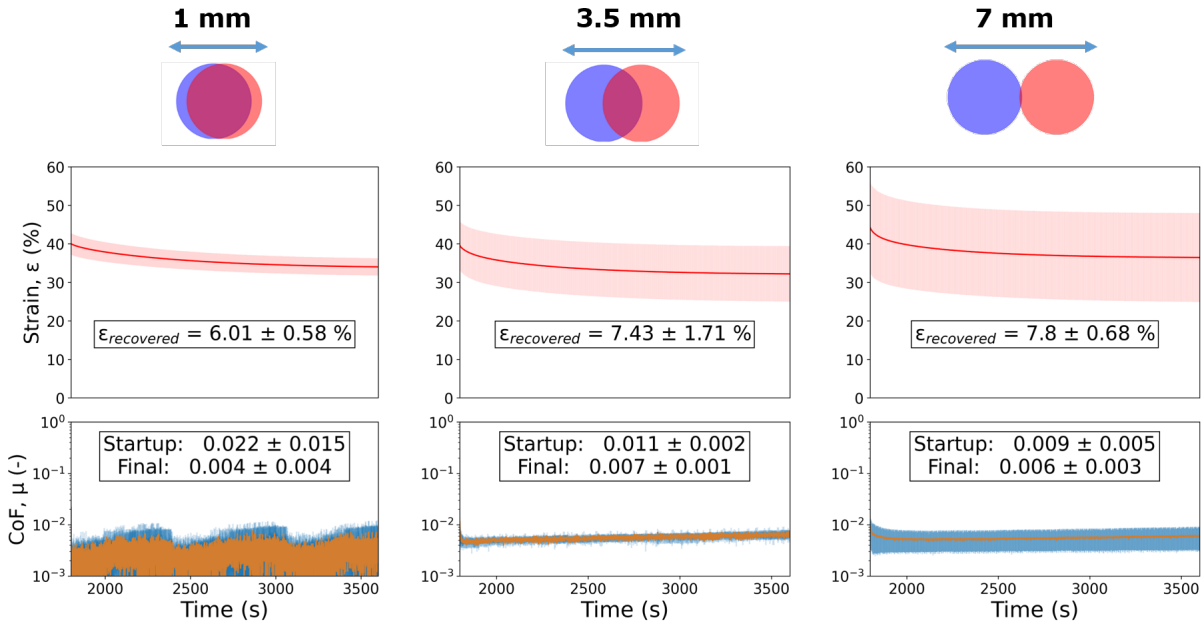

Figure 4.6: Compression and CoF data for the just the sliding phase of the rehydration cycle for sliding with a stroke length of (a) 1 mm (b) 3.5 mm (c) 7 mm.

Strain recovery for both the overlapped (1 mm, 3.5 mm stroke) and non-overlapped (7 mm stroke) conditions exhibit comparable CoF behaviour with low startup μ_S between 0.03 - 0.01, and in all cases rapidly reaching a sustained steady state CoF with $\mu_F < 0.01$. Total strain recovery during sliding was commensurate with increasing sliding distance. The shortest 1 mm reciprocating distance exhibited the lowest $\varepsilon_r = 6.0 \pm 0.6\%$, followed by 3.5 mm sliding with $\varepsilon_r = 7.4 \pm 1.7\%$, and finally 7 mm sliding $\varepsilon_r = 7.8 \pm 0.7\%$. Compared to the 20 mm stroke rehydration cycle (Fig. 4.3b) which exhibited $\varepsilon_r = 8.1 \pm 1.2\%$, the predominantly overlapped condition of 1 mm sliding showed a reduced ability to recover interstitial fluid.

4.5 Discussion

This study elucidates the efficacy of SPMK-g-PEEK to facilitate low friction and modulate cartilage hydration through a novel mechanism of tribological rehydration. Our findings reveal that SPMK-g-PEEK significantly enhances strain recovery during sliding consistently in the conditions outlined. Soft biomimetic interfaces may be a key advance in biomaterials utilised within articulating surfaces for joint prostheses, addressing the limitation of conventional polymeric and metallic surfaces that fail to emulate the intrinsic biphasic and hydrated tribology of articular cartilage. The subsequent sections will delineate the promising performance of the SPMK-g-PEEK - cartilage interface and the mechanisms underlying the SPMK polyelectrolyte

ability to maintain low friction and facilitate interstitial fluid recovery.

4.5.1 SPMK-g-PEEK Tribological Rehydration

By employing a rehydration cycle (Fig. 4.2) it was possible to directly observe and quantify compression recovery of cartilage during sliding. Unfunctionalised PEEK demonstrated continued compression at the onset of sliding, characteristic of a cartilage SCA which provides no entrainment zone for fluid recovery, subsequently throughout the test CoF continued to increase as biphasic lubrication diminished, depriving the contact area of lubricating interstitial fluid [17]. This yielded an increasing CoF of 0.23 up to 0.38, which is consistent with previous 30 - 60 minute tests for SCA cartilage sliding against a hard planar counter-face [18, 19, 20].

For the same SCA configuration with SPMK-g-PEEK, cartilage was able to re-uptake interstitial fluid during sliding characterised by a reduced strain along with a rapidly stabilised μ_F of 0.005. SPMK-g-PEEK surfaces provide an interface with performance akin to natural cartilage-cartilage biomechanics [18]. Notably, even in adverse conditions where the surface of cartilage has been abraded or the rehydration has been inhibited by an osmotic gradient, SPMK-g-PEEK continued to facilitate low CoF of ~ 0.01 at the interface along with tribological rehydration to reduce overall strain. The low friction coefficients achieved in this study are the same magnitude as MPC functionalised Co-Cr-Mo sliding against cartilage [21]. Whilst this previous study briefly postulates that the MPC polymer brush provides a water source for rehydration of cartilage contributing to a sustained low CoF, our findings go a step further by providing empirical evidence of the rehydration mechanism through direct observation of cartilage strain recovery, a process underpinned by a highly hydrated multiphase interface composed of hydrophilic polyelectrolytes.

The CoF and strain recovery observed in this study for the SPMK-g-PEEK and SCA cartilage contact pair are similar in magnitude to studies by Burris on tribological rehydration of cSCA cartilage on glass [16, 15]. Adopting a similar rehydration protocol of 30 minutes compression followed by 30 minutes sliding, strain recovery (ε_r) was reported between 3% and 7%, initially presenting relatively high startup CoF of 0.17 - 0.20 before settling to lower equilibrium CoF of 0.03 - 0.06 [16, 15]. However, in these studies all tribological rehydration was contingent on a cSCA cartilage plug and high speeds of 80 mm/s, which facilitates fluid entrainment borne through convergent wedge hydrodynamics [5, 22]. Contrasting with these findings, the SPMK-

g-PEEK-mediated rehydration demonstrated in this study occurs under flat SCA conditions and at significantly reduced speeds (10 mm/s). This observation not only expands the conventional scope of tribological rehydration but also suggests alternative mechanisms at play beyond convergent wedge hydrodynamic entrainment.

The low friction achieved by tethered polyelectrolytes is lower than cartilage-cartilage contacts in a migrating contact geometry (MCA), which exhibit steady state CoF in the range 0.02 - 0.04 along with tribological rehydration [18, 23]. While our study corroborates the rehydration that underpins biphasic lubrication for cartilage interfaces, for SPMK-g-PEEK the markedly lower startup CoF and rapid approach to equilibrium CoF of less than 0.01 can be attributed to the inherent low friction characteristics of hydration shells which provide a highly lubricious aqueous interface [24].

The consistency of low CoF and rehydration, irrespective of healthy cartilage biomechanical function, underscores the promising tribological properties of SPMK-g-PEEK as a material choice for cartilage interfacing implant surfaces for patients with early-stage cartilage disease. In this study, the observed peak cartilage strains of approximately 30 - 40% are significantly higher than the typical *in vivo* strains of 5 - 10% [25]. However, prior research indicates that strains within this range do not compromise the mechanical integrity of the cartilage [26]. Additionally, a previous study investigating SCA cartilage interfaced with SPMK-g-PEEK under identical loading conditions reported no cartilage fibrillation after 2.5 hours of sliding [1]. Therefore, these higher strains likely do not introduce an error related to damage in the collagen matrix when examining tribological rehydration post-compression. Effective tribological rehydration has been shown to mitigate cartilage cell death by supporting a high fluid load fraction and lubricity [27]. Elevated fluid pressurisation not only reduces friction but also provides essential mechanical support to cartilage, mitigating degenerative effects often seen in early stage cartilage disease [28, 29].

4.5.2 Role of Polyelectrolyte Lubrication

SPMK polyelectrolyte interfaces are innately lubricious due to the hydrophilic sulfonic acid groups which facilitate hydration lubrication [30]. This explains the overall lower startup CoF (< 0.02) observed for all tests against SPMK-g-PEEK, compared to previous experiments on cSCA cartilage against glass which exhibited startup CoF of $\mu_S \sim 0.17$ - 0.20 [16, 15].

Conventional understanding of sustained cartilage lubrication requires competing interstitial fluid recovery to closely match efflux, sustaining interstitial fluid pressure and a constant supply of lubricant at the cartilage interface. For a MCA or cSCA contact configuration, the temporal CoF response of cartilage in sliding ($\mu(t)$) can be represented as a function of solid phase friction (μ_{eq}) and the interstitial fluid load fraction (F') shown in Equation 1.2 [20, 31]. This relationship demonstrates that low friction can only be sustained with a high degree of interstitial fluid pressure, which has a non-linear relationship to cartilage strain [31, 32].

However, the impeded rehydration of cartilage against SPMK-g-PEEK conducted in 2 mol/L NaCl (Fig. 4.5) only recovered 1.6% strain throughout sliding whilst rapidly stabilising a low friction of 0.005, the same CoF evolution observed for SPMK-g-PEEK in PBS where uninhibited rehydration recovered 8.4% strain (Fig. 4.3b). The presence of surface tethered SPMK polyelectrolytes offers a persistent boundary lubricant with viscous fluid characteristics [33, 34]. This indicates that the lubrication performance of SPMK-g-PEEK against cartilage is primarily controlled by the highly hydrated SPMK polyelectrolyte interface, with a minimal reliance on the effectiveness of biphasic lubrication arising from interstitial pressurisation.

4.5.3 Mechanism of polyelectrolyte-enhanced tribological rehydration

After the compression phase, the strain (ε_C) in both PEEK and SPMK-g-PEEK samples was approximately 40%, as shown in Table 4.2. This result indicates that the presence of the SPMK interface does not influence interstitial fluid efflux under static conditions. The rehydration of these materials only occurs upon the initiation of sliding, suggesting that the SPMK-g-PEEK interface activates a dynamic lubrication mechanism that is not reliant on alterations to the porosity of the cartilage. Specifically, the sliding motion appears to generate sufficient fluid pressure to overcome the interstitial fluid pressure of the cartilage, thereby facilitating fluid ingress towards a reduced strain equilibrium. This tribological rehydration mechanism, observed in experiments using a flat SCA cartilage contact model, deviates from the mechanisms described in existing literature, which typically involve hydrodynamic pressurisation at a convergent inlet in models using a larger curved cSCA cartilage contact [5, 22].

Primarily, the presence of a swollen, highly hydrated polyelectrolyte layer acts as a replenishing source of water, thus facilitating the rehydration of articular cartilage [1]. The mechanisms underlying polyelectrolyte-enhanced tribological rehydration of cartilage is hypothesised to be

a combination of micro elastohydrodynamic lubrication (μEHL) and polyelectrolyte enhanced elastohydrodynamic lubrication (PB-EHL) [33, 35, 3]. Established theories of μEHL theories suggest that the surface roughness of cartilage, which has a relatively low elastic modulus, is smoothed by two orders of magnitude under modest loading conditions. This smoothing effect facilitates the formation of a fluid film, enabling effective lubrication at the cartilage contact [35, 36, 37].

Polyelectrolytes and gel layers substantially enhance elastohydrodynamic lubrication (EHL) film thickness and lower the transition speed required to achieve an EHL regime in aqueous lubrication [38, 39]. Optical interferometry tribological assessments of various hydrophilic polymer brush interfaces reveal that these materials maintain a stable aqueous film approximately 30 - 35 nm thick at low entrainment speeds (around 10^{-3} mm/s), attributed to the hydration effects of the polymer brushes [40, 41]. At speeds increase to $\sim 10^{-2}$ mm/s, a low speed transition is observed to a PB-EHL regime with fluid films rapidly expanding up to 100 nm thick [41, 33]. Contrasting to classical EHL theories which necessitate viscous lubricants for a separating fluid film. In aqueous systems, the presence of a swollen polymer brush layer itself can behave as a viscous lubricant to produce PB-EHL at low speeds [41, 30, 42, 40, 38]. At the nanoscale, it is hypothesised that compression of the swollen, hydrophilic SPMK polyelectrolyte concentrates water molecules, thereby enhancing EHL formation through increased fluid pressurisation [1, 3].

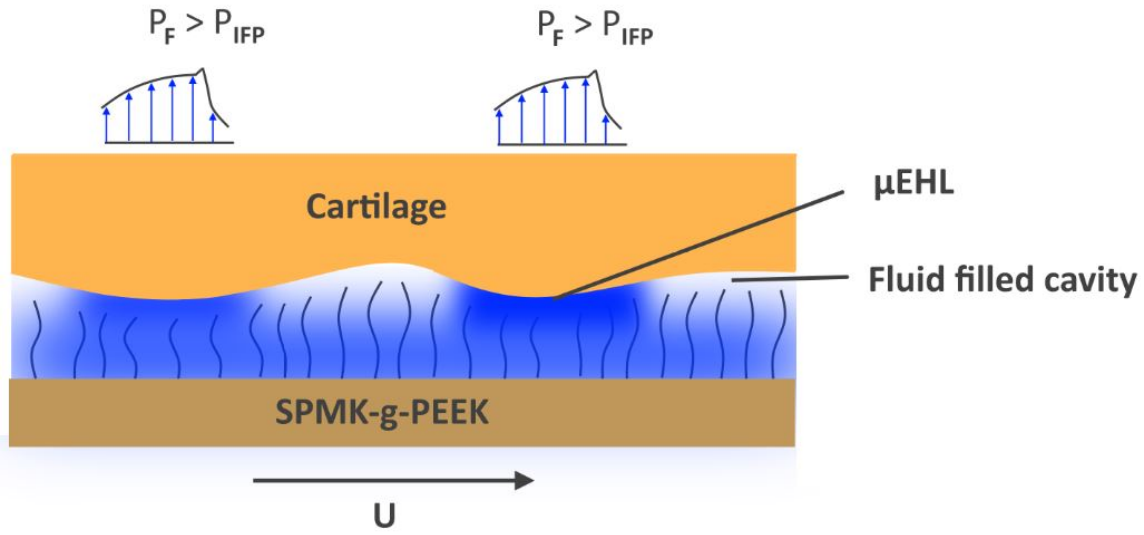

Figure 4.7: Proposed lubrication regime showing cartilage deformation giving rise to local regions of μEHL where a polyelectrolyte enhanced fluid film is present. Postulating where the fluid pressure is greatest (P_F) this overcomes the interstitial pressure of the cartilage ($P_F > P_{IFP}$) fluid can be imbibed back into cartilage, facilitating polyelectrolyte-enhanced tribological rehydration.

Figure 4.7 shows the proposed lubrication regime for polyelectrolyte enabled tribological rehydration. At regions of μEHL fluid film formation, the PB-EHL enhanced viscosity of the water lubricating layer may give rise to a fluid pressure gradient. Nearest the outlet of the contact where the fluid pressure (P_F) is the highest and overcomes the interstitial fluid pressure of cartilage ($P_F > P_{IFP}$) water can be recovered by the cartilage, leading to tribological rehydration and overtime reducing the overall strain of cartilage during sliding. The presence of polyelectrolytes can reduce the speeds required for the evolution of EHL lubrication fluid films and due to the enhanced local viscosity, PB-EHL can give rise to greater local fluid pressures and thicker fluid films than water alone. This is akin to a mode of boosted lubrication, whereby the presence of biological macromolecular polyelectrolytes native to synovial fluid (i.e. hyaluronic acid, lubricin) in the contact gap can increase viscosity leading to enhanced hydrodynamic pressurisation at reduced speeds [43, 44, 45]. Biological polyelectrolyte constituents of synovial fluid have been widely compared to polymer brush tribology, providing both a highly effective boundary lubricant and affinity to maintain fluid film lubrication [46, 47]. For SPMK-g-PEEK, instead of relying on entrainment and confinement of polyelectrolytes, the SPMK is tethered to the PEEK substrate providing unabating boosted lubrication localised at the contacting asperities of the SCA cartilage counterface [3].

For SPMK-g-PEEK sliding against an SCA cartilage plug the total strain recovery plateaued following an exponential decay in total strain until a reduced strain equilibrium is reached. For undamaged PEEK sliding at 10 mm/s the total recovery was $\varepsilon_r = 8.1 \pm 1.2\%$ demonstrating a mechanistic limit to overall strain recovery of cartilage. The hypothesis presented here posits an equilibrium state is reached between the fluid film pressure, denoted as P_F, and the interstitial fluid pressure of cartilage, P_{IFP}. Cartilage mimicking early signs of degradation the cartilage abraded with 250 μm grit sandpaper exhibits a greater overall strain recovery (Fig. 4.4b, $\varepsilon_r = 12.1 \pm 2.0\%$) compared to the undamaged control (Fig. 4.3b, $\varepsilon_r = 8.1 \pm 1.2\%$). Suggesting that the rougher, abraded cartilage surface will yield higher local asperity pressurisation leading to increased local fluid pressures and hence a greater degree of cartilage interstitial fluid recovery. However, further studies with larger sample sizes and higher experimental repeats are required to confirm this hypothesis. Additionally, inducing controlled cartilage degradation using trypsin or employing clinically relevant scoring methods for cartilage damage would provide more robust insights [48].

4.5.4 Effect of Overlapping Contact on Rehydration

Hydrogel and cartilage lubrication requires the contact area to remain hydrated, for short distance reciprocating contacts exhibiting an overlapping contact area, friction characteristically increases as the lubricant is unreplenished in the overlapped sliding area [13, 14]. Similarly, polymer brush tribology relies heavily on sustained hydration to ensure lubricity [30, 33]. Additionally, under compressive forces, surfaces functionalised with polyelectrolytes undergo dehydration, leading to a partial collapse of the brush structure, a reduction in water volume, and consequently, increased friction [49, 50].

Testing overlapped contact areas (Fig. 4.6) demonstrates reduced strain recovery for the overlapped 1 mm sliding distance $\varepsilon_r = 6.0 \pm 0.6\%$ compared to the $\varepsilon_r \sim 8\%$ for longer sliding distances. Upon modelling the strain recovery time constant (τ) using a single-phase exponential decay function (Equation 4.1), the 1 mm stroke condition corresponding to the greatest overlap area exhibits a protracted recovery time of $\tau = 611$ s. In contrast, the 7 mm (Fig 4.6c) and 20 mm (Fig 4.3b) non-overlapped conditions demonstrate nearly equivalent, and notably shorter, rehydration times of 358 s and 384 s respectively shown in Figure 4.8. Despite the reduced strain recovery (τ) for the 1 mm overlapping contact condition, CoF still remains characteristically low, with startup and rapid stabilisation to the final CoF observed for all conditions ~ 0.01 (Fig. 4.6). This suggests that the hydrophilic SPMK polyelectrolyte, even under persistent compression in the overlapped sliding area, maintains a substantial water content, thereby providing an effective swollen lubricating interface. Similar ATRP produced polymer brush interfaces (MPC & SPMK) with hydrophilic functional groups necessitate pressures of above 100 MPa before dehydration and subsequent breakdown of lubricity occurs [51, 52]. For SPMK the tenaciously bound hydration shells due to the anionic sulfonic acid groups can effectively resist dehydration under the 0.75 MPa physiological contact pressures used in this study.

The rehydration of the cartilage is hypothesised to arise from a synergistic effect of augmented fluid films, attributable to PB-EHL, in conjunction with the water-retentive properties of the hydrophilic SPMK polyelectrolyte, which acts as a fluid reservoir for rehydration. The observed diminution in overall rehydration and the decelerated strain recovery rate associated with shorter overlapping stroke lengths can likely be attributed to the incomplete formation of the fluid film. Conventional hydrodynamic film development necessitates a stroke length exceeding twice the

contact width for full fluid film development [14, 53]. Nevertheless, notable cartilage rehydration is observed even at the minimal 1 mm reciprocating distance, with ε_r recorded at 6.0 ± 0.6%, suggesting that the rehydration mechanism is predominantly facilitated by the hydrophilic SPMK, which serves as an effective fluid reservoir.

$$\varepsilon_{sliding}(t) = \varepsilon_C + \varepsilon_r \cdot e^{(\frac{-t}{\tau})} \tag{4.1}$$

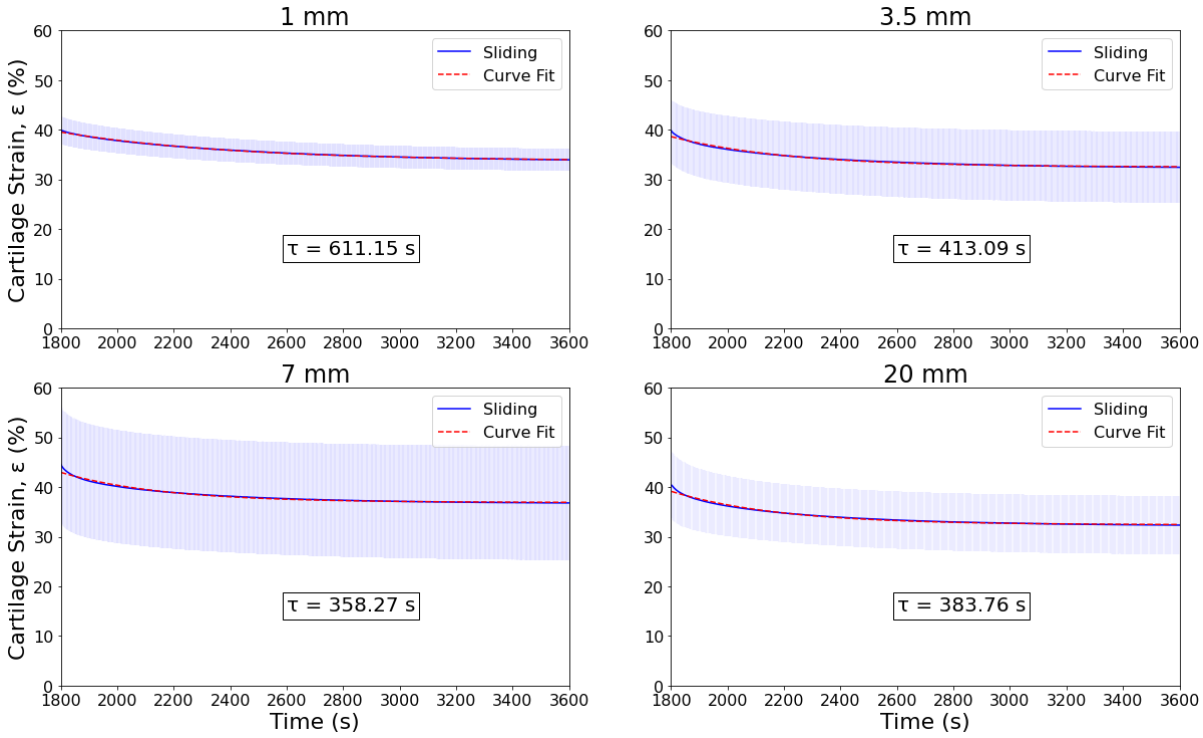

Figure 4.8: Rate of tribological rehydration strain recovery τ calculated for 1 mm, 3.5 mm, 7 mm, and 20 mm reciprocating distances for SCA cartilage against SPMK-g-PEEK.

4.5.5 Limitations & Future Work

Comparative clinical data suggest that healthy knee cartilage should experience strains between 5 - 10% during gait activities [25], whereas the final strain observed with SPMK-g-PEEK implants was approximately 30%. This discrepancy may also be influenced by the rate of cartilage loading, as *in vivo* cartilage experiences both constant and dynamic loading conditions. Whilst a major finding of this study is the novel demonstration of polyelectrolyte tribological rehydration, it is necessary to understand the cumulative strain recovery through a combined cSCA/MCA and SPMK-g-PEEK tribological study. The authors speculate that the combined tribological rehydration effects of a conformal or convergent contact geometry and the boosted

cartilage rehydration facilitated by SPMK-g-PEEK could closer emulate physiological cartilage interstitial fluid mechanics and support.

The scope of this paper honed in on empirical evidence of polyelectrolyte mediated cartilage strain recovery, with experiments designed to elucidate the underpinning roles of hydration lubrication and contact dynamics which reimbibe fluid into cartilage. As such, all experiments have been performed in hour long tests in a contact configuration unlike the conformal geometry of synovial joints. In order to escalate technology readiness, longer tests will be performed along with physiological duty cycles (e.g. gait) to understand the long term performance and potential failure mechanisms of SPMK-g-PEEK.

Finally, Section 4.5.3 which explores the PB-EHL mechanism of tribological rehydration relies on EHL theory developed for classical engineering bearings, non-aqueous systems, or confined polymer brush systems [33, 42, 53]. Whilst contextualisation of this study against the aforementioned literature provides insight into the SPMK contact dynamics, there exists a gap in the literature that fully encapsulates the complex tribological interplay observed in this research. The interface formed by polyelectrolyte surfaces interfaced with cartilage requires an intricate model encompassing the permeable poroviscoelastic mechanics of cartilage along with the macromolecular and nanorheological dynamics of SPMK. PB-EHL is a plausible hypothesis for the observed cartilage rehydration, an upcoming study will seek to further validate the PB-EHL hypothesis across a range of speeds and contact configurations.

4.6 Conclusions

Three key characteristics of SPMK-g-PEEK have been identified which elucidate the unique demonstration of sustained lubrication and tribological rehydration for a flat stationary contact area cartilage plug. Firstly, the SPMK polyelectrolyte provides a boundary lubricant which provides a highly hydrated viscous lubricious interface, and against cartilage offers a highly lubricious counter-face even in absence of biphasic lubrication. Secondly, the high density of surface tethered hydrophilic sulfonic acid groups provides an aqueous reservoir as a source for cartilage interstitial fluid recovery. And thirdly, tribological rehydration is facilitated by polyelectrolyte enhanced elastohydrodynamic lubrication, akin to boosted lubrication, where the surface tethered SPMK enhance the local viscosity to provide substantial pressurised fluid films.

This study presents SPMK-g-PEEK as a compelling biocompatible coating for orthopaedic implants articulating against cartilage. Providing support for the native biomechanics of articular cartilage, offering both low friction $\mu \sim 0.01$ along with enhanced interstitial fluid load support and cartilage strain recovery of $\sim 8\%$. Notably, SPMK-g-PEEK maintains consistent tribological performance even under conditions where cartilage surfaces are damaged or incapable of sustaining normal interstitial fluid homeostasis. The SPMK polyelectrolyte interface provides further insight into modes of tribological rehydration beyond prevailing theories contingent on high speed, convergent geometry hydrodynamic fluid pressurisation [18, 17, 14].

SPMK-g-PEEK surface exhibits lubrication characteristics that surpass traditional hydrodynamic and biphasic lubrication models, achieving lower friction coefficients at reduced sliding speeds. This expands the scope of tribological applications to include conditions where high-speed fluid entrainment is not feasible, such as in low-mobility patients or in smaller planar joints where large articulating motions are limited. The tribological performance of synthetic polymers in contact with cartilage has substantial implications for orthopaedic applications, particularly for the next generation of hemiarthroplasty and focal cartilage resurfacing. Furthermore, this has expanded the scope of mechanisms underpinning tribological rehydration and highlights the substantive tribological efficacy of hydrophilic macromolecules, providing further insight into the role of biopolyelectrolytes, such as lubricin and hyaluronic acid, in synovial biotribology.

References

[1] Robert J Elkington, Richard M Hall, Andrew R Beadling, Hemant Pandit, and Michael G Bryant. Highly lubricious spmk-g-peek implant surfaces to facilitate rehydration of articular cartilage. *Journal of the Mechanical Behavior of Biomedical Materials*, page 106084, 2023.

[2] Yunlong Yu, Marco Cirelli, Pengfei Li, Zhichao Ding, Yue Yin, Yucheng Yuan, Sissi De Beer, G Julius Vancso, and Shiyong Zhang. Enhanced stability of poly (3-sulfopropyl methacrylate potassium) brushes coated on artificial implants in combatting bacterial infections. *Industrial & Engineering Chemistry Research*, 58(47):21459–21465, 2019.

[3] Robert J Elkington, Richard M Hall, Andrew R Beadling, Hemant Pandit, and Michael G Bryant. Brushing up on cartilage lubrication: Polyelectrolyte-enhanced tribological rehydration. *Langmuir*, 2024.

[4] Robert Elkington, Andrew Beadling, Richard Hall, Hemant Pandit, and Michael Bryant. Biomimetic highly lubricious polyelectrolyte functionalized peek surfaces for novel hemiarthroplasty implants and focal resurfacing. In *Orthopaedic Proceedings*, volume 103, pages 34–34. Bone & Joint, 2021.

[5] David L Burris and Axel C Moore. Cartilage and joint lubrication: new insights into the role of hydrodynamics. *Biotribology*, 12:8–14, 2017.

[6] Motoyasu Kobayashi and Atsushi Takahara. Tribological properties of hydrophilic polymer brushes under wet conditions. *Chemical Record*, 10(4):208–216, 2010.

[7] Motoyasu Kobayashi and Atsushi Takahara. Polyelectrolyte brushes : a novel stable lubrication system in aqueous conditions. pages 403–412, 2012.

[8] W A Hodge and W H Harris. Contact pressures in the human hip joint measured in vivo. 83(May):2879–2883, 1986.

[9] Richard A Brand. Joint contact stress: a reasonable surrogate for biological processes? *The Iowa orthopaedic journal*, 25:82, 2005.

[10] Eiji Tanaka, Tatsunori Iwabe, Diego A Dalla-Bona, Nobuhiko Kawai, Theo van Eijden, Masao Tanaka, Shoji Kitagawa, Takashi Takata, and Kazuo Tanne. The effect of experimental cartilage damage and impairment and restoration of synovial lubrication on friction in the temporomandibular joint. *Journal of orofacial pain*, 19(4), 2005.

[11] Edward H Chiang, Timothy J Laing, Charles R Meyer, Jennifer L Boes, Jonathan M Rubin, and Ronald S Adler. Ultrasonic characterization of in vitro osteoarthritic articular cartilage with validation by confocal microscopy. *Ultrasound in medicine & biology*, 23(2):205–213, 1997.

[12] Salvatore Federico and Walter Herzog. On the anisotropy and inhomogeneity of permeability in articular cartilage. *Biomechanics and modeling in mechanobiology*, 7:367–378, 2008.

[13] Mario Alberto Accardi, Daniele Dini, and Philippa M Cann. Experimental and numerical investigation of the behaviour of articular cartilage under shear loading—interstitial fluid pressurisation and lubrication mechanisms. *Tribology International*, 44(5):565–578, 2011.

[14] Elze Porte, Philippa Cann, and Marc Masen. A lubrication replenishment theory for hydrogels. *Soft Matter*, 16(45):10290–10300, 2020.

[15] Margot S Farnham, Kyla F Ortved, Jeffrey S Horner, Norman J Wagner, David L Burris, and Christopher Price. Lubricant effects on articular cartilage sliding biomechanics under physiological fluid load support. *Tribology Letters*, 69:1–14, 2021.

[16] Margot S Farnham, Riley E Larson, David L Burris, and Christopher Price. Effects of mechanical injury on the tribological rehydration and lubrication of articular cartilage. *Journal of the Mechanical Behavior of Biomedical Materials*, 101:103422, 2020.

[17] Axel C Moore and David L Burris. Tribological rehydration of cartilage and its potential role in preserving joint health. *Osteoarthritis and cartilage*, 25(1):99–107, 2017.

[18] Matteo Caligaris and Gerard A Ateshian. Effects of sustained interstitial fluid pressurization under migrating contact area, and boundary lubrication by synovial fluid, on cartilage friction. *Osteoarthritis and Cartilage*, 16(10):1220–1227, 2008.

[19] Gerard A Ateshian. The role of interstitial fluid pressurization in articular cartilage lubrication. *Journal of biomechanics*, 42(9):1163–1176, 2009.

[20] H Forster and J Fisher. The influence of loading time and lubricant on the friction of articular cartilage. *Proceedings of the Institution of Mechanical Engineers, Part H: Journal of Engineering in Medicine*, 210(2):109–119, 1996.

[21] Masayuki Kyomoto, Toru Moro, Ken-ichi Saiga, Fumiaki Miyaji, Hiroshi Kawaguchi,

Yoshio Takatori, Kozo Nakamura, and Kazuhiko Ishihara. Lubricity and stability of poly (2-methacryloyloxyethyl phosphorylcholine) polymer layer on co–cr–mo surface for hemi-arthroplasty to prevent degeneration of articular cartilage. *Biomaterials*, 31(4):658–668, 2010.

[22] DL Burris, L Ramsey, BT Graham, C Price, and AC Moore. How sliding and hydrodynamics contribute to articular cartilage fluid and lubrication recovery. *Tribology Letters*, 67:1–10, 2019.

[23] Maria Parkes, Francesca Tallia, Gloria R Young, Philippa Cann, Julian R Jones, and Jonathan RT Jeffers. Tribological evaluation of a novel hybrid for repair of articular cartilage defects. *Materials Science and Engineering: C*, 119:111495, 2021.

[24] Weifeng Lin and Jacob Klein. Hydration lubrication in biomedical applications: From cartilage to hydrogels. *Accounts of materials research*, 3(2):213–223, 2022.

[25] Chinmay S Paranjape, Hattie C Cutcliffe, Steven C Grambow, Gangadhar M Utturkar, Amber T Collins, William E Garrett, Charles E Spritzer, and Louis E DeFrate. A new stress test for knee joint cartilage. *Scientific reports*, 9(1):2283, 2019.

[26] CP Brown, RW Crawford, and Adekunle Oloyede. An alternative mechanical parameter for assessing the viability of articular cartilage. *Proceedings of the Institution of Mechanical Engineers, Part H: Journal of Engineering in Medicine*, 223(1):53–62, 2009.

[27] Margot S Farnham, Kyla F Ortved, David L Burris, and Christopher Price. Articular cartilage friction, strain, and viability under physiological to pathological benchtop sliding conditions. *Cellular and Molecular Bioengineering*, 14(4):349–363, 2021.

[28] M Wong and DR Carter. Articular cartilage functional histomorphology and mechanobiology: a research perspective. *Bone*, 33(1):1–13, 2003.

[29] Dennis R Carter, Gary S Beaupré, Marcy Wong, R Lane Smith, Tom P Andriacchi, and David J Schurman. The mechanobiology of articular cartilage development and degeneration. *Clinical Orthopaedics and Related Research®*, 427:S69–S77, 2004.

[30] Motoyasu Kobayashi and Atsushi Takahara. Tribological properties of hydrophilic polymer brushes under wet conditions. *The Chemical Record*, 10(4):208–216, 2010.

[31] Axel C Moore, Jordyn Lee Schrader, Jaclyn J Ulvila, and David L Burris. A review of

methods to study hydration effects on cartilage friction. *Tribology-Materials, Surfaces & Interfaces*, 11(4):202–214, 2017.

[32] Michael A Soltz and Gerard A Ateshian. Experimental verification and theoretical prediction of cartilage interstitial fluid pressurization at an impermeable contact interface in confined compression. *Journal of biomechanics*, 31(10):927–934, 1998.

[33] Piotr Mocny and Harm Anton Klok. Tribology of surface-grafted polymer brushes. *Molecular Systems Design and Engineering*, 1(2):141–154, 2016.

[34] Wufang Yang and Feng Zhou. Polymer brushes for antibiofouling and lubrication. *Biosurface and Biotribology*, 3(3):97–114, 2017.

[35] D Dowson and Zhong-Min Jin. Micro-elastohydrodynamic lubrication of synovial joints. *Engineering in medicine*, 15(2):63–65, 1986.

[36] JB Medley, D Dowson, and V Wright. Transient elastohydrodynamic lubrication models for the human ankle joint. *Engineering in medicine*, 13(3):137–151, 1984.

[37] G. N. de Boer, N. Raske, S. Soltanahmadi, D. Dowson, M. G. Bryant, and R. W. Hewson. A porohyperelastic lubrication model for articular cartilage in the natural synovial joint. *Tribology International*, 149(May 2019):105760, 2020.

[38] Nicholas D Spencer. *Aqueous lubrication: natural and biomimetic approaches*, volume 3. World Scientific, 2014.

[39] A Gopinath and L Mahadevan. Elastohydrodynamics of wet bristles, carpets and brushes. *Proceedings of the Royal Society A: Mathematical, Physical and Engineering Sciences*, 467(2130):1665–1685, 2011.

[40] LI Jinpeng, YANG Shuyan, WU Yang, LI Xinming, GUO Feng, and ZHOU Feng. Correlation between water film thickness and tribological behavior of polymer brush in aqueous lubrication. *Tribology*, 41(6):858–869, 2021.

[41] Motoyasu Kobayashi, Hiroyoshi Tanaka, Myo Minn, Joichi Sugimura, and Atsushi Takahara. Interferometry study of aqueous lubrication on the surface of polyelectrolyte brush. *ACS Applied Materials & Interfaces*, 6(22):20365–20371, 2014.

[42] Robert M Bielecki, Maura Crobu, and Nicholas D Spencer. Polymer-brush lubrication in oil: sliding beyond the stribeck curve. *Tribology Letters*, 49:263–272, 2013.

[43] D L Burris, L Ramsey B T Graham C Price, and A C Moore. How Sliding and Hydrodynamics Contribute to Articular Cartilage Fluid and Lubrication Recovery. *Tribology Letters*, 67(2):1–10, 2019.

[44] Eric L Radin, David A Swann, and Paul A Weisser. Separation of a hyaluronate-free lubricating fraction from synovial fluid. *Nature*, 228(5269):377–378, 1970.

[45] PS Walker, D Dowson, MD Longfield, and VERNA Wright. " boosted lubrication" in synovial joints by fluid entrapment and enrichment. *Annals of the rheumatic diseases*, 27(6):512, 1968.

[46] Clementine Pradal, Gleb E Yakubov, Martin AK Williams, Michael A McGuckin, and Jason R Stokes. Lubrication by biomacromolecules: mechanisms and biomimetic strategies. *Bioinspiration & Biomimetics*, 14(5):051001, 2019.

[47] Bruno Zappone, Marina Ruths, George W Greene, Gregory D Jay, and Jacob N Israelachvili. Adsorption, lubrication, and wear of lubricin on model surfaces: polymer brush-like behavior of a glycoprotein. *Biophysical journal*, 92(5):1693–1708, 2007.

[48] Linda Troeberg and Hideaki Nagase. Proteases involved in cartilage matrix degradation in osteoarthritis. *Biochimica et Biophysica Acta (BBA)-Proteins and Proteomics*, 1824(1):133–145, 2012.

[49] Seido Yarimitsu, Toru Moro, Masayuki Kyomoto, Kenichi Watanabe, Sakae Tanaka, Kazuhiko Ishihara, and Teruo Murakami. Influences of dehydration and rehydration on the lubrication properties of phospholipid polymer-grafted cross-linked polyethylene. *Proceedings of the Institution of Mechanical Engineers, Part H: Journal of Engineering in Medicine*, 229(7):506–514, 2015.

[50] Stephen B Abbott, Wiebe M De Vos, Laura LE Mears, Beatrice Cattoz, Maximilian WA Skoda, Robert Barker, Robert M Richardson, and Stuart W Prescott. Is osmotic pressure relevant in the mechanical confinement of a polymer brush? *Macromolecules*, 48(7):2224–2234, 2015.

[51] Motoyasu Kobayashi, Masami Terada, and Atsushi Takahara. Polyelectrolyte brushes: a

novel stable lubrication system in aqueous conditions. *Faraday discussions*, 156(1):403–412, 2012.

[52] Odeya Tairy, Nir Kampf, Michael J Driver, Steven P Armes, and Jacob Klein. Dense, highly hydrated polymer brushes via modified atom-transfer-radical-polymerization: structure, surface interactions, and frictional dissipation. *Macromolecules*, 48(1):140–151, 2015.

[53] K Ikeuchi, S Fujita, and M Ohashi. Analysis of fluid film formation between contacting compliant solids. *Tribology international*, 31(10):613–618, 1998.

Chapter 5

Brushing Up On Cartilage Lubrication: polyelectrolyte-enhanced tribological rehydration

5.1 Abstract

This study presents new insight on the potential role of polyelectrolyte interfaces in regulating low friction and interstitial fluid pressurisation of cartilage. Polymer brushes composed of hydrophilic 3-sulfopropyl methacrylate potassium salt (SPMK) tethered to a PEEK substrate (SPMK-g-PEEK) are a compelling biomimetic solution for interfacing with cartilage, inspired by the natural lubricating biopolyelectrolyte constituents of synovial fluid. These SPMK-g-PEEK surfaces exhibit a hydrated compliant layer approximately 5 μm thick, demonstrating the ability to maintain low friction coefficients ($\mu \sim 0.01$) across a wide speed range (0.1 - 200 mm/s) under physiological loads (0.75 - 1.2 MPa). A novel polyelectrolyte-enhanced tribological rehydration mechanism is elucidated, capable of recovering up to $\sim$ 12 % cartilage strain, and subsequently facilitate cartilage interstitial fluid recovery, under loads ranging from 0.25 to 2.21 MPa. This is attributed to the combined effects of fluid confinement within the contact gap and the enhanced elastohydrodynamic behaviour of polymer brushes.

Contrary to conventional theories that emphasise interstitial fluid pressurisation in regulating cartilage lubrication, this work demonstrates that SPMK-g-PEEK's frictional behaviour with cartilage is independent of these factors and provides unabating aqueous lubrication. polyelectrolyte-enhanced tribological rehydration can occur within a static contact area and operates independently of known mechanisms of cartilage interstitial fluid recovery established for converging or migrating cartilage contacts. These findings challenge existing paradigms, proposing a novel polyelectrolyte - cartilage tribological mechanism not exclusively reliant on interstitial fluid pressurisation or cartilage contact geometry. The implications of this research extend to a broader understanding of synovial joint lubrication, offering insights into the development of joint replacement materials that more accurately replicate the natural functionality of cartilage.

5.2 Introduction

The primary objective of this study is to deepen the understanding of cartilage-polyelectrolyte tribology by investigating the role of polymer brushes in facilitating tribological rehydration [1]. This research hypothesises that cartilage-polyelectrolyte interfaces, characterised by surface-grafted polyelectrolytes that maintain hydration under mechanical load [2, 3], exhibit high compliance [4], and increase aqueous film thickness [5, 6, 7], may generate elevated fluid pressures at the interface. Such pressures are theorised to support the recovery of cartilage interstitial fluid [1, 8]. This supposition underpins our examination of friction and tribological rehydration within a hydrodynamic framework, necessitating a detailed tribological analysis of cartilage-SPMK interfaces across various speed and load conditions. Specifically, this study seeks to identify and quantify the critical speed and load parameters that facilitate observable strain recovery in cartilage interfaced with SPMK-g-PEEK, thereby providing evidence of tribological rehydration. Secondly, this study aims to explore the current mechanistic numerical [9] and empirical models [10] for tribological rehydration alongside interstitial fluid pressurisation to form a hypothesis on the mechanism of polyelectrolyte-enhanced tribological rehydration. Experiments will use a SCA cartilage contact, for which no demonstration of tribological rehydration exists [11]. This seeks to not only elucidate the underlying principles of polyelectrolyte-enhanced tribological rehydration, but also to contribute to the development of functional biomimetic cartilage repair materials and deeper insight into the potential mechanisms of biopolyelectrolytes within the

superficial macromolecular complex.

5.3 Methods

5.3.1 Sample Preparation

Materials

SPMK monomer, PBS, and 5 mm thick PEEK (450G. Victrex, UK) sectioned into 25 × 25 mm square samples with a surface roughness (R_a) of approximately 100 nm are employed in this study, as detailed in Section 3.3.1. For all experiments, SPMK-g-PEEK interfaces are explored in the context of biomedical implant materials and hence in an isotonic PBS environment to mimic physiological ion concentrations and osmolarity, containing 137 mM sodium chloride (Na^+Cl^-), 10 mM phosphate buffer (K^+), and 2.7 mM potassium chloride (K^+Cl^-) with a pH of approximately 7.4.

SPMK-g-PEEK

SPMK-g-PEEK surfaces with a polyelectrolyte thickness of approximately 400 nm featuring a high density of hydrophilic anionic sulfonic acid groups were produced following the methodology described in Section 3.3.3).

Cartilage Samples

SCA cartilage plugs, ⊘ 4.0 mm and ⊘ 7.2 mm diameter, were extracted from the patellofemoral grooves of bovine stifle joints using the methodology described in Section 3.3.2.

5.3.2 Surface Analysis

A NPFLEX (Bruker, USA) optical interferometer was used to measure the surface roughness of the polished unfunctionalised PEEK and SPMK-g-PEEK samples using a non-contact vertical scanning interferometry (VSI) method, analysing surface reflections to create interference fringes at a 50× optical magnification. Three different 250 × 250 μm areas of each sample were scanned using a high intensity monochromatic green light to enhance reflection and minimise data loss. Optical profilometry data was processed using Bruker Vision64 software to calculate the mean arithmetic roughness (R_a) for each sample area.

A Tescan Amber X plasma focused ion beam-scanning electron microscope (FIB-SEM) was used to measure the hydrated polyelectrolyte height of SPMK-g-PEEK surfaces. SPMK-g-PEEK samples were hydrated by submerging in PBS for 10 minutes before being placed in a Quorum PP3010 cryo preparation chamber and frozen in slushed nitrogen ($\sim$ -210 °C) before being transferred to the SEM under vacuum to prevent ice formation [12]. The SPMK-g-PEEK samples was then sputter coating with a 20 nm thick platinum layer before FIB was used to mill a 100 L $\times$ 40 W $\times$ 100 D μm cross section. Cross section images were taken using SEM to identify the SPMK layer which was validated using Energy Dispersive X-ray Spectroscopy (EDX) to locate sulfonic acid groups. PBS was specifically used to model the hydrated thickness of SPMK-g-PEEK in isotonic environments, where the polyelectrolyte layer will be sensitive to the presence of ionic species, partially collapsing the brush structure due to screening out of electrostatic repulsion along with exclusion of water from the brushes[13, 6, 14].

A Bruker Dimension Icon Atomic Force Microscope (AFM) was used to map the elastic modulus of swollen SPMK-g-PEEK samples submerged in PBS. Measurements were performed using SAA-SPH-10UM (Bruker AFM Probes, USA) AFM probes due to their low precalibrated 0.25 N/m spring constant and large 10 μm probe radius suitable for measuring soft samples in the sub kPa range. Indentation force measurements were performed in a 16 $\times$ 16 grid (256 total) over a 50 $\times$ 50 μm area, two force maps were each performed on two SPMK-g-PEEK samples. Each force-displacement curve was performed with a ramp size of 5.0 μm at a 2 $\mu m/s$ indentation velocity, as used in similar soft contact research [15, 16]. Data was analysed using a custom Python script to identify the contact displacement at which the probe engaged with surface indicated by a reduction in noise and subsequently identify the data region that complies with Hertztian contact theory to calculate elastic modulus [15, 17]. The elastic modulus was only calculated for the first 1 μm of indentation to isolate substrate effects.

5.3.3 Mechanical Testing

To understand the tribological behaviour of SPMK-g-PEEK, speed sweep experiments analogous to Stribeck analysis [18] were conducted to explore SCA cartilage over a short 5 minute loading period, in order mitigate the effects of rising friction contributions due to the time dependant loss of interstitial fluid pressurisation. Figure 5.1a shows the pin-on-disk configuration of a MTM (Micro Traction Machine, PCS Instruments, UK) which was used to perform a speed sweep analysis of a flat $\oslash$ 4.0 mm SCA cartilage plug against unfunctionalised PEEK and

SPMK-g-PEEK disks. Both increasing speed sweeps of 1 - 200 mm/s and decreasing sweeps of 200 - 1 mm/s were performed three times for each test condition. A 15 N constant load was applied throughout the test, which for a ⊘ 4.0 mm cartilage plug corresponds to a ∼ 1.2 MPa contact pressure assuming full contact over the SCA contact. Three repeats were taken for each test condition. To ensure a physiological isotonic gradient all testing was performed fully submerged in PBS. The coefficient of friction (CoF μ, Eq. 3.1), the ratio of the tangential force (F_X) to the applied load (F_Z), was recorded throughout the test at a frequency of 1 Hz.

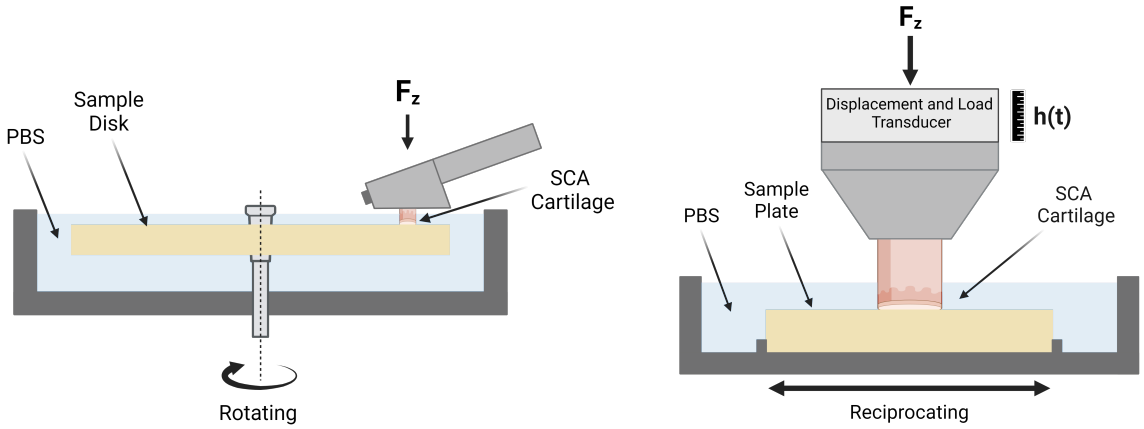

(a) (b)

Figure 5.1: 5.1a. MTM pin-on-disc configuration showing the PEEK/SPMK-g-PEEK sample disk submerged in PBS and ⊘ 4.0 mm SCA cartilage plug mounted in the pin holder. 5.1b. UMT pin-on-plate configuration showing the affixed sample plate in a bath of PBS linearly reciprocating over a distance of 20 mm against a ⊘ 7.2 mm SCA cartilage plug. A constant normal load, F_Z, is applied throughout the rehydration cycle, regulated via PID control. Additionally, a displacement transducer is employed to record variations in cartilage height ($h(t)$) throughout testing.

Figure 5.1b shows the UMT TriboLab (Bruker, USA) equipped with a reciprocating linear drive and custom built lubricant bath used to measure the compression and subsequently strain recovered due to tribological rehydration of a flat ⊘ 7.2 mm SCA cartilage plug sliding against SPMK-g-PEEK. Throughout testing samples remained fully submerged in PBS and closed loop PID control maintained constant F_Z loading with an accuracy of ± 0.5 N and concurrently measured changes in cartilage compression ($h(t)$). The full details of this test setup are described in a previous publication [1]. A rehydration cycle, lasting 3600 seconds, was conducted to evaluate the tribological rehydration of SCA cartilage interfacing with SPMK-g-PEEK under varying conditions of load and sliding speed. The cycle was divided into two phases: an initial phase of unconfined compression (no sliding) for 1800 seconds, followed by a 1800 s sliding phase

under a constant normal load. The experiments were conducted under three load conditions: $F_Z = 10$ N, $F_Z = 30$ N, and $F_Z = 90$ N which correspond to contact pressures of 0.25 MPa, 0.74 MPa, and 2.21 MPa, respectively, assuming uniform contact across the cartilage surface, representative of the physiological pressures encountered by tibiofemoral articular cartilage during human gait [19]. To assess the impact of sliding speed on tribological rehydration, specifically focusing on compression recovery during sliding due to cartilage interstitial fluid recovery, each load condition was tested across a range of speeds (ν) set at 0.1, 0.5, 1, 2, 5, and 10 mm/s each linearly reciprocating across a 20 mm sliding distance. CoF (μ, Eq. 3.1) was only recorded for the $F_Z = 30$ N load condition, as this scenario optimally aligned with the calibrated ranges of tangential load cells available.

Following testing, each cartilage plug was placed in PBS for 1 hour to free swell and recover the compressed height, and then stored in a phosphate buffered formalin solution. The uncompressed height of each cartilage plug (h_0) was then measured using a calibrated Keyence VHX-7000 optical microscope with a 20× magnification, the detailed measurement protocol is detailed in a previous chapter (Sec. 3.3.8) [1]. This enabled calculation of the cartilage compression in terms of overall strain ($\varepsilon(t) = h(t)/h_0$). Strain recovery ($\varepsilon_r$), defined in Equation 5.1, was quantified as the difference in total strain observed at the conclusion of the 1800-second compression phase ($\varepsilon_C = \varepsilon(t = 1800s)$) and the final strain measured at the end of the 3600-second sliding phase ($\varepsilon_F = \varepsilon(t = 3600s)$). This calculation facilitates a direct comparison of the strain recovery capabilities of the cartilage, attributable to tribological rehydration facilitated by the SPMK-g-PEEK interface, under varying speed and load conditions.

$$\varepsilon_r = \varepsilon_C - \varepsilon_F = \varepsilon(t = 1800\ s) - \varepsilon(t = 3600\ s) \tag{5.1}$$

5.4 Results

5.4.1 Surface Analysis

Surface roughness of the unfunctionalised PEEK measured a mean roughness of $R_a = 101 \pm 10$ nm (N = 3), and mean roughness of the SPMK-g-PEEK measured $R_a = 304 \pm 11$ nm (N = 3). The increase in R_a value for SPMK-g-PEEK indicates grafting of SPMK has markedly altered the topography of PEEK specifically introducing additional surface features along with

increasing the prominence of existing ones. Once hydrated the SPMK surface features will become obscured as the hydrophilic polymer chains swell to provide an aqueous interface.

Figure 5.2 presents the Cryo-FIBSEM imaging and EDX analysis conducted to determine the swollen height of the SPMK layer on the PEEK substrate. SEM imaging alone fails to distinctly delineate the SPMK interlayer, obscured by the presence of frozen water and density variations in the swollen SPMK [20]. The thickness of the SPMK layer is identified by the region exhibiting the highest sulphur content, attributed to the sulfonic acid groups within the polyelectrolyte layer, with an estimated height of approximately 5 μm. This region lies beneath an oxygen-rich area indicative of frozen water, and above a carbon-rich zone representing the PEEK substrate. The spatial resolution limit of EDX composition analysis, typically around 1 μm due to the volumetric interaction of the electron beam [21], implies that the measured height of the SPMK layer, while indicative, cannot be precisely quantified through EDX, rendering the derived height as an approximate estimate rather than an exact measurement.

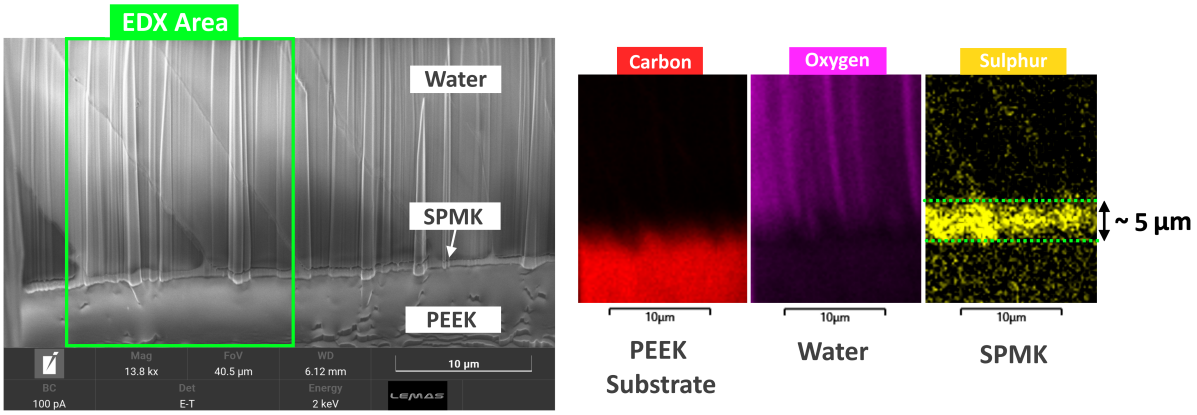

Figure 5.2: Left: CryoSEM image of swollen SPMK-g-PEEK cross section showing area of EDX analysis. Right: EDX analysis of carbon (red), oxygen (purple) and sulphur (yellow) corresponding to the PEEK substrate, frozen water, and SPMK layers respectively. Measuring a swollen polyelectrolyte layer of approximately 5 μm.

The elastic moduli of the swollen polyelectrolyte interfaces submerged in PBS for SPMK-g-PEEK was determined using AFM force mapping to be $E = 505$ Pa with a standard deviation of $\pm$ 111 Pa. This value indicates variability in the mechanical properties, with the observed range spanning from 166 to 1055 Pa, as depicted in Figure 5.3a. This analysis was based on 1024 indentation measurements conducted across two samples of SPMK-g-PEEK. Specifically, Figure 5.3b shows a representative 50×50 μm area where the elastic moduli were assessed in a 16×16 grid. During the evaluation process, any force-displacement curves that either

did not align with Hertzian contact mechanics or demonstrated significant error were excluded. Consequently, a total of 792 modulus measurements were retained for analysis. A representative force-displacement indentation curve is presented in Figure 5.3c, indicating that indentation depths of 1 μm consistently resulted in forces below 5 nN. Moreover, the curves did not adhere to Hertzian contact theory at forces approximately lower than 0.5 nN. The accurate determination of surface contact for soft materials poses a significant challenge, requiring the mathematical delineation of the indentation range that accurately fits the Hertz model (Fig. 5.3c) [15, 17].

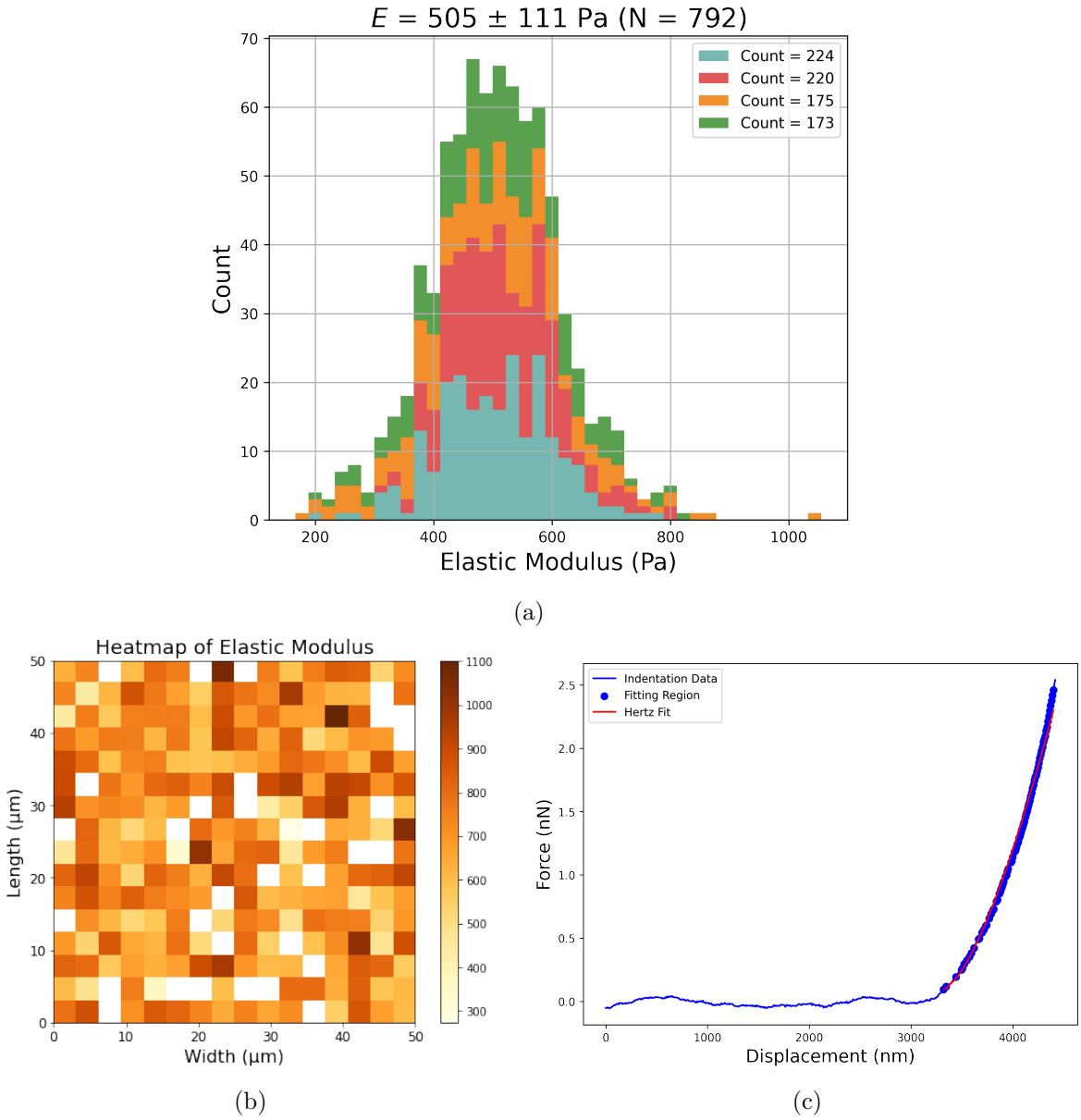

Figure 5.3: 5.3a. Histogram of elastic modulus values, mean $E = 505 \pm 111$ Pa. Range: 166 - 1055 Pa. Interquartile range: 140 Pa. *Count* corresponds to the number of indentation curves (out of 256) exhibiting compliance with Hertzian contact mechanics and hence retained for analysis. 5.3b. Elastic modulus measured in a 16 × grid across a 50 × 50 μm area of SPMK-g-PEEK submerged in PBS (Count = 224). 5.3c. Force-displacement indentation curve for a 10 μm radius colloidal probe indenting SPMK-g-PEEK submerged in PBS, showing the region which is compliant with Hertzian contact fitting for calculating elastic modulus.

5.4.2 SPMK & PEEK Speed Sweep Analysis

Figures 5.4a and 5.4b show the CoF evolution for SCA cartilage against SPMK-g-PEEK and unfunctionalised PEEK during sweeps of increasing speed 1 - 200 mm/s and decreasing speed 200 - 1 mm/s, respectively. In both scenarios, SPMK-g-PEEK demonstrated a remarkable stability of CoF, exhibiting minimal variation with mean CoF of $\mu = 0.012 \pm 0.002$ and $\mu =$

0.011 ± 0.002 for the decreasing and increasing speed sweeps respectively. Conversely, the CoF response of unfunctionalised PEEK exhibited significant variation dependent on the speed sweep direction. For the increasing speed case, CoF rises steadily up to a maximum $\mu = 0.11 \pm 0.036$, and begins to reduce at speeds above 120 mm/s to a final CoF of $\mu = 0.071 \pm 0.025$. In contrast, for the decreasing speed sweep, the CoF increased steadily, starting from $\mu = 0.034 \pm 0.004$ at a sliding speed of 200 mm/s and reaching a peak of $\mu = 0.22 \pm 0.068$ at 5 mm/s, before exhibiting a slight decrease when the sliding speed further reduced to 1 mm/s.

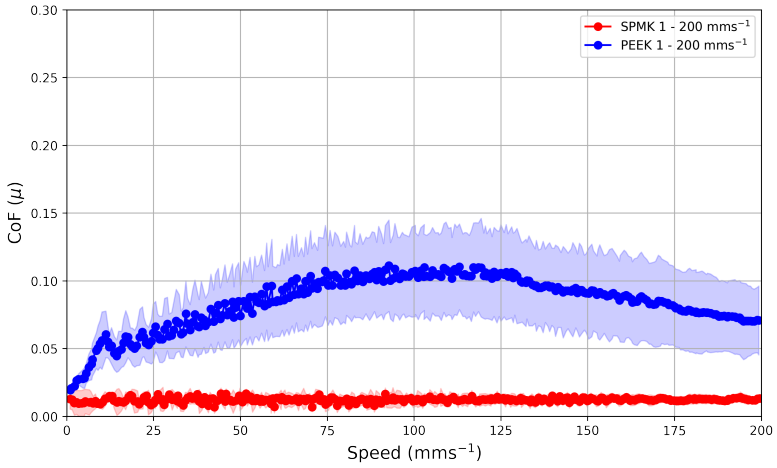

(a)

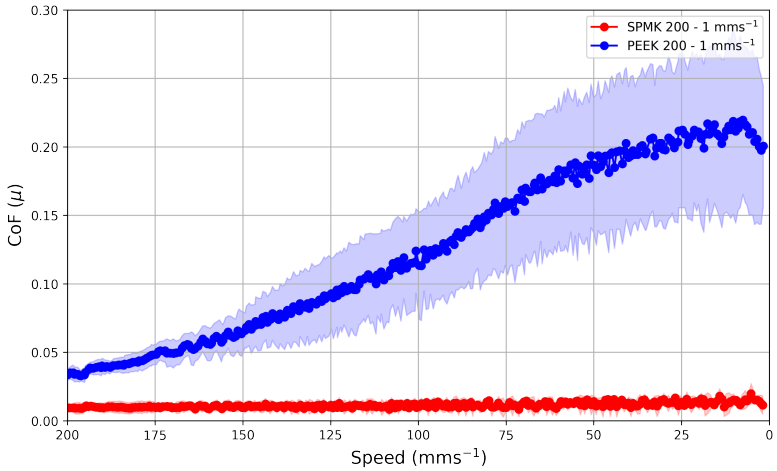

(b)

Figure 5.4: SPMK-g-PEEK (N = 3) and PEEK (N = 3) disc versus flat ⊘ 4 mm SCA cartilage plug for 5.4a. increasing speed sweep from 1 - 200 mm/s and 5.4b. decreasing speed sweep from 200 - 1 mm/s.

5.4.3 Strain Recovery & Tribological Rehydration

Representative strain datum ($\varepsilon(t)$) for the 90 N rehydration cycles are shown in Figure 5.5 for the 10 mm/s (Fig. 5.5a) and 0.1 mm/s (Fig. 5.5b) conditions, demonstrating $\varepsilon_r \sim 11$ % and $\varepsilon_r \sim$ -5

% respectively during the sliding phase. During the first 30 minutes of unconfined compression the cartilage interstitial fluid exuded at a decaying rate towards a static equilibrium. Upon the onset of sliding rehydration of the cartilage can occur, reducing the overall compression as fluid is reimbibed by the cartilage, which is clearly observed for the 10 mm/s condition (Fig. 5.5a).

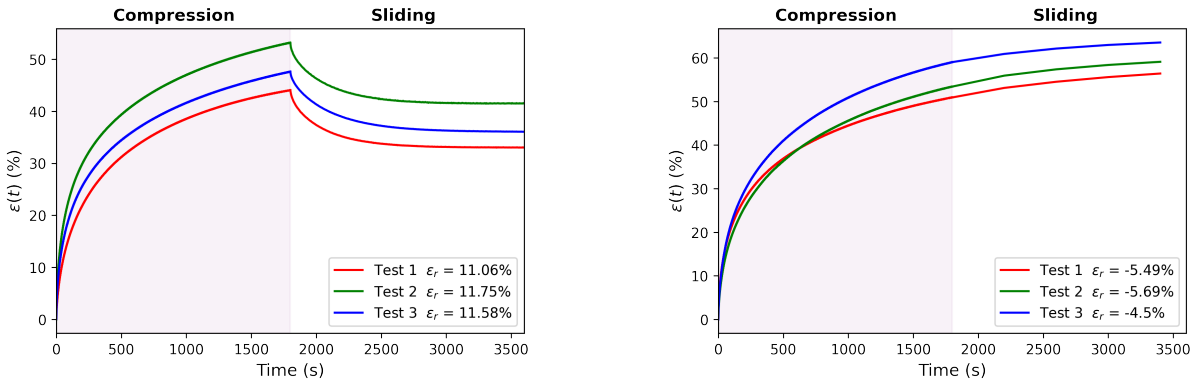

(a) 10 mm/s (b) 0.1 mm/s

Figure 5.5: Strain evolution during the compression and sliding phases under an applied load of 90 N of ⌀ 7.2 mm SCA cartilage sliding against SPMK-g-PEEK at (a) 10 mm/s and (b) 0.1 mm/s.

The mean strain recovery (ε_r, Equation 5.1) was calculated for each speed and load condition, with a sample size of N = 3 for each group. Figure 5.6a shows the evolution of the mean strain recovery ($\varepsilon_r(t)$) throughout all sliding phases for the 30 N load condition. The overall mean strain recovery for each condition is plotted in Figure 5.6b and aggregated in Table 5.1 along with the mean strain at the end of the compression phase (ε_C) for each load condition. Figure 5.6b shows across all load conditions, an increase in strain recovery (ε_r) was observed in correlation with increments in sliding speed. Notably, at a minimal speed of $\nu = 0.1\ mm/s$, the overall cartilage strain persistently augmented throughout the sliding phase, culminating in a negative recovery strain of approximately $\varepsilon_r \sim -5\%$ across all load conditions. Strain recovery due to tribological rehydration became pronounced at speeds exceeding $\nu = 1\ mm/s$, with the highest strain recovery for each condition being attained at the highest speed, $\nu = 10\ mm/s$. The analysis revealed that samples subjected to a 10 N load exhibited the least overall strain recovery at $\nu = 10\ mm/s$, with $\varepsilon_r = 8.87 \pm 0.79\%$, whereas the 30 N and 90 N conditions demonstrated comparably higher maximum strain recoveries of $\varepsilon_r = 11.24 \pm 0.68\%$ and $\varepsilon_r = 11.46 \pm 0.29\%$ respectively. Though this is partially due to the greater initial strain before sliding at higher loads. The variability in cartilage strain recovery, indicated by a standard deviation range of ± 0.11 - 2.37%, aligns with findings from prior studies exploring tribological rehydration induced

strain recovery in bovine cartilage [22, 23]. This observed strain error represents the inherent mechanical, poroviscoelastic, and thickness variations in cartilage samples harvested across a range of bovine specimens and patellofemoral locations [24].

The observation of strain recovery and subsequent cartilage rehydration increasing with sliding speed demonstrated consistency across all compressive stresses applied to the cartilage, quantified as $\varepsilon_C = 26.1 \pm 1.3\%$, $42.0 \pm 1.4\%$, and $51.8 \pm 3.0\%$ for the 10 N, 30 N, and 90 N load conditions respectively, as summarised in Table 5.1. Analysing net strain recovery (ε_r), Figure 5.6b illustrates that at lower sliding speeds of $\nu \leq 1.0\ mm/s$, the 10 N condition facilitated a greater recovery of cartilage strain. A transition is evident at higher speeds, specifically $\nu \geq 5.0\ mm/s$, where enhanced strain recovery is observed under the higher 30 N and 90 N load conditions. This trend underscores the role of sliding speed, and subsequently hydrodynamic effects, in augmenting cartilage interstitial fluid recovery, evidenced by the increased cartilage strain recovery attributed to tribological rehydration facilitated by the polyectrolyte SPMK interface.

Figure 5.6c shows the mean sliding phase CoF (μ) for the $F_Z = 30$ N load condition, with the data aggregated in Table 5.2. For all sliding speeds, SPMK-g-PEEK facilitated low friction with $\mu < 0.016$ throughout the sliding cycle, aligning with previous research demonstrating the lubricating efficacy of polyelectrolyte - cartilage contacts [1]. For increasing speeds between 0.5 - 10 mm/s a decrease in CoF was observed from a maximum of $\mu = 0.016 \pm 0.003$ to a minimum of $\mu = 0.005 \pm 0.001$. This is commensurate with enhanced interstitial fluid pressurisation evidenced by greater strain recovery across the increasing speed range (Fig. 5.6a) and broadly aligns with the interstitial fluid pressurisation hypothesis (Eq. 1.3).

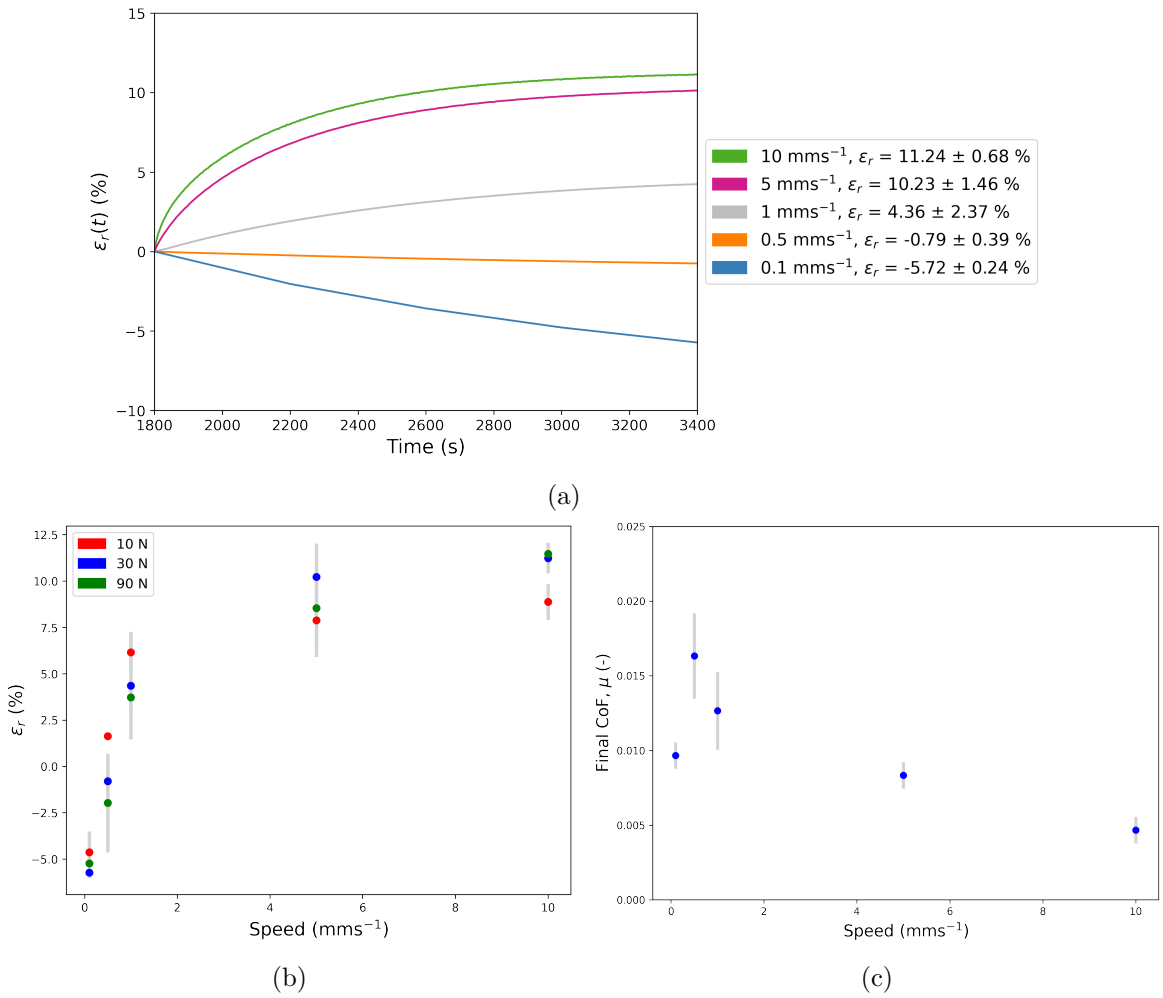

Figure 5.6: 5.6a. Evolution of mean strain recovery ($\varepsilon_r(t)$) for the 30 N load during the sliding phase of the rehydration cycle for all sliding speeds. Error bars are omitted for clarity. 5.6b. Strain recovery (ε_r) for all tests conditions (Tab. 5.1) plotted for each speed condition with standard deviation error bars shown. 5.6c. Mean CoF (μ) for the 30 N load during the sliding phase of the rehydration cycle for all sliding speeds with standard deviation error bars shown (Tab. 5.2).

Table 5.1: Summary of strain recovery (ε_r) calculated across each specified and load condition with a sample size of N = 3 for each group. Along with the cartilage strain at the end of the compression phase (ε_C) for each load conditions, with a samples size of N = 15 for each group.

Load	**Compression**	**Rehydration**, ε_r (%)				
F_Z	ε_C (%)	0.1 mm/s	0.5 mm/s	1 mm/s	5 mm/s	10 mm/s
10 N	26.1 ± 1.31	-4.63 ± 0.93	1.63 ± 0.11	6.15 ± 0.88	7.89 ± 1.62	8.87 ± 0.79
30 N	42.0 ± 1.39	-5.72 ± 0.24	-0.79 ± 0.39	4.36 ± 2.37	10.23 ± 1.46	11.24 ± 0.68
90 N	51.8 ± 2.91	-5.23 ± 0.52	-1.97 ± 2.18	3.73 ± 0.65	8.54 ± 1.87	11.46 ± 0.29

Table 5.2: Summary of mean CoF (μ) of the 30 N load condition at speeds of 0.1 - 10 mm/s with a sample size of N = 3 for each group.

Load	**CoF**, μ (-)				
F_Z	0.1 mm/s	0.5 mm/s	1 mm/s	5 mm/s	10 mm/s
30 N	0.010 ± 0.001	0.016 ± 0.003	0.013 ± 0.003	0.008 ± 0.001	0.005 ± 0.001

5.5 Discussion

The interface between SPMK-g-PEEK and cartilage represents a significant advancement in the development of biomaterials aimed at mimicking the natural lubrication and mechanical properties of superficial macromolecular complexes on cartilage. This section explores the structural characterisation of SPMK-g-PEEK, highlighting the swollen height, mechanical properties and polyelectrolyte conformation designed to mimic synovial biopolyelectrolytes. Analysis of the tribological and strain recovery behaviour of cartilage interfaced with SPMK-g-PEEK reveals sustained low friction akin to physiological levels and ability to augment interstitial fluid load support, both necessary for maintaining the long-term function of cartilage. These findings are contextualised within the broader scope of cartilage lubrication models, culminating in a new hypothesis of polyelectrolyte-enhanced tribological rehydration.

5.5.1 SPMK-g-PEEK Interface

The swollen height of SPMK measured in this study was $\sim$ 5 μm (Fig. 5.2), an order of magnitude greater than the $R_a \sim$ 100 nm roughness of PEEK, which protects interfacing cartilage from hard asperity contact and hence provide a lubricious compliant interface. This is similar to the measured $\sim$ 1 - 10 μm MPC polymer brushes on steel [12] and polyethylene [25] substrates in the context of biomedical implants. Previous measurement of the dry height of the SPMK layer grafted to PEEK using FIB-SEM measured a 397 ± 47 nm thick polyelectrolyte layer [1], meaning the SPMK exhibits a swelling ratio of approximately 12×. The measured SPMK thickness demonstrates that swelling and compression of the polyelectrolyte is too small to contribute to the overall strain recovery of articular cartilage. Typical cartilage thickness was approximately 1200 μm which when considering strain recovery in the region of $\varepsilon_r \sim$ -5 - 12 % corresponds to an approximate height change of 60 - 200 μm.

The nanomechanical analysis of the SPMK-g-PEEK demonstrated the SPMK-g-PEEK surface

submerged in PBS has a modulus of E = 505 ± 111 Pa, exhibiting a highly compliant surface consistent with extended polyelectrolyte chains with a high fluid content [17]. This reflects the highly compliant 1 - 4 μm thick [26, 27, 28, 29] superficial macromolecular complex on cartilage with a modulus of E = 9 ± 2 kPa [29]. The SPMK surface moduli is markedly lower than previous literature exploiting biomedical applications of polyelectrolytes. AFM force mapping of brush terminated hydrogels designed to mimic hydrophilic proteins native to corneal or synovial surfaces exhibit moduli of $E \sim 3$ - 44 kPa [30, 17, 31]. These are orders of magnitude lower than previously reported biomedical applications of MPC grafted to rough polyethylene ($R_a = 650$ μm) hip replacement implants with swollen MPC height $\sim$ 1400 nm thick and AFM nanomechanical studies measuring a variable modulus of $E = 73 \pm 72$ kPa due to varying substrate effects [25].

The observed low moduli and ~ 5 μm swollen height demonstrates that grafting-from of SPMK monomer (Fig. 5.7a) onto PEEK substrates yields a dense end-tethered polymer surface (Fig. 5.7b) enriched with sulfonic acid groups [13, 1]. The sulfonic acid groups possess hydrophilic and ionisable characteristics, enabling them to dissociate in aqueous environments leaving negatively charged sulfonate ions (SO_3^-) tethered to the polymer back bone, the same hydrophilic functional groups present on proteoglycans in synovial fluid [32]. Electrostatic repulsion among the negatively charged SO_3^- groups and osmotic pressure of hydrated counter-ions around the charged chains cause the polymer chains to extend away from the substrate and form a brush like configuration [33, 4, 34, 32, 35]. The highly hydrophilic sulfonate groups form tight hydration shells contributing to the solvation of the polymer brush supporting its extended formation and facilitating hydration lubrication [36]. Such polymer brush structures can resist deformation under compressive loading due to the conformational entropy and exclude volume effect of the hydrated SPMK polyelectrolyte causing a repulsive force under loading [35, 37].

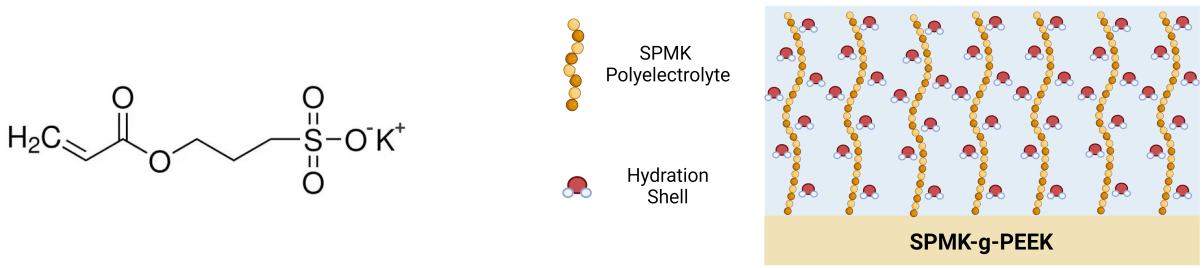

(a) (b)

Figure 5.7: 5.7a. 3-Sulfopropyl methacrylate potassium salt (SPMK) monomer. 5.7b. Polymer brush conformation of SPMK-g-PEEK showing the presence of bound hydration shells on the sulfonic acid groups.

5.5.2 SPMK-g-PEEK - Cartilage Tribology

This study clearly demonstrates SPMK-g-PEEK's tribological efficacy as a cartilage counterface under physiological loads of 0.75 - 2.21 MPa. Hydrated SPMK provides a highly lubricious surface capable of maintaining an invariably low CoF of $\mu \sim 0.01$ across a speed range of 1 - 200 mm/s and mechanism to augment cartilage strain recovery of up to $\varepsilon \sim 11.5$ %. Under constant loading, the rehydration cycle demonstrates recovery of cartilage interstitial fluid increases with sliding speed (Fig. 5.6b), evidenced by the increasing strain (Eq. 1.3), highlighting the role of hydrodynamics in facilitating polyelectrolyte-enhanced tribological rehydration. At higher sliding speeds, greater strain recovery appears to facilitate lower friction coefficients, as shown by the CoF trend analysis for $F_Z = 30$ N (Fig. 5.6c) which exhibits the lowest $\mu = 0.005 \pm 0.001$ at the high speed condition of $\nu = 10$ mm/s along with the greatest strain recovery $\varepsilon_r = 11.24 \pm 0.68$ %. Maintenance of low friction and the reduction of cartilage strain positions SPMK-g-PEEK as a promising material for maintaining cartilage health. Effective rehydration of articular cartilage is important to maintain cell viability [38] and provide fluid flow for solute transport and removal of metabolic waste from the tissue [39, 40]. Furthermore, both effective rehydration and high lubricity are crucial for shielding the collagen matrix from high shear and normal forces to prevent wear [41, 42].

The speed sweep analysis (Fig. 5.4) of unfunctionalised PEEK is representative of current understanding of SCA models, exhibiting the lowest CoF $\mu \sim 0.02$ - 0.04 at the start of sliding and hence at the point of the minimum strain, irrespective of the 1 mm/s and 200 mm/s starting speeds. For PEEK, the increasing 1 - 200 mm/s speed condition shows a peak CoF $\mu \sim 0.11$ at speeds of 120 mm/s recovering slightly at higher speeds likely due the onset of a soft-

EHL regime [43]. Whereas the decreasing speed condition the peak CoF $\mu \sim 0.22$ occurred at the end of testing corresponding to maximum temporal strain. SPMK-g-PEEK demonstrated invariably low CoF for both increasing and decreasing speeds sweeps with $\mu < 0.012$ in both scenarios, maintaining high lubricity that is unaffected by variations in loading time (i.e. contact strain), speed, or lubrication regime. Highlighting that for aqueous lubrication systems with the ability to hold water at the surface, friction cannot necessarily be associated with a change in lubrication regime [3]. Similar speed independent CoF ($\mu \sim 0.02$, $\nu = 0.1$ - 50 mm/s) has been shown for the aqueous lubrication of hydrophilic poly(ethylene glycol) brushes [44, 45] and brush terminated hydrogels in self mated gemini contacts [46, 47]. This has been attributed to an elastoviscous regime, where the extended polymer chains can influence the interfacial viscosity which has a net smoothing effect to damp frictional transitions between boundary and fluid film lubrication regimes [47]. Furthermore at low speeds in confined interfaces, high polyelectrolyte concentration can increase effective viscosity and produce substantially higher film thickness than expected for conventional elastohydrodynamic theory at low speeds, giving rise to a low speed (≥ 0.1 mm/s) onset of fluid film lubrication [44, 5, 7, 18]. The lubricating efficacy of SPMK-g-PEEK is attributed to the confined polyelectrolyte behaving as a viscous lubricant to produce lubricating fluid films at low speeds [44, 5, 7]. When considering the high roughness of cartilage ($R_a \sim 500$ nm [48]) it is likely that this is a localised phenomena in regions of cartilage asperity contact. Notably, CoF decreases with increasing speed in tandem with increasing strain recovery during longer term testing of the rehydration cycle (Fig. 5.6c). Demonstrating that polyelectrolyte-enhanced lubricating fluid films exhibit a reduction in viscosity with increased shear rate [49], promoting low friction while maintaining interstitial fluid pressurisation.

Early cadaveric hip pendulum studies to simulate gait show that for human joints CoF was typically between a range of $\mu \sim 0.01$ - 0.04 [50, 51, 52] and are corroborated by recent benchtop cartilage-cartilage tribology studies showing CoF as low as $\mu \sim 0.001$ - 0.015 [42, 53]. However, the current state of research applies a reductionist approach to discern between three modes of MCA, cSCA and SCA tribological rehydration [11, 54]. Studies using a hard impermeable counterface (i.e. glass, PEEK) show that during sustained sliding MCA and cSCA cartilage conditions friction can remain consistently as low as $\mu \sim 0.03$ as a result of maintaining low cartilage strain and high interstitial fluid pressurisation (Eq. 1.3) [53, 10]. MCA cartilage on glass exhibit low CoF of 0.01 - 0.07 between speed ranges of 0.05 - 4.5 mm/s, maintaining fluid load support of $F' \sim 0.85$ - 0.9 [53, 55, 56]. Tribological rehydration of cSCA cartilage is shown

to only occur at speeds above 30 mm/s when hydrodynamic pressures are sufficient to promote interstitial fluid recovery, demonstrating low CoF $\mu \sim 0.01$ - 0.03 at high speeds of 80 mm/s ($F' \sim 0.9$) and high CoF of $\mu \sim 0.1$ - 0.4 at lower speeds of 1 - 20 mm/s below the speed threshold for effective interstitial fluid recovery [57, 10, 22]. SCA cartilage sliding experiments are analogous to cartilage in unconfined compression, exhibiting no evidence of fluid imbibement to compete with the interstitial fluid efflux during loading [1, 53]. At low speeds of 1 mm/s, SCA cartilage exhibits a CoF of $\mu \sim 0.19$ [53], increasing up to $\mu \sim 0.3$ - 0.5 at speeds of 80 mm/s [57, 10]. The CoF observed in the presented rehydration cycles consistently remain low ($\mu \sim 0.01$), reflecting the physiological friction coefficients present in synovial joints [50, 51, 52, 42, 53]. This studies observation of SCA cartilage maintaining low friction at low velocities ($\nu = 0.1$ - 10 mm/s) diverges from current cartilage rehydration frameworks, demonstrating tribological and rehydration dynamics akin to those elucidated in MCA and cSCA cartilage models [57, 10, 53, 55, 56]. Which highlights an unexplored avenue of tribological rehydration facilitated by polyelectrolyte boundary lubrication interfaces, mirroring the configuration of endogenous superficial macromolecular complexes, yet neglected by prevailing MCA and cSCA paradigms.

The mean strain recovery (ε_r) for all speed and load conditions (5.6b) shows as speed increases, the recovered strain and subsequently the interstitial fluid pressurisation increases. Compared to cSCA tribological rehydration which only occurs at speeds of above 30 mm/s [57, 10, 22], the polyelectrolyte-enhanced tribological rehydration demonstrates a net recovery of strain even in low speed conditions of $\nu = 0.1$ - 0.5 mm/s. This is hypothesised to be underpinned by the low speed affinity of polyelectrolytes for enhanced fluid film formation [44, 5, 7] promoting hydrodynamic pressurisation and restoration of interstitial fluid. Strain recovery (ε_r) becomes asymptotic in all speed conditions, corroborating similar findings that an equilibrium is reached between the interfacial and interstitial pressure fields [23, 22, 10]. Maximum strain recovery (ε_r) observed at $\nu = 10$ mm/s is lower for the $F_Z = 10$ N condition ($\varepsilon_r = 8.76 \pm 0.79$ %) compared to the higher load conditions of $F_Z = 30$ & 90 N which exhibit $\varepsilon_r \sim 11$ %, which intuitively demonstrate at greater loads, greater fluid pressurisation occurs, leading to greater strain recovery [18]. A transition around $\nu = 1$ mm/s is observed, below this threshold greater strain recovery occurs for the 10 N load, whereas above this transition the strain recovery rate for 30, 90 N load conditions become greater than at $F_Z = 10$ N. Permeability of cartilage is inversely proportional to compressive strain [58], which for low loads will mean the net fluid flow

of cartilage can occur at a greater rate for (Darcy's Law [59]). The speed transition observed in Figure 5.6b corroborates the previous hypothesis of greater fluid pressurisation at higher speeds, yielding a greater rate of interstitial fluid recovery towards equilibrium.

5.5.3 Hypothesis of polyelectrolyte-enhanced tribological rehydration

Coupling of hydrodynamic and interstitial fluid pressure fields have been developed for explaining tribological rehydration of cSCA cartilage [10, 9]. Specifically, this has been undertaken as a percolation based approach to mixed lubrication of cartilage treated as a porous material [60, 9]. Within this interface, modelling of hydrodynamic forces induced by a wedge effect hypothesises fluid pressure peaks at the contact inlet, facilitating interstitial fluid recovery. Additionally, rehydration within the loaded contact zone occurs as fluid trapped at asperity contacts becomes pressurised, forming localised rehydration channels [9]. This process leverages the intrinsic roughness of cartilage to create percolating channels. Compliant tribological systems such as cartilage have been shown to flatten at moderate pressures, which is advantageous for reducing friction in hydrodynamic lubrication [49, 61]. The percolation approach models cartilage as a material with multiple roughness scales, postulating that the micro-roughness of cartilage must be present at the contact interface to maintain lubrication and facilitate rehydration [60].

Understanding the lubrication of SPMK-g-PEEK - cartilage interfaces necessitates an adaptive multimode lubrication model [62] due to the dominating role of interstitial fluid pressurisation in supporting the majority of applied load [63, 64, 65], along with the boundary lubrication expected to occur when pressurisation subsides and cartilage contact occurs [63, 3]. To the authors knowledge there have been no theoretical or experimental studies on the role of biological or synthetic polyelectrolytes for cartilage rehydration. Experimental [66, 67] and modelling [26] approaches have explored the role of the presence of polyelectrolytes on cartilage, showing that the superficial macromolecular complex acts as a low permeability barrier, providing flow resistance to sustain cartilage interstitial pressure which is congruent with our initial published studies [1]. However, this does not explain the net strain recovery observed during at the onset of sliding (Fig. 5.6b). Any potential cushioning effect of the ~ 5 μm thick low moduli SPMK interface providing rehydration through passive swelling are contradicted by previous studies, which have shown no notable reduction in cartilage strain when comparing PEEK and SPMK-g-PEEK [1] and passive swelling rates being slower than tribological rehydration [68] suggesting a reduced load-speed dependency than observed (Fig. 5.6b). Instead, cartilage rehydration is

an active process onset by sliding (Fig. 5.5a) that competes with fluid exudation under loading [10].

Figure 5.8 presents a hypothetical mechanism of polyelectrolyte-enhanced tribological rehydration, a similar percolation approach is considered by assuming at the microscale level cartilage still exhibits some roughness [9], giving rise to localised regions of compressed polyelectrolyte at cartilage asperities. Upon the onset of sliding there will be a lubricant flow incurred, giving rise to a viscous fluid film enhanced by polyelectrolyte elastohydrodynamic lubrication [5]. Compression of the hydrated SPMK polyelectrolyte will reduce the volume available for water molecules, and compounded by the increased relaxation times of polymer brushes in compression [69], produce pressurised regions of water which overcome the cartilage interstitial fluid pressure and facilitate rehydration [4, 3]. Increased strain recovery at greater speeds is expected to be a convolution of enhanced fluid film formation due to the polyelectrolyte [44, 5, 7], resulting in a greater quantity of fluid at the interface, along with a greater percolating flux exposing the cartilage asperities to more polyelectrolyte per unit time [9].

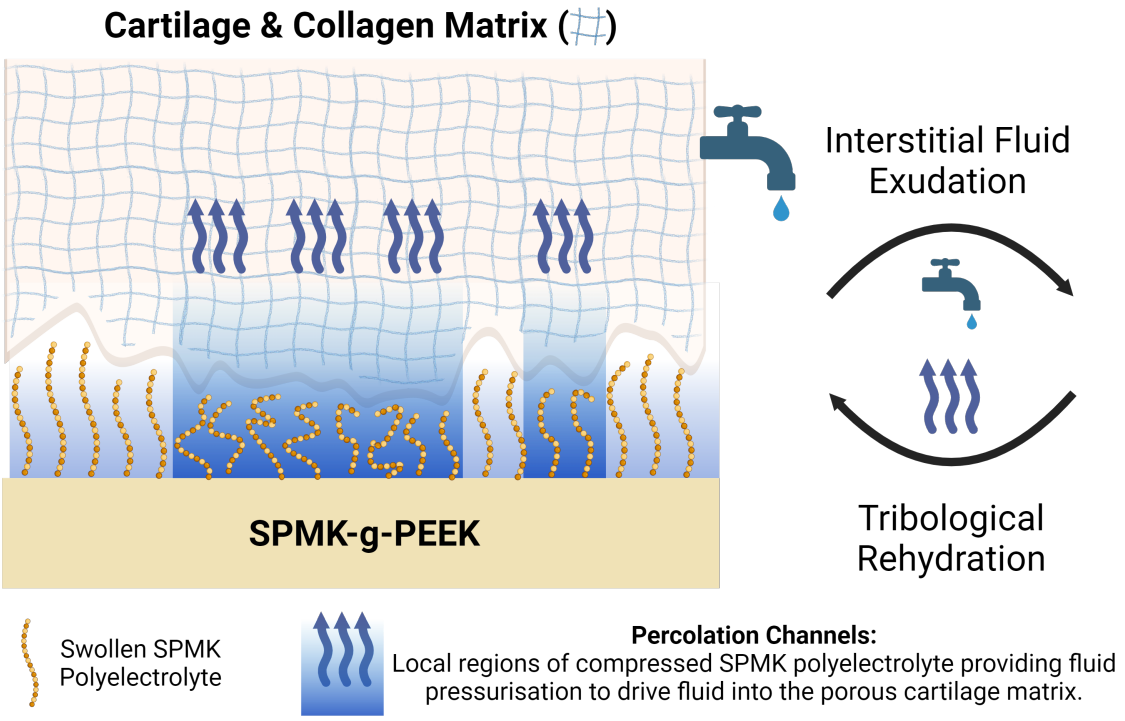

Figure 5.8: Hypothesised mechanism of polyelectrolyte-enhanced tribological rehydration. This process is conjected to occur through localised compression of the SPMK polyelectrolyte at cartilage asperities during sliding, which generates pressurised fluid regions within percolation channels to facilitate cartilage rehydration. Low friction is expected to be maintained by a polyelectrolyte enhanced elastohydrodynamic fluid film and the highly hydrated SPMK boundary interface.

Current cartilage models posit that interstitial fluid pressurisation is the dominant mechanism to maintain low CoF in cartilage and overlooks the role of biological polyelectrolytes [10, 9, 70, 53]. The holistic role of lubricating biopolyelectrolytes found in synovial fluid remains contentious in biotribology research. Limited studies demonstrate addition of synovial fluid into MCA and cSCA contacts show a slight reduction in friction and hence augmentation of interstitial fluid pressure [53, 22]. In contrast a cornucopia of tribological research asserts the lubrication benefits of synovial fluid macromolecular complexes demonstrated at the nanoscale [32, 3, 42], in SCA and MCA cartilage contacts [53, 71, 72, 73, 74], and in whole joint models [75, 76]. However, these studies do not address the potential mechanisms by which these complexes might contribute to the rehydration of cartilage. The demonstration of polyelectrolyte-enhanced tribological rehydration in the present study benefits from a precisely controlled chemical composition of direct attachment of SPMK to the substrate. Whereas the *in vivo* superficial macromolecular complex relies on electrostatic interaction with the negatively charged cartilage surface to remain attached [64, 3], which inevitably becomes challenging to maintain within the contact area during *in vitro* tribology studies particularly during testing of unmatched cartilage contacts [53, 22]. Engineering of surface grafted polyelectrolytes provide a compelling solution for not only emulating the *in vivo* performance of cartilage but also as a versatile model for understanding the tribological phenomena of natural synovial lubrication.

5.5.4 Future Work & Limitations

CryoSEM offers only an approximate measure of the swollen height of the SPMK polyelectrolyte while illustrating the distribution of the sulfonic acid groups. However, the spatial resolution of EDX, limited to 1 μm [21], necessitates additional methods such as ellipsometry [69] for precise measurement of the swollen height at the SPMK-g-PEEK interface. Initial efforts to gauge the thickness of SPMK under hydrated conditions have proved challenging. This difficulty is largely due to the high water content and low relative polymer content, which result in a minimal change in polarisation signal. Consequently, this measurement is still under active investigation.

No discussion in this study has pertained to potential interaction between the SPMK polyelectrolyte and any superficial macromolecular complex present on the cartilage samples. Previous cartilage studies have shown that extensive washing with PBS can diminish the superficial layer [29, 77], and consideration of how the surface would become degraded through exposure to PBS during cutting, storage or pre-test free swelling in PBS was unaccounted.

Discerning between the impact on friction due to the SPMK-g-PEEK interface which provides an unabating highly lubricious sliding interface and interstitial fluid pressurisation remains uncertain. The decrease in friction observed in this study for increased states of cartilage rehydration (Fig. 5.6c) suggest a synergy between between cSCA and polyelectrolyte induced tribological rehydration is possible. Future studies should explore the behaviour SPMK-g-PEEK using a cSCA cartilage model.

The cartilage - SPMK-g-PEEK interface presented in this study presents a challenging numerical modelling problem, requiring interfacing the interstitial fluid flow and strain of cartilage with the local fluid pressurisation of compressed polyelectrolyte chains. Necessitating the combination of a molecular dynamics problem [78] coupled with a poroviscoelastic cartilage model which accounts for the multi-mode lubrication regime and strain dependant cartilage topography [79].

5.6 Conclusions

Hydrophilic SPMK polymer brush surfaces tethered to PEEK substrates have been developed as an advanced biomaterial to interface directly with cartilage and support native biotribology, These surfaces draw inspiration from the macromolecular constituents of synovial fluid, aiming to replicate its lubricating properties. The development of SPMK-g-PEEK surfaces, featuring a hydrated tethered layer approximately 5 μm thick, facilitates low friction coefficients ($\mu \sim 0.01$) over a broad speed range ($0.1 - 200$ mm/s) under physiological loading conditions ($0.75 - 1.2$ MPa). A pivotal finding of this study is the discovery of a novel polyelectrolyte-enhanced tribological rehydration mechanism, capable of recovering cartilage interstitial fluid under loads ranging from 0.25 to 2.21 MPa. This recovery is attributed to the synergistic effects of fluid confinement within the contact gap and the enhanced elastohydrodynamic performance of the polymer brushes.

Going beyond prevailing theories that attribute cartilage lubrication to interstitial fluid pressurisation and tribological rehydration through conformal geometries, our findings demonstrate that physiological friction coefficients of SPMK-g-PEEK interfaced with cartilage can occur independently of interstitial fluid recovery and pressurisation. This discovery challenges existing paradigms and suggests a novel mechanism of lubrication that does not solely rely on the established models of interstitial fluid pressurisation. The implications of this research extend beyond the specific interactions of SPMK-g-PEEK with cartilage, offering a broader under-

standing of synovial joint lubrication. By synthesising materials that replicate the superficial macromolecular complex of cartilage, we have elucidated a new mechanism for the regulation of cartilage interstitial fluid. This advances our comprehension of joint lubrication and opens new avenues for the development of joint replacement materials that more closely mimic the natural function of cartilage.

5.7 Supplementary Information: NPFlex Roughness Measurements

A NPFLEX (Bruker, USA) optical interferometer was used to measure the surface roughness of the polished unfunctionalised PEEK and SPMK-g-PEEK samples using a non-contact vertical scanning interferometry (VSI) method, analysing surface reflections to create interference fringes at a 50× optical magnification. Three different 250 × 250 μm areas of each sample were scanned using a high intensity monochromatic green light to enhance reflection and minimise data loss. Optical profilometry data was processed using Bruker Vision64 software to calculate the mean arithmetic roughness (R_a) for each sample area.

Table 5.3 summarises the average roughness for three (N = 3) areas of both dry PEEK and SPMK-g-PEEK. Surface roughness of the unfunctionalised PEEK measured a mean roughness of R_a = 101 ± 9.8 nm (N = 3), and mean roughness of the SPMK-g-PEEK measured R_a = 304 ± 10.9 nm (N = 3).

Table 5.3: Average roughness (R_a) of three (N = 3) 250 × 250 μm areas of dry PEEK and SPMK-g-PEEK along with the calculated mean and one standard deviation (S.D.) for each sample.

	Average R_a (μm), (N = 3)			Mean ± S.D. (μm)
PEEK	92	99	115	101 ± 9.8
SPMK-g-PEEK	289	310	314	304 ± 10.9

Representative roughness measurements for dry unfunctionalised PEEK and SPMK-g-PEEK are shown in Figure 5.9.

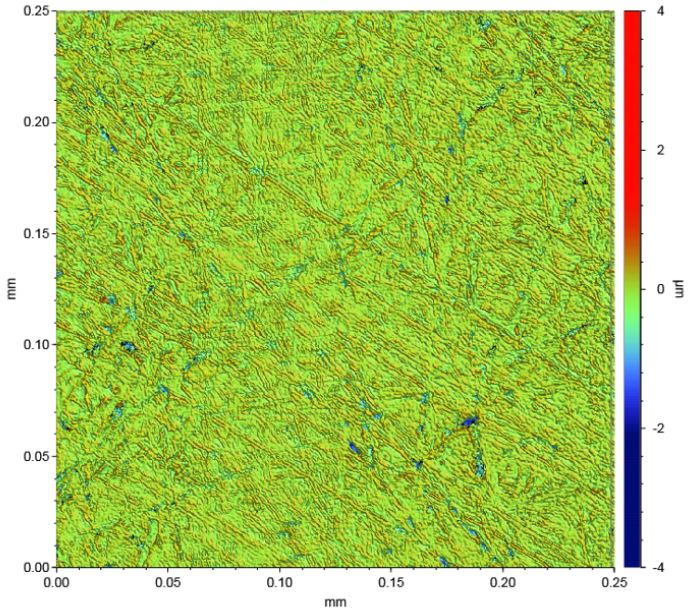

(a)

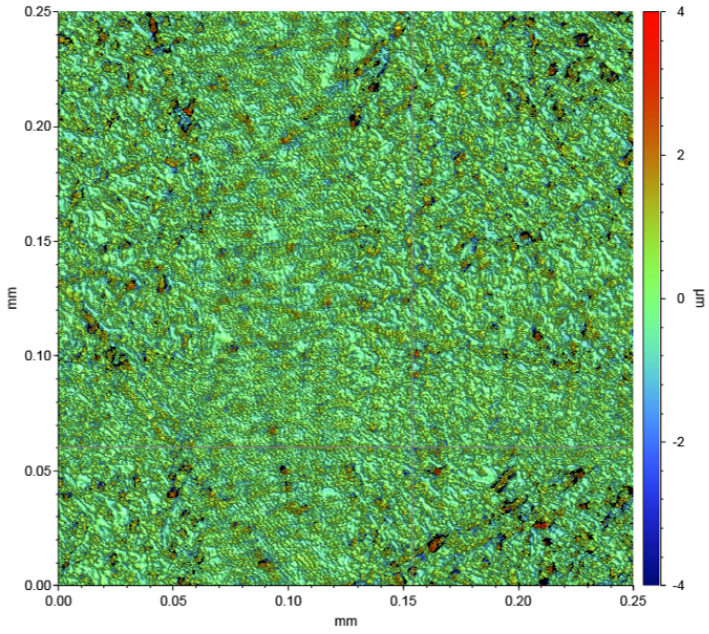

(b)

Figure 5.9: Representative height maps measuring the surface profile heights of 5.9a PEEK (R_a = 101 ± 9.8 nm (N = 3)) and 5.9b SPMK-g-PEEK (R_a = 304 ± 10.4 nm (N = 3)).

References

[1] R J Elkington, R M Hall, A R Beadling, H Pandit, and M G Bryant. Highly lubricious spmk-g-peek implant surfaces to facilitate rehydration of articular cartilage. *J. Mech. Behav. Biomed. Mater.*, 147:106084, 2023.

[2] Weifeng Lin and Jacob Klein. Hydration lubrication in biomedical applications: From cartilage to hydrogels. *Acc. Mater. Res.*, 3(2):213–223, 2022.

[3] Nicholas D Spencer. *Aqueous lubrication: natural and biomimetic approaches*, volume 3. World Scientific, 2014.

[4] Piotr Mocny and Harm-Anton Klok. Tribology of surface-grafted polymer brushes. *MSDE*, 1(2):141–154, 2016.

[5] Motoyasu Kobayashi, Hiroyoshi Tanaka, Myo Minn, Joichi Sugimura, and Atsushi Takahara. Interferometry study of aqueous lubrication on the surface of polyelectrolyte brush. *ACS Appl. Mater. Interfaces.*, 6(22):20365–20371, 2014.

[6] Motoyasu Kobayashi and Atsushi Takahara. Tribological properties of hydrophilic polymer brushes under wet conditions. *Chem. Rec.*, 10(4):208–216, 2010.

[7] LI Jinpeng, YANG Shuyan, WU Yang, LI Xinming, GUO Feng, and ZHOU Feng. Correlation between water film thickness and tribological behavior of polymer brush in aqueous lubrication. *Tribology*, 41(6):858–869, 2021.

[8] Robert Elkington, Andrew Beadling, Richard Hall, Hemant Pandit, and Michael Bryant. Biomimetic highly lubricious polyelectrolyte functionalized peek surfaces for novel hemiarthroplasty implants and focal resurfacing. In *Orthop. Proc.*, volume 103, pages 34–34. Bone & Joint, 2021.

[9] Carmine Putignano, David Burris, Axel Moore, and Daniele Dini. Cartilage rehydration: The sliding-induced hydrodynamic triggering mechanism. *Acta Biomater.*, 125:90–99, 2021.

[10] A C Moore and David L B. Tribological rehydration of cartilage and its potential role in preserving joint health. *Osteoarthritis Cartilage*, 25(1):99–107, 2017.

[11] Axel C Moore, Jordyn Lee Schrader, Jaclyn J Ulvila, and David L Burris. A review of

methods to study hydration effects on cartilage friction. *Tribol. - Mater. Surf. Interfaces*, 11(4):202–214, 2017.

[12] Sufia Fatima. *Bio-inspired surfaces using zwitterionic polymer for functional aqueous lubrication (PhD Thesis)*. PhD thesis, Univ. Leeds, 2022.

[13] JL Lanigan, S Fatima, TV Charpentier, A Neville, D Dowson, and M Bryant. Lubricious ionic polymer brush functionalised silicone elastomer surfaces. *Biotribology*, 16:1–9, 2018.

[14] Shengwei Xiao, Baiping Ren, Lei Huang, Mingxue Shen, Yanxian Zhang, Mingqiang Zhong, Jintao Yang, and Jie Zheng. Salt-responsive zwitterionic polymer brushes with anti-polyelectrolyte property. *Curr. Opin. Chem. Eng.*, 19:86–93, 2018.

[15] Md Mahmudul Hasan, Christopher L Johnson, and Alison C Dunn. Soft contact mechanics with gradient-stiffness surfaces. *Langmuir*, 38(31):9454–9465, 2022.

[16] Tooba Shoaib, Joerg Heintz, Josue A Lopez-Berganza, Raymundo Muro-Barrios, Simon A Egner, and Rosa M Espinosa-Marzal. Stick–slip friction reveals hydrogel lubrication mechanisms. *Langmuir*, 34(3):756–765, 2018.

[17] Alison C Dunn, Juan Manuel Uruena, Yuchen Huo, Scott S Perry, Thomas E Angelini, and W Gregory Sawyer. Lubricity of surface hydrogel layers. *Tribol. Let.*, 49:371–378, 2013.

[18] Gwidon Stachowiak and Andrew W Batchelor. *Engineering tribology*. Butterworth-Heinemann, 2013.

[19] Kjirste C Morrell, W Andrew Hodge, David E Krebs, and Robert W Mann. Corroboration of in vivo cartilage pressures with implications for synovial joint tribology and osteoarthritis causation. *PNAS*, 102(41):14819–14824, 2005.

[20] Yuji Higaki, Motoyasu Kobayashi, Tomoyasu Hirai, and Atsushi Takahara. Direct polymer brush grafting to polymer fibers and films by surface-initiated polymerization. *Polym. J.*, 50(1):101–108, 2018.

[21] D Imeson. On the spatial resolution of edx composition determination. *Ultramicroscopy*, 9(3):307–310, 1982.

[22] Margot S Farnham, Kyla F Ortved, Jeffrey S Horner, Norman J Wagner, David L Burris,

and Christopher Price. Lubricant effects on articular cartilage sliding biomechanics under physiological fluid load support. *Tribol. Let.*, 69:1–14, 2021.

[23] Margot S Farnham, Riley E Larson, David L Burris, and Christopher Price. Effects of mechanical injury on the tribological rehydration and lubrication of articular cartilage. *J. Mech. Behav. Biomed. Mater.*, 101:103422, 2020.

[24] Daniel M Espino, Duncan ET Shepherd, and David WL Hukins. Viscoelastic properties of bovine knee joint articular cartilage: dependency on thickness and loading frequency. *BMC Musculoskelet. Disord.*, 15(1):1–9, 2014.

[25] Na Wang, Ana-Maria Trunfio-Sfarghiu, Daniel Portinha, Sylvie Descartes, Etienne Fleury, Yves Berthier, and Jean-Paul Rieu. Nanomechanical and tribological characterization of the mpc phospholipid polymer photografted onto rough polyethylene implants. *Colloids Surf. B: Biointerfaces*, 108:285–294, 2013.

[26] JinJing Liao, David W Smith, Saeed Miramini, Bruce S Gardiner, and Lihai Zhang. Investigation of role of cartilage surface polymer brush border in lubrication of biological joints. *Friction*, pages 1–18, 2021.

[27] P Kumar, M Oka, J Toguchida, M Kobayashi, E Uchida, T Nakamura, and K Tanaka. Role of uppermost superficial surface layer of articular cartilage in the lubrication mechanism of joints. *J. Anat.*, 199(3):241–250, 2001.

[28] Yoshinori Sawae, Teruo Murakami, Kenji Matsumoto, and Masayuki Horimoto. Study on morphology and lubrication of articular cartilage surface with atomic force microscopy. *J. Jap. Soc. Tribol.*, 45(2):150–157, 2000.

[29] R Crockett, S Roos, P Rossbach, C Dora, W Born, and H Troxler. Imaging of the surface of human and bovine articular cartilage with esem and afm. *Tribol. Lett.*, 19:311–317, 2005.

[30] CL Johnson and AC Dunn. Tribological characterization of gradient-density polyacrylamide hydrogel surfaces. *Exp. Mech.*, 61:829–842, 2021.

[31] Angela A Pitenis, Juan Manuel Urueña, Andrew C Cooper, Thomas E Angelini, and W Gregory Sawyer. Superlubricity in gemini hydrogels. *J. Tribol.*, 138(4):042103, 2016.

[32] Weifeng Lin and Jacob Klein. Recent progress in cartilage lubrication. *J. Adv. Mater.*, 33(18):2005513, 2021.

[33] Rigoberto C Advincula, William J Brittain, Kenneth C Caster, and Jürgen Rühe. *Polymer brushes: synthesis, characterization and applications.* John Wiley & sons, 2006.

[34] Yunlong Yu, Marco Cirelli, Pengfei Li, Zhichao Ding, Yue Yin, Yucheng Yuan, Sissi De Beer, G Julius Vancso, and Shiyong Zhang. Enhanced stability of poly (3-sulfopropyl methacrylate potassium) brushes coated on artificial implants in combatting bacterial infections. *Ind. Eng. Chem. Res.*, 58(47):21459–21465, 2019.

[35] Yuji Higaki, Motoyasu Kobayashi, Daiki Murakami, and Atsushi Takahara. Anti-fouling behavior of polymer brush immobilized surfaces. *Polym. J.*, 48(4):325–331, 2016.

[36] Sabrina Jahn and Jacob Klein. Hydration lubrication: the macromolecular domain. *Macromolecules*, 48(15):5059–5075, 2015.

[37] Uri Raviv, Suzanne Giasson, Nir Kampf, Jean-François Gohy, Robert Jérôme, and Jacob Klein. Lubrication by charged polymers. *Nature*, 425(6954):163–165, 2003.

[38] Margot S Farnham, Kyla F Ortved, David L Burris, and Christopher Price. Articular cartilage friction, strain, and viability under physiological to pathological benchtop sliding conditions. *CMBE*, 14(4):349–363, 2021.

[39] Alan J Grodzinsky, Marc E Levenston, Moonsoo Jin, and Eliot H Frank. Cartilage tissue remodeling in response to mechanical forces. *Annu. Rev. Biomed. Eng.*, 2(1):691–713, 2000.

[40] Brian T Graham, Axel C Moore, David L Burris, and Christopher Price. Sliding enhances fluid and solute transport into buried articular cartilage contacts. *Osteoarthritis Cartilage*, 25(12):2100–2107, 2017.

[41] Van C Mow and Rik Huiskes. *Basic orthopaedic biomechanics & mechano-biology.* Lippincott Williams & Wilkins, 2005.

[42] Sabrina Jahn, Jasmine Seror, and Jacob Klein. Lubrication of articular cartilage. *Annu. Rev. Biomed. Eng.*, 18:235–258, 2016.

[43] Nigel Marx, Johan Guegan, and Hugh A Spikes. Elastohydrodynamic film thickness of soft ehl contacts using optical interferometry. *Tribol. Int.*, 99:267–277, 2016.

[44] Seunghwan Lee and Nicholas D Spencer. Aqueous lubrication of polymers: Influence of surface modification. *Tribol. Int.*, 38(11-12):922–930, 2005.

[45] Nicholas D Spencer. Aqueous lubrication with poly (ethylene glycol) brushes. *Tribology Online*, 9(4):143–153, 2014.

[46] Yuki A Meier, Kaihuan Zhang, Nicholas D Spencer, and Rok Simic. Linking friction and surface properties of hydrogels molded against materials of different surface energies. *Langmuir*, 35(48):15805–15812, 2019.

[47] Alison C Dunn, W Gregory Sawyer, and Thomas E Angelini. Gemini interfaces in aqueous lubrication with hydrogels. *Tribol. Lett.*, 54:59–66, 2014.

[48] Seonghun Park, Kevin D Costa, and Gerard A Ateshian. Microscale frictional response of bovine articular cartilage from atomic force microscopy. *J. Biomech.*, 37(11):1679–1687, 2004.

[49] Seunghwan Lee and Nicholas D Spencer. Achieving ultralow friction by aqueous, brush-assisted lubrication. In *Superlubricity*, pages 365–396. Elsevier, 2007.

[50] IC Clarke, R Contini, and RM Kenedi. Friction and wear studies of articular cartilage: a scanning electron microscope study. *J. Lubr. Technol.*, 97(3):358–366, 1975.

[51] A Unsworth, D Dowson, and V Wright. Some new evidence on human joint lubrication. *Ann. Rheum. Dis.*, 34(4):277, 1975.

[52] A Unsworth, D Dowson, and V Wright. The frictional behavior of human synovial joints—part i: natural joints. 1975.

[53] Matteo Caligaris and Gerard A Ateshian. Effects of sustained interstitial fluid pressurization under migrating contact area, and boundary lubrication by synovial fluid, on cartilage friction. *Osteoarthritis Cartilage*, 16(10):1220–1227, 2008.

[54] Margot S Farnham and Christopher Price. Translational cartilage tribology: How close are we to physiologically relevant benchtop articular cartilage testing? *Tribol. Lub. Tech., TLT Arch.*, pages 1–10, 2020.

[55] ED Bonnevie, VJ Baro, L Wang, and David L Burris. In situ studies of cartilage microtribology: roles of speed and contact area. *Tribol. Lett.*, 41:83–95, 2011.

[56] Axel C Moore and David L Burris. An analytical model to predict interstitial lubrication of cartilage in migrating contact areas. *J. Biomech.*, 47(1):148–153, 2014.

[57] David L Burris and Axel C Moore. Cartilage and joint lubrication: new insights into the role of hydrodynamics. *Biotribology*, 12:8–14, 2017.

[58] JOSEPH M Mansour and Van C Mow. The permeability of articular cartilage under compressive strain and at high pressures. *JBJS*, 58(4):509–516, 1976.

[59] Stephen Whitaker. Flow in porous media i: A theoretical derivation of darcy's law. *Transp. Porous Media*, 1:3–25, 1986.

[60] Carmine Putignano, Luciano Afferrante, Giuseppe Carbone, and Giuseppe P Demelio. A multiscale analysis of elastic contacts and percolation threshold for numerically generated and real rough surfaces. *Tribol. Int.*, 64:148–154, 2013.

[61] Gerard A Ateshian, Michael A Soltz, Robert L Mauck, Ines M Basalo, Clark T Hung, and W Michael Lai. The role of osmotic pressure and tension-compression nonlinearity in the frictional response of articular cartilage. *Transp. Porous Media*, 50:5–33, 2003.

[62] Teruo Murakami and Atsushi Suzuki. Superior tribological behaviors of articular cartilage and artificial hydrogel cartilage. *Encyclopedia of Biocolloid and Biointerface Science*, pages 278–291, 2016.

[63] Gerard A Ateshian. The role of interstitial fluid pressurization in articular cartilage lubrication. *J. Biomech.*, 42(9):1163–1176, 2009.

[64] Matej Daniel. Boundary cartilage lubrication: Review of current concepts. *WMW*, 164(5-6):88–94, 2014.

[65] Ramaswamy Krishnan, Monika Kopacz, and Gerard A Ateshian. Experimental verification of the role of interstitial fluid pressurization in cartilage lubrication. *J. Orthop. Res.*, 22(3):565–570, 2004.

[66] Alanna R Gannon, Thomas Nagel, and Daniel J Kelly. The role of the superficial region in determining the dynamic properties of articular cartilage. *Osteoarthritis Cartilage*, 20(11):1417–1425, 2012.

[67] Benjamin G Cooper, TB Lawson, Brian D Snyder, and Mark W Grinstaff. Reinforcement of articular cartilage with a tissue-interpenetrating polymer network reduces friction and modulates interstitial fluid load support. *Osteoarthritis Cartilage*, 25(7):1143–1149, 2017.

[68] Steven Voinier, AC Moore, Jamie M Benson, C Price, and David Lawrence Burris. The modes and competing rates of cartilage fluid loss and recovery. *Acta Biomater.*, 138:390–397, 2022.

[69] Rosa M Espinosa-Marzal, Robert M Bielecki, and Nicholas D Spencer. Understanding the role of viscous solvent confinement in the tribological behavior of polymer brushes: A bioinspired approach. *Soft Mat.*, 9(44):10572–10585, 2013.

[70] Michael A Soltz and Gerard A Ateshian. Experimental verification and theoretical prediction of cartilage interstitial fluid pressurization at an impermeable contact interface in confined compression. *J. Biomech.*, 31(10):927–934, 1998.

[71] Teruo Murakami, Seido Yarimitsu, Kazuhiro Nakashima, Yoshinori Sawae, and Nobuo Sakai. Influence of synovia constituents on tribological behaviors of articular cartilage. *Friction*, 1:150–162, 2013.

[72] Matteo Caligaris, Clare E Canal, Christopher S Ahmad, Thomas R Gardner, and Gerard A Ateshian. Investigation of the frictional response of osteoarthritic human tibiofemoral joints and the potential beneficial tribological effect of healthy synovial fluid. *Osteoarthritis Cartilage*, 17(10):1327–1332, 2009.

[73] TA Schmidt and RL Sah. Effect of synovial fluid on boundary lubrication of articular cartilage. *Osteoarthritis Cartilage*, 15(1):35–47, 2007.

[74] AHA Damen, CC van Donkelaar, RM Cardinaels, J-M Brandt, TA Schmidt, and Keita Ito. Proteoglycan 4 reduces friction more than other synovial fluid components for both cartilage-cartilage and cartilage-metal articulation. *Osteoarthritis Cartilage*, 29(6):894–904, 2021.

[75] J O'kelly, A Unsworth, D Dowson, DA Hall, and V Wright. A study of the role of synovial fluid and its constituents in the friction and lubrication of human hip joints. *Eng. Med.*, 7(2):73–83, 1978.

[76] A Unsworth. Tribology of human and artificial joints. *Proc. Inst. Mech. Eng. H: J. Eng. Med.*, 205(3):163–172, 1991.

[77] R Crockett, A Grubelnik, S Roos, C Dora, W Born, and H Troxler. Biochemical compo-

sition of the superficial layer of articular cartilage. *J. Biomed. Mater. Res. A, Jap. Soc. Biomat., and Aus. Soc. Biomat. & Korean Soc. Biomat.*, 82(4):958–964, 2007.

[78] Manjesh K Singh, Patrick Ilg, Rosa M Espinosa-Marzal, Martin Kroger, and Nicholas D Spencer. Polymer brushes under shear: Molecular dynamics simulations compared to experiments. *Langmuir*, 31(16):4798–4805, 2015.

[79] GN De Boer, N Raske, S Soltanahmadi, D Dowson, MG Bryant, and RW Hewson. A porohyperelastic lubrication model for articular cartilage in the natural synovial joint. *Tribol. Int.*, 149:105760, 2020.

Chapter 6

Performance Parity In Cartilage Repair: SPMK-g-PEEK Versus Cartilage-Cartilage Interfaces

6.1 Abstract

Effective fluid exudation and rehydration are essential for the low-friction function of healthy articular cartilage, facilitating interstitial fluid pressurisation, solute transport, and aqueous lubrication. However, current metallic biomaterials used in focal cartilage repair or hemiarthroplasty compromise this fluid-pressure-dependent load support, leading to the erosion of the interfacing cartilage. This study investigates bioinspired hydrophilic 3-sulfopropyl methacrylate potassium salt (SPMK) polymer grafted onto a PEEK substrate (SPMK-g-PEEK) as a potential solution. SPMK-g-PEEK aims to mimic the natural tribology of cartilage by providing an aqueous low friction interface and polyelectrolyte-enhanced tribological rehydration (PETR), supporting fluid recovery and interstitial fluid pressurisation during cartilage sliding. The tribological characteristics of physiological cartilage-cartilage interfaces, which rely on osmotic swelling and hydrodynamic tribological rehydration, are compared with PETR enabled by SPMK-g-PEEK interfaces.

This study introduces a bespoke Fuzzy-PI controlled biotribometer for *in vitro* cartilage contact assessment. Employing a dual-phase testing method, static compression followed by sliding, al-

lows simultaneous measurement of friction and cartilage strain recovery, indicative of interstitial fluid recovery following compressive exudation. Cartilage condyle, unfunctionalised PEEK, and SPMK-g-PEEK surfaces were investigated against flat cartilage plugs, which provide no hydrodynamic entrainment zone for tribological rehydration, and convex cartilage plugs, which create a convergent hydrodynamic zone for tribological rehydration. Matched cartilage-cartilage contacts exhibited low friction coefficients of ~ 0.04 and strain recovery of up to $\sim 14\%$ during the sliding phase. SPMK-g-PEEK surfaces sliding against convex cartilage plugs demonstrated similar strain recovery of $\sim 13\%$ and reduced friction coefficients of ~ 0.01, due to the combined effects of PETR and hydrodynamic tribological rehydration. In contrast, unfunctionalised PEEK surfaces, similar to current hard biomaterials employed in cartilage resurfacing, showed significantly higher friction and inhibited rehydration. SPMK-g-PEEK effectively mimics the physiological rehydration of connatural articular cartilage surfaces, highlighting its potential as a biomimetic material for cartilage resurfacing.

6.2 Introduction

For synovial joints cartilage fluid recovery has widely been attributed to articulation induced free swelling at exposed surfaces [1, 2]. Nonetheless, *in vivo* studies show the cartilage often remains in contact during unloading [3, 4]. While passive swelling can occur in the cartilage contact area during unloading, studies comparing these separate mechanisms highlight tribological rehydration can occur at a 7× greater rate than passive swelling [1]. Alternatively, fluid exchange and synovial rehydration in the cartilage contact gap has been theorised, by computational modelling, to occur due to interfacial gaps created by the opposing rough ($R_a \sim 2.0$ μm) cartilage surfaces [5, 6]. Further details of synovial mechanisms which support interstitial fluid pressurisation and rehydration are discussed in Section 1.3.4.

However, synergy between synovial rehydration (i.e. fluid exchange and osmotic swelling) within the cartilage contact gap and the macroscale geometry enabling tribological rehydration in conformal synovial joints has yet to be investigated directly. Free swelling (MCA) cartilage rehydration has been demonstrated with matched cartilage-cartilage interfaces demonstrating sustained low CoF, but does not elucidate additional rehydration behaviours (i.e. measure strain) [7]. Tribological rehydration has only been shown in a cSCA configuration against impermeable (glass) interfaces to isolate the effects of free swelling, demonstrating both sus-

tained low CoF and strain recovery [8, 9]. PETR has been demonstrated with SCA cartilage interfaced with SPMK-g-PEEK, isolating the hydrodynamic effects of tribological rehydration, demonstrating both strain recovery and low CoF due to effective aqueous boundary lubrication [10, 11, 12]. The SPMK polyelectrolyte interface enhances fluid confinement and pressurisation in the contact gap to augment fluid exchange within the loaded contact area [12, 11].

This study aims to establish an *in vitro* expanded testing framework presented in Figure 1.7b, comparing strain recovery indicative of rehydration in matched cartilage-cartilage contacts with that of cartilage paired with materials designed to enhance rehydration (SPMK-g-PEEK). There are limited studies of cartilage-cartilage interfaces, partly due to the uncertainty and challenges introduced by uneven and compliant condyle surfaces, and are limited to only studying friction rather than strain [13, 14, 15, 7]. The initial phase of the study will concentrate on quantifying tribological and fluid recovery properties of cartilage-cartilage interfaces, requiring precise adaptive load control to accommodate the dynamic nature of cartilage strain and contact area during sliding [16]. Subsequently, this will then be used as a comparative benchmark to SPMK-g-PEEK and unfunctionalised PEEK control surfaces mated against SCA and cSCA cartilage. This aims to compare hydrodynamic tribological rehydration of hard impermeable biomaterials against the combined action of PETR and hydrodynamic tribological rehydration facilitated with SPMK-g-PEEK. This approach seeks to quantitatively evaluate if SPMK-g-PEEK is a viable focal cartilage repair surface for reproducing physiological cartilage-cartilage interstitial fluid recovery and low friction.

6.3 Methods

6.3.1 Materials

SPMK monomer, PBS, and 5 mm thick PEEK (450G. Victrex, UK) sectioned into 25 × 25 mm square samples with a surface roughness (R_a) of approximately 100 nm are employed in this study, as detailed in Section 3.3.1.

SPMK-g-PEEK surfaces with a polyelectrolyte thickness of approximately 400 nm featuring a high density of hydrophilic anionic sulfonic acid groups were produced following the methodology described in Section 3.3.3).

SCA cartilage plugs, ⌀ 7.2 mm diameter, were extracted from the patellofemoral grooves of

bovine stifle joints using the methodology described in Section 3.3.2. Larger cSCA explants were harvested from the lateral and medial femoral condyles using a 20 mm holesaw with an internal diameter of 18 mm. These methods and explant dimensions follow previous work which obtain flat ⌀7.2 mm SCA contacts [12, 11] and convex ⌀18 mm cSCA contacts [17, 18]. Any samples with surface defects or SCA samples with a planar height difference of > 0.2 mm were discarded. Following extraction all cartilage samples were cryopreserved ($-18°$C) in PBS, prior to testing samples were thawed for at least 12 hours in a refrigerator followed by acclimatisation to room temperature for an additional 2 hours.

6.3.2 Fuzzy-PI Enabled Tribometer

Figure 6.1 shows the bespoke tribometer employing two Precision Linear Stages (PLS) (Phyisk Instrumente GmbH and Co, Germany); an indenter PLS (Z-axis, L-509 Precision Linear Stage) to apply normal force and a sliding PLS (X-axis, L-511 High-Precision Linear Stage) to facilitate sliding perpendicular to the direction of loading. The indenter PLS has a maximum velocity of 20 mm/s, the larger sliding PLS has a maximum velocity of 90 mm/s with linear position (X) tracked by a Linear Variable Differential Transformer (LVDT) with a resolution of 0.1 μm. A six-axis load cell (ATI Industrial Automation Inc, USA) was mounted perpendicular to the test cell along with a cartilage plug mount, fixed to the stage of the indenter PLS. The load cell can measure maximum loads of 145 N with a resolution of 62.5 mN, in this setup only the forces in the Z and X directions were used to measure the normal force (F_Z) and tangential force (F_X) respectively. A detailed schematic of the test cell is also shown in Figure 6.1 showing a cSCA cartilage plug mounted on the 6-axis load cell with a SPMK-g-PEEK plate submerged in PBS in the test cell bath. This setup was controlled using a custom LabVIEW programme interfaced with a CompactRIO embedded controller (National Instruments, USA). Normal force (F_Z) was maintained throughout testing using Fuzzy-PI control [19]. The advanced controller integrates a Fuzzy 'supervisor' with a PI 'slave' in a synergistic manner. As the system operates,the error generated by the PI controller is used as an input variable for the Fuzzy controller. The interface engine of the Fuzzy controller then calculates the new Proportional (P) and Integral (I) gains in real time, which the PI controller uses to dynamically adjust its feedback parameters. This approach ensures that the controller adapts to the changing cartilage contact deformation resulting from temporal variations in hydration and strain during testing.

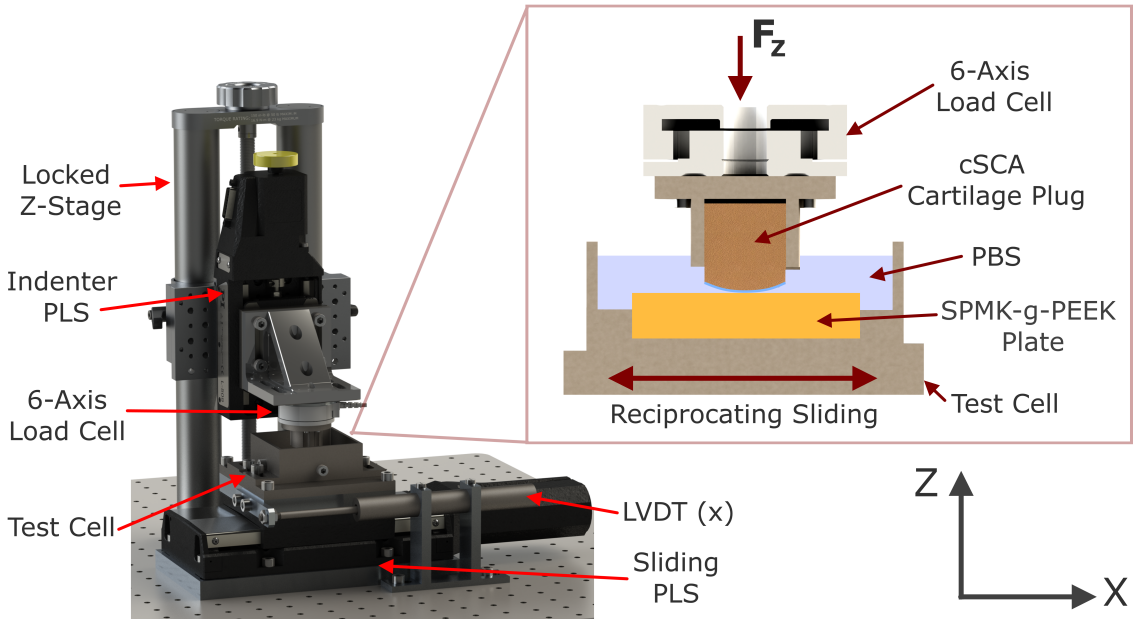

Figure 6.1: Schematic of the Fuzzy-PI tribometer instrumented with load cell, indenter and sliding PLS, and LVDT labelled with callout view of test cell show cSCA cartilage sliding against a SPMK-g-PEEK plate submerged in PBS.

6.3.3 Experimental Overview

To evaluate the tribological performance and rehydration characteristics, both the SCA (no tribological rehydration) and cSCA (tribological rehydration) cartilage pins were subjected to a rehydration cycle comprising of a compression phase followed by sliding. These tests were conducted against three distinct substrates: a physiological control of a condyle plate (synovial rehydration), unfunctionalised PEEK (no PETR rehydration), and SPMK-g-PEEK (PETR rehydration). The rationale for each substrate-cartilage pin combination are summarised in Table 6.1.

Table 6.1: Overview of rehydration cycle experiments conducted with SCA and cSCA cartilage pins against cartilage condyle, unfunctionalised PEEK, and surface modified SPMK-g-PEEK substrates.

Pin Geometry-Substrate Contact	**Rehydration Mechanisms**
SCA-Condyle (N = 3)	Synovial Rehydration
cSCA-Condyle (N = 3)	Tribological + Synovial Rehydration
SCA-PEEK (N = 3)	No Rehydration
cSCA-PEEK (N = 3)	Tribological Rehydration
SCA-SPMK (N = 3)	PETR
cSCA-SPMK (N = 3)	Tribological + PETR Rehydration

Akin to Figure 1.7b, the rehydration cycle consisted of an 1800 s compression period (0 ≤

$t < 1800s$) followed by 1800 s of reciprocating sliding ($1800 \leq t \leq 3600s$) at a frequency of 1 Hz over a 10 mm linear sliding distance. Throughout the whole rehydration cycle a constant normal load of 20 N was maintained using Fuzzy-PI control [19]. The contact pressure under a 20 N load across a 7.2 mm diameter flat SCA is calculated to be approximately 0.50 MPa. This estimate is also consistent for the larger 18 mm convex cSCA, where optical measurements against impermeable surfaces (glass) suggest a similar effective contact area of about $\sim$ 7 mm [17], resulting in a comparable contact pressure of 0.50 MPa. These values fall within the typical physiological spatially and temporally averaged contact stresses in the range of 0.1 - 5.0 MPa for mammalian joints [20, 10]. All tests were conducted in a fully submerged environment of phosphate buffered saline (PBS), serving dual purposes. Primarily, PBS acted as an aqueous medium, facilitating the rehydration of cartilage throughout the sliding phase. Secondly, PBS maintained a stable osmotic gradient to sustain physiological cartilage swelling.

6.3.3.1 Sliding and Measurement of Coefficient of Friction

The tribometer enabled reciprocating sliding motion at 1 Hz, with a linear displacement (X) of $\pm$ 10 mm and a peak velocity of 31.4 mm/s. To capture the dynamic changes in the Coefficient of Friction (CoF, μ), both normal (F_Z) and tangential (F_X) forces were sampled at a frequency of 50 Hz. CoF, Equation 6.1, is calculated as the mean value of data sampled during the middle 50% of each linear reciprocation ($2.5 \leq X \leq 7.5$ mm). This range, encompassing the speed range of 22.1 to 31.4 mm/s, is highlighted in the shaded regions of Figure 6.2 showing a representative X displacement versus tangential force F_x plot. This specific range can be considered the steady-state period of the sliding cycle. Of particular note are the CoF upon the startup of the sliding cycle (μ_S, t = 1800 s) and the final CoF achieved at the end of sliding (μ_F, t = 3600 s).

$$\mu = \frac{F_x}{F_z} \tag{6.1}$$

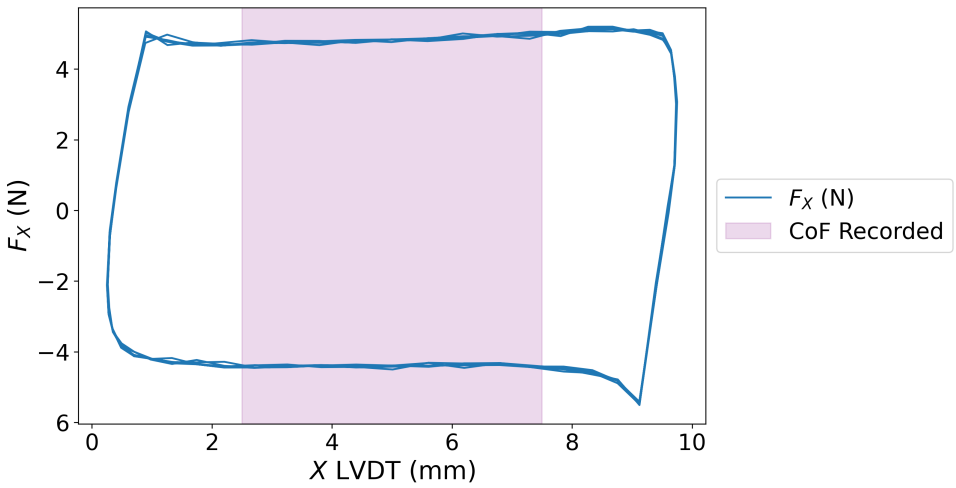

Figure 6.2: Representative plot of X displacement versus tangential force (F_X) illustrating the region (shaded) used for calculating the coefficient of friction (CoF) values. CoF is computed as the mean value within this shaded area ($2.5 \leq X \leq 7.5$ mm). This plot depicts five X-F_X curves for the cSCA-PEEK condition (Table 6.1).

6.3.3.2 Cartilage Compression

Vertical displacement was monitored using the PLS inbuilt linear encoder for direct position measuring with a sampling frequency of 5 Hz. Vertical displacement is calculated as the average change in sample height over every five consecutive reciprocating cycles, indicating the strain response of the cartilage pin. Cartilage strain recovery during the sliding phase ($\varepsilon_r(t)$, Equation 6.2) was determined by subtracting the vertical displacement of the contact pair at the start of sliding ($Z(t = 1800\ s)$) from the time dependant vertical displacement ($Z(t)$), and normalising this difference by the swollen, uncompressed cartilage height (h_0) (Sec. 3.3.8). This quantifies the cartilage strain recovery, attributing positive values of $\varepsilon_r(t)$ to sliding induced interstitial fluid recovery, and negative values to sustained fluid loss exhibited as continued compression. Referring to IFP theory (Eq. 1.3), the initial 30-minute compression phase aims to induce cartilage strain toward the equilibrium state ($\varepsilon_C \Rightarrow \varepsilon_{eq}$). Therefore, increasing strain recovery ($\varepsilon_r(t)$) during sliding is expected to result in a lower steady-state coefficient of friction (μ_F) compared to the startup coefficient (μ_S).

It is important to note that SPMK-g-PEEK and PEEK samples are treated as incompressible materials. In comparison, the compression phase against compliant cartilage condyles results in deformation of both the pin and the condyle surface over a larger contact area, and correspondingly lower contact pressures. Therefore, to measure the change in height attributable to the cartilage pin, the X-positions of the deformed condyle following compression phase were

excluded from the calculation of average $Z(t)$ displacement. This complicates direct comparison to IFP theory discussed in Equation 1.3, as the equilibrium strain (ε_{eq}) of the cartilage plug cannot be precisely determined at the end of the compression phase (ε_C). However, calculation of the overall strain recovery ($\varepsilon_r(t = 3600s)$), denoted as ε_r, remains consistent with previous protocols utilised to quantify strain recovery attributable to tribological rehydration on cSCA cartilage [21, 9] and PETR of SCA cartilage [11, 12].

$$\varepsilon_r(t) = \frac{Z(t = 1800\ s) - Z(t)}{h_0} \tag{6.2}$$

6.3.3.3 Statistical Analysis

Independent t-tests were conducted to compare the mean overall strain recovery (ε_r), startup CoF (μ_S) and final CoF (μ_F) across different contact pairs (Table X). The t-tests were used to determine if there were significant differences between the means of two independent groups under different conditions. The *t-statistic* quantifies the difference between the sample means in terms of standard deviations; a higher absolute t-statistic value indicates a greater difference between the groups. The *p-value* represents the likelihood that the observed differences are due to experimental error. In this study, a significance level of 0.05 was used, meaning p-values below 0.05 were considered statistically significant. Independent t-tests were performed to compare:

- **Contact Geometry**: SCA vs. cSCA for each substrate (PEEK, Condyle, SPMK), elucidating the contribution of tribological rehydration facilitated by the cSCA contact.
- **Substrate Effects:** PEEK and SPMK-g-PEEK vs. matched cartilage for both SCA and cSCA conditions, elucidating the contribution of substrate hydration to replicate the tribology of matched cartilage (physiological condition).

This focused statistical approach allows for the quantitative assessment of the effects of geometric and surface interactions on cartilage tribology and rehydration. The full pairwise t-tests results across all contact conditions are provided in the supporting information (Tab. A1). Primarily, this approach seeks to determine if PETR (i.e. SPMK-g-PEEK substrates) can mimic native synovial rehydration of matched cartilage (i.e. condyle substrates).

6.4 Results & Discussion

Table 6.2 summarises the mean applied load, F_Z ± one standard deviation, throughout the sliding phase. Variability of applied load was most pronounced when interacting with cartilage condyle surfaces (Supplementary Figure A1) and in the case of the highest strain PEEK conditions leading a maximum deviation of ± 1.53 N. The Fuzzy-PI controllers capability to dynamically tune the PI controller [19] was effective in responding to the temporal cartilage deformation and maintaining an approximately constant 20 N load throughout sliding. Notably, matched cartilage tribology studies often do not disclose the normal load error nor state the deviation [7, 22, 23, 24, 25]. This lack of reporting makes direct comparisons challenging. However, the observed maximum deviation of ± 1.53 N is relatively small (∼ 7.5% of the target load of 20 N), whereas previous studies on matched cartilage have shown that for contact pressures with a 25% difference (ranging from 0.3 - 0.4 MPa) steady state CoF remains consistent at approximately $\mu \sim 0.03$ [24]. This studies level of F_Z deviation is unlikely to significantly impact the tribological performance or the general conclusions drawn from the study.

Table 6.2: Summary of the mean applied normal load (F_Z), mean overall strain recovery (ε_r), mean initial startup CoF (μ_S), and mean final CoF (μ_F) for each test configuration. The values are based on tests conducted in accordance with the parameters specified in Table 6.1. Each test was performed in triplicate (N = 3), and the data are presented as mean ± one standard deviation.

Test (N = 3)	**Applied Load** F_Z (N)	**Strain Recovery** ε_r (%)	**Startup CoF** μ_S (-)	**Final CoF** μ_F (-)
SCA-Condyle	19.87 ± 1.53	8.77 ± 3.10	0.133 ± 0.032	0.049 ± 0.012
cSCA-Condyle	19.69 ± 1.39	14.11 ± 4.15	0.125 ± 0.025	0.038 ± 0.020
SCA-PEEK	19.89 ± 0.81	-4.69 ± 1.60	0.300 ± 0.045	0.269 ± 0.064
cSCA-PEEK	19.77 ± 1.01	4.15 ± 1.01	0.282 ± 0.069	0.148 ± 0.037
SCA-SPMK	20.21 ± 0.29	7.04 ± 1.71	0.038 ± 0.024	0.011 ± 0.006
cSCA-SPMK	19.98 ± 0.39	12.95 ± 2.55	0.043 ± 0.012	0.007 ± 0.004

Table 6.2 also summarises the mean overall strain recovery (ε_r), the mean startup CoF (μ_S, measured at t = 1800 s) and the mean final CoF (μ_F, measured at t = 3600 s) with one standard deviation of error for all test scenarios detailed in Table 6.1. Strain recovery (ε_r) was noted for five out of six contact conditions explored during the sliding phase coinciding with decreasing CoF, broadly complying with the principles of IFP theory (Eq. 1.3). The only sample that did not exhibit reducing strain or CoF was PEEK - SCA cartilage which is

expected, as this configuration facilitates no rehydration mechanism. The specific relationship between CoF and strain recovery for each contact pair are discussed in subsequent sections. Principally, this methodology attempts to replicate the fluid recovery processes inherent to physiological cartilage-cartilage interactions and contrast with the rehydration capabilities of SPMK-g-PEEK [12, 10, 11].

6.4.1 Effect of Contact Geometry (SCA vs. cSCA)

Greater cartilage strain recovery (ε_r) and subsequently lower final CoF are expected for cSCA geometry cartilage pins. This geometry facilitates tribological rehydration through hydrodynamic pressurisation in the convergent-wedge inlet, in contrast to SCA, which lacks a convergent wedge and operates independently of tribological rehydration [18, 11]. Table 6.3 summarises the independent *t*-tests performed for each substrate (PEEK, SPMK-g-PEEK, cartilage condyle) interfaced with cartilage in SCA and cSCA conditions. For all contact pairs, the startup CoF (μ_S) is unaffected by contact geometry ($p > 0.7$), which is expected as this corresponds to the cartilage pin is in the highest strain state ahead of any rehydration. Overall strain recovery (ε_r) is enhanced by tribological rehydration (cSCA conditions) against engineered PEEK and SPMK-g-PEEK substrates ($p < 0.05$). Whereas against a cartilage condyle, the contribution of strain recovery attributed to tribological rehydration is reduced ($p = 0.15$), suggesting fluid recovery is dominated by alternate synovial surface rehydration effects. In contrast, for the condyle and SPMK-g-PEEK cases, the contact geometry (SCA versus cSCA) does not significantly impact the final CoF (μ_F, $p > 0.4$), implying that alternate substrate effects dominate the friction response. Further discussion of statistical significance is provided in subsequent sections alongside the experimental data to delineate specific fluid recovery and tribological mechanisms.

Table 6.3: **Contact Geometry:** Comparison of mean overall strain recovery (ε_r), startup CoF (μ_S) and final CoF (μ_F) between each substrate in SCA and cSCA configurations using independent t-tests. The t-statistic measures the difference between the sample means in terms of standard deviations, and the p-value indicates the statistical significance of the observed differences.

Sample Pair	Strain Recovery (ε_r)		Startup CoF (μ_S)		Final CoF (μ_F)	
	t-statistic	p-value	t-statistic	p-value	t-statistic	p-value
SCA-Condyle vs cSCA-Condyle	-1.79	0.15	0.34	0.75	0.82	0.47
SCA-PEEK vs cSCA-PEEK	-8.09	0.01	0.39	0.73	2.84	0.06
SCA-SPMK vs cSCA-SPMK	-3.68	0.04	-0.32	0.77	0.96	0.40

6.4.1.1 Cartilage vs. Cartilage Condyle

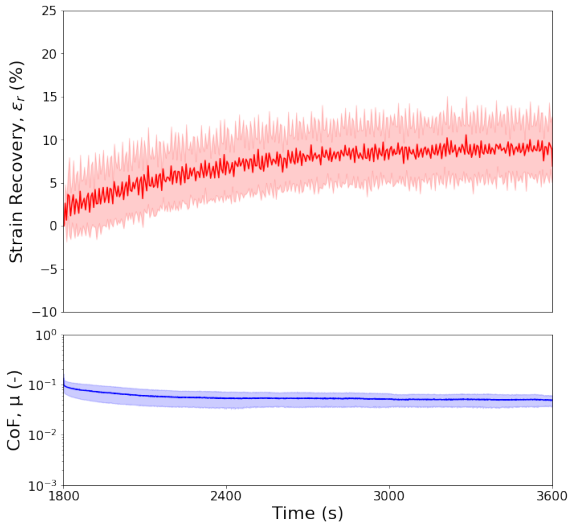

(a) SCA-Condyle (N = 3).

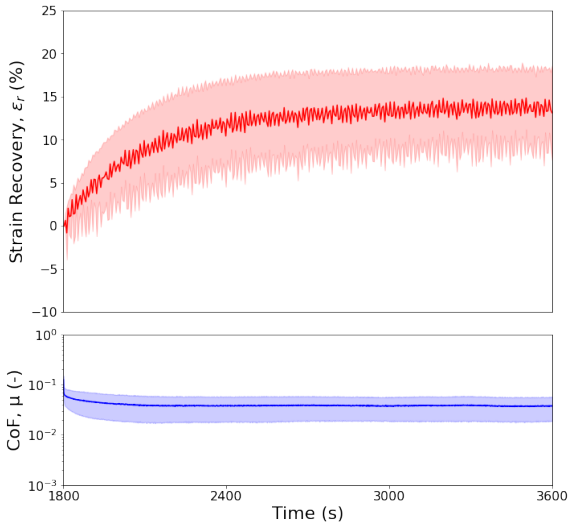

(b) cSCA-condyle (N = 3).

Figure 6.3: Strain recovery ($\varepsilon_r(t)$) and CoF ($\mu(t)$) data for the sliding phase of SCA and cSCA cartilage pins against a bovine condyle.

Figure 6.3 illustrates strain recovery from which fluid recovery is inferred for SCA and cSCA cartilage plugs throughout sliding against a cartilage condyle, indicating the recovery of interstitial fluid. Cartilage condyles sliding against the SCA plug (Fig. 6.3a) exhibited strain recovery of $\varepsilon_r = 8.77 \pm 3.10\%$. A greater strain reduction was observed for the cSCA condition (Fig. 6.3b) of $\varepsilon_r = 14.11 \pm 4.15\%$, though this result is not statistically significant ($p = 0.15$). In both instances the startup CoF at the onset of sliding was approximately $\mu_S \sim 0.13$ ($p = 0.75$), and decreased throughout sliding towards similar final CoF of $\mu_F = 0.049 \pm 0.012$ and $\mu_F = 0.038 \pm 0.020$ for the SCA and cSCA cases respectively ($p = 0.47$). Observation of strain recovery in both instances corresponds to a substantially reduced final CoF (μ_F), broadly complying with IFP theory (Eq. 1.3) [8, 7]. The authors recognise that the low sample size (N = 3) limits the statistical power of this study. Hence the contribution of tribological rehydration (cSCA condition) to strain recovery is not conclusively elucidated within this experiment, and is indicated by a low non-significant p-value ($p = 0.15$). However, the high strain recovery observed in the SCA condition ($\varepsilon_r = 8.77 \pm 3.10\%$), clearly suggests that matched cartilage rehydration appears to be dominated by alternate fluid recovery mechanisms native to interfacing synovial tissue. Potential mechanisms are discussed in later sections (Sec. 6.4.2).

The matched cartilage configuration bridges the experimental gap between the biomechanical fidelity of conformal hip pendulum experiments and the simplified conditions of pin-on-plate

studies, offering a more physiologically representative contact of conformal synovial joint mechanics [26]. Previous studies on self-mated cartilage, using both human hip pendulum experiments and multiaxial joint simulators, have consistently reported low CoF values between 0.01 - 0.06, implying sustained IFP for maintaining low friction [27, 28, 29]. Benchtop pin-on-plate studies of matched cartilage-cartilage contacts also typically examine only CoF, sustained in the region of 0.01 - 0.05 during $\leq$ 1 hour long testing [30, 25, 24, 7]. The self-mated cartilage experiments detailed in this study (Fig. 6.3) demonstrate a CoF (μ_F) of < 0.05, comparable to anticipated values, with the addition of in-situ quantification of strain recovery quantifying reuptake of interstitial fluid.

6.4.1.2 Cartilage vs. PEEK

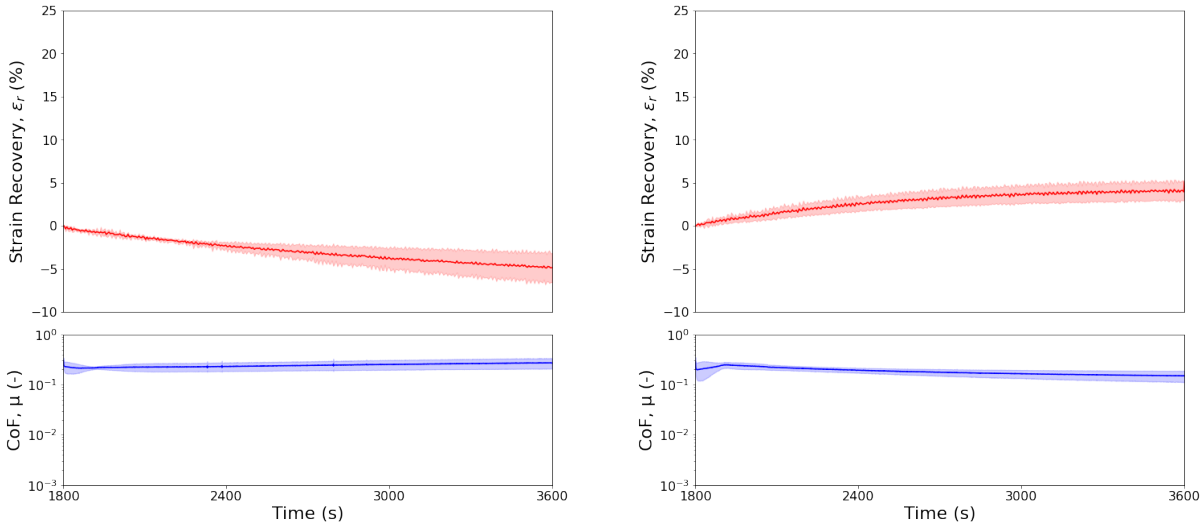

(a) SCA-PEEK (N = 3). (b) cSCA-PEEK (N = 3).

Figure 6.4: Strain recovery ($\varepsilon_r(t)$) and CoF ($\mu(t)$) data for the sliding phase of SCA and cSCA cartilage pins against unfunctionalised PEEK.

No strain recovery, indicating no rehydration, was observed for SCA cartilage sliding against PEEK plates (Fig. 6.4a), exhibited as a continuous strain increase throughout sliding (ε_r = -4.69 $\pm$ 1.60%). This observation is consistent with prior research, resembling unconfined compression, within which the flat SCA geometry fails to generate a hydrodynamic pressurisation zone necessary for facilitating fluid recovery in cartilage [10, 11, 7, 31]. Contrary to IFP theory (Eq. 1.3) and earlier findings that correlate increased strain with higher CoF [7, 11]. A marginal reduction in CoF during the SCA-PEEK sliding phase was observed, from $\mu_S = 0.300 \pm 0.045$ to $\mu_F = 0.269 \pm 0.064$. Considering the high margin of CoF error, both these results essentially

align with the maximal equilibrium CoF for SCA-PEEK [10, 11]. Indicating that the marginal differences observed are indicative of no effective fluid recovery, and the loss of IFP following compression completely inhibits cartilage lubrication.

The cSCA-PEEK condition (Fig. 6.4b) significantly enhances interstitial fluid recovery ($p = 0.003$) resulting in a strain recovery of $\varepsilon_r = 4.15 \pm 1.01\%$, indicating effective tribological rehydration [31]. Correspondingly, the reduction from a high startup CoF ($\mu_S = 0.282 \pm 0.069$) to a final CoF ($\mu_F = 0.148 \pm 0.037$) approached significance ($p = 0.06$). Indicating effective tribological rehydration consistent with IFP theory (Eq. 1.3) [31, 9]. However, the resultant final CoF, significantly exceeds safe physiological friction levels ($\sim \mu \leq 0.1$) [8], suggesting that only partial restoration of IFP was achieved. Comparatively, previous studies of glass interfaced with cSCA cartilage at a lower 7 N load ($\sim$ 0.2 MPa) demonstrate speeds of 60 - 80 mm/s are required to achieve sufficient tribological rehydration for sustaining a physiological CoF of $<$ 0.04 [31, 17, 21], corresponding to a strain recovery of $\varepsilon_r \sim 6\%$ [21, 9]. The lower sliding speeds used in this study of 22.1 - 33.4 mm/s are consistent with the speed threshold for initiating tribological rehydration [17, 21, 31], with similar studies observing CoF in the range of 0.1 - 0.3 [17, 21] and strain recovery of $\varepsilon_r \sim 1\%$ at 30 mm/s [21]. The greater strain recovery of $\varepsilon_r = 4.15 \pm 1.01\%$ observed herein is attributed to the application of a higher load of 20 N ($\sim$ 0.50 MPa). This higher load predisposes the cartilage to a greater degree of compression-induced strain, facilitating a more substantial recovery along with increased hydrodynamic pressurisation during sliding, thereby promoting more fluid recovery [17, 12, 24].

6.4.1.3 Cartilage vs. SPMK-g-PEEK

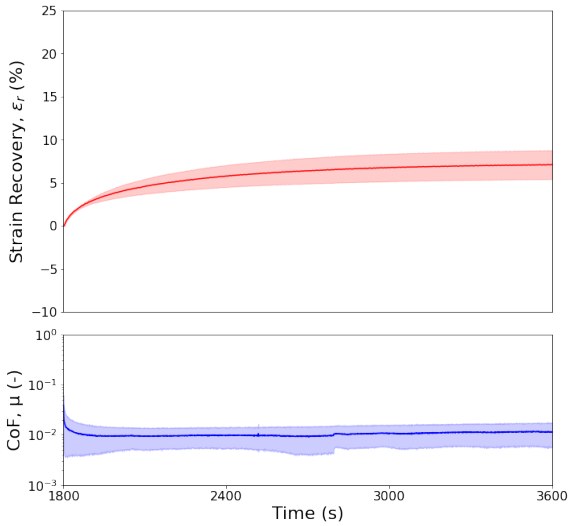

(a) SCA-SPMK (N = 3).

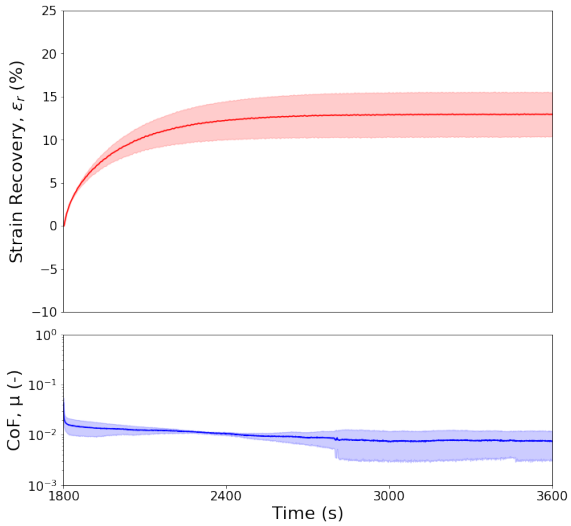

(b) cSCA-SPMK (N = 3).

Figure 6.5: Strain recovery ($\varepsilon_r(t)$) and CoF ($\mu(t)$) data for the sliding phase of SCA and cSCA cartilage pins against SPMK-g-PEEK.

Strain recovery indicative of rehydration occurred for both the SCA and cSCA cartilage pins sliding against SPMK-g-PEEK, as shown in Figure 6.5. SCA-SPMK (Fig, 6.5a) resulted in a total strain recovery of $\varepsilon_r = 7.04 \pm 1.71\%$, and cSCA-SPMK (Fig. 6.5b) exhibited a significantly greater strain recovery of $\varepsilon_r = 12.95 \pm 2.55\%$ ($p = 0.04$). Minor discrepancies between low CoF measurements (i.e., ranges below $\mu < 0.05$) are often attributed to sample misalignment rather than mechanistic differences [32]. Therefore respective startup and final CoF for the SCA-SPMK and cSCA-SPMK conditions (Table. 6.2) are considered nominally equivalent and are statistically insignificant. For both contact geometries against the highly lubricious SPMK-g-PEEK surface, the onset of sliding yielded a startup CoF of $\mu_S \sim 0.04$ ($p = 0.77$) before reaching a steady state $\mu_F \sim 0.01$ ($p = 0.40$). Concurrent strain recovery and CoF reduction during the sliding phase suggest compliance with the principles of IFP (Eq. 1.3) with increasing fluid load support corresponding to attenuated friction.

Demonstration of rehydration ($\varepsilon_r = 7.04 \pm 1.71\%$) for the SCA-SPMK interface aligns with previous studies of PETR in the same contact conditions at higher loads of 30 N (~ 0.75 MPa) at 10 mm/s exhibiting $\varepsilon_r \sim 8$ - 11% [11, 12]. The greater overall strain recovery observed for the cSCA-SPMK condition ($\varepsilon_r = 12.95 \pm 2.55\%$, $p = 0.04$), compared to the SCA condition, indicates the mechanisms of PETR and convergent contact tribological rehydration are additive, resulting in an enhanced strain recovery. This provides greater fluid recovery than observations

of cSCA tribological rehydration exclusive to convergent wedge effects, as observed against the unfunctionalised PEEK (Fig. 6.4b) and in previous studies [9, 11, 21]. Notably, enhanced strain recovery does significantly correspond to reduced final CoF between SCA and cSCA contacts (μ_F, $p = 0.40$), highlighting that the aqueous lubrication of SPMK-g-PEEK substantially influences cartilage friction.

The SPMK-g-PEEK surface introduces a highly hydrated polyelectrolyte interface, providing effective aqueous boundary lubrication. Previous studies have shown that lubricity of SPMK-g-PEEK is independent of speed, maintaining constant low CoF (< 0.02) across a speed range of 1 - 200 mm/s up to 1.2 MPa contact pressures against cartilage [12]. The inherent lubricity of the SPMK-g-PEEK interface facilitates low CoF even after compressive cartilage dehydration, with both SCA and cSCA contacts exhibiting a startup CoF of $\mu_S \sim 0.04$. The SPMK-g-PEEK startup CoF observed within this study is marginally higher than previous studies ($\mu_S < 0.02$, sliding speed = 10 mm/s) [11]. Whilst this discrepancy maybe be attributed experimental hardware differences in sample alignment [32], greater shear forces resulting from higher sliding speeds likely increase friction in cartilage following compression, where rehydration has not yet occurred to supplement fluid load support.

6.4.2 Substrate Effects

Table 6.4 summarises the independent t-tests performed for each cartilage contact geometry condition (SCA, cSCA) interfaced with each substrate (PEEK, SPMK, cartilage condyle). Aside from tribological rehydration afforded by a cSCA cartilage geometry, there are clear indications of rehydration attributed to substrate effects. Comparing cartilage condyle and PEEK substrates in both SCA and cSCA configurations, demonstrated significantly greater overall strain recovery (ε_r, $p < 0.05$), lower startup CoF (μ_S, $p < 0.05$), and lower final CoF (μ_F, $p < 0.03$) for cartilage condyle surfaces. The greater overall strain recovery and low friction of matched cartilage is attributed to the increased availability of water in the contact area, as both cartilage can exude water interstitial water and support biphasic fluid-structure interactions to promote rehydration and lubrication [33, 34]. Furthermore, compliance of low-modulus matched cartilage contacts promote uniform distribution of contact pressures [35, 36], which may support fluid film lubrication [34, 37]. Synovial rehydration mechanisms can be attributed to fluid exchange within the contact gap [5, 6] and osmotic swelling [1], both of which rely on transient loading within the contact area during sliding, supported by the high compliance distributing contact

pressures and roughness of cartilage (i.e. fluid confinement between asperities). However, this study does not isolate specific contributions of synovial tissue rehydration mechanisms, focusing instead on the overall performance of matched cartilage. Conversely, hard biomaterials such as PEEK result in higher contact pressures and comparatively smaller contact areas, resulting in accelerated fluid exudation and higher shear forces [38, 39, 36]. Cartilage rehydration and aqueous lubrication are reduced as PEEK surfaces do not provide a hydrated, porous, compliant counterface necessary for effective fluid exchange within the contact area [10]. The same trend is observed when comparing SPMK-g-PEEK and PEEK substrates in both SCA and cSCA configurations (Tab. 6.4), demonstrating significantly greater overall strain recovery (ε_r, $p < 0.02$), lower startup CoF (μ_S, $p < 0.01$), and lower final CoF (μ_F, $p < 0.02$) for SPMK-g-PEEK substrates. Prior studies measure the SPMK swollen surface height of 5 μm and low modulus of ~500 Pa, indicating a hydrated, cushioning interface that enhances fluid pressurisation within cartilage asperity gaps to facilitate rehydration [12]. Hydrophilic SPMK-g-PEEK counterfaces facilitate aqueous lubrication (low μ_S and μ_F) and an aqueous reservoir to support cartilage interstitial fluid recovery (high ε_r) through PETR [12, 10, 11].

Table 6.4 shows strain recovery promoted by SPMK-g-PEEK substrates attributed to PETR, and strain recovery promoted by condyle substrate attributed to synovial rehydration mechanisms are comparable in both SCA (ε_r, $p = 0.44$) and cSCA conditions (ε_r, $p = 0.71$). The greatest strain recovery was observed in the cSCA condition, with cSCA-SPMK exhibiting $\varepsilon_r = 12.95 \pm 2.55\%$, and cSCA-Condyle exhibiting $\varepsilon_r = 14.11 \pm 4.15\%$ ($p = 0.71$). Providing an initial empirical demonstration that SPMK-g-PEEK can effectively mimic synovial rehydration mechanisms. However, there are distinct differences in lubrication mechanisms. In both SCA and cSCA conditions, SPMK-g-PEEK surfaces exhibit a significantly lower startup CoF ($\mu_S \sim 0.04$) compared to the high startup CoF ($\mu_S \sim 0.13$) observed for cartilage condyles ($p < 0.02$). IFP recovery and enhanced fluid load support, indicated by strain recovery, results in lower final CoF for SPMK-g-PEEK ($\mu_F \sim 0.01$) and condyle ($\mu_F \sim 0.05$) surfaces. Comparing respective contact geometries, there is a statistically greater reduction of final CoF for SCA conditions ($p = 0.02$) than for cSCA conditions ($p = 0.11$). Which is attributed to the greater contribution of tribological rehydration observed for the cSCA-SPMK condition (Tab. 6.3). As discussed previously, the lubrication performance of SPMK-g-PEEK is largely independent of IFP, as the high hydration of the SPMK-g-PEEK interface provides unabating aqueous lubrication [12, 10, 11]. Notably, the startup CoF observed for SPMK-g-PEEK contacts ($\mu_S \sim 0.04$) is

similar in magnitude to the final CoF for matched cartilage condyles ($\mu_F \sim 0.05$). Demonstrating that the lubrication performance of SPMK-g-PEEK can replicate physiological CoF even in contact conditions following compressive fluid exudation with reduced cartilage IFP (Fig. 6.5). Conversely, lubrication of matched cartilage relies on IFP [7], and hence is dependant on strain recovery to restore IFP (Fig. 6.3).

Table 6.4: **Substrate effects:** Comparison of mean overall strain recovery (ε_r), startup CoF (μ_S) and final CoF (μ_F) between PEEK and SPMK-g-PEEK and matched cartilage substrates for both SCA and cSCA conditions using independent t-tests. The t-statistic measures the difference between the sample means in terms of standard deviations, and the p-value indicates the statistical significance of the observed differences.

Sample Pair	Strain Recovery (ε_r)		Startup CoF (μ_S)		Final CoF (μ_F)	
	t-statistic	p-value	t-statistic	p-value	t-statistic	p-value
SCA-Condyle vs SCA-PEEK	6.68	0.01	-5.24	0.01	-5.85	0.02
cSCA-Condyle vs cSCA-PEEK	4.04	0.05	-3.75	0.05	-4.53	0.02
SCA-SPMK vs SCA-PEEK	10.43	0.01	-8.90	0.01	-6.95	0.02
cSCA-SPMK vs cSCA-PEEK	5.56	0.02	-5.91	0.02	-6.56	0.02
SCA-Condyle vs SCA-SPMK	0.91	0.44	4.11	0.02	4.91	0.02
cSCA-Condyle vs cSCA-SPMK	0.41	0.71	5.12	0.02	2.63	0.11

6.4.3 Clinical Significance

Current use of hard biomaterials (e.g. Cobalt-Chromium-Molybdenum) for focal joint repair or hemiarthroplasty compromise fluid-pressure dependant load support of interfacing cartilage, leading to high friction and cartilage erosion [40, 41]. Indicating that these biomaterials do not facilitate the sustainable, competitive rehydration essential for supporting healthy cartilage biomechanics [42, 43]. In contrast, matched cartilage surfaces provide a continuous pathway for fluid exchange, supporting hydraulic permeability and osmotic rehydration [35]. Cartilage fluid recovery to counteract compressive exudation holds significant physiological relevance. Foremost rehydration is required for sustaining IFP and CoF < 0.1 [31, 8, 7], above which can lead to wear of cartilage and pathogenesis of osteoarthritis [44, 45, 46]. Additionally rehydration underpins biological functions (i.e. solute transport and cellular mechanotransduction) [47, 16, 48] with observations that activity can prevent osteoarthritis [49] or joint space narrowing by reversing cartilage dehydration due to inactivity [50, 51].

This study demonstrates interfacing hard biomaterials, such as PEEK (Fig. 6.4), against cartilage results in vastly reduced strain recovery and higher CoF, highlighting the inadequacy of hard biomaterials in supporting cartilage lubrication and rehydration [10, 11]. Whereas, fric-

tion and interstitial fluid recovery of cartilage is significantly influenced by the surface hydration of opposing cartilage (condyle substrates) or polyelectrolytes (SPMK-g-PEEK substrates) [7, 12, 52]. Compared to PEEK in the SCA condition, cartilage condyle interfaces result in enhanced strain recovery ($\varepsilon_r = 8.77 \pm 3.10\%$, $p = 0.01$) resulting in a substantially lower final CoF ($\mu_F = 0.049 \pm 0.012$, $p = 0.02$). Similarly SPMK-g-PEEK in the SCA condition, compared to PEEK, results in enhanced strain recovery ($\varepsilon_r = 7.04 \pm 1.71\%$, $p = 0.01$) and a substantially lower CoF ($\mu_F = 0.011 \pm 0.006$, $p = 0.02$). The SCA condition operates independently of tribological rehydration [31, 11], and therefore isolates the contributions of each substrate. The contribution of tribological rehydration enhanced overall strain recovery for all substrates (Tab. 6.2). Correspondingly, the greatest strain recovery in this dataset was observed for the cSCA-SPMK ($\varepsilon_r = 12.95 \pm 2.55\%$) and cSCA-Condyle ($\varepsilon_r = 14.11 \pm 4.15\%$) experiments. A key finding of this study is that PETR by SPMK-g-PEEK substrates can reproduce comparable levels matched cartilage (condyle) synovial rehydration, demonstrated by the insignificant strain recovery (ε_r) p-values comparing both SCA, $p = 0.44$, and cSCA conditions, $p = 0.71$ (Tab. 6.4). Furthermore, the superior aqueous lubrication properties of SPMK-g-PEEK are able to facilitate physiological CoF levels at the start of sliding ($\mu_S \sim 0.04$) [7, 8], where cartilage IFP is diminished, contrasting to the higher startup CoF observed for cartilage condyle surfaces ($\mu_S \sim 0.13$). These results confer SPMK-g-PEEK as a compelling biomimetic interface for facilitating cartilage rehydration, and therefore the biological function of cartilage [47], and also facilitate low friction comparable to the final CoF of matched cartilage interfaces following effective rehydration and IFP recovery ($\mu_F \sim 0.05$, Fig. 6.3). Previous studies of low cartilage friction afforded by SPMK-g-PEEK interfaces have been demonstrated to substantially mitigate cartilage wear compared to unfunctionalised biomaterials [10] and facilitate low CoF of damaged cartilage [11].

Present literature on high water content materials for cartilage resurfacing, hydrogels or polymer brush interfaces, often only consider CoF to evaluate performance against impermeable counterfaces (e.g. glass) [53, 54, 55, 56, 57, 58, 59] or cartilage explants [60, 61, 62]. These approaches fail to directly measure the materials' ability to regulate cartilage interstitial fluid recovery. The inference of sustained hydration is often indirectly made through observations of maintained physiological CoF levels, leveraging the understanding of the biphasic nature of these materials [58, 59]. However, the reliance on CoF as a sole performance indicator may be misleading, posing the risk that materials exhibiting low CoF due to aqueous lubrication

alone may not adequately support fluid transport requisite for maintaining cartilage health [47]. SPMK-g-PEEK is an example of a material that facilitates physiological low cartilage CoF, irrespective of cartilage IFP [11, 12], which is demonstrated by the low CoF observed for cartilage interfaced with SPMK-g-PEEK at the onset of sliding ($\mu_S \sim 0.04$, Fig. 6.5). The specific PETR mechanism underpinning cartilage strain recovery interfaced with SPMK-g-PEEK has been explicated in a previous study [12]. However future studies of alternate hydrated materials for articulating against cartilage (e.g. hydrogels) should employ studies which evaluate the materials capacity for facilitating cartilage rehydration.

6.4.4 Limitations

The statistical power of this study is constrained by the small sample size (N = 3), providing only an initial indication of SPMK-g-PEEK's efficacy in replicating the fluid exchange and tribological properties of matched articular cartilage. *In vitro* analysis of cartilage tribology inherently faces uncertainties due to the variability in tissue quality and geometry [8]. The most significant errors were observed in the matched cartilage contacts (Fig. 6.3), with a strain standard deviation of approximately 3-4%. In contrast, previous studies on SCA cartilage strain against PEEK substrates reported standard deviations around 2% [11]. The higher standard deviation in matched cartilage contacts is attributed to the compliance of both mated cartilage surfaces, which leads to greater temporal variation in compressive strain. These errors are further compounded by the low sample size. Specifically, this study did not reliably quantify the synergistic effects of cSCA tribological rehydration and synovial rehydration (e.g. fluid exchange or osmotic swelling). Future studies should incorporate a larger sample size and aim to optimise the Fuzzy-PI feedback parameters to enhance feedback rate and improve load control.

The development of a tribometer that simulates physiological matched cartilage interactions has limited the accuracy of data collection, particularly in measuring contact area or strain under zero interstitial pressure. Additionally, the experiments involving matched cartilage (condyle) and SPMK-g-PEEK interfaces did not strictly adhere to the numerical predictions of IFP theory (Eq. 1.3), likely due to additional friction dissipation mechanisms beyond biphasic theory (i.e. aqueous boundary lubrication). To fully elucidate the temporal biomechanical behaviour of cartilage interfaced with candidate biomaterials, future studies should incorporate accurate calculations of interstitial fluid flow using poroviscoelastic models [63], alongside detailed ex-

perimental analyses.

The role of dynamic physiological loading (i.e. gait) in cartilage tribology and fluid pressurisation remains a topic of debate in the literature [64, 65]. This study focused on loads maintained at 20 N. Follow on studies using the Fuzzy-PI tribometer (Fig. 6.1) will explore the role of variable loading on both cartilage-cartilage tribological rehydration and the effectiveness of SPMK-g-PEEK to emulate this behaviour under physiological duty cycles. Furthermore, this dynamically responsive *in vitro* apparatus and associated techniques could feasibly be employed for validating other soft viscoelastic materials for tissue and cartilage repair [66, 67].

6.5 Conclusions

This study demonstrates the efficacy of SPMK-g-PEEK as a biomimetic material for focal cartilage repair, capable of facilitating sustained low friction and interstitial fluid recovery comparable to matched cartilage-cartilage interfaces. The development of a Fuzzy-PI controlled biotribometer for *in vitro* assessment of cartilage contact models facilitated concurrent measurement of friction and strain recovery attributable to interstitial fluid maintenance. Through a dual-phase testing approach, encompassing compression and subsequent compression-sliding, this methodology permits direct quantification of cartilage's interstitial fluid recovery after static exudation phases, revealing rehydration dynamics.

Our results demonstrate the rehydration of matched cartilage contacts with fluid exchange attributable to osmotic swelling and hydrodynamic tribological rehydration, establishing a physiological benchmark for strain recovery ($\varepsilon_r \sim 14\%$) and low friction ($\mu \sim 0.04$) following a period of compressive cartilage dehydration. In contrast, PEEK surfaces hinder fluid influx, leading to high CoF and limited interstitial fluid recovery during sliding. SPMK-g-PEEK surfaces, with an engineered polyelectrolyte-enhanced tribological rehydration mechanism, exhibited comparable tribological behaviour to matched cartilage contacts, resulting in strain recovery of $\varepsilon_r \sim 13\%$ and lower friction, $\mu \sim 0.01$. This highlights the effectiveness of SPMK-g-PEEK in maintaining near-surface hydration, which is synonymous with cartilage lubrication and rehydration, offering inherent advantages over currently employed hard biomaterials used in cartilage repair. Overall, SPMK-g-PEEK presents a promising biomimetic solution for cartilage repair, effectively mimicking the natural rehydration and lubrication mechanisms essential for joint health and longevity.

6.6 Supporting Information

Figure A1 shows the boxplots of F_Z applied throughout the sliding phase for each cartilage contact pair. Demonstrating a consistent interquartile range below ± 1 N, indicating minimal fluctuation in applied load. The largest load fluctuations were observed for the matched cartilage-cartilage contact pairs due to the variation in surface height of the cartilage condyles.

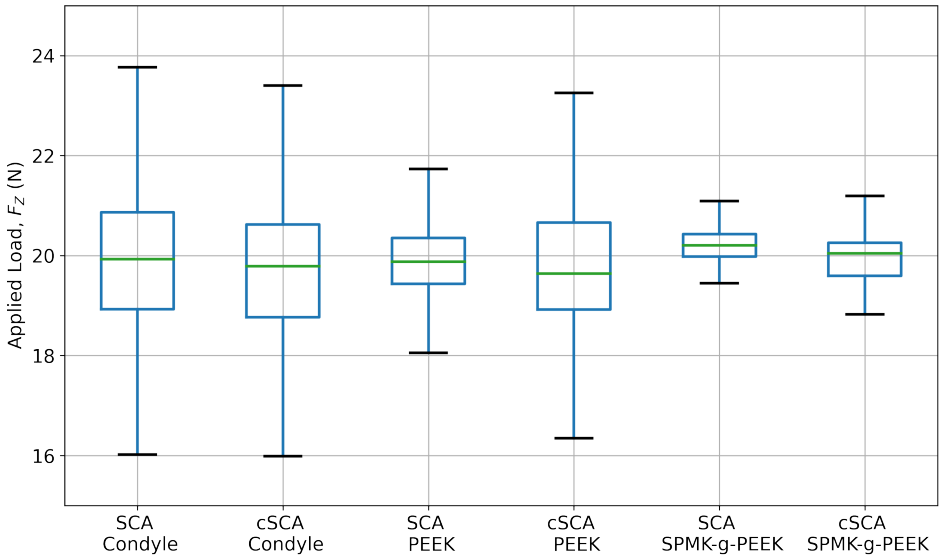

Figure A1: Boxplots of the applied normal load (F_Z) for each testing scenario showing the variation of load control throughout the sliding phase of each test.

Table A1 summarises the results of pairwise t-tests for all contact pairs between PEEK, SPMK-g-PEEK and cartilage condyle surfaces in both SCA and cSCA contact conditions.

Table A1: Results of pairwise t-tests for all contact pairs

Sample Pair	Strain Recovery		Startup CoF		Final CoF	
	t-statistic	p-value	t-statistic	p-value	t-statistic	p-value
SCA-Condyle vs cSCA-Condyle	-1.786	0.154	0.341	0.751	0.817	0.469
SCA-Condyle vs SCA-PEEK	6.683	0.007	-5.238	0.008	-5.852	0.024
SCA-Condyle vs cSCA-PEEK	2.454	0.112	-3.393	0.047	-4.408	0.033
SCA-Condyle vs SCA-SPMK	0.910	0.442	4.114	0.017	4.906	0.017
SCA-Condyle vs cSCA-SPMK	-1.804	0.148	4.561	0.028	5.751	0.018
cSCA-Condyle vs SCA-PEEK	7.321	0.009	-5.888	0.009	-5.967	0.017
cSCA-Condyle vs cSCA-PEEK	4.039	0.046	-3.705	0.046	-4.530	0.019
cSCA-Condyle vs SCA-SPMK	2.851	0.089	4.348	0.012	2.240	0.135
cSCA-Condyle vs cSCA-SPMK	0.412	0.705	5.122	0.016	2.633	0.110
SCA-PEEK vs cSCA-PEEK	-8.092	0.003	0.378	0.727	2.835	0.061
SCA-PEEK vs SCA-SPMK	-10.433	0.001	8.898	0.003	6.952	0.019
SCA-PEEK vs cSCA-SPMK	-10.149	0.001	9.558	0.007	7.077	0.019
cSCA-PEEK vs SCA-SPMK	-3.335	0.029	5.785	0.017	6.331	0.021
cSCA-PEEK vs cSCA-SPMK	-5.557	0.016	5.911	0.024	6.562	0.021
SCA-SPMK vs cSCA-SPMK	-3.681	0.041	-0.323	0.768	0.961	0.398

References

[1] Steven Voinier, AC Moore, Jamie M Benson, C Price, and David Lawrence Burris. The modes and competing rates of cartilage fluid loss and recovery. *Acta Biomaterialia*, 138:390–397, 2022.

[2] Frank C Linn. Lubrication of animal joints: I. the arthrotripsometer. *JBJS*, 49(6):1079–1098, 1967.

[3] S Hinterwimmer, M Gotthardt, R von Eisenhart-Rothe, S Sauerland, M Siebert, T Vogl, Felix Eckstein, and H Graichen. In vivo contact areas of the knee in patients with patellar subluxation. *Journal of biomechanics*, 38(10):2095–2101, 2005.

[4] Christopher E Henderson, Jill S Higginson, and Peter J Barrance. Comparison of mri-based estimates of articular cartilage contact area in the tibiofemoral joint. 2011.

[5] Yabin Wu and Stephen J Ferguson. The influence of cartilage surface topography on fluid flow in the intra-articular gap. *Computer methods in biomechanics and biomedical engineering*, 20(3):250–259, 2017.

[6] JinJing Liao, David W Smith, Saeed Miramini, Namal Thibbotuwawa, Bruce S Gardiner, and Lihai Zhang. The investigation of fluid flow in cartilage contact gap. *Journal of the Mechanical Behavior of Biomedical Materials*, 95:153–164, 2019.

[7] Matteo Caligaris and Gerard A Ateshian. Effects of sustained interstitial fluid pressurization under migrating contact area, and boundary lubrication by synovial fluid, on cartilage friction. *Osteoarthritis and Cartilage*, 16(10):1220–1227, 2008.

[8] Axel C Moore, Jordyn Lee Schrader, Jaclyn J Ulvila, and David L Burris. A review of methods to study hydration effects on cartilage friction. *Tribology-Materials, Surfaces & Interfaces*, 11(4):202–214, 2017.

[9] Margot S Farnham, Kyla F Ortved, Jeffrey S Horner, Norman J Wagner, David L Burris, and Christopher Price. Lubricant effects on articular cartilage sliding biomechanics under physiological fluid load support. *Tribology Letters*, 69:1–14, 2021.

[10] Robert J Elkington, Richard M Hall, Andrew R Beadling, Hemant Pandit, and Michael G Bryant. Highly lubricious spmk-g-peek implant surfaces to facilitate rehydration of articular cartilage. *Journal of the Mechanical Behavior of Biomedical Materials*, 147:106084, 2023.

[11] Robert J Elkington, Richard M Hall, Andrew R Beadling, Hemant Pandit, and Michael G Bryant. Engineering tribological rehydration of cartilage interfaces: assessment of potential polyelectrolyte mechanisms. *Tribology International*, 2024.

[12] Robert J Elkington, Richard M Hall, Andrew R Beadling, Hemant Pandit, and Michael G Bryant. Brushing up on cartilage lubrication: Polyelectrolyte enhanced tribological rehydration. *Preprint Submitted to Langmuir*, 2024.

[13] H Forster and J Fisher. The influence of loading time and lubricant on the friction of articular cartilage. *Proceedings of the Institution of Mechanical Engineers, Part H: Journal of Engineering in Medicine*, 210(2):109–119, 1996.

[14] Tannin A Schmidt, Nicholas S Gastelum, Quynhhoa T Nguyen, Barbara L Schumacher, and Robert L Sah. Boundary lubrication of articular cartilage: role of synovial fluid constituents. *Arthritis & Rheumatism*, 56(3):882–891, 2007.

[15] Robert L Trevino, Jonathan Stoia, Michel P Laurent, Carol A Pacione, Susan Chubinskaya, and Markus A Wimmer. Establishing a live cartilage-on-cartilage interface for tribological testing. *Biotribology*, 9:1–11, 2017.

[16] Oliver R Schätti, Luigi M Gallo, and Peter A Torzilli. A model to study articular cartilage mechanical and biological responses to sliding loads. *Annals of biomedical engineering*, 44:2577–2588, 2016.

[17] David L Burris and Axel C Moore. Cartilage and joint lubrication: new insights into the role of hydrodynamics. *Biotribology*, 12:8–14, 2017.

[18] Axel C Moore. *Independent and competing roles of fluid exudation and rehydration in cartilage mechanics and tribology*. University of Delaware, 2017.

[19] Kaushikk Ravender Iyer, David Keeling, and Richard M Hall. A novel and advanced control method based on fuzzy-pi for joint wear simulators. *Open Research Europe*, 4(6):6, 2024.

[20] Richard A Brand. Joint contact stress: a reasonable surrogate for biological processes? *The Iowa orthopaedic journal*, 25:82, 2005.

[21] Meghan E Kupratis, Ahmed E Gure, Kyla F Ortved, David L Burris, and Christopher Price. Comparative tribology: articulation-induced rehydration of cartilage across species. *Biotribology*, 25:100159, 2021.

[22] Y Merkher, S Sivan, I Etsion, A Maroudas, G Halperin, and A Yosef. A rational human joint friction test using a human cartilage-on-cartilage arrangement. *Tribology Letters*, 22:29–36, 2006.

[23] CJ Bell, E Ingham, and J Fisher. Influence of hyaluronic acid on the time-dependent friction response of articular cartilage under different conditions. *Proceedings of the Institution of Mechanical Engineers, Part H: Journal of Engineering in Medicine*, 220(1):23–31, 2006.

[24] J Katta, SS Pawaskar, ZM Jin, E Ingham, and J Fisher. Effect of load variation on the friction properties of articular cartilage. *Proceedings of the Institution of Mechanical Engineers, Part J: Journal of Engineering Tribology*, 221(3):175–181, 2007.

[25] E Northwood, J Fisher, and R Kowalski. Investigation of the friction and surface degradation of innovative chondroplasty materials against articular cartilage. *Proceedings of the institution of mechanical engineers, part H: Journal of Engineering in Medicine*, 221(3):263–279, 2007.

[26] Yanhong Bei and Benjamin J Fregly. Multibody dynamic simulation of knee contact mechanics. *Medical engineering & physics*, 26(9):777–789, 2004.

[27] A Unsworth, D Dowson, and V Wright. Some new evidence on human joint lubrication. *Annals of the rheumatic diseases*, 34(4):277–285, 1975.

[28] A Unsworth, D Dowson, and V Wright. The frictional behavior of human synovial joints—part i: natural joints. 1975.

[29] L McCann, I Udofia, S Graindorge, E Ingham, Z Jin, and J Fisher. Tribological testing of articular cartilage of the medial compartment of the knee using a friction simulator. *Tribology International*, 41(11):1126–1133, 2008.

[30] Jarrett M Link, Evelia Y Salinas, Jerry C Hu, and Kyriacos A Athanasiou. The tribology of cartilage: Mechanisms, experimental techniques, and relevance to translational tissue engineering. *Clinical Biomechanics*, 79:104880, 2020.

[31] Axel C Moore and David L Burris. Tribological rehydration of cartilage and its potential role in preserving joint health. *Osteoarthritis and cartilage*, 25(1):99–107, 2017.

[32] DL Burris and WG Sawyer. Addressing practical challenges of low friction coefficient measurements. *Tribology letters*, 35:17–23, 2009.

[33] Jay J Shim, Steve A Maas, Jeffrey A Weiss, and Gerard A Ateshian. Finite element implementation of biphasic-fluid structure interactions in febio. *Journal of biomechanical engineering*, 143(9):091005, 2021.

[34] JS Hou, MH Holmes, WM Lai, and VC Mow. Boundary conditions at the cartilage-synovial fluid interface for joint lubrication and theoretical verifications. *J Biomech Eng.*, 1989.

[35] Sainath Shrikant Pawaskar, John Fisher, and Zhongmin Jin. Robust and general method for determining surface fluid flow boundary conditions in articular cartilage contact mechanics modeling. *Journal of Biomechanical Engineering*, 132(3):031001, 2010.

[36] Ryan Willing, Michael Lapner, Graham JW King, and James A Johnson. In vitro assessment of the contact mechanics of reverse-engineered distal humeral hemiarthroplasty prostheses. *Clinical Biomechanics*, 29(9):990–996, 2014.

[37] Christian J Schwartz and Shyam Bahadur. Investigation of articular cartilage and counterface compliance in multi-directional sliding as in orthopedic implants. *Wear*, 262(11-12):1315–1320, 2007.

[38] Carolyn Berkmortel, G Daniel G Langohr, Graham King, and James Johnson. Hemiarthroplasty implants should have very low stiffness to optimize cartilage contact stress. *Journal of Orthopaedic Research®*, 38(8):1719–1726, 2020.

[39] Alana Khayat. *Effect of hemiarthroplasty implant contact geometry and material on early cartilage wear*. The University of Western Ontario (Canada), 2015.

[40] Sainath Shrikant Pawaskar, Eileen Ingham, John Fisher, and Zhongmin Jin. Fluid load support and contact mechanics of hemiarthroplasty in the natural hip joint. *Medical engineering & physics*, 33(1):96–105, 2011.

[41] Theresa Diermeier, Arne Venjakob, Kevin Byrne, Rainer Burgkart, Peter Foehr, Stefan Milz, Andreas B Imhoff, and Stephan Vogt. Effects of focal metallic implants on opposing cartilage–an in-vitro study with an abrasion test machine. *BMC Musculoskeletal Disorders*, 21(1):1–7, 2020.

[42] Debora Rossetti. *Early Biological Response of Articular Cartilage to Hemiarthroplasty Wear*. PhD thesis, The University of Western Ontario (Canada), 2022.

[43] Farshid Guilak, David L Butler, and Steven A Goldstein. Functional tissue engineering:

the role of biomechanics in articular cartilage repair. *Clinical Orthopaedics and Related Research®*, 391:S295–S305, 2001.

[44] CP Neu, AH Reddi, K Komvopoulos, TM Schmid, and PE Di Cesare. Increased friction coefficient and superficial zone protein expression in patients with advanced osteoarthritis. *Arthritis & Rheumatism*, 62(9):2680–2687, 2010.

[45] Sevan R Oungoulian, Krista M Durney, Brian K Jones, Christopher S Ahmad, Clark T Hung, and Gerard A Ateshian. Wear and damage of articular cartilage with friction against orthopedic implant materials. *Journal of biomechanics*, 48(10):1957–1964, 2015.

[46] SMT Chan, CP Neu, K Komvopoulos, AH Reddi, and PE Di Cesare. Friction and wear of hemiarthroplasty biomaterials in reciprocating sliding contact with articular cartilage. 2011.

[47] Brian T Graham, Axel C Moore, David L Burris, and Christopher Price. Sliding enhances fluid and solute transport into buried articular cartilage contacts. *Osteoarthritis and cartilage*, 25(12):2100–2107, 2017.

[48] Michael B Albro, Nadeen O Chahine, Roland Li, Keith Yeager, Clark T Hung, and Gerard A Ateshian. Dynamic loading of deformable porous media can induce active solute transport. *Journal of biomechanics*, 41(15):3152–3157, 2008.

[49] Paul T Williams. Effects of running and walking on osteoarthritis and hip replacement risk. *Medicine and science in sports and exercise*, 45(7):1292, 2013.

[50] Ragnar Ekholm and INGELMARK BE. Functional thickness variations of human articular cartilage. *Acta Societatis Medicorum Upsaliensis*, 57(1-2):39–59, 1952.

[51] BE Ingelmark and RAGNAR EKHOLM. A study on variations in the thickness of articular cartilage in association with rest and periodical load; an experimental investigation on rabbits. *Upsala lakareforenings forhandlingar*, 53(1-2):61–74, 1948.

[52] T Murakami, Y Sawae, M Horimoto, and M Noda. Role of surface layers of natural and artificial cartilage in thin film lubrication. In *Tribology Series*, volume 36, pages 737–747. Elsevier, 1999.

[53] Piers E Milner, Maria Parkes, Jennifer L Puetzer, Robert Chapman, Molly M Stevens,

Philippa Cann, and Jonathan RT Jeffers. A low friction, biphasic and boundary lubricating hydrogel for cartilage replacement. *Acta biomaterialia*, 65:102–111, 2018.

[54] Yu-Song Pan, Dang-Sheng Xiong, and Ru-Yin Ma. A study on the friction properties of poly (vinyl alcohol) hydrogel as articular cartilage against titanium alloy. *Wear*, 262(7-8):1021–1025, 2007.

[55] Mark E Freeman, Michael J Furey, Brian J Love, and Jeanne M Hampton. Friction, wear, and lubrication of hydrogels as synthetic articular cartilage. *Wear*, 241(2):129–135, 2000.

[56] Michelle M Blum and Timothy C Ovaert. Low friction hydrogel for articular cartilage repair: evaluation of mechanical and tribological properties in comparison with natural cartilage tissue. *Materials Science and Engineering: C*, 33(7):4377–4383, 2013.

[57] Kai Chen, Xuehui Yang, Dekun Zhang, Linmin Xu, Xin Zhang, and Qingliang Wang. Biotribology behavior and fluid load support of pva/ha composite hydrogel as artificial cartilage. *Wear*, 376:329–336, 2017.

[58] D Baykal, RJ Underwood, K Mansmann, M Marcolongo, and SM Kurtz. Evaluation of friction properties of hydrogels based on a biphasic cartilage model. *Journal of the mechanical behavior of biomedical materials*, 28:263–273, 2013.

[59] Teruo Murakami, Seido Yarimitsu, Kazuhiro Nakashima, Nobuo Sakai, Tetsuo Yamaguchi, Yoshinori Sawae, and Atsushi Suzuki. Biphasic and boundary lubrication mechanisms in artificial hydrogel cartilage: A review. *Proceedings of the Institution of Mechanical Engineers, Part H: Journal of Engineering in Medicine*, 229(12):864–878, 2015.

[60] Masayuki Kyomoto, Toru Moro, Ken-ichi Saiga, Fumiaki Miyaji, Hiroshi Kawaguchi, Yoshio Takatori, Kozo Nakamura, and Kazuhiko Ishihara. Lubricity and stability of poly (2-methacryloyloxyethyl phosphorylcholine) polymer layer on co–cr–mo surface for hemi-arthroplasty to prevent degeneration of articular cartilage. *Biomaterials*, 31(4):658–668, 2010.

[61] Feng Li, Anmin Wang, and Chengtao Wang. Analysis of friction between articular cartilage and polyvinyl alcohol hydrogel artificial cartilage. *Journal of Materials Science: Materials in Medicine*, 27:1–8, 2016.

[62] Feng Li, Yonglin Su, Jianping Wang, Gang Wu, and Chengtao Wang. Influence of dynamic

load on friction behavior of human articular cartilage, stainless steel and polyvinyl alcohol hydrogel as artificial cartilage. *Journal of Materials Science: Materials in Medicine*, 21:147–154, 2010.

[63] GN De Boer, N Raske, S Soltanahmadi, D Dowson, MG Bryant, and RW Hewson. A porohyperelastic lubrication model for articular cartilage in the natural synovial joint. *Tribology International*, 149:105760, 2020.

[64] Hamid Sadeghi, DET Shepherd, and DM Espino. Effect of the variation of loading frequency on surface failure of bovine articular cartilage. *Osteoarthritis and Cartilage*, 23(12):2252–2258, 2015.

[65] Ramaswamy Krishnan, Elise N Mariner, and Gerard A Ateshian. Effect of dynamic loading on the frictional response of bovine articular cartilage. *Journal of biomechanics*, 38(8):1665–1673, 2005.

[66] V Timothy Nayar, James D Weiland, and Andrea M Hodge. Macrocompression and nanoindentation of soft viscoelastic biological materials. *Tissue Engineering Part C: Methods*, 18(12):968–975, 2012.

[67] Ahmet Erdemir, Craig Bennetts, Sean Davis, Akhil Reddy, and Scott Sibole. Multiscale cartilage biomechanics: technical challenges in realizing a high-throughput modelling and simulation workflow. *Interface focus*, 5(2):20140081, 2015.

Chapter 7

Discussion

7.1 Introduction

This thesis provides novel insights into the role of polyelectrolyte interfaces in regulating low friction and interstitial fluid pressurisation in cartilage. Specifically, polyelectrolytes composed of hydrophilic 3-sulfopropyl methacrylate potassium salt (SPMK) end-grafted onto a PEEK substrate (SPMK-g-PEEK) are explored as a biomimetic solution for cartilage interfacing surfaces. Both SPMK and PEEK have been demonstrated to be biocompatible materials [1, 2]. The resulting surface modification possesses a high density of sulfonic acid groups with hydrophilic and ionisable characteristics. In aqueous environments, these groups dissociate, leaving negatively charged sulfonate ions (SO_3^-) tethered to the polymer backbone forming hydration shells [3]. These hydrophilic functional groups mimic those present on proteoglycans within the articular cartilage supramolecular complex and in synovial fluid [4], eliciting a biomimetic interface inspired by the natural lubricating biopolyelectrolytes found in synovial tissues. The SPMK-g-PEEK surfaces leverage hydration lubrication, a mechanism where a thin layer of water molecules is maintained by biopolyelectrolytes present within the superficial articular cartilage interface [4], creating a highly hydrated environment that closely mimics the natural conditions within synovial joints.

This body of work begins by endorsing the bioinspired attributes of surface grafted polyelectrolytes and their applications for orthopaedic medical devices. However, few groups have attempted to exploit their use for cartilage interfacing bearing surfaces (Sec. 1.4.5). The high affinity for hydration lubrication and consonantly high interfacial hydration posits their poten-

tial as surrogate cartilage counterfaces, providing physiological CoF and modulating IFP. The majority of this thesis utilises SCA cartilage contact configurations to assess the tribological performance and rehydration characteristics of SPMK-g-PEEK surfaces. Through systematic *in vitro* testing, these configurations allow for a comprehensive evaluation of the material's ability to maintain low CoF and sustain interstitial fluid pressurisation under physiological loading conditions. Key contributions of this study are:

- Demonstration that SPMK-g-PEEK provides highly effective aqueous boundary lubrication of articular cartilage, achieving sustained low coefficients of friction ($\mu < 0.02$).
- Development of *polyelectrolyte-enhanced tribological rehydration* (PETR) theory for facilitating cartilage strain recovery and interstitial fluid reuptake.
- Verification that friction and strain recovery magnitudes for cartilage interfaced with SPMK-g-PEEK are comparable to those of healthy cartilage-cartilage interfaces.

The findings presented herein not only advance our understanding of cartilage lubrication mechanisms but also the methods and materials required for developing biomimetic therapeutic strategies in cartilage resurfacing.

7.2 Research Objectives & Publication Review

Section 2.1 outlines the four research objectives, each corresponding to one of the four publications that comprise this thesis. The following subsections summarise each research objective and corresponding key research findings:

7.2.1 Development and Validation of Biocompatible Polyelectrolyte Functionalised Biomaterial

Chapter 3 introduces the UV photopolymerisation *grafting from* synthesis of a $\sim$ 400 nm (dry thickness) SPMK polyelectrolyte end-grafted to PEEK, and confirms the presence of sulfonic acid groups along with increased wettability, which reflect the desired biomimetic properties. Continuous sliding of SCA bovine cartilage plugs demonstrates the effective aqueous boundary lubrication of SPMK-g-PEEK, evidenced by its low physiological CoF ($\mu_F \sim 0.02$), which is significantly lower compared to unfunctionalised PEEK ($\mu_F \sim 0.45$) or CoCr ($\mu_F \sim 0.35$) interfaces (Fig. 3.7). Cartilage strain recorded throughout each 2.5-hour sliding test demon-

strates that SPMK-g-PEEK reduces the rate of cartilage fluid exudation (Fig. 3.9) and overall strain by approximately 50% compared to unfunctionalised PEEK and CoCr. This indicates enhanced retention of interstitial fluid and hence improved fluid load support in cartilage. This study provides initial evidence that SPMK-g-PEEK substantially mitigates cartilage wear (Fig. 3.8), sustains physiological friction coefficients, and proves the hypothesis that polyelectrolytes enhance IFP.

7.2.2 Characterisation of Rehydration Capability

Chapter 4 assesses sliding-induced strain recovery, indicating interstitial fluid rehydration, of SCA cartilage following a period of static compression against SPMK-g-PEEK and unfunctionalised PEEK. The preloading of cartilage was expected to lead to high startup CoF (μ_S) due to diminished IFP. This is the case for unfunctionalised PEEK control, which during the sliding phase exhibits a high startup CoF ($\mu_S \sim 0.23$) and continues to rise ($\mu_F \sim 0.38$) due to no cartilage rehydration (Fig. 4.3a). Conversely, SPMK-g-PEEK facilitate consistently low CoF ($\mu_S \approx \mu_F \sim 0.01$) and hence effective aqueous boundary lubrication irrespective of cartilage IFP (Fig. 4.3b), furthermore consistently low CoF were also observed in an altered osmotic environment where cartilage fluid recovery was completely inhibited (Fig 4.5). Throughout sliding, SPMK-g-PEEK facilitated strain recovery, indicating interstitial fluid rehydration and enhanced IFP against both pristine and abraded SCA cartilage samples (Fig. 4.4b). Additionally, using low sliding speeds (10 mm/s) and SCA cartilage, contrasting to tribological rehydration demonstrated with cSCA contacts [5], introduces a novel mode of interstitial fluid recovery attributed to polyelectrolytes distinct from fluid pressurisation in a convergent wedge zone. This study empirically demonstrates the efficacy of the hydrated SPMK interface in providing aqueous boundary lubrication and serving as fluid reservoir to facilitate fluid recovery.

7.2.3 Mechanistic Tribological Framework For Polyelectrolyte - Cartilage Interfaces

Chapter 4 culminates in proposing that sliding-induced rehydration is driven by μEHL. In these regions, the polyelectrolyte increased effective viscosity generates high hydrodynamic pressures, which in turn create higher fluid pressures, leading to rehydration (Fig. 4.7). Chapter 5 provides a focused study on the rehydration modalities of polyelectrolyte - cartilage interfaces, establishing the theory of *polyelectrolyte-enhanced tribological rehydration* (PETR) (Sec. 5.5.3).

This study extended prior SCA cartilage strain recovery experiments to explore a range of contact pressures (0.25 - 2.1 MPa) and speeds (0.1 - 10 mm/s) against SPMK-g-PEEK. Greater strain recovery, which indicates higher contact fluid pressurisation, was observed with increasing load and speed, demonstrating the PETR mechanism is driven by a hydrodynamic process (Fig. 5.6). PETR is attributed to the synergistic effects of fluid confinement within the contact gap and polyelectrolyte enhanced μEHL (Sec. 5.5.3). Additionally, this study measured the swollen properties of the SPMK interface, revealing a hydrated thickness of $\sim$ 5 μm (Fig. 5.2) and a low modulus of $\sim$ 500 Pa (Fig. 5.3), analogous to the superficial macromolecular complex present on articular cartilage (Sec. 1.3.3 & 5.5.1). Subsequently, establishing the hypothesis that PETR may occur naturally in synovial joints, drawing parallels to the biomimetic design of the SPMK interface.

7.2.4 Comparative Analysis of Biomimetic Capabilities

Chapter 6 compared the tribological characteristics of physiological matched cartilage contacts, which rely on osmotic swelling and tribological rehydration, with PETR facilitated by SPMK-g-PEEK interfaces. A similar dual-phase testing approach, involving static compression followed by sliding at higher physiological speeds ($\sim$ 30 mm/s), demonstrated that low CoF and strain recovery attributable to interstitial fluid reuptake were comparable (Tab. 6.4) for matched cartilage (Fig. 6.3) and SPMK-g-PEEK (Fig. 6.5). Specifically, for SPMK-g-PEEK interfaced with cSCA cartilage, PETR and conventional tribological rehydration are demonstrated to operate synergistically (Sec. 6.4.1.3). For the cSCA condition, matched cartilage exhibited a final strain recovery of $\varepsilon_r \sim 14\%$ which was effectively emulated by SPMK-g-PEEK which exhbited a strain recovery of $\varepsilon_r \sim 13\%$ (Tab. 6.2). Furthermore, the innate surface hydration of SPMK-g-PEEK is able to invariably imitate physiological friction coefficients of matched cartilage. Specifically the low startup CoF of SPMK-g-PEEK ($\mu_S \sim 0.04$) is comparable to the final CoF of matched cartilage ($\mu_F \sim 0.05$), which is strongly dependant on IFP recovery (Sec. 6.4.2). These findings highlight that SPMK-g-PEEK is comparable to native cartilage-cartilage interfaces in maintaining near-surface hydration for aqueous lubrication and cartilage rehydration. Supporting future work for orthopaedic applications and tribological advantages of SPMK-g-PEEK interfaces over current use of non-hygroscopic hard biomaterials such as PEEK or CoCr (6.4.3).

7.3 Implications Of Research Findings

SPMK-g-PEEK biomimetic materials interfaces have been developed to support the natural tribological function of interfacing articular cartilage. Aqueous lubrication of SPMK-g-PEEK is attributed to hydration lubrication and formation of a hydrated boundary layer, sustaining physiologically consistent CoF of $\mu < 0.02$. CoF is consistently low even in conditions designed to disrupt hydrodynamic lubrication modes demonstrated with overlapping contact areas (Fig. 4.6) and Stribeck analysis (Fig. 5.4). Furthermore, low CoF is observed irrespective of cartilage strain (Fig. 4.5 and 5.6), and thus can compensate for diminished cartilage fluid load support, which would otherwise facilitate biphasic lubrication of cartilage (IFP, Eq. 1.3) [5]. A corollary of this is that observed low CoF of lubricious biomaterials interfaced with cartilage does not necessarily indicate effective IFP or rehydration of cartilage. This study goes beyond conventional tribological testing for candidate biomaterials, which only focus on CoF (Sec. 1.3.5), by developing *in vitro* validation methods inclusive of strain measurement and hence the interstitial fluid flow within interfacing cartilage.

SPMK-g-PEEK facilitates strain recovery of SCA cartilage (Fig. 3.7 & 4.3b), a contact configuration that isolates the effects of conventional tribological rehydration [5] or migrating contact free swelling [6]. Previous studies have shown that sliding SCA cartilage against hard non-hygroscopic counterfaces (e.g., glass, PEEK or CoCr) is analogous to unconfined compression, exhibiting increasing strain (reduced IFP) and a correspondingly rising CoF (Fig. 3.7 & 4.3a) [5, 6, 7]. The demonstration of polyelectrolyte-enhanced tribological rehydration introduces a novel cartilage interstitial fluid recovery mechanism. Contrary to models that hypothesise polyelectrolytes reduce contact permeability [8], this study shows negligible differences in cartilage interstitial fluid loss between SPMK-g-PEEK and PEEK during static compression (Fig. 3.7), meaning polyelectrolyte interfaces do not preclude the exudation of interstitial fluid from cartilage.

PETR is a sliding induced mechanism, underpinned by polyelectrolyte enhanced μEHL and fluid confinement within the contact gap (Sec. 5.5.3). This mechanism becomes effective from speeds > 0.5 mm/s (Fig. 5.6). Similarly, tribological rehydration is also a hydrodynamic mechanism, which relies on fluid pressurisation borne solely through fluid mechanics, due to a convergent wedge (cSCA) contact geometry and which requires speeds of > 30 mm/s [5]. PETR broadens the scope of conventional tribological rehydration, demonstrating cSCA carti-

lage interfaced with SPMK-g-PEEK enhances overall strain recovery and cartilage rehydration (Fig. 6.5). This highlights the inherent benefits of polyelectrolyte-functionalised biomaterials over conventional non-functionalised biomaterials for cartilage interfacing surfaces, particularly in supporting cartilage fluid reuptake.

For matched cartilage contacts, this study demonstrates the native hydration of articular cartilage, supported by synovial biopolyelectrolytes, sustains interstitial fluid pressurisation, strain recovery and lubrication (Sec. 6.4.1.1 & 6.4.3). The 5 μm swollen thickness, low elastic moduli of $\sim$ 500 Pa, and presence of ionic hydration shells of SPMK-g-PEEK is analogous to the physiological superficial macromolecular complex on articular cartilage ($\sim$ 1 - 4 μm thickness [9, 10], $\sim$ 9 kPa moduli [11]). Various research groups have investigated the role of synovial fluid constituents which are hypothesised to form a viscous gel-like boundary interface to support aqueous boundary lubrication and sustain CoF $<$ 0.03 along with supporting fluid confinement and interstitial fluid pressurisation within the polyelectrolyte [12, 13, 14]. The polyelectrolyte conformation and tribological performance is consistent with those observed for SPMK-g-PEEK. Notably, the novel demonstration of PETR fluid recovery facilitated by SPMK-g-PEEK interfaced with cartilage expands the postulated role of the superficial macromolecular complex, supporting the hypothesis of fluid flow leading to rehydration within the cartilage contact gap [15].

SPMK-g-PEEK is positioned as an enabling biomaterials solution for cartilage resurfacing, addressing current issues with high friction hard biomaterials (e.g. CoCr or ceramics) leading to cartilage erosion [16, 17]. This solution has been demonstrated to physiologically consistent low CoF with matched cartilage interfaces within this study (Fig. 6.3) and studies of whole joint models (μ $<$ 0.04) [18, 19]. Notably, the strain recovery of cartilage interfaced with SPMK-g-PEEK clearly indicates enhanced fluid reuptake and augmented IFP. These factors are crucial for the biological functions of cartilage, such as solute transport and cellular mechanotransduction [20, 21], chondrocyte survival [22], and for reversing dehydration due to inactivity [5]. This study advances tribological analysis by including measurement of strain recovery, demonstrating that SPMK-g-PEEK is a highly effective counterface for rehydrating cartilage, thereby supporting cartilage biological function. SPMK-g-PEEK lubrication is also effective when interfacing with damaged cartilage (Fig. 4.4) and in conditions designed to limit fluid reuptake (Fig. 4.5), highlighting that this could be a suitable counterface for cartilage in

the early stages of osteoarthritis where fluid load support and lubrication are often diminished [23, 24]. This body of work underscores the role of interfacial fluid-structure interactions in the design of cartilage resurfacing orthopaedic implants, offering insights that move beyond the limitations of conventional hard, impermeable metallic biomaterials. These findings contribute to a deeper understanding of how implant materials and interfaces can better mimic native articular cartilage, ultimately guiding the development of minimally invasive focal repair implants that conserve cartilage function and longevity in clinical applications.

7.4 Limitations

7.4.1 Clinical Relevance

The short-term (1 - 3 hour) tribological testing, employed under constant loads and primarily in PBS, is not representative of the long-term performance that an orthopaedic implant must endure over a 5+ year lifetime. This study does not explore *in vivo* environmental conditions inclusive of the complex biochemical composition of synovial fluid, the presence of proteins such as albumin and lubricin, variations in pH, and the fluctuating mechanical stresses and temperatures encountered within the synovial joint environment. The failure of Aquala (Kyocera Medical, Japan) implants [25], despite rigorous ISO 14242 hip simulator preclinical validation, underscores the challenges associated with the clinical application of polyelectrolyte-functionalised interfaces. Primarily highlighting the susceptibility of ester based polymers to degraft in *in vivo* environments, which could be attributed to hydrolysis and accelerated by changes in pH [1, 26]. Previous studies have demonstrated that SPMK-g-PEEK is susceptible to hydrolytic degrafting of SPMK. However, in PBS, this degradation only becomes significant after several days [1]. In this study, a new sample of SPMK-g-PEEK was utilised for each test, and short-term (1 - 3 hour) tribological tests were conducted in PBS to mitigate any performance degradation due to surface deterioration. No notable performance reduction was observed within the test duration, suggesting that this issue was not significant during testing.

This thesis provides an early stage *in vitro* study, corresponding to a technology readiness level of 1 - 2, which focuses on material properties and functional tribological assessment of SPMK-g-PEEK. However, the scope of these studies does not address the long term mechanical or chemical stability of SPMK-g-PEEK, its potential interactions with synovial fluid constituents, or adverse *in vivo* conditions (e.g. changes in pH due to inflammation [27]). Furthermore, the

study did not account for potential interactions between the SPMK polyelectrolyte and any naturally occurring superficial macromolecular complexes on the cartilage surface, which may affect the tribological performance. Future work should both address the chemical stability of SPMK interfaces (Section 7.5.3) along with physiologically representative long term testing (Section 7.5.4) for translation towards a viable medical device.

7.4.2 Quantifying Interstitial Fluid Pressurisation

This study does not measure or quantitatively address the ratio of cartilage fluid load support (F') facilitated by PETR fluid recovery of SPMK-g-PEEK. Aqueous boundary lubrication is demonstrated to be independent of temporal cartilage strain. Consequently, the observed effective CoF (μ_{eff}) remains consistently low ($\mu_S \approx \mu_F$), even when measured immediately following cartilage compression ($\mu_S \not\approx \mu_{eq}$). Whereas typical cartilage equilibrium CoF are reported as μ_{eq} = 0.2 - 0.3 in saline [28]. This indicates IFP theory cannot be directly applied to calculate fluid load support (Eq. 1.2) due to the effective aqueous boundary lubrication facilitated by SPMK-g-PEEK. Low cartilage strain and strain recovery empirically demonstrate that SPMK-g-PEEK facilitates cartilage fluid recovery and therefore enhances fluid pressurisation [28] compared to unfunctionalised controls; however, the resultant fluid load support is not quantified. The absence of this data limits the ability to fully profile the effectiveness of SPMK-g-PEEK in replicating the natural biomechanics of cartilage. Future studies (Section 7.5.2) should include direct measurement techniques such as pressure sensors or imaging methods to capture the dynamics of IFP during cartilage articulation with SPMK-g-PEEK surfaces [29, 28]. This will provide a more comprehensive understanding of the fluid load support and elucidate the effectiveness of PETR in maintaining cartilage health and function.

7.4.3 Surface Conformation

SPMK-g-PEEK interfaces were developed following a one step polymer brush self-initiated grafting protocol for MPC to PEEK [30]. However, the resultant measurements of SPMK dry thickness ($\sim$ 500 nm, Fig. 3.6) and swollen thickness ($\sim$ 5 μm, Fig. 5.2) are notably thicker than typical polymer brush interfaces, which usually exhibit dry thickness $<$ 150 nm and swollen thickness $<$ 1 μm [31, 32]. The employed grafting method does not involve a crosslinker, meaning that SPMK can only be end-grafted to the PEEK substrate. This study, however, does not measure the grafting density, chain length, polydispersity, or density gradient of the resultant

SPMK interface. Consequently, it remains uncertain within the scope of this study whether these systems are strictly polymer brushes or if other chain mobility dynamics, such as chain entanglement, could be present. To this end, the reader may note the terms *polymer brush* and *polyelectrolyte interface* are used interchangeably throughout this thesis.

This study attempts to contrast the surface dynamics of SPMK-g-PEEK with the superficial macromolecular complex on articular cartilage. However, the natural complex conformation is still not fully understood [33]. Key differences include the mobility of physical adsorption, rather than higher enthalpy chemical adsorption, and presence of larger bottle-brush polymers, such as lubricin [4]. Remarks of similarity between SPMK-g-PEEK and natural synovial macromolecular complexes are based on their comparable tribological behaviour, hydration lubrication efficacy, and isomorphic material characteristics. Despite these analogies, it is important to acknowledge that there are inherent conformational differences which have not been directly tested.

7.5 Future Work

Two aspects of this thesis should be developed further, firstly investigating what this study demonstrates for native *in vivo* synovial lubrication, and secondly developing polyelectrolyte functionalised implant surfaces for clinical use in cartilage resurfacing.

7.5.1 Potential of *in vivo* mechanism

This research proposes a novel mechanism of cartilage rehydration facilitated by polyelectrolytes (PETR), however no studies have directly addressed whether synovial biopolyelectrolytes contribute to this process *in vivo*. Fluid confinement and associated rehydration in the cartilage contact gap is attributed to interfacial gaps created by high roughness of cartilage, however this has only been modelled theoretically inclusive of the high viscosity of synovial fluid [15]. This approach overlooks the hydrated gel-like interface provided by the superficial macromolecular complex, which has been emulated with SPMK-g-PEEK interfaces. An experimental matched-cartilage study using the rehydration analysis developed in this thesis could compare surfaces with the superficial macromolecular complex removed by sodium dodecyl sulfate [9] to unperturbed cartilage. This would provide initial insights into the role of biopolyelectrolytes in supporting cartilage rehydration. However, extensive washing, and by extension sliding, in

PBS has been shown to remove the superficial complex [11]. Conducting these experiments in synovial fluid would likely reintroduce biopolyelectrolytes back into the contact gap for the diminished superficial complex cartilage samples. Therefore, these experiments would either need to be limited to a short time frame or explore alternate strategies to inhibit physical adsorption or recovery of synovial constituents on the superficial cartilage surface throughout sliding.

7.5.2 Understanding IFP

Understanding the role of PETR in modulating cartilage fluid load support should be explored both experimentally and through computational modelling approaches.

Experimentally this could be achieved by instrumenting cartilage with a pressure transducer and directly measure fluid pressurisation [29], however in order to facilitate the SPMK - cartilage contact interface, the transducer would need to be mounted behind the cartilage sample, which would measure the overall interstitial fluid pressurisation over longer consolidation times. Alternatively, optical methods offer non-invasive methods to elucidate enhanced fluid flow. Glass surfaces can be functionalised with SPMK using a silanisation process, which introduces functional groups onto the glass surface to facilitate the grafting of SPMK [34]. This would then facilitate optical contact area measurements [28] and potentially allow optical thin film interference measurements of the fluid film between SPMK-glass and cartilage interfaces [35]. These measurements would enable the calculation of fluid pressure within the contact gap and, by varying the SPMK concentration profile, elucidate the relationship between enhanced fluid film pressurisation and PETR.

Computational modelling of the presented experimental strain data could calculate fluid pressurisation of cartilage. The interface formed by SPMK-g-PEEK interfaced with cartilage requires an intricate model encompassing the permeable poroviscoelastic mechanics of cartilage [36] along with the macromolecular and nanorheological dynamics of SPMK [37]. This model would need to extend beyond current cartilage models, which often solely focus on entrained fluid film formation, to incorporate a hydrated polyelectrolyte interlayer representing the SPMK interface.

7.5.3 Reinforcement of SPMK-g-PEEK for *in vivo* applications

A significant limitation hindering the *in vivo* use of ester-based polyelectrolytes is their susceptibility to hydrolysis of covalent ester bonds in aqueous environments. Surfaces grafted with SPMK exhibit substantial degradation following immersion in PBS, with over a 95% reduction in dry thickness after 32 days [1]. Reinforcement strategies such as macroinitiators to strengthen the polyelectrolytes connection the substrate with multiple bonds [38, 1] or the incorporation of hydrophobic groups into the polymer backbone, which can shield ester bonds from water molecules and reduce their susceptibility to hydrolytic degradation could be explored [39, 1].

7.5.4 Translation to a Medical Device

Regulatory approval requires rigorous testing to demonstrate consistent performance, safety, and efficacy over extended periods, which involves both *in vitro* and *in vivo* studies. Learning from the failure of MPC functionalised polyethylene (Aquala) implants [25], which showed promise after extensive ISO 14242 hip simulator testing but ultimately failed in clinical application, extra care should be taken when exploring polyelectrolyte interfaces for *in vivo* use. The next stage of validation for polyelectrolyte functionalised materials should involve testing in physiologically representative environments. This includes long-term immersion testing and subsequent surface analysis to assess the grafted polyelectrolyte stability when immersed in physiological fluids (e.g. PBS, and inflammation representative pH ranges) over extended periods. The next stage of clinical translation would be extended joint simulator testing against cartilage using physiological duty cycles to mimic the mechanical environment of a joint [40], evaluating the friction, wear, and overall performance of the material when interfacing with cartilage. Successful validation in these stages would provide a robust foundation for the clinical translation of polyelectrolyte functionalised biomaterials for cartilage repair and resurfacing. Leading to *in vivo* long-term animal studies to observe the material's behaviour in a living system, ensuring its biocompatibility, durability, and efficacy in supporting cartilage health. These steps are critical to validate the material's long-term potential and safety before considering human trials.

7.6 Concluding Remarks

The project was developed on the basis of exploring polyelectrolyte functionalised biomaterials for their use as cartilage interfacing implant surfaces. SPMK-g-PEEK was employed as a paradigmatic polyelectrolyte functionalised biomaterial, and subsequently used to develop systematic *in vitro* tests which demonstrate aqueous boundary lubrication and develop the theory of polyelectrolyte-enhanced tribological rehydration which supports cartilage interstitial fluid recovery. SPMK-g-PEEK surfaces effectively reduce friction and promote cartilage interstitial fluid pressurisation, achieving results comparable to those observed in connatural cartilage-cartilage interfaces. The findings of this study highlight the potential of polyelectrolyte functionalised biomaterials to mimic the native lubrication and hydrated properties of cartilage, offering promising avenues for the development of orthopaedic cartilage resurfacing implants. Furthermore, the structural and functional similarity between grafted SPMK and the biopolyelectrolyte superficial macromolecular complex on articular cartilage suggests that synovial biopolyelectrolytes could enhance fluid confinement in the contact gap and augment interstitial fluid recovery. This novel mechanism (polyelectrolyte enhanced tribological rehydration) could operate in tandem with presupposed mechanisms of hydrodynamic convergent wedge tribological rehydration and free swelling, representing a third paradigm in cartilage rehydration.

This work has developed techniques for the initial tribological validation of interfaces designed for cartilage counterfaces, primarily emphasising the requirement of appraising cartilage strain recovery. Whilst maintaining low CoF is essential for mitigating cartilage erosion, supporting interstitial fluid recovery is incontrovertibly necessary for maintaining the biological functions of cartilage. This critical factor is often overlooked in tribological studies which explore high water content biomaterials, such as hydrogels or polymer brush interfaces, positioned as low friction biomimetic cartilage materials. Additionally, this work has identified critical areas for further research to evaluate the long-term chemical and mechanical stability of SPMK-g-PEEK in more complex physiological environments. Ultimately this thesis concedes that SPMK would likely fail *in vivo* due to the susceptibility of hydrolytic degradation, requiring the development of reinforced polyelectrolyte interfaces optimised for physiological environments. Addressing these challenges will be crucial for advancing from *in vitro* validation to clinical application.

In summary, this thesis contributes to the field of cartilage repair with engineered interfaces

demonstrating the feasibility and effectiveness of polyelectrolyte functionalised surfaces. It provides a robust framework for future research and development, paving the way for the clinical translation of these enabling materials. The outcomes of this research hold the potential to improve joint health and patient outcomes, providing a *soft solution to the hard problem* of addressing the limitations of current hard biomaterials used in cartilage resurfacing applications. While the aspiration remains that tissue engineering approaches will eventually fully restore articular cartilage, these methods currently face long healing times and unreliable clinical outcomes. For younger patients who require immediate load-bearing and functional interventions, engineered resurfacing materials are the most viable interim solution. Thus, further exploration and development of polyelectrolyte functionalised focal cartilage repair interfaces is strongly advocated.

References

[1] Yunlong Yu, Marco Cirelli, Pengfei Li, Zhichao Ding, Yue Yin, Yucheng Yuan, Sissi De Beer, G Julius Vancso, and Shiyong Zhang. Enhanced stability of poly (3-sulfopropyl methacrylate potassium) brushes coated on artificial implants in combatting bacterial infections. *Industrial & Engineering Chemistry Research*, 58(47):21459–21465, 2019.

[2] Jeffrey M Toth. Biocompatibility of peek polymers. In *PEEK biomaterials handbook*, pages 107–119. Elsevier, 2019.

[3] Dietmar Paschek and Ralf Ludwig. Specific ion effects on water structure and dynamics beyond the first hydration shell. *Angew. Chem., Int. Ed*, 50(2):352–353, 2011.

[4] Weifeng Lin and Jacob Klein. Recent progress in cartilage lubrication. *Advanced Materials*, 33(18):2005513, 2021.

[5] Axel C Moore and David L Burris. Tribological rehydration of cartilage and its potential role in preserving joint health. *Osteoarthritis and cartilage*, 25(1):99–107, 2017.

[6] Matteo Caligaris and Gerard A Ateshian. Effects of sustained interstitial fluid pressurization under migrating contact area, and boundary lubrication by synovial fluid, on cartilage friction. *Osteoarthritis and Cartilage*, 16(10):1220–1227, 2008.

[7] Robert J Elkington, Richard M Hall, Andrew R Beadling, Hemant Pandit, and Michael G

Bryant. Engineering tribological rehydration of cartilage interfaces: assessment of potential polyelectrolyte mechanisms. *Tribology International*, 2024.

[8] JinJing Liao, David W Smith, Saeed Miramini, Bruce S Gardiner, and Lihai Zhang. Investigation of role of cartilage surface polymer brush border in lubrication of biological joints. *Friction*, pages 1–18, 2022.

[9] S Graindorge, W Ferrandez, E Ingham, Z Jin, P Twigg, and J Fisher. The role of the surface amorphous layer of articular cartilage in joint lubrication. *Proceedings of the Institution of Mechanical Engineers, Part H: Journal of Engineering in Medicine*, 220(5):597–607, 2006.

[10] Joe T Rexwinkle, Heather K Hunt, and Ferris M Pfeiffer. Characterization of the surface and interfacial properties of the lamina splendens. *Frontiers of Mechanical Engineering*, 12:234–252, 2017.

[11] R Crockett, S Roos, P Rossbach, C Dora, W Born, and H Troxler. Imaging of the surface of human and bovine articular cartilage with esem and afm. *Tribology letters*, 19:311–317, 2005.

[12] Teruo Murakami, Seido Yarimitsu, Kazuhiro Nakashima, Yoshinori Sawae, and Nobuo Sakai. Influence of synovia constituents on tribological behaviors of articular cartilage. *Friction*, 1:150–162, 2013.

[13] Tannin A Schmidt, Nicholas S Gastelum, Quynhhoa T Nguyen, Barbara L Schumacher, and Robert L Sah. Boundary lubrication of articular cartilage: role of synovial fluid constituents. *Arthritis & Rheumatism*, 56(3):882–891, 2007.

[14] Vinay Sharma, Xinfeng Charlie Shi, George Yao, Ying Zheng, Nicholas D Spencer, and James Yuliang Wu. Fluid confinement within a branched polymer structure enhances tribological performance of a poly (2-methacryloyloxyethyl phosphorylcholine)-surface-modified contact lens. *Royal Society Open Science*, 11(10):240957, 2024.

[15] JinJing Liao, David W Smith, Saeed Miramini, Namal Thibbotuwawa, Bruce S Gardiner, and Lihai Zhang. The investigation of fluid flow in cartilage contact gap. *Journal of the Mechanical Behavior of Biomedical Materials*, 95:153–164, 2019.

[16] SMT Chan, CP Neu, K Komvopoulos, AH Reddi, and PE Di Cesare. Friction and wear

of hemiarthroplasty biomaterials in reciprocating sliding contact with articular cartilage. 2011.

[17] RJH Custers, DBF Saris, WJA Dhert, AJ Verbout, MHP Van Rijen, SC Mastbergen, FPJG Lafeber, and LB Creemers. Articular cartilage degeneration following the treatment of focal cartilage defects with ceramic metal implants and compared with microfracture. *JBJS*, 91(4):900–910, 2009.

[18] L McCann, I Udofia, S Graindorge, E Ingham, Z Jin, and J Fisher. Tribological testing of articular cartilage of the medial compartment of the knee using a friction simulator. *Tribology International*, 41(11):1126–1133, 2008.

[19] Elizabeth I Drewniak, Gregory D Jay, Braden C Fleming, and Joseph J Crisco. Comparison of two methods for calculating the frictional properties of articular cartilage using a simple pendulum and intact mouse knee joints. *Journal of biomechanics*, 42(12):1996–1999, 2009.

[20] Brian T Graham, Axel C Moore, David L Burris, and Christopher Price. Sliding enhances fluid and solute transport into buried articular cartilage contacts. *Osteoarthritis and cartilage*, 25(12):2100–2107, 2017.

[21] Zhenxing Zhao, Yifei Li, Mengjiao Wang, Sen Zhao, Zhihe Zhao, and Jie Fang. Mechanotransduction pathways in the regulation of cartilage chondrocyte homoeostasis. *Journal of cellular and molecular medicine*, 24(10):5408–5419, 2020.

[22] Margot S Farnham, Kyla F Ortved, David L Burris, and Christopher Price. Articular cartilage friction, strain, and viability under physiological to pathological benchtop sliding conditions. *Cellular and Molecular Bioengineering*, 14(4):349–363, 2021.

[23] Yaghoub Dabiri and LePing Li. Focal cartilage defect compromises fluid-pressure dependent load support in the knee joint. *International journal for numerical methods in biomedical engineering*, 31(6):e02713, 2015.

[24] Manoj Rajankunte Mahadeshwara, Maisoon Al-Jawad, Richard M Hall, Hemant Pandit, Reem El-Gendy, and Michael Bryant. How do cartilage lubrication mechanisms fail in osteoarthritis? a comprehensive review. *Bioengineering*, 11(6):541, 2024.

[25] Takashi Hosoi, Masahiro Hasegawa, Elia Marin, Narifumi Kishida, Akihiro Sudo, Wenliang Zhu, and Giuseppe Pezzotti. MPC-grafted highly cross-linked polyethylene liners retrieved

from short-term total hip arthroplasty : Further evidences for the unsuitability of the MPC method. (February):1–11, 2020.

[26] Olga Borozenko, Robert Godin, Kai Lin Lau, Wayne Mah, Gonzalo Cosa, WG Skene, and Suzanne Giasson. Monitoring in real-time the degrafting of covalently attached fluorescent polymer brushes grafted to silica substrates effects of ph and salt. *Macromolecules*, 44(20):8177–8184, 2011.

[27] Paul S Treuhaft and Daniel J McCarty. Synovial fluid ph, lactate, oxygen and carbon dioxide partial pressure in various joint diseases. *Arthritis & Rheumatism: Official Journal of the American College of Rheumatology*, 14(4):475–484, 1971.

[28] Axel C Moore, Jordyn Lee Schrader, Jaclyn J Ulvila, and David L Burris. A review of methods to study hydration effects on cartilage friction. *Tribology-Materials, Surfaces & Interfaces*, 11(4):202–214, 2017.

[29] Seonghun Park, Ramaswamy Krishnan, Steven B Nicoll, and Gerard A Ateshian. Cartilage interstitial fluid load support in unconfined compression. *Journal of biomechanics*, 36(12):1785–1796, 2003.

[30] Masayuki Kyomoto, Toru Moro, Shihori Yamane, Masami Hashimoto, Yoshio Takatori, and Kazuhiko Ishihara. Poly (ether-ether-ketone) orthopedic bearing surface modified by self-initiated surface grafting of poly (2-methacryloyloxyethyl phosphorylcholine). *Biomaterials*, 34(32):7829–7839, 2013.

[31] Motoyasu Kobayashi, Yuki Terayama, Moriya Kikuchi, and Atsushi Takahara. Chain dimensions and surface characterization of superhydrophilic polymer brushes with zwitterion side groups. *Soft Matter*, 9(21):5138–5148, 2013.

[32] Jörg Habicht, Markus Schmidt, Jürgen Rühe, and Diethelm Johannsmann. Swelling of thick polymer brushes investigated with ellipsometry. *Langmuir*, 15(7):2460–2465, 1999.

[33] Bruno Zappone, Marina Ruths, George W Greene, Gregory D Jay, and Jacob N Israelachvili. Adsorption, lubrication, and wear of lubricin on model surfaces: polymer brush-like behavior of a glycoprotein. *Biophysical journal*, 92(5):1693–1708, 2007.

[34] Bogdan Zdyrko and Igor Luzinov. Polymer brushes by the "grafting to" method. *Macromolecular rapid communications*, 32(12):859–869, 2011.

[35] Rahul Kumar, Mohammad Sikandar Azam, Subrata Kumar Ghosh, and Sanjay Yadav. 70 years of elastohydrodynamic lubrication (ehl): a review on experimental techniques for film thickness and pressure measurement. *Mapan*, 33(4):481–491, 2018.

[36] GN De Boer, N Raske, S Soltanahmadi, D Dowson, MG Bryant, and RW Hewson. A porohyperelastic lubrication model for articular cartilage in the natural synovial joint. *Tribology International*, 149:105760, 2020.

[37] Manjesh K Singh, Patrick Ilg, Rosa M Espinosa-Marzal, Martin Kroger, and Nicholas D Spencer. Polymer brushes under shear: Molecular dynamics simulations compared to experiments. *Langmuir*, 31(16):4798–4805, 2015.

[38] Yunlong Yu, G Julius Vancso, and Sissi de Beer. Substantially enhanced stability against degrafting of zwitterionic pmpc brushes by utilizing pgma-linked initiators. *European polymer journal*, 89:221–229, 2017.

[39] Robert Quintana, Maria Gosa, Dominik Janczewski, Edit Kutnyanszky, and G Julius Vancso. Enhanced stability of low fouling zwitterionic polymer brushes in seawater with diblock architecture. *Langmuir*, 29(34):10859–10867, 2013.

[40] L McCann, E Ingham, Z Jin, and J Fisher. An investigation of the effect of conformity of knee hemiarthroplasty designs on contact stress, friction and degeneration of articular cartilage: a tribological study. *Journal of biomechanics*, 42(9):1326–1331, 2009.